PGS Ex. 1120

(Referred to in Dr. Triantafyllou's August 27, 2015 deposition transcript as Ex. 1076 in IPR2014-01477)

Ex. PGS 1076

Supplement to Ex. PGS 1041

LEAST SQUARES FILTERING AND TESTING FOR POSITIONING AND QUALITY CONTROL DURING 3D MARINE SEISMIC SURVEYS

VASSILIS N GIKAS

Surveying Engineering N.T.U.A.

Thesis submitted for the Degree of
Doctor of Philosophy

Department of Surveying
University of Newcastle upon Tyne
August 1996

ABSTRACT

Three-dimensional seismic exploration has been widely accepted as an integral part of the development of new oil and gas fields and as a fundamental tool in exploiting additional reserves in existing fields. Positioning is an important ingredient to the success of a 3-D seismic survey. In recent years the problem has become extremely complex, mainly due to the expansion of the type and quantity of survey data collected. Moreover it has become increasingly common for clients to require proof in real-time that the survey 'quality' specifications are being met.

This research project has aimed to develop a completely general, rigorous and integrated methodology which will enable multi-source surveying observables derived during offshore hydrocarbon prospecting, to be integrated to evaluate the relative position and quality measures of the seismic sources, hydrophones and associated hardware in real-time during modern multi-source, multi-streamer operations.

In order to achieve this, a unified algorithm has been developed in which Kalman filtering adopted as the basic stochastic process. The significant innovation of the method is centred upon its ability to cope with any geometrical configuration (i.e. any number of vessels, sources and streamers) while the number of states in the system is reduced to a minimum. The full system has been programmed and successfully tested using two sets of real marine positioning data. Substantial practical support including real data and detailed technical discussions on the subject has been offered by the exploration industry.

Analysis with real data has shown, for the first time, that a completely rigorous solution to the problem is feasible. More specifically, analysis showed that single polynomials can be adopted as a realistic representation of the seismic streamer shape. Source nodes and hydrophone groups deployed at modern single vessel configurations can be located with a positional precision of about 2.0-3.0 metre 2drms and 4.0-5.0 metre 2drms respectively. Maximum external reliability at any node in the network varies between 4.0-8.0 metre. Also, analysis showed that the computational cycle time is typically less than the shot interval.

ACKNOWLEDGEMENTS

I wish to thank my supervisor, Prof. Paul Cross, for giving me the opportunity to undertake the work, having faith in my ability to carry the project through to the end and for his continuous enthusiasm and advice.

This project has been undertaken in association with QC Tools, Inc., who supplies software, systems and consultancy to the exploration industry. Therefore, thanks are due to everyone who has helped over the three years, especially Alex Asiama Akuomoa, Dave Ridyard and Duncan Griffiths for their sustained efforts in providing the data sets that have been analysed during the course of this research and the detailed technical discussions on the current state of the art. I would also like to acknowledge Winnie and Stanley Herr for showing me the bright lights and warm hospitality of Houston during my stay in Texas.

I am indebted to all those in the department who have helped over my research period with ideas and computing related matters, especially Rahmi Celik, Chris Pinel, Paul Denys and Joel Barnes. Special thanks are also due to Noel Zinn of Western Atlas International for his valuable technical comments and suggestions and interest in this research.

Great appreciation is due to Commission of the European Communities, Athens Academy, Eugenides Foundation and Onassis Foundation for their generous financial support of research into streamer modelling at the University of Newcastle upon Tyne.

My thanks also go to all those at my home University in Athens for their support and advice, especially Ass. Prof. Demitris Paradissis for listening to my ideas and encouraging me to pursue such avenues.

Finally, thanks must go to my family, my parents Nicholas and Paraskevi, and my brothers Petros and Sotiris for their continued support and encouragement throughout my years in Newcastle.

LIST OF CONTENTS

LIST OF FIGURES

LIST OF TABLES

LIST OF ACRONYMS

2-D	Two dimensional
3-D	Three dimensional
AS	Anti spoofing
ASCII	American Standard Code for Information Interchange
B-method	Baarda method
BLUE	Best linear unbiased estimator
c-o	computed - observed
C/A	Coarse/Acquisition GPS signal
CDP	Common depth point
CEP	Circular error probable
CGG	Companie Generale du Geophysique
DGPS	Differential GPS
DIA	Detection Identification Adaptation (statistical testing procedure for geodetic networks)
DMO	Dip move-out
DoD	Department of Defense
drms	distance root mean square
EAGE	European Association of Geoscientists and Engineers
ED50	European datum 1950
ER	External reliability
GME	Geometric mean error
GOM	Global overall model
GPS	Global Positioning System
HF	High frequency
HGS	Halliburton's Geophysical Services
HMP	Horizontal mid-point
Hz	Hertz
INS	Integrated navigation system
IR	Internal reliability
JPO	Joint Program Office
KHz	Kilo Hertz
Km	kilometre
L1	GPS L-band signal 1 (1575.42 MHz)
L2	GPS L-band signal 2 (1227.6 MHz)

LBL	Long baseline (positioning method)
LOM	Local overall model
LOP	Line of position
LORAN	Long Range Navigation System
LS	Local slippage (test statistic)
LSM	Least square method
m	metre
MDE	Marginally detectable error
MHS	Maximum horizontal shift
MHz	Mega Hertz
NCL_NET	Newcastle Network
NMO	Normal move-out
NRP	Navigation reference point
NTUA	National Technical University of Athens
P-code	Precision code
PMRL	Post mission receiver location
PRN	Pseudorandom noise
QA	Quality assurance
QC	Quality control
QI	Quality improvement
QUEST	Quality Engineering and Survey Technology Ltd.
RGPS	target tracking GPS
SA	Selective Availability
SBL	Sort baseline (positioning method)
sd	standard deviation
SEG	Society of Exploration Geophysicists
SIPS	Seismic Integrated Positioning System
SSBL	Super sort baseline (positioning method)
t/b	tailbuoy
TQM	Total quality management
UHF	Ultra high frequency
UKOOA	United Kingdom Offshore Operation Association
UMPI	Uniformly most powerful invariant (test statistic)
USBL	Ultra sort baseline (positioning method)
WGS84	World Geodetic System 1984
Y-code	Encrypt P-code
ε_{rms}	root mean square error

INTRODUCTION

OVERVIEW

In order to explore the continental shelf seabed and the structures beneath it, seismic surveys are usually undertaken. These surveys involve large vessels towing seismic sources ('guns') and several long (possibly 6km) 'streamers', each carrying (possibly several hundred) hydrophones that sense the arrival of the reflected and refracted sound waves. By measuring their amplitudes and travel times it is possible to reconstruct an image of the sub-surface geology. The displays which result from seismic processing are used by oil companies to determine where to drill future exploration and production wells.

In order to do this analysis it is necessary to know the position of each gun and hydrophone for each measurement. Earlier systems leading just to two-dimensional profiling did not place great accuracy requirements on the hydrographic surveying positioning. During the time of 2-D seismic recording the navigation lines were widely spaced (possibly several kilometre) so that prospective hydrocarbon targets could be identified (to some extent) by correlated geological characteristics. For such an acquisition scheme the impact of marine positioning inaccuracies on the resolution of the processed seismic data in most cases is minimum.

Over the last decade the situation has dramatically changed. Geophysical and economic pressures have led to an increasing number of multiple line data collection techniques. Today, 3-D survey exploration is the rule. These surveys are carried out to provide imaging information for the subsurface (mainly dipping horizons) that cannot be obtained through 2-D processing, and therefore, to determine spatial relations in three dimensions, as opposed to determine components along separated survey lines in 2-D jobs. A detailed 'picture' of the reservoir, greater resolution and placement of geologic faults as well as greater structural delineation are the primary objectives of a 3-D seismic survey.

The attainment of this ultimate demand, for better sub-surface positioning accuracies, depends (among such other parameters as, binning without proper relocation corrections, application of NMO correction in the case of non-hyperbolic traveltime curves, constant velocity DMO processing without corrections, time migration in the presence of velocity variations, neglect of anisotropy, etc.) on the absolute and relative accuracy with which the surface elements (sources and receivers) are located. Hence the seismic industry, in order to meet this requirement for better surface positioning accuracies, has responded with increasingly complex marine seismic networks, in which the type and quantity of the survey data collected has expanded to more than thirty times the original amount for the first 2-D jobs. Moreover, in recent years the problem has become extremely complex since it has become increasingly common for clients to require proof, often in real time, that the survey 'quality' specifications are being met.

The processing algorithms currently used to solve the positioning problem proved inadequate to provide a general solution. This is because most of these algorithms treat each epoch, and each measuring system, more or less independently in a rather arbitrary way. Therefore, these systems are highly 'case dependent', i.e. relatively small changes to the configuration or measurement set-up may lead to major changes in the processing software. Secondly, and probably most importantly, it is extremely difficult to analyse the error propagation through such a process and therefore it is almost impossible to describe the precision and reliability of the final gun and hydrophone positions.

This research aims to develop and test new, completely general (for flexibility purposes), rigorous and integrated (for error propagation, and therefore QA/QC purposes) mathematical models for the determination of source and hydrophone positions within modern offshore exploration configurations.

The project has been undertaken in association with QC Tools, Inc., a consultancy company for the exploration industry. QC Tools contribution is limited to providing an almost infinite amount of real positioning data, existing software related to the project objectives and offers to hold detailed technical discussions on the current state of the art.

RESEARCH OBJECTIVES AND SCIENTIFIC RESULTS EXPECTED

The overall aim of the project has already been outlined, namely to develop a general, integrated and rigorous approach to the positioning and quality control in real time of marine seismic networks. In order to achieve this, emphasis has been placed on a number of objectives

- Determination of an optimum general mathematical description of the streamer shape by preliminary fitting of streamer models to compass data.
- Acquisition of a formal description of the geometry of the whole configuration by integrating all positioning data types into a single functional model.
- Computation of the real-time position and quality measures of any point deployed in a seismic network by adopting a Kalman (or other) filter as the basic stochastic process.
- Test the integrated model for appropriateness and for its sensitivity to detect and identify expected biases in the raw data by incorporating a uniform testing procedure.
- Assessment and testing of the correctness of the mathematics and the feasibility of the associated algorithms in terms of convergence, solubility and computational efficiency by preparing software for the various parts of the process and testing with real offshore data.
- Refinement of functional and stochastic models based on detailed analysis using alternative model hypotheses.

The results are tested mathematical models, in the form of computational algorithms, for the following

- The shape of the seismic streamers.
- The dynamics of 3D seismic configurations during data collection.
- The real-time positions and quality measures for offshore seismic surveys.
- The effect of the network geometry and the relative stochastic properties on seismic network positioning and quality control.

RESEARCH METHODOLOGY

The methodology adopted to verify the correctness of the mathematical models and the feasibility of the of the associated algorithms and software has involved

- The examination of time series of the filter solution, and the time series of the predicted and filtered positions and velocities of the various nodes involved in the seismic network.
- The assessment of innovation sequence (predicted residuals of the positioning data), namely mean values and standard deviations, and their covariance matrices. This helps in identifying trends and problems in the observation data, e.g. spikes, biases, missing and noisy observations.
- The implementation of independent checks in order to identify gross and systematic errors in the raw data. These tests are concerned with the comparison of identical quantities computed using completely different data.

Moreover, in summary, the methodology used to study the effect of the design parameters on the filter solution and the estimates derived from it, in an attempt to refine both observation and dynamic models, has included

- The testing of different streamer models.
- The implementation of alternative stochastic models for the observation and dynamic models.
- The evaluation of the effect of the measurement geometry by eliminating selected navigation sensors.

THESIS OUTLINE

For readers unaccustomed to the details of the acquisition and analysis phases of the navigation part of the seismic processing an overview and current state of the art is given in Chapter One. More specifically, the various methods and techniques of acquiring marine positioning data today are reviewed. The evolution of positioning in marine seismic networks, the details of positioning requirements and the need for quality assurance are also examined. Finally, a brief description of currently used methods for integrated processing of marine positioning data as well as the data types and instrumentation for positioning are given.

Chapter Two concentrates on the issue of streamer modelling. The first part of the chapter deals with the basic principles and limitations arising from an approach based on a hydrodynamic model. Also, the most well known numerical methods used to simulate the shape of the streamer are discussed and evaluated. In the second part of the chapter, a polynomial curve fitting model is described and tested with real data for use by the integrated positioning algorithm. To validate the selected method the results derived from this part of the analysis are compared with the results obtained from other curve fitting methods.

Chapters Three and Four describe the Kalman filter and the concepts of quality assurance and quality measures applied to offshore positioning. Chapter Three gives a brief review of the advantages of using a Kalman filter versus simple least squares in the offshore environment and introduces the Kalman filter models and algorithms. The Kalman filter principles and terms associated with it are also discussed. Particular emphasis is placed on the so-called Bayes filter, a slightly different form of the standard Kalman filter algorithms. Chapter Four concentrates on the Kalman filter quality measures, namely precision and reliability. A classification of measures of precision is given in the first half of the chapter. In the second half, the concept of statistical testing as a part of the quality assessment process is discussed. However, a more concise description of the B-method (a uniform testing procedure for bias identification) for use in dynamic systems is given in Appendix B. The concept of reliability, and the associated formulae used to compute it, are also discussed in detail.

An integrated algorithm for positioning offshore seismic networks is presented in Chapter Five. More specifically, a few remarks related to the whole idea of the proposed algorithm and the coordinate systems associated with it are given, followed by a review of the functional and stochastic models required to implement the method. Finally, the formulae that are used to locate the various elements of a seismic network and to compute their associated quality measures are discussed.

Chapter Six outlines the software which is written to test the algorithm presented in Chapter Five. The main features of the program, a functional overview as well as the various problems and improvement modifications related with it are presented in this chapter. An introductory design specification proposal developed to provide a general layout to initiate the mathematical processes of the proposed algorithm is given in Appendix D.

To test the performance of the integrated algorithm, the software has been used to process two sets of real offshore data and a number of the analyses of the results has been performed. These include those based on the statistics of the predicted residuals of the observations, the filter solution and independent checks. These analyses and checks are presented in Chapter Seven.

Chapter Eight describes the main trials that have been in place to study the effect of the functional and stochastic models on position and precision of a seismic spread. These include examination of alternative streamer models, geometry configurations and stochastic models for the observation and dynamic models. The overall aim of this chapter is to refine both functional and stochastic models as well as to touch on the question of the design of new systems.

Chapter Nine describes all the reliability trials and results (in the form of marginally detectable errors in the observations and horizontal shift on the network positions) obtained during the analysis. Particular attention is paid to the effect of the geometry configuration and observation distribution and redundancy.

Finally, a summary of the conclusions and suggestions for further research are given in Chapter Ten.

CHAPTER ONE

ACQUISITION AND POSITIONING 3D MARINE SEISMIC SURVEYS - AN OVERVIEW

1.1 INTRODUCTION

Exploration seismology is a geophysical method in which the aim is to reconstruct as detailed as possible an image of the sub-surface geology. The product of a seismic survey over an exploration area is a geological model that can be evaluated for the presence of hydrocarbons. The evaluation process includes interpretation steps in terms of geological structure, lithological variation, stratigraphy, and hydrocarbon prospectivity (McQuillin et al, 1984; Berg and Woolverton, 1985; Kerr, 1982).

The implementation of the seismic method for hydrocarbon prospecting involves three basic steps

1. Data acquisition.
2. Data processing.
3. Display of the processed data.

In the present chapter the details of the acquisition and analysis phases of the navigation part of the seismic processing are discussed. For the phases of the processing and display of the processed data is simply mentioned that these are meant to eliminate the seismic signal of noise, refractions and multiple events, to enhance resolution, to combine redundant observations and image the events in space. Display of the processed data concerns with the visualization of the seismic attributes in order to be used for geological interpretation (Rayson, 1996).

1.2 ACQUISITION OF MARINE SEISMIC AND NAVIGATION DATA

1.2.1 General

The process of data acquisition during marine seismic exploration can be summarized as follows

1. Generation of a pulse of sound (disturbance) which meets as near as possible pre-defined requirements of total energy, duration, frequency content, maximum amplitude and phase (McQuillin et al, 1984).
2. Recording the wavefield (reflected and refracted) as a function of time and space.
3. Observation of the position of the vessel(s), sources, hydrophones and horizontal mid-points (HMP is the average of the positions of a gun target and a receiver) and their quality measures (Figure 1.1).
4. Real-time onboard control to ensure the required areal coverage.

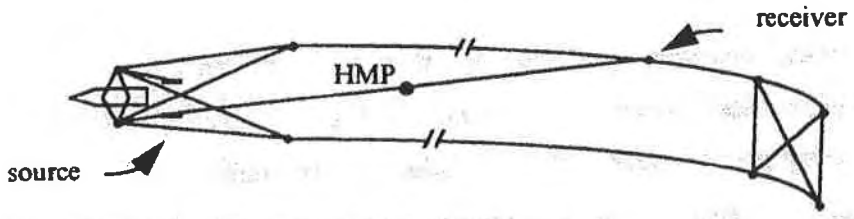

Figure 1.1 Horizontal Midpoint Position (HMP)

This study concentrates on the third step of the process, namely on the surveying problem of seismic data acquisition. The need for accurate and reliable positioning of the marine seismic networks is mainly a result of the demand for better resolution of the subsea geological image. During 2-D seismic acquisition the navigation lines are widely spaced (possibly several kilometre) so that prospective hydrocarbon targets may be identified by correlated geological characteristics (Northon et al, 1990). Alternatively, 3-D recording is the method to provide imaging information for the subsurface (mainly dipping horizons) that cannot be obtained through 2-D processing, i.e. to determine spatial relations in three dimensions, as opposed to determine components along separated survey lines in 2-D jobs (Figure 1.2).

Morgan, (1983) and (1992) states that the primary objectives of a 3-D seismic survey are

1. to provide a detailed 'picture' of the reservoir.
2. to provide greater resolution and placement of geologic faults, and
3. to provide greater structural delineation.

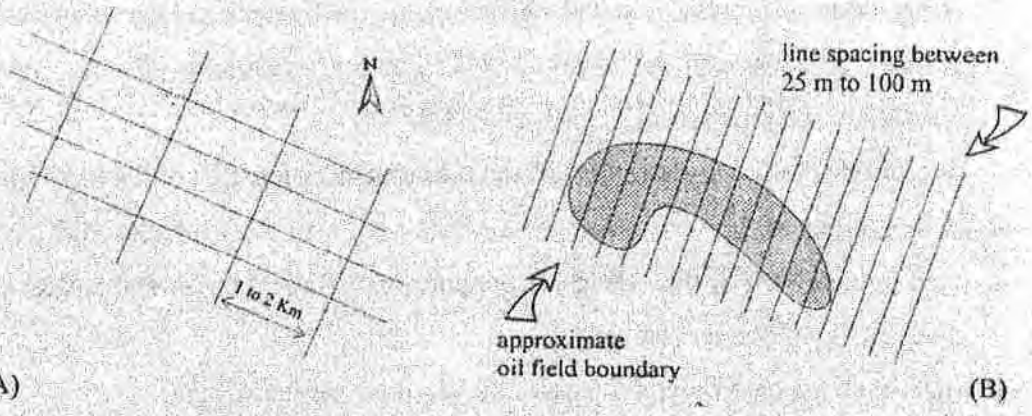

Figure 1.2 2D conventional seismic grid (A), and 3D seismic grid (B)

When these objectives are satisfied, then the 3-D method helps significantly to determine optimum locations for drilling wells, and to quantify estimates of oil and gas reserves in the reservoirs. Use of advanced technology and collaborative survey management during the acquisition phase of the seismic process places an important role in achieving optimum high-quality and cost-effective results.

1.2.2 Acquisition Methods

1.2.2.1 Towed Streamer Technique

The basic configuration of an offshore seismic exploration survey during data acquisition is as follows. One or more vessels (Figure 1.3) sail in approximately straight lines whilst towing a number of 'streamers' (often 3-6 kilometre long) and 'seismic sources'. The streamers carry a number of hydrophones (typically 50-100 per kilometre) and are towed just bellow the surface of the water (Morgan, 1992; Naylor, 1990; van Zeelst, 1991) - see Figure 1.4. At specified distance interval (typically every

20-25 metre) one of the guns is fired resulting in seismic waves which travel through the water and penetrate the subsurface (Figure 1.5). The times of arrival of reflected and/or refracted signals are then measured by the hydrophones. The surveying problem is to determine the position of the guns and hydrophones, and their associated quality measures, at the instants of firing and reception respectively.

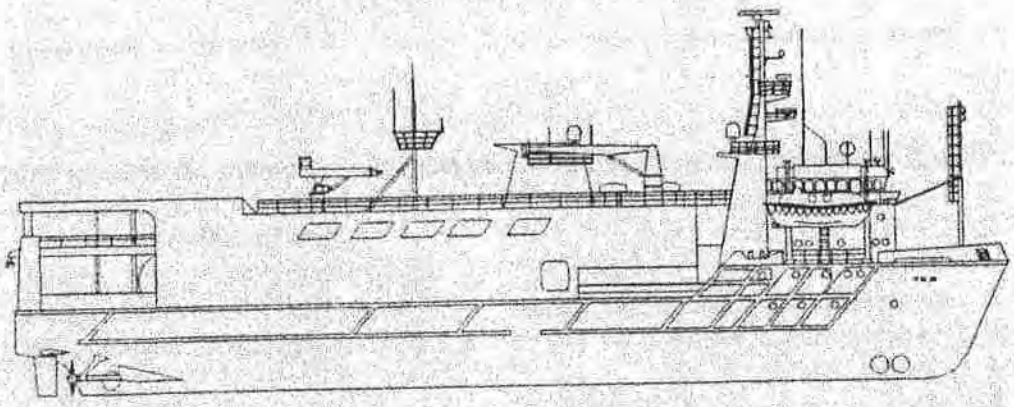

Figure 1.3 Marine seismic vessel, RV Sea Star (HGS fleet, 1993)

The first seismic surveys offshore date back to the early seventies in which simple 2-D jobs were conducted using configurations consisted of one vessel, one energy source and one streamer. Since then, in order to address the needs for higher resolution, increased efficiency and faster acquisition and processing, driven by the geophysical requirements of the implementation of the 3-D method, more complicated geometries are increasingly used. A dual-vessel, quad-source, quad-streamer configuration ('Quad/Quad' technique) was first used in 1988 by GECO-PRAKLA recording 16 Common Depth Point (CDP) lines per survey line increasing significantly coverage and efficiency of the 3-D method (Naylor, 1990). To increase productivity, obtain improved results, reduce turnaround time and achieve lower costs per subsurface kilometre the same seismic contractor was the first company to conduct 6 and 8-streamer dual source surveys (Schlumberger Geco-Prakla, 1996). Also, larger vessels have entered the arena allowing the use of bigger and more complicated seismic networks. For instance, PGS Exploration boats are capable of towing 12 or 16 streamers (PGS Exploration, 1996). WESTERN ATLAS vessels recently set a record with 7600-metre streamers and plan to tow even longer streamers for suitable prospects (Western Atlas International, 1996).

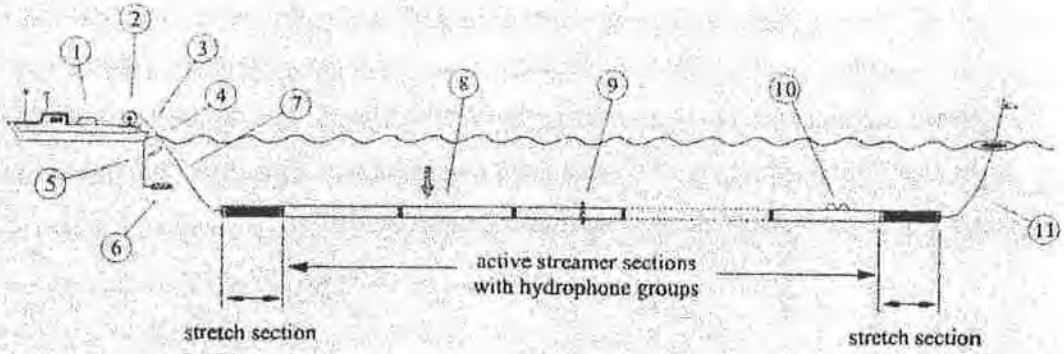

Figure 1.4 Marine streamer system and related acoustic sources of streamer noise:
1. Shipborne noise (machine and other)
2. Cable reel on stern of ship
3. Jerks of tow cable by pitch and roll
4. Interaction tow cable surface waves
5. Propeller and propulsion
6. Airgun
7. Vibrations of tow cable in water
8. Transmission of surface water
9. Vibrations and turbulence by depth controllers
10. Flow noise (interaction streamer - water)
11. Induced noise by the tailbuoy

The typical network configuration during seismic acquisition outlined above. However, alternative geometry configurations and shooting strategies have been introduced for use under specific circumstances. For instance, the presence of production platforms make closely spaced 3-D deep water marine acquisition difficult. In such cases it is necessary to implement different network geometries. These may include a receiver boat and a source boat (with or without 'mini-streamer') sailing beside, or inline, on either side of the hazard (Duncan and Nelson, 1989). Several typical shooting configurations are shown in Figure 1.6.

Another important factor related to the design of the acquisition surveys of seismic data is the shooting direction, or the so-called 'question of azimuths'. The shooting direction affects dramatically the quality of the imaged data and particularly the regularity of offset sampling mainly for DMO (Dip-Moveout, correction for the reflection-point smear that results when reflectors dip), and for velocity determination (Lansley, 1995).

Also, obstructing constructions, ships, strong currents, as well as cost are factors to bear in mind when selecting the orientation of a 3-D marine seismic survey. However, each survey is unique so the relative importance of these factors needs to be examined on a project by project basis (Egan and Kupoor, 1990). For instance, alternative geometry consisting of concentric circles (instead of parallel lines) has been introduced in a project which lends itself to image salt domes (Durrani, 1987).

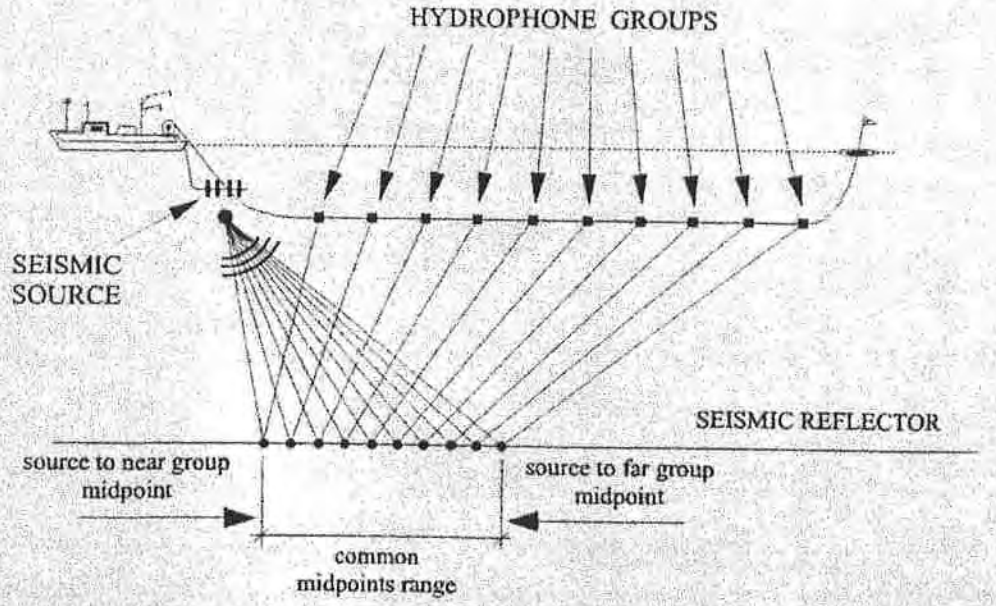

Figure 1.5 Marine seismic acquisition

1.2.2.2 Ocean Bottom Cable Technique (Transition Zone)

The ocean bottom cable technique is a relatively new acquisition method of deploying receivers on a cable which is led on the seabed. The method is particularly effective not only in shallow transitional congested or obstructed areas but also in harsh sea states that would shut down a streamer crew. Moreover, since the receivers are stationary on the sea bottom the method offers high quality seismic data for surveys around obstructions such as oil platforms (Rayson, 1996).

In 3-D bottom cable seismic operations the recording vessel deploys on the ocean bottom (in water depths ranging from the very shallow to 150 metre) one or more

cables (typically 15-20 kilometre long). When the cables are deployed the recording vessel anchors, connects to the cables and checks the electrical integrity of cables and sensor groups. Shooting is undertaken by another vessel (shooting vessel), which tows only the seismic source array, that shoots a swath of lines parallel to the bottom cables. After the swath is covered the cable is laid out and redeployed for the next swath until a 3-D seismic survey is complete (Barr et al, 1990). The geometry of a typical acquisition spread is illustrated in Figure 1.7.

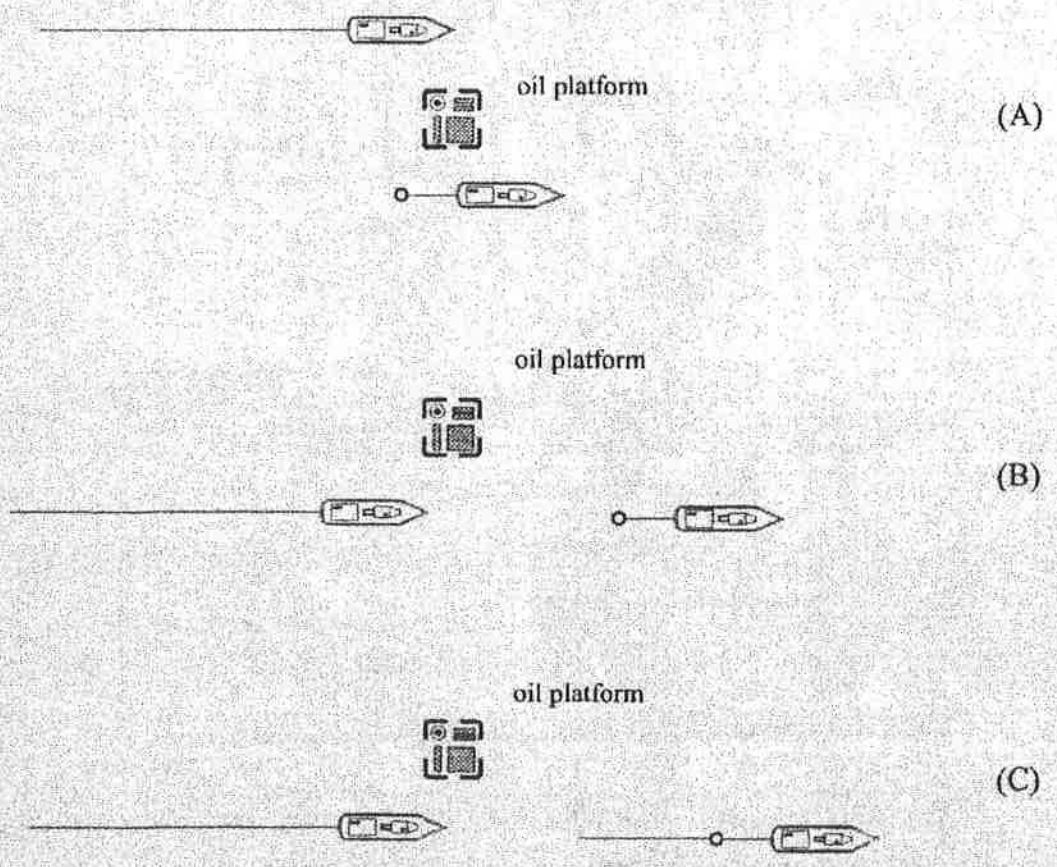

Figure 1.6 Common used shooting configurations near production platforms

1.2.2.3 Vertical Cable

This is an alternative method of exploration mainly used in like sub-salt reservoirs. During vertical cable seismic operations a group of receivers are deployed vertically on a cable which is kept under tension by an anchor at the bottom and syntactic foam buoys

at the sea surface. Krail, (1993) states that, in 1989 such an experiment was conducted offshore Louisiana in 550 metre of water which has shown that high quality seismic results can be acquired with a vertical cable.

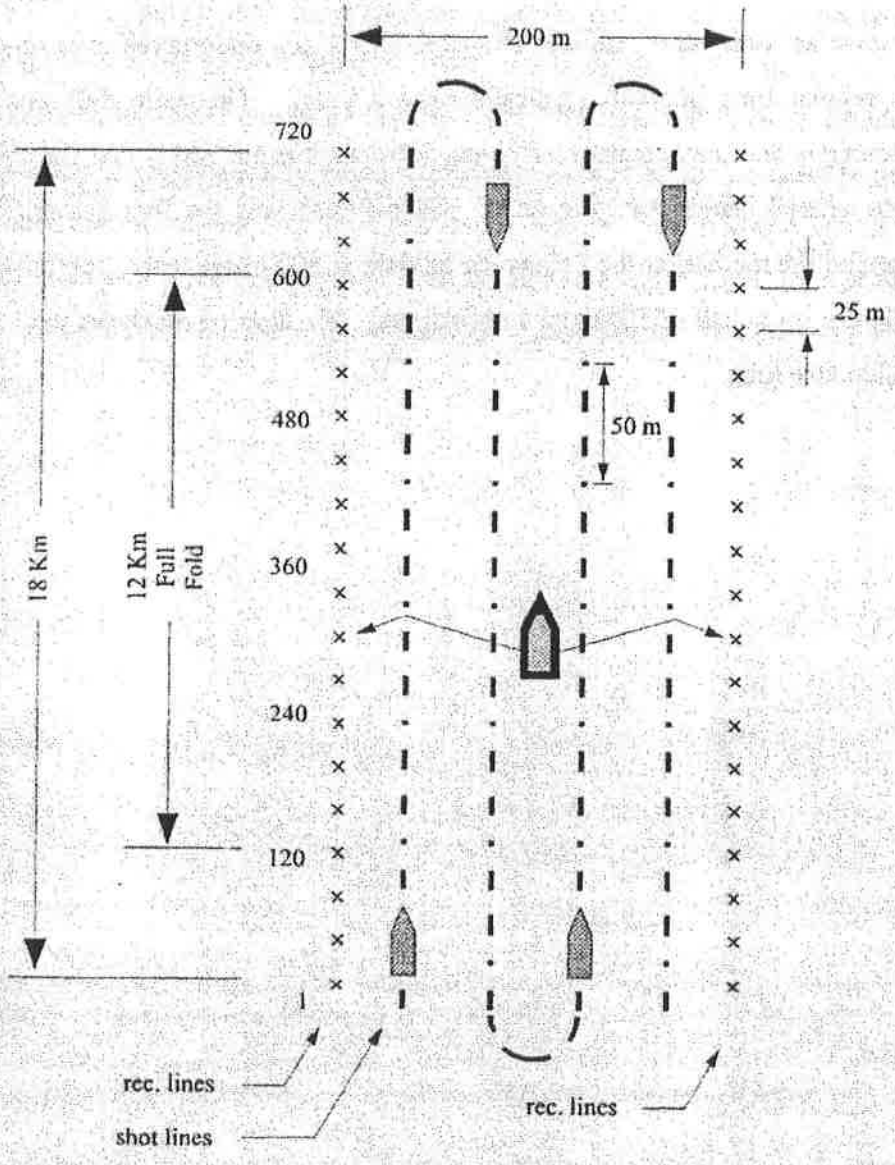

Figure 1.7 Ocean bottom cable shooting configuration. 3D H-spread technique (Syntron, Inc.)

Record 240 channels x 2 lines
25 metre receiver spacing
50 metre shot spacing
50 metre shotline spacing

Approx. 8 hours shooting
2.4 square kilometre
120 fold/12.5 metre x 25 metre cells

1.2.2.4 Buried Cable (4D Seismic Recording)

Buried cable surveys have recently deployed as a reservoir monitoring acquisition scheme in order to study the reservoir characteristics (oil migration) as these change with time. In order to study these changes usually a number of seismic surveys, also known as 'time lapse' surveys (Rayson, 1996), are undertaken over an area of interest at regular time intervals (typically once a year). The main difference between this technique and the conventional ocean bottom cable method is that the cable is ploughed into seabed instead of lying on it. Geco-Prakla was the first seismic contractor that applied the method at the Foinhaven oil field at 500 metre water depth, west of Shetland Islands, on behalf of BP Expo International. Six lines of receivers were used, each 5-6 Kilometre long.

1.3 THE EVOLUTION OF POSITIONING IN MARINE SEISMIC NETWORKS

The implementation of the 3-D seismic method, to better define complex producing reservoirs, has led the seismic industry to find ways of improving the positioning methods offshore. Over the last couple of decades the oil community has seen an enormous increase of the type and quantity of the survey data collected and increasingly complicate acquisition configurations. The development of positioning methods can be categorized into three main periods (Canter et al, 1989)

1. Fixed offset period.
2. Vessel relative and semi-integrated positioning network period.
3. Integrated positioning network period.

A brief review of evolution and the road ahead of these systems is given in the following sections.

1.3.1 Fixed Offset Period

On the first 2-D seismic surveys simplicity was a demand due to the technology which was available during this time. These surveys were recorded with only vessel positioning. The vessel navigation reference point was located with an estimated accuracy 3 to 5 metre by means of radio positioning (Canter et al, 1989; Morgan, 1986). Nominal offset values from the tow point to source nodes and head of the streamers were used to locate these points. Usually, the vessel gyro (typically estimated to an accuracy level of one degree) was used to stepback to the towpoint. Also, the first compass on the streamer was used to provide overall azimuth control for the head point of the cable. When twin streamer surveys were conducted in order to increase confidence, acoustic equipment was used to measure cable separation and skew. Finally, in order to minimize the effect of feathering (drift of the streamer at an angle to the planed seismic line due to cross-currents) 'active' tailbuoys (radio positioning system is included in the taibuoy) were increasingly used. Usually, this was done by rotating the compass data so that the misclosure between radio positioning and compass

derived position at the end was minimized. Nevertheless, the differences found using tailbuoy position could not be isolated into compass, magnetic declination corrections, or corrections on the tailbuoy positions. The typical bin size during the mid-seventies was 100-200 metre cross-line and 50 metre in-line (Chevron Training Course, 1992).

1.3.2 Vessel Relative and Semi-Integrated Positioning Network Period

The emphasis on front-end positioning led to the vessel relative period which utilized positioning sensors on the vessel to improve the quality of the position of the gun arrays and the front-end of the streamers. Sort and ultra sort baseline acoustic transducers (Kelland, 1994) were mounted on the vessel's hull while acoustic receivers were placed on the source nodes and the cable heads (Court, 1991). Although the method allows a good fix geometry from the vessel to the sensors deployed on the cables and guns it suffers of a number of problems. Canter et al (1989), and Tiong Ha (1990) state that the hull mounted transducer must operate efficiently through the wake of the vessel, the propeller wash, and the bubbles from the airgun firing, and therefore, the raw data requires heavy filtering unless careful attention in installation and operation is performed. Also bottom and surface reflections occur and interfere with the original signal if the signal exceeds certain length in time.

To improve front-end positioning in addition to acoustic systems laser systems were increasingly used to measure the travel time from the vessel to surface reflector targets located on the sources, the front of the streamers, or on auxiliary floating structures. Moreover, the use of radio positioning systems to locate the vessel Navigation Reference Point (NRP) and the tail/head buoys became a rule. In more recent configurations DGPS systems were also used in relation with radio navigation systems.

The most common approach applied to the positioning problem (still widely used) was to treat each epoch, and each measuring system, more or less independently. So both the laser and acoustic measurements were used to transfer the position of the vessel to the floats, while the front-end acoustics related the floats to the guns and front-end of the streamer, and then the compasses determined the streamers shape. The rear-end

acoustics and the tailbuoy positioning served to provide some control of the orientation and stretch of the streamers. Typically the process would involve some sort of curve fitting operation for the compasses, e.g. as in Ridyard (1989), and several independent 'network adjustments' for the acoustic and laser networks. It is possible that the process would involve 'iterating' several times through the various data types in order to 'best fit' (in some rather general sense) all of the measurements.

Alternative semi-integrated methods that suggest integrated processing of acoustics and compass azimuths have also been developed and implemented (Court, 1990; Court, 1993). Moreover, direct comparisons of tailbuoy positions derived using different positioning systems (Stingant, 1989) have been used to ensure the positioning of seismic networks offshore. Similarly, for the same purpose especially designed experiments involving comparisons of the streamer position derived using conventional positioning systems deployed on the seismic spread, and those derived using long baseline tracking arrays located in deep water have been conducted (Cotton et al, 1985).

1.3.3 Integrated Positioning Network Period

As stated earlier in this section both the frequency and complexity of marine 3-D seismic surveys have increased dramatically over the last decade. Nowadays, in a typical configuration (Figure 1.8) measurements will include compass orientations at points along the streamer (typically 4-7 per kilometre), laser ranges from the vessel to a variety of floats (for instance those carrying the guns and those at the front of the streamer), underwater acoustic measurements (of the distance) between a number of points at the front and back of the system (referred to as the 'front-end' and 'rear-end' acoustic networks), the position of the tailbuoy and the position of the vessel (both typically, but not necessarily, by DGPS). More complicated systems may also include acoustics throughout the length of the streamer and additional navigation devices on the vessel. It is also possible in order to improve the triangulation geometry in the front-end network to include towfish structures, with a mounted transpoder on them, suspended from cantilever arms (which when lowered extend typically 10 metre from the sides of

the boat) built at each side of the vessel (Court, 1990). Moreover, in the case of several vessels operating simultaneously, between vessel measurements would also be made.

The processing algorithms currently used to solve the positioning problem, discussed earlier in this section, proved inadequate to provide an integrated and rigorous approach. Although these methods are probably perfectly satisfactory from an accuracy point of view they suffer from two major disadvantages. Firstly they are highly 'case dependent', i.e. relatively small changes to the configuration or measurement set may lead to major changes in the processing software - something that is especially difficult in real-time (or quasi real-time) quality control. Secondly, and probably most importantly, it is extremely difficult to analyze the error propagation through such a process - hence it is almost impossible to describe the precision and reliability of the final gun and hydrophone positions. This aspect is becoming increasingly important as clients require proof (often in real time) that the survey specifications are being met.

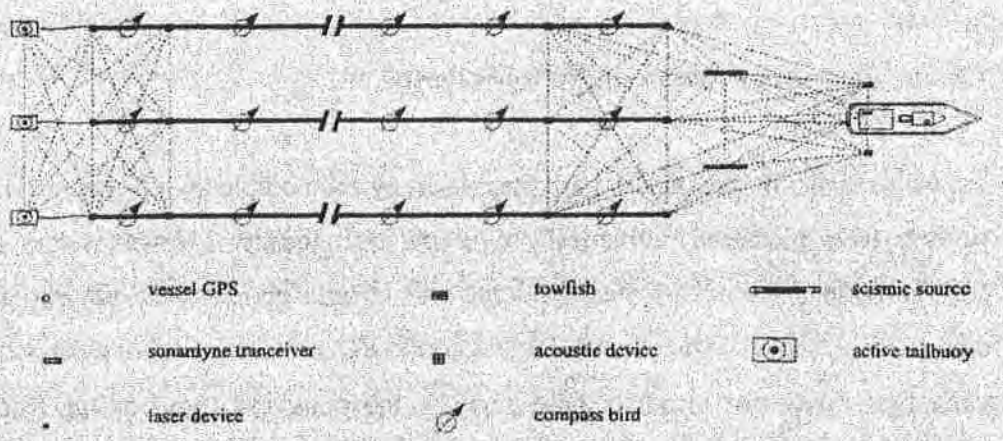

Figure 1.8 One vessel, dual source, triple streamer survey configuration

These vital questions have driven the seismic industry gradually to develop and implement integrated and rigorous (in a mathematical manner) positioning systems. These systems should, in principle, be flexible enough to describe the geometry of any likely practical set-up, handle any set of observations, and provide the position and associated quality measures of any point of interest throughout the spread. Kalman filtering is the most well known stochastic process that can be used to exploit the

potential of the dynamic environment in which they operate. The various advantages of the use of integrated networks are clearly stated by Zinn and Rapatz, (1995), while the specific advantages of Kalman filtering over simple 'epoch by epoch' least squares may be found in Section 3.1.2 in this study.

1.3.4 Ocean Bottom Cable Positioning Methods

During bottom cable operations the problem of locating accurately the receiver groups is not as big an issue as it is for the surface streamer since the receivers remain stationary during shooting. However, as the cable sinks it, and consequently the receivers, drift from the navigation line owing to currents and to a lesser extent the method of deployment (Rigsby et al, 1987). Currently receiver location systems use a single-point high-frequency acoustic source transmitter on the shooting vessel and special acoustic receivers at the centre of each receiver group. Using the transmitter location, relatively to the vessel navigation reference point location, at different times as 'base stations', and the time picks from the acoustic receivers as ranges the receiver position is estimated by a simple least square computation (Chevron Training Course, 1992).

An alternative of estimating the positions of the bottom cable receivers, known as PMRL (Post Mission Receiver Location) technique, uses the first arrival times of two near seismic traces from two near shooting lines, the shot (seismic source) coordinates and water and near-surface velocities (Rigsby et all, 1987).

1.4 POSITIONING AND QUALITY ASSURANCE REQUIREMENTS

1.4.1 Positioning Requirements

Absolute positioning and repeatability of positioning are important for drilling operations. Morgan, (1983) states that the grid of reflection points must be known (with respect to shore) with an accuracy of 30 metre. Also, positions should be able to be relocated to within 10 metre. What is, however, of interest in this study is the relative positioning requirements within a seismic spread.

To reach a set of positioning specifications for the various elements involved in a 3-D seismic survey (namely, the vessel, source nodes and receiver groups), it is necessary to consider of the positioning requirements that relate directly to the geophysical needs. During 3-D seismic acquisition the survey vessel steers along parallel lines separated by tens of metre spread across the prospect area. The acquired seismic data are sorted among bins according to midpoint locations for unmigrated data, or according to reflecting points for migrated data (Sheriff, 1994). The size of bins, which are in the form of a horizontal grid, is usually defined by the spacing of the seismic lines (cross-track direction), and the spacing of the hydrophone groups interval (along-track direction). Currently, typical bin dimensions are 12.5 metre along-track and 25 metre cross-track (Morgan, 1992). In seismic processing reflection points which fall within a bin are 'stacked' together to obtain the output trace for this bin. Morgan, (1992) states that, the seismic acquisition and processing technology currently dictates an accuracy level for the reflection points of about 25% of the bin length and width. Thus, for a 12.5 metre by 25 metre bin the relative accuracy of the reflection points is specified 3 metre in-line, and 6.25 metre cross-track. In order to meet this subsurface reflection point position requirements (see Figure 1.5 and Morgan, (1983)) the maximum error in the position allowed at the sea surface for the source and receiver points is up to twice the error allowed for the subsurface bin, i.e. for a bin of size 12.5 metre by 25 metre this maximum error is estimated 6 metre in-line and 12.5 metre cross-line. The main assumption to reach this conclusion is, however, a flat seismic reflector and no variations in elevation between source and receiver points. It is important to stress that

the effect of the navigation errors on the seismic quality is a major issue and one that is not examined in detail in this study. Interested readers are recommended to study Hampson and Jakubowicz (1990), Homman and Ogtrop (1993), Levin (1983), Levin (1984), Levin (1996) and Paffenholz, Monk and Fryar (1993).

It is rather common today, for seismic operators to specify acceptable seismic navigation results in terms of bin size and HMP precision (Zinn and Rapatz, 1995). For this purpose, source and receiver errors can be easily propagated to estimate HMP precision. Zinn, (1991) demonstrates that the HMP in-line and cross-line errors are at most the average of the in-line and cross-line errors of the source and hydrophone points and can be as little as zero.

Nevertheless, assessment of the quality of positioning a seismic spread offshore is not confined only in the computation of precision measures. Reliability measures are increasingly used to assess the ease with which biases (gross measurement errors in the navigation data) may be detected (internal reliability) and the impact of undetected biases on the source and receiver positions, and finally HMP (external reliability). Today, it is not rare for clients to require maximum external reliability values of 8-10 metre (Zinn, 1996).

Both precision and reliability measures are concerned with the concept of quality control and quality assurance (QC/QA) of positioning the role of which is essential to the success of a 3-D seismic survey. This issue is briefly discussed in the following section.

1.4.2 Quality Assurance Requirements

The concept of quality assurance (QA) often is constrained to the narrow traditional meaning of finding and implementing 'better' ways, means or techniques to solve a problem. The meaning of QA is expanded, however, to a more general definition. Martens and Riemersma, (1986) define it as 'all those planned or systematic actions necessary to provide confidence that a product or service will satisfy defined needs', and Ridyard, (1993) as a 'conformance to requirements'. QA should be treated,

therefore, as an integrated procedure that incorporates all the operational techniques of quality planning and quality control of a system.

Jensen and Nicolai, (1990) extend the concept of QA one step further. The integration of QA and quality improvement programmes (QI) (the positive feedback in the system) leads to a methodology known as total quality management (TQM) - see Figure 1.9. The various stages of such a proposed scheme of total quality management for positioning a marine seismic survey are detailed by Jensen, (1988) and Jensen and Nicolai, (1990). The main points of the procedure for the different phases of the process are reproduced here

1. Project requirements
   - These include establishment of the scope of the work to be conducted, and of the client/project requirements, including parameters as maximum error ellipse semi-major axis value, significance level of the test and power of the test (for reliability computations).

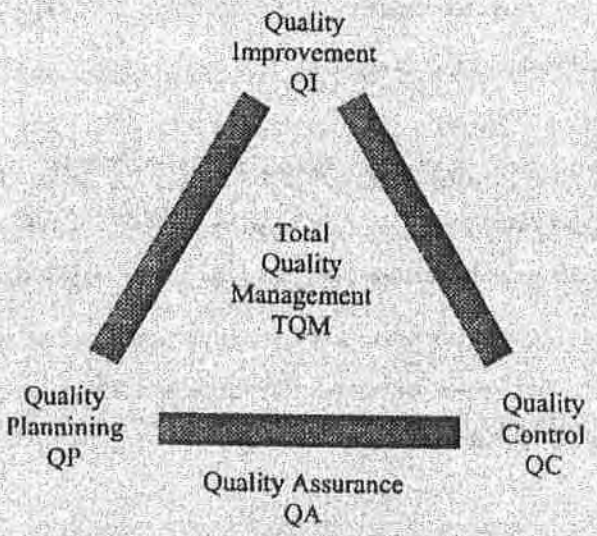

Figure 1.9 Quality management policy scheme for positioning marine seismic surveys

2. Survey design
   - Formulate a design for the proposed positioning network including sufficient redundant observations.

- Define the a priori covariance matrix for the observations based on previous experience.
- Compute relative and absolute precision, and internal and external reliability of the network. Compare these with the project requirements and establish tolerances for internal reliability to be used through the operational QC stage.

3. Operational QC
   - Quality control and safety supervision of on-line positioning data acquisition including progress control and coordination of operations.
   - Compute predicted residuals for all observations and measures of precision and reliability (using the B-method) for all points of interest involved in the network.
   - For any large set of data (possibly per seismic line) examine for biases due to various common causes (combination of outliers, station coordinates, etc.), if required.
   - Produce a time series plots of the observation statistics (predicted residuals and their variances), and of the quality measures (precision and reliability) describing the network, showing the percentage over the marginal values established in the project requirements stage.
4. Post-processing QC
   - Post-(mission) processing of the raw data involves further QC either to detect and identify biases and finally adapt the system, or to improve on the real time results. Although today post-processing is a common practice it remains possible in some cases to avoid this step. In fact, in post processing most of the QC steps taken in real-time are repeated (Houtenbos, 1989). To do this it is not, however, only the additional time and personnel required but also massive storage is required to log all different types of the raw data. The challenge today is that no post-processing should be required in most cases (Jensen, 1992).
5. Feedback
   - Provide the proposed revisions for the survey design, operational QC and specifications.

The procedure outlined above in a way that is constrained exclusively to the positioning problem of 3-D seismic surveys. It is, however, important to understand that the

navigation problem is an integral part of the seismic acquisition process. The big challenge during acquisition is to ensure that the seismic data collected during the survey is correct and complete (there is no excessive coverage, or 'holes', or lack of coverage in some parts of the prospect) before the seismic vessel has left the area.

To address this need a TQM system should integrate the navigation and binning (a means of determining areal coverage and collating data for seismic processing) processes of the seismic acquisition in real-time (CENSUS User's Guide, 1994; Hume et al, 1994; Nash and Ridyard, 1987; Ridyard, 1993; Stigant, 1993).

1.5 EXCHANGE FORMATS AND INTEGRATED PROCESSING OF POSITIONING DATA

1.5.1 Types of Positioning Data and Standard Exchange Formats

Prior to seismic data analysis and interpretation the seismic method involves the implementation of three basic steps, namely the actual acquisition activity, the position computation and the binning computation. These processes require the use of three types of data. These include

1. Raw observation positioning data.
2. Processed source and receiver positioning data.
3. Binned data, i.e. positioning data sorted among bins according to midpoint location.

There are many formats are that used for transfering positioning data between companies involved in seismic exploration. These are mainly concerned with the standard exchange of field survey positioning observational data and post-plot shotpoint locations. In the following sections a brief description of the most common used formats among the exploration industry are given.

1.5.1.1 Exchange Formats for Raw Marine Positioning Data

This type of exchange formats is concerned with the exchange of field-acquired marine positioning data. These can be generally classified in three categories. Those developed by

1. Individual seismic contractors, mainly for their own use.
2. The Society of Exploration Geophysicists (SEG) - SEG P2 (1983).
3. The United Kingdom Offshore Operators Association (UKOOA) - UKOOA P2/86, UKOOA P2/91 and UKOOA P2/94.

Today, the UKOOA format is accepted worldwide by the offshore community as the standard exchange format. The most recent versions (P2/91 and P2/94) have been designed to best cover the requirements arising from complex survey configurations in

terms of completeness and readability. Completeness means that no need is required to refer to external supporting documents to describe all relevant raw positioning data. Readable refers to a sufficiently structured format that allows some degree of visual interpretation and inspection by the user. Some of the most important points of P2/91 and P2/94 versions (which are extension of P2/86) are (UKOOA_SPC, 1986 and 1994; Nicolai, 1992; Celik, 1996)

1. All information is stored in records of 80 bytes (as in previous versions) 'card image', the columns of which are numbered 1 through 80.
2. Four main types of records have been defined
   - *Survey header records* - H. These records provide information such as, survey definition, definition of the geodetic datums and shifts, definition related to vessel(s), guns, streamers etc.
   - *Comment records* - C. This type of records does not appear in previous versions. It provides comments valid for the whole project, for a whole line or just for an event.
   - *Event records* - E (implicit time reference). Under 'E' records is stored all raw positioning data information.
   - *Inter-event records* - T (explicit time reference). This is also a new type of record that allows to record time information for each observation recorded.
3. P2/91 and P2/94 require one file per seismic line, meaning that a new set of header records are required for every line.
4. Quality information about the observations is allowed to be recorded. A priori (or expected), and actual (or measured) quality information is allowed for network observations and only actual quality information for non-network observations.
5. P2/91 and P2/94 allow time to be recorded with any observation, i.e. observations do not refer to shotpoint time.

1.5.1.2 Exchange Formats for Processed Marine Positioning Data

Similar to exchange formats for raw marine positioning data, the UKOOA exchange format for processed data has been almost universally accepted among the seismic industry. P1/84 format was defined by UKOOA for the exchange of processed source

and receiver coordinates. P1/90 is a revised version of P1/84 which expanded to cover issues such as multi-source, multi-streamer acquisition. Four types of records have been defined (CENSUS User's Guide, 1994)

1. *Header records* - This type of records holds similar information as the header files of UKOOA P2 formats.
2. *Point position records* - These records are used to identify the point being positioned. The most common are, source fired (S), vessel (V, P1/90 only), and tailbuoy (T, P1/90 only). The source records contain also information such as line number, shotpoint number, date/time and water depth.
3. *Receiver records* - Receiver records contain information such as receiver ID flag, receiver position (easting and northing), and cable depth.
4. *Relation records* - This type of records is an extension to the format and is used to prevent the pointless repetition of unchangeable information for different shots.

In addition to the UKOOA format other exchange data formats have been developed such as, SEG P1 (1983) as well as industry standard formats such as, the Shell's SPS format, the Advance Geophysical's ProMAX database format and the Green Mountain's MESA format.

1.5.2 Geophysical Contractors' Navigation and Binning Systems

It is a general conclusion from the discussion so far that the trend seems to be a movement of the seismic industry towards faster multi-tasking integrated software and central processing units (UNIX based workstations). Almost all major geophysical contractors/companies have developed (and continuously improve) their own navigation and binning/processing systems to meet this demand. The main characteristics of these systems are outlined bellow

1. During acquisition usually some of the data are synchronized with shot time (as compass azimuths and network acoustics), and some are recorded at the sensor time (Syledis, GPS, RGPS).
2. Storage at the UKOOA P2/91/94 formats and real-time graphic display of acquisition is a common practice.

3. Some systems, as GIN 2000 developed by CGG, compute source and receiver positions based on least squares algorithms for the various networks of the spread (vessel-buoy, relative head and relative tail networks as well as streamer shape). Other systems, as TotalNet, developed by WESTERN ATLAS, implement integrated network solutions by means of a Kalman filter.
4. Quality control, including monitoring of the quality of the recorded data (setup, configuration, spread geometry, data integrity, and statistical analysis) is an essential feature in today's systems.
5. On-board binning systems provide real time monitoring of CMP distribution throughout a 3-D survey. Also, most binning systems' capabilities include, flex binning, editing and rebinning algorithms.

In Table 1.1 a list of the navigation and binning systems of some major geophysical contractors is given.

Contractor	Navigation System	Binning / Processing System
WESTERN	WISDOM II	FLEX QC / CNAVCHK
GECO / PRAKLA	TRINAV	TRINAV / QC
CGG	GIN 2000	GIN 2000
DIGICON	MAGNAVOX 200 / SCOPE III	BIRDOG

Table 1.1 Contractors' navigation and binning/processing systems

1.6 POSITIONING DATA TYPES AND SYSTEMS

To locate accurately a complex marine seismic network today typically a total of more than 250 observations, of several data types, is required to be collected per time event (Western Atlas International, 1994b). These data types include (Houtenbos, 1989; Nicolai, 1992; Zinn and Rapatz 1993)

1. Ranges from the vessel and floating auxiliary stations to shore stations and/or seabed acoustic targets.
2. Range differences from the vessel and floating auxiliary stations to shore master and slave stations.
3. Pseudo-ranges and carrier wave phase from satellites to vessel or floating auxiliary stations.
4. Bearings from vessel to shore and seabed acoustic targets.
5. Acoustic ranges between the pingers and receivers fixed on the vessel hull, and ranges between the vessel and the guns and front-end streamer receivers. Also, acoustic ranges at the front-end, rear-end and middle of the cables, and between vessels.
6. Laser ranges and directions, over the water, between the vessel and various prisms mounted on the gun tube buoys, paravanes or navigation buoys.
7. Angles and distances from the vessel to tailbuoys.
8. Gyrocompass measurements on the vessel.
9. Compass bearings along streamers.
10. Depth of streamer sensors.

In the following sections a brief description of the various types of the positioning systems used by the seismic industry to acquire the observations outlined above is given.

1.6.1 Acoustic Systems

Today, acoustic systems play an important role in accurately and reliable positioning of seismic spreads offshore. These systems usually consist of devices such as acoustic pingers, responders, hydrophones, tranceivers, or transducers fixed on the hull of a

vessel, on mobile targets and seabed positions. The transmission type is a sound wave (typically 10-1000 KHz) and the measured quantity is the one-way travel time between the source of the signal and the receiver. The basic formula that is used to obtain a range D from an acoustic signal is (Chevron Training Course, 1992)

$$D = v\left(t' - t_d \pm e\right) = vt \qquad 1.1$$

where

D	: is the distance parallel by the sound pulse
v	: is the velocity of propagation, typically 1500 metre/sec
t'	: is the raw time measurement
t_d	: is the known equipment delays
e	: is the residual timing error

Three acoustic positioning methods are mainly used by the offshore industry. These are referred as

1. Long Baseline Method (LBL)
2. Sort Baseline Method (SBL)
3. Ultra Sort Baseline Method (USBL)

LBL acoustic systems are used to provide accurate position fixing over a wide area by observing the distance from a sensor on the hull of a vessel, or from a sensor on a towed float or underwater target, to three or more transponders deployed at known positions on the ocean bottom. The line connecting the seabottom transponders (baseline) usually varies between 5 Kilometre to less than 50 Kilometre.

USBL acoustic systems, or Super Sort Baseline (SSBL), are used to locate a single target placed on the seabed or on a mobile structure. They consist of an array of transducers in a single assembly fixed on the vessel's hull. Their operation is based on phase comparison techniques to measure the angle of arrival of an acoustic signal in both the horizontal and vertical planes. Hence, a single point located on the sea bottom or on a mobile station is fixed by measuring its range and bearing relative to the vessel. Although USBL acoustic systems are more convenient to install than LBL systems they

do not provide redundant information, and therefore they are less reliable (Kelland, 1994).

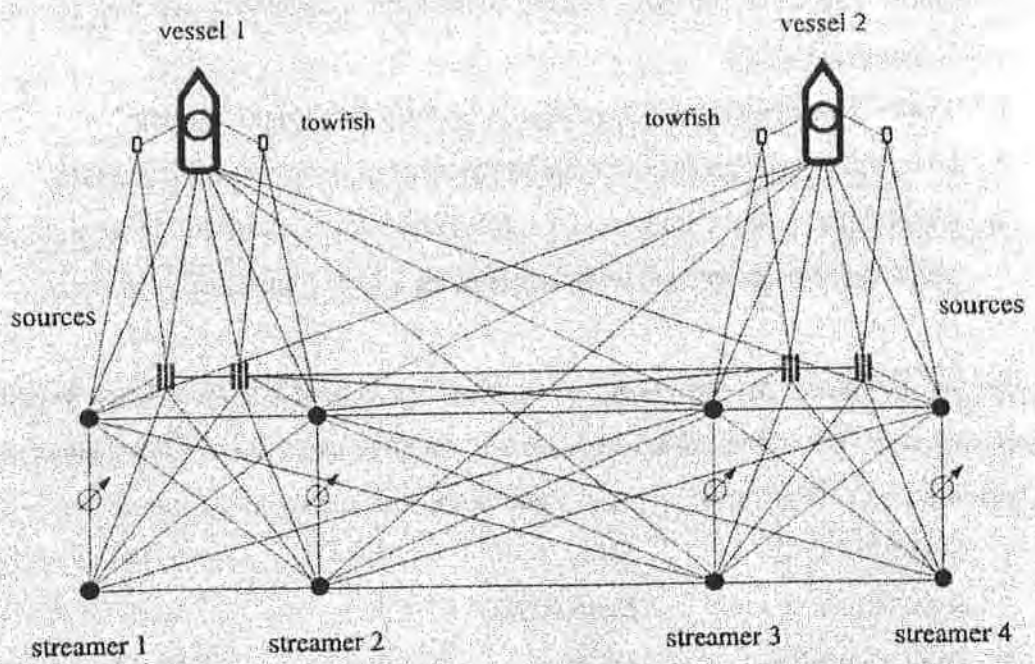

Figure 1.10 Dual vessel, quad source, quad streamer symmetric survey configuration. Simplified front-end acoustic network

During 3-D seismic operations SBL acoustic systems are typically used (in combination with other measurements) to locate the various elements involved within a seismic spread, and therefore they will be discussed in more detail.

During seabed surveys, structure installation and drilling operations several acoustic devices (typically hydrophones) fixed on the hull of a vessel (typically separated by distances of 10 to 100 metre) are used to locate points on the seabed. In seismic surveys an acoustic network comprises transceivers and transducers mounted beneath the seismic vessel, on source arrays, navigation buoys and towfish or deployed along the streamers. Direct ranges are measured in either direction between transceivers to build an acoustic network. A typical modern seismic configuration usually consists of three acoustic networks, one at the front-end, one at the rear-end, and one in the middle

(Figure 1.10). Also, configurations involving acoustics throughout the length of the seismic streamers are increasingly used.

The most important problems related to acoustic positioning systems are (Houston, 1987; Tiong Ha 1990)

1. The effect of the air bubbles produced by the guns during shooting.
2. Interference problems caused due to the wake of the of the seismic vessel.
3. Reflections from the bottom and surface can interfere with the original signal if the signal exceeds certain length in time (Figure 1.11).

Proper design of modern acoustic systems has eliminated, to a large extent, these problems. The three most well known manufacturers of SBL systems and their products used today in seismic applications are

1.	SONARDYNE	SIPS
2.	SYNTRON	MultiTRAK
3.	DigiCOURSE	ECHO

All three systems operate in the band width between 50 KHz - 100 KHz. Their resolution varies between 0.10 metre - 0.15 metre. Maximum operating ranges can reach 1000 metre between devices fixed on the tailbuoys of a typical dual vessel configuration. This reduces, however, to under 500 metre at the front-end of the network due to the effect of the air bubbles (Kelland, 1994). Both SYNTRON and DigiCOURSE systems are relatively new products.

Finally, as stated earlier, USBL systems are used by the exploration industry. Such a system is the HPR-Simrad that uses a transmitter/receiver which is mounted on the end of a perch under the vessel. The receivers are mounted at points that need to be accurately located, e.g. on sub-arrays on each source (before the first gun cluster), and on streamer heads (before the first streamer trace).

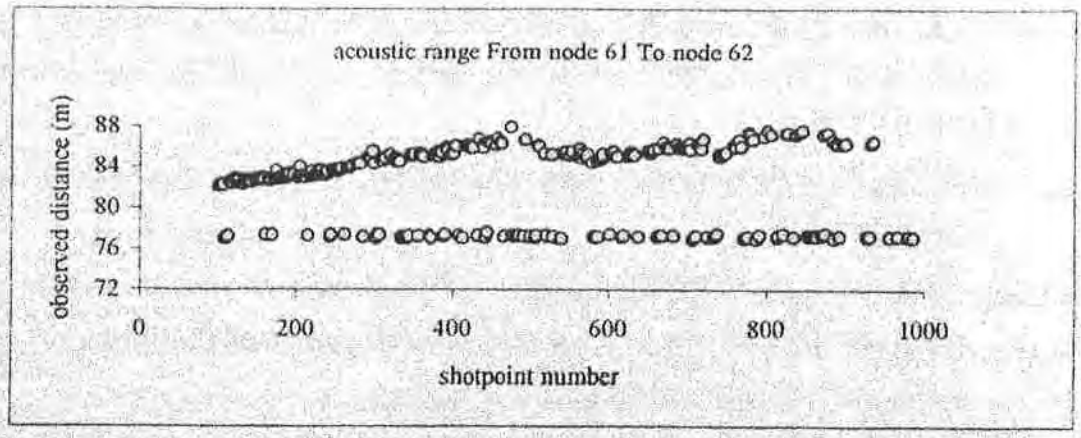

Figure 1.11 Time series of raw acoustic distance measurements between two acoustic nodes fixed on the frond-end of the same streamer. Due to the physical connection between these sensors the observed range should be more or less fixed (in this case approx. 77 metre). It is clearly visible that these signals are strongly affected by (combined sea bottom and/or surface) reflections, Irish Sea 1993 (see Appendix E2)

1.6.2 Laser Systems

Another way to observe a distance or a direction is that by using a laser system. The principle of computing a range from measurements of laser beams is almost the same as for an acoustic system. In this case, however, since a laser beam consists of highly coherent light waves (light amplification by the stimulated emission of radiation), the propagation velocity v in Equation 1.1 refers to the speed of light, and the time t to the one-way travel time from the laser device to the reflector target, i.e. half of the two-way measured time.

In 3-D seismic operations laser systems deployed on the vessel stern to measure the travel time to surface reflectors located on the sources, the front of the streamers, or on auxiliary floating structures. The method has a highly success in identifying a target and is easier to install because no electrical connections are required since the reflectors are passive devices. Typical accuracy level of the laser systems is ±1 metre for ranges and ±0.1 degree for measured directions (Chevron Training Course, 1992).

Though the basic principle of the method is fairly simple the complexities are introduced by the environment in which the system operates. Some of the major problems are (Tiong Ha, 1990)

1. During heavy downpour or foggy conditions, the rain or fog can block out the laser beam completely.
2. Since the retro-reflectors are passive devices there is no way to ascertain that the rays reflected back come from a particular reflector. For this reason only a small number of well separated reflectors can be used.
3. Because the laser beam does not transmit well in water only surface targets can be used.
4. Is vital to develop efficient techniques of holding up the retro-reflectors above the water and sea waves.

1.6.3 Magnetic Cable Compass

Since 1976, cable compasses have been used to provide a major portion of the position solution during marine seismic surveys. Today, cable compasses must be more accurate and repeatable than ever. What makes this challenging is the fact that cable compasses use the earth's magnetic field to determine the orientation of the streamer segments. The orientation of a cable compass is measured only with the horizontal component of the earth's magnetic field which differs the world over. Two major errors are concerned with magnetic compasses, magnetic declination (or variation), and magnetic deviation.

Magnetic declination is the difference between the geographic and magnetic north and can be as large as several degrees and, known with an uncertainty of the order of 0.5 degrees. An erroneous value of magnetic declination will introduce a specious rotation to all streamer shapes, resulting in a coordinate shift which can amount to hundreds of metre depending on the magnitude of error (Norton et al, 1990).

Magnetic deviation concerns with local effects of every single compass caused by misalignment of the compass card with respect to the earth's magnetic field superimposed upon the earth's magnetic field. This difference can be measured in the

laboratory and can be expressed by a number of correction coefficients. The correction is approximated by the following equation (Gerber, 1987)

$$\text{Deviation correction} = A + B\sin(\phi) + C\cos(\phi) \qquad 1.2$$

where

- A : defines the correction for the compass bias or off-set.
- B, C : are the corrections adjust for permanent magnetic anomalies within the compass, which exhibit a single-cycle sinusoidal error with compass rotation.
- ϕ : is the compass heading.

The magnetic deviation can be estimated with an accuracy of 0.05 degrees (Chevron Training Course, 1992). This correction must be applied to each compass individually and for all possible headings. It should be stressed that even relatively small discrepancies, of the order of 0.5 degrees, can produce errors of tens of metre in the final hydrophone positions in configurations with typical inter-compass spacing of 300 metre (Norton et al, 1990).

In addition to this correction (static calibration), calibration in the field (dynamic calibration) is necessary to verify the correct performance of each compass. The purpose of this calibration procedure is to derive a fixed correction value for the survey area (and compare with published magnetic declination values) as well as to identify biases resulting from the static calibration, the mounting of the compasses on the streamers, and the dynamic behavior of the compass (Gerber, 1987). A detailed description of the calibration procedures may be found in Gerber, (1987) and in DigiCOURSE paper reference, (1995).

Today, cable compass manufacturers produce compasses that usually combine depth keeping 'birds'. These depth controller devices comprise movable vanes which are used to maintain the streamer at a predetermined depth. Cable compass accuracy is of the order 0.5 degrees and resolution of 0.1-0.5 degrees while the depth controllers

resolution is of the order of 0.15 metre. Among others, SYNTRON and DigiCOURSE are well known cable compass manufacturers.

1.6.4 Gyrocompass

A gyrocompass is an instrument that it is used to measure the true azimuth of a heading line. It is based on a gyroscope that is forced to hold its spin axis in the direction of the meridian. This is possible by using an unbalanced mass which makes the axis of rotation precess about true north. If a torque tries to change the plane of rotation of the gyroscope, the gyroscope axis will rotate about an axis perpendicular both to the gyroscope's axis of spin and the torque (Sheriff, 1994; Tetley and Calcutt, 1991).

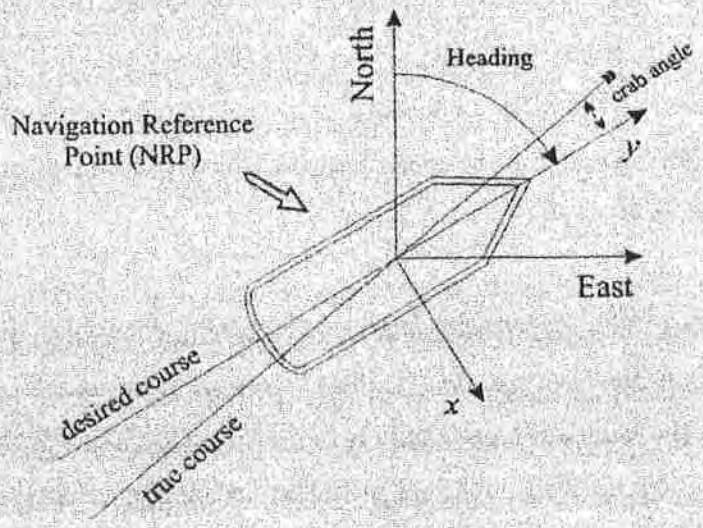

Figure 1.12 Vessel crab angle

A gyrocompass is today almost a mandatory instrument for all survey vessels in order to provide the azimuth of the vessel's heading, i.e. the azimuth of the desired course. Estimated accuracy of gyros used on geophysical vessels is about 0.7-1.0 degrees (Houston, 1987). It is essential that integrated navigation systems today combine gyro observations with other positioning systems, such as Syledis or DGPS, to improve the quality of the navigation results (Celik and Cross, 1994).

Due to external forces acting on the vessel, such as wind and cross currents, this it cannot sail along a predetermined line. The difference between the vessel's true course and the desired course (Figure 1.12) is termed as crab angle. In any navigation algorithm crab angle should be placed at the state vector and recover from all other measurements.

1.6.5 Terrestrial Radio Ranging Systems

These are classified as range-range and hyperbolic radio positioning systems. The intersection of at least two lines of positions (LOP) is required to fix a point using terrestrial navigation aids. In the range-range (or circular) mode direct measurement of time or phase places the user on circular LOPs, while by taking the difference between two direct time or phase measurements places the user on LOPs that are hyperbolas. A point is, therefore, fixed at the intersection of two circular and hyperbolic LOPs respectively. In practice redundant observations are, however, used to improve the quality of a position fix.

Another way to classify radio ranging systems is according to the frequency at which they operate. Radio positioning systems used by the oil industry to locate the vessel Navigation Reference Point (NRP) and other targets, as head/tailbouy floating structures, operate in the band widths 5-10 GHz, 400-450 MHz, 1-4 MHz, and 100 KHz. In general, the higher the frequency, the greater the accuracy potential, and the lower the frequency the greater the range potential (Morgan, 1986). A list of the more common radio positioning systems is given in Table 1.2 (Celik, 1996; Morgan, 1986). For a more detailed description the reader is referred to Ackroyd and Lorimer, (1990); ANON, (1986); Forssell, (1991) and Ingham, (1975).

The standard industry radio positioning system for 3-D seismic surveys is Syledis - see Table 1.2. The main advantages of the system are the high level of accuracy (typically ±5 metre for a well calibrated system), the possibility to support head/tailbuoys, and its reasonable cost. However, the system set up and calibration procedure can be complex and time consuming. Moreover, multiple units of equipment are required for shallow

water, or large complex streamer surveys. Apart from Syledis, Hyperfix and ARGO systems are used by the oil exploration industry. These systems, although they can operate at ranges as long as 400 Kilometre (daytime) from the shore stations and provide a maximum accuracy of 10-15 metre, do not support head/tailbuoys and are susceptible to bad weather. Hyperfix and ARGO represent a reasonable solution to radio positioning of exploration 3-D surveys only under 'relaxed' geophysical requirements and as a good back up to Syledis under difficult circumstances (Chevron Training Course, 1992).

Positioning System	Manufacturer Country	Frequency (approx.)	User Mode	Range (Km)	Accuracy (metre)
Mini Ranger	Motorola Inc. Temple, Arizona	5.4-5.9 GHz	Circular	25-50	5-20
Trisponder	Del Norte Technology Inc. New Orleans, Lousiana	8.8-9.5 GHz	Circular	25-50	3-12
Syledis	Sercel Carquefou, France	420-450 MHz	Circular	60-110	5-10
Maxiran	Navigation Management Inc. Florida	420-450 MHz	Circular	60-150	10-50
ARGO	Cubic Western Data San Diego, California	1.6-2.0 MHz	Circular	150-500	8-25
SPOT	Offshore Navigation Inc. New Orleans, Louisiana	1.6-2.0 MHz	Circular	800-1000	10-50
Hyperfix	Racal Decca Survey Ltd Leatherhead, UK	1.6-3.4 MHz	Circular	150-700	10-30
Geolog	Sercel Carquefou, France	2.0 MHz	Circular	800-1000	10-50
Loran C	USA	100 KHz	Hyperbolic	300-1500	50-500
Pulse/8	Racal Decca Survey Ltd. Leatherhead, UK	100 KHz	Hyperbolic	300-800	30-500

Table 1.2 Radio positioning systems

The main error sources of the radio positioning systems refer to changes of the atmospheric conditions (temperature, pressure, humidity) of the various layers the radio waves travel. Errors in the time and phase measurement process as well as beacons (chain) geometry affect the accuracy of radio positioning systems.

1.6.6 Satellite Systems

Since 1969, the oil industry has been using satellite systems for navigation, positioning and communications. The Global Positioning System (GPS) has become the most extensively used positioning and navigation tool in the world. Available worldwide, GPS consists of a constellation of 24 satellites and provides users with position accuracy of 100 metre (2drms at 95% probability level) 24 hours a day. Significantly enhancing the accuracy of the system, differential GPS (DGPS) techniques have matured to become the most advanced and accurate implementation of GPS providing the user with horizontal position accuracy of better than 3 metre up to ranges of 1000 kilometre from the reference stations. In the following sections the basic principles and characteristics of the system, as well as its application to 3-D marine seismic environment will be summarized.

1.6.6.1 Working Principle and Observables

GPS is deployed and operated by the Joint Program Office (JPO) located at the US Air Force Systems Commands Space Division which is directed by the US Department of Defense (DoD). It comprises three major segments (Hofmann-Wellenhof et al, 1994; Corbett, 1994)

1. The space segment that consists of the GPS satellites in orbit around the earth. The satellites broadcast signals (radio frequency ranging codes) and navigation messages.
2. The control segment that consists of the Master Control Station (MCS) and a number of monitor stations responsible for tracking and managing the satellites.
3. The user segment consists of the user equipment sets that receive the satellite signals and process the information to obtain position, velocity and time.

GPS satellites transmit on two frequencies (both of which are multiples of a precisely controlled atomic clock) known as Link-1 (L1) and Link-2 (L2) which are multiples of a fundamental frequency of 10.23 MHz. These two frequencies (known as carriers as well) are modulated by up to two binary codes which consist of pseudorandom noise

(PRN) sequence of zeros and ones. The two primary PRN sequences used by GPS are the Coarse/Acquisition (C/A) code, and the precision (P) code (Hofmann-Wellenhof et al, 1994; Corbett, 1994).

The principles of radio positioning from satellites are fundamentally the same as those for terrestrial radio positioning systems. In the case of satellites the transmitter locations are the known orbital positions (satellites) at very precise time marks. There are essentially two methods of positioning using GPS, using either pseudoranges or carrier phases. Using pseudoranges the receiver code (each receiver replicates the C/A and/or the P code at an equivalent time at which it was generated within the satellite) is correlated against the satellite code. The time offset is scaled by the speed of light to compute a distance measurement. The latter method uses the much more precise carrier phase observations to compute baselines between two positions. The principle of the method is simple. If the signals (L1, L2) are generated within the receiver at the same time as those in the satellites a phase difference measurement may be measured very accurately within the receiver. The basic problem remains, however, to solve for the whole number of complete wavelengths (integer ambiguities) between the satellite and receiver. This is usually carried out by postprocessing using linear combinations of the two frequencies and differencing techniques (Talbot, 1992 and Chen, 1992). In marine applications combination of pseudorange and phase data reduces the noise error within the pseudorange measurement resulting in a much higher positioning accuracy (Celik, 1996). Today, new fast ambiguity resolution techniques (on-the-fly) are being developed to solve for integer ambiguities in a single epoch to provide very high baseline positioning in real-time (Corbett, 1993).

1.6.6.2 Differential GPS

Differential GPS technique relies on the assumption that the errors in the position at one point are similar to those for all points within the same area. DGPS involves the use of at least two correlating receivers. One of them, the reference station, is stationary and located at a known point while the second one is a mobile receiver with the desired result being its position and possibly its velocity.

The reference receiver is used to calculate corrections to the GPS derived position or to the measured code ranges. Therefore, two correction methods are in use to improve the accuracy of the mobile receiver position. In the first method the stationary receiver computes its position using the same set of satellites as the mobile one. The position corrections are derived by the difference between its known and estimated position. These corrections are then passed to the moving receiver to compute an improved position. In the latter method pseudoranges observed at the reference station are compared to what is expected in order to determine corrections which if applied to the pseudoranges improve the position fix. The effect of DGPS on the position source errors, for level of accuracy required to conduct a 3-D seismic survey, is given in Table 1.3 (Chevron Training Course, 1992).

ERRORS REMOVED BY DGPS	
selective availability	removed by DGPS
ionospheric group delay	almost complete compensation at close range, degrading as monitor-mobile separation increases
tropospheric group delay	almost complete compensation at close range, degrading as monitor-mobile separation increases
ephemeris error	removed by DGPS
satellite clock error	removed by DGPS

Table 1.3 The effect of DGPS on the main error sources of the GPS system

1.6.6.3 GPS Error Sources

GPS is affected by a number of error sources that must be eliminated or modeled to improve the quality of a position fix. The most important of them can be classified in satellite, atmospheric, receiver, and multipath errors.

Satellite error sources involve natural and artificial errors, namely

1. Selective Availability (SA) and Anti-Spoofing (AS) are intentional errors placed on the GPS system by the US DoD to degrade the accuracy level for civilian users. SA is concerned with the modification of the satellite transmission to degrade

deliberately the pseudorange measurement. This can be done by altering the ephemeris data (by a procedure known as epsilon), or by dithering the satellite clocks. AS alters the GPS signal by changing the characteristics of the P code (Roberts, 1993).

2. Natural errors concerned with ephemeris errors and satellite clock errors. Errors in the ephemeris data are related with poor prediction of the satellite orbit, and therefore its position (satellite computed position should lie within 20 metre of its true position (QUEST Training Course, 1995)), while satellite clock errors result from time drifts from GPS time.

Atmospheric propagation errors refer to ionospheric and tropospheric effects. Ionosphere may cause a delay as much as 150 metre to a GPS signal due to the change of its travel time caused by the ionized constituent of the gas-molecules layers. Tropospheric effects are caused by delays of the GPS signals passing through this medium (Hofmann-Wellenhof et al, 1994; Cohen et al, 1992).

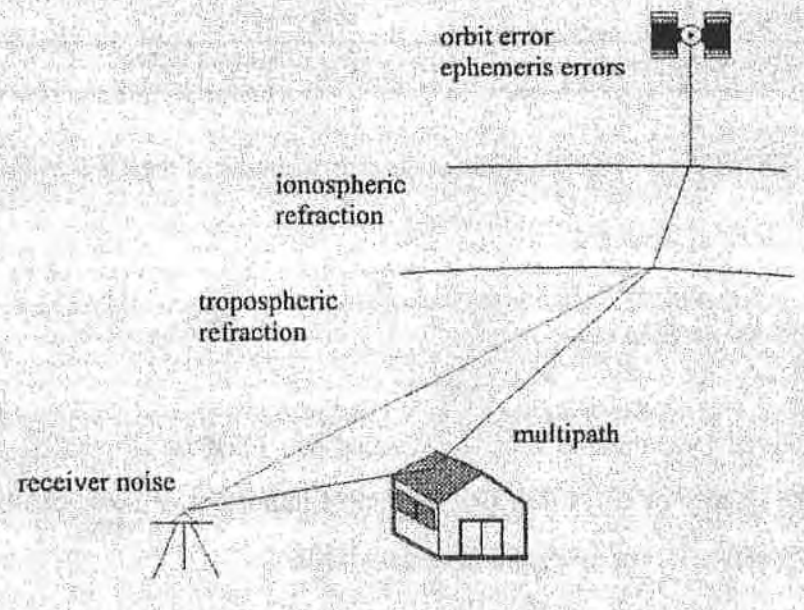

Figure 1.13 Main GPS error sources

A number of possible error sources are associated with GPS receiver themselves. These include receiver clock errors, code correlation ability, antenna phase centre variation, tracking bandwidth and internal electronic noise (QUEST Training Course, 1995).

Finally, multipath is the effect whereby the GPS signal does not travel directly to the receiver but via two or more paths, namely reflected signals. A schematic view of the GPS error sources is illustrated in Figure 1.13

1.6.6.4 DGPS in Offshore 3-D Seismic Surveying

DGPS in offshore seismic exploration is not used only for vessel navigation purposes. Another use of DGPS is that of target tracking. Today, it is a rule that active tailbuoys (also head and navigation buoys), namely floats equipped with terrestrial or satellite positioning systems, are used to improve the quality of positioning a 3-D seismic network. During GPS target tracking (RGPS) the pseudoranges observed at the floating station are transmitted back to the vessel via a UHF telemetry system. The main processing that is performed onboard the vessel yields to a range and bearing which are finally converted to local coordinates relative to vessel (QUEST Training Course, 1995) - see Figure 1.14.

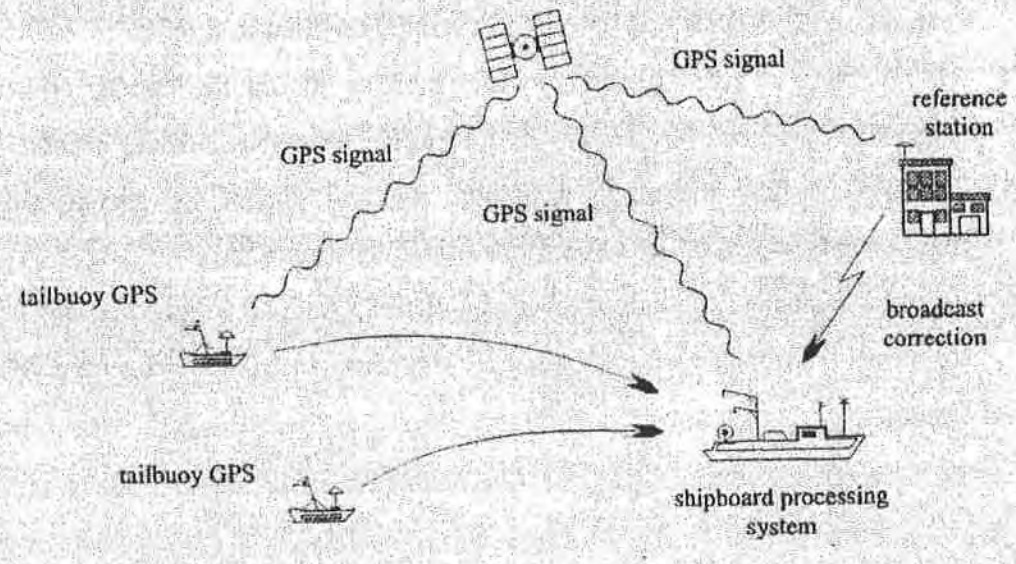

Figure 1.14 RGPS target tracking

There is no doubt that tailbuoy/vessel DGPS systems offer today a significant improvement in offshore seismic positioning, especially after the complete 24-satellite constellation became available. Moreover, it is generally accepted among the seismic industry that DGPS can be used as a stand-alone primary positioning system during seismic exploration. The UKOOA, which consists of offshore exploration companies acting in UK, plays a significant role in establishing standards and guidelines for the offshore industry, including seismic positioning data. This is implemented by organizing DGPS and seismic acquisition workshops and by publishing their results. Some of the consensus points related to DGPS for use by the exploration industry, derived from earlier and more resent meetings (May 22 and December 11, 1991; January 15, 1992; 23-25 April, 1993), are summarized as follows (Guidelines for the Use of Differential GPS in Offshore Surveying, 1994; Jensen, 1992)

1. For offshore surveying, and particularly offshore seismic, a minimum of five satellites is required at all times since satisfactory height-aiding is critical to the acceptance of DGPS.
2. True range corrections should be transmitted by the reference stations to vessel. This essentially means that reference stations should not compute positions for use in obtaining pseudorange corrections.
3. Postprocessing should be seen as something that should be carried out only when necessary (because of a problem) and not as a matter of course. The aim should be that real-time, or quasi real-time solutions to be the final solutions.
4. All raw data at reference stations and mobiles should be logged, primarily for 'insurance purposes', but possibly for performance enhancements as needed.
5. The use of fully integrated navigation systems should be encouraged. QC requirements should be seen as a major reason for integration.
6. Research is needed to study the benefits of using multi-reference stations in DGPS solutions, the possible value of using L2 frequency in DGPS and on the QC of the system.

CHAPTER TWO

STREAMER MODELLING

2.1 INTRODUCTION

One of the major challenges in acquiring a high quality 3D seismic survey is to locate accurately the hydrophone groups deployed at intervals along the length of the seismic streamers. Since the compasses and other measuring devices are not co-located with the hydrophones it is necessary, in any approach, to have a mathematical model that describes the shape of the streamer. Moreover, because of the numerous hydrodynamic forces acting on the cable in the underwater environment, the cable shape it is likely to be significantly distorted from a nominal straight line - so a simple linear model is very unlikely to be sufficient.

In fact the problem is confined in modelling the shape of the seismic streamer in the horizontal plane in real time. It is assumed that the shape of the cable has no deviations in shape vertically since the use of 'birds' along the cable maintain the streamer in practically constant depth (Amrine et al, 1989; Jakubowicz, 1980).

To estimate this distorted shape three alternatives can be considered. In the first approach a physical model of the hydrodynamic forces acting on the cable could be used to derive the streamer shape. The second approach is to consider an 'empirical' numerical approach in which the solution to the problem is deduced by adopting a 'model curve' that best fit the observed data. Finally a hybrid method can be used in which the streamer location is computed based on a physical model together with a set of positioning observations.

This chapter attempts to assess the various approaches to the problem of streamer modelling. More specifically this chapter aims to investigate, describe and test a solution to the problem that can be easily incorporated and performed in a single operational navigation system such as one based on a Kalman filter.

The first part of the chapter deals with the basic principles and limitations arising from an approach based on a physical model. The very basic steps of the implementation of a method which is based on information derived from both physical principles and geodetic measurements are also discussed. Finally in the same part the use of different fitting procedures is considered and evaluated. The second part of the chapter attempts to examine in more detail and test the approach which is selected to be incorporated in the integrated algorithm for positioning seismic networks given in Chapter Five, i.e. a polynomial streamer model.

2.2 STREAMER MODELLING

2.2.1 A Hydrodynamic Approach to Streamer Modelling

It is known that tension forces due to the vessel pull, and drag forces due to the resistance of the cable through the water, determine the three dimensional shape of the seismic streamer. Knowledge of the system dynamics can be used in constructing a physical model that describes the motions of the cable in response to the various external forces.

Any change in the vessel's speed and any fluctuation in the sea waves, or those generated by the vessel, the wind load or the water currents, would mean changes in the towing tension and drag forces respectively. Such a model can only be applied when these external forces acting on the cable are known with a reasonable accuracy. It should be stressed, however, that, even if these quantities are known, a system of several streamers and floats would lead to models that would be too complicated and inflexible for the construction and implementation of a practically useful positioning algorithm. It is therefore unlikely that, although they have been used for vessel motion, (Cross and Pritcett, 1986) hydrodynamic models will be adopted for positioning purposes in the foreseeable future.

It has been mentioned earlier that a similar approach to this is one where the shape of the streamer is determined using knowledge of both the system's hydrodynamics as well as measurements such as compass bearings and acoustic derived ranges. A full description and testing of such a model may be found in Krail and Brysk (1989). In the following paragraphs, only the main points of this approach are given.

It is assumed that the shape of the cable is such that tension forces due to vessel pull and the presence of the tailbuoy are balanced by drag forces due to the resistance of the cable through the water. This condition of equilibrium leads to differential equations which if integrated analytically yield a formal expression of the cable tension. Another

analytic integration leads to an expression which relates the arc length of the cable to the tangent angle. The procedure of analytical integration and the mathematical operations help so that a multiplicity of constants including the tension of the cable at the stern, the cross current velocity and the drag coefficients can be eliminated. However this expression contains two integration constants that remain to be computed. These are the two tangent angles at the front and rear ends of the cable. It is proposed that these constants are determined by applying a least squares fit to the compass measurements. The functional model in this case is based on the expression that relates the cable length to the tangent angle. With the integration constants being determined from the compass readings, the shape of the streamer can be easily expressed in Cartesian coordinates by eliminating the tangent angle between the parametric equations which relate the along and cross positions to the tangent angle.

The main difference between this approach and any other conventional curve fitting procedure is basically that the functional model that is used to fit the compass data is derived from the analysis of the physics of the problem rather than based on an ad-hoc numerical fit. Nevertheless such a model is practically impossible to use in a Kalman filter model for real time positioning and quality control from mixed data sources for a number of reasons.

First, the foregoing analysis assumes that the streamer is affected by a cross current of steady flow over its full length. Moreover the assumption of a flexible cable in equilibrium suggests that the vessel is sailing with constant velocity in a constant velocity cross current. Obviously these assumptions become invalid when the vessel's speed changes significantly or when the sea state or current fluctuations are abrupt. It should be also noted that all these constraints have a much greater effect at the ends of the cable where the presence of the vessel and tailbuoy upsets entirely the validity of these assumptions.

2.2.2 Curve Fitting Procedures

For the estimation of the streamer shape it is assumed that noisy corrupted measurements of the tangent azimuths at various points along the length of the streamer are available. Interpretation of the compass data to derive the streamer position has always proved difficult. Several numerical methods can be adopted to obtain the streamer shape. Jakubowicz, (1980) states that 'since the behavior of the cable is not known it is not possible to choose a basis set in which to expand the required functions from physical arguments. Hence the choice of a fitting procedure depends mostly on the consideration of any particularly attractive mathematical properties of a method together with its efficiency and ease of computation'.

It is a principle requirement in this study that the selected fitting method should be one with well defined mathematical properties and such that can be incorporated easily in a unified recurrent process such as a Kalman filter. More explicitly, it is necessary that the selected curve be continuous and continuously differentiable at every point of the cable as well as to describe the complete streamer shape using only one set of coefficients, i.e. to be a single function. In the following paragraphs the most well known methods used to simulate the shape of a streamer are considered and assessed.

Straight Line Fit

The simplest method to represent the streamer's shape is to consider the streamer as a straight line which follows exactly the track of the vessel. Although this approach would be very simple in practice, significant differences from the final expected position may result, not only because of the angle between the vessel's track and the cable baseline (feathering), but also because of the 'deformed' shape of the cable. Only in processing and interpretation of the streamer shape in the early days of 2D seismic surveys was it assumed to be a straight line since no positioning systems were available on the streamer. The streamer feathering with the planned survey line was then measured and checked by means of a radar bearing to the tailbuoy (Zeijlmaker, 1990).

Arc of Circles Fit

One of the most well known conventional modelling algorithms is the arc of circles method (Zinn, 1991; Zinn and Rapatz, 1995). In this approach it is assumed that the seismic cable is a circular arc between any pair of adjacent compass units. Under this assumption with only the known compass azimuths at the ends of the circular are and its length (distance between the compasses), the chord azimuth and the straight line cord distance of the circular arc can be easily computed. Therefore given the coordinates for one of the ends of the arc the coordinates of any point on the arc (acoustic device, hydrophone, etc.;) can be computed as a function of the chord azimuth and the straight line chord distance between the ends (compasses) of the circular arc.

This method of fitting compass data can be incorporated easily in a positioning algorithm where the positions of any node in the network (cable acoustic sensors, compasses, tailbuoy GPS stations, etc.;) are states in the system. The position of any hydrophone group can then be easily computed given its offset value from the head of the streamer. Variations of this technique have been implemented, and operate successfully in integrated positioning algorithms, by widely known companies as Western Geophysical (Western Atlas International, 1994b; Zinn and Rapatz, 1995). Clearly, and as stated earlier in this section, such an approach cannot be used in the algorithm proposed in Chapter Five because a completely different observation model has been adopted.

Conner and Ponton (1994) outline two more characteristics of the method. First it is the disability of the streamer to bend between two active compass units. This obviously means that the streamer shape is restricted to a second order fit and therefore it cannot be determined whether a bend exists between compasses. This point is becomes crucial if a compass(es) for some reason are disabled. The second point to note is that the arc fitting routine results in a curve which is not smooth at the points where adjacent arcs are spliced together.

Cubic Spline Fit

Another way to address this problem it might be to use a mathematical function such as a cubic spline. However, even though a cubic spline gives a curve continuous and

continuously differentiable, and one which is capable of fitting the data very closely, it is not the best solution to the problem. This is because its coefficients vary along the length of the cable (i.e. the streamer shape is not represented by a single function) and its incorporation into a single operational study, is extremely difficult. Moreover, because the cubic spline is technically capable of representing faithfully each compass reading, it is hyper-sensitive to compass errors leading to the possibility of a completely unrealistic final curve. Finally its implementation is computationally cumbersome.

Least Squares Polynomial Fit

A more attractive way to address this problem might be to apply a mathematical approximation such as a least squares polynomial fit. This approach is one of the best known since it has been widely used in the past to build up algorithms that describe the shape of a seismic streamer offshore. The method it has been well described in the literature in a number of texts, for example Court (1993a), Egeland (1982), Gilbert (1980), Owsley (1981) and Jakubowicz (1980).

Nevertheless, single polynomials suffer from two disadvantages and therefore they are not very popular in some sections of the exploration industry. The first problem is concerned with the requirement of breaking the polynomial at acoustic and laser nodes in order to integrate the observed ranges. The second one originates in the mathematical properties of the polynomial functions. Polynomial fitting models, depending on the quality of the compass data, the number of compasses and the polynomial order, may result in high risk extrapolations at the ends of the cable. However, this risk, in the algorithm discussed in Chapter Five, is practically eliminated because the acoustic measurements and the use of a tailbuoy at the front and rear ends all contribute together to the determination of the streamer's shape.

Furthermore using least squares polynomials leads to a curve which describes the complete streamer's shape using only one set of coefficients, and the resultant curve is continuous and continuously differentiable at every point of the cable. As a result this method can be incorporated much more easily in a unified recurrent process such as a

Kalman filter. Hence in this study an 'n-order' polynomial is one model that has been utilized.

A variation of the simple least squares polynomial method of fitting compass data may be found in Conner and Ponton (1994). In an attempt to improve the results that can be derived from a curve fitting model using actual compass data they suggest that pseudo compasses are generated for various points along the streamer. The values of these compasses are a function of the actual compass values that are placed behind and ahead of the pseudo compass position. The significant innovation of the method is that the values of the compasses generated are computed using compass reading information obtained from previous and following shots in a sense that the dynamics of the cable are also taken into account. Obviously this method can only be applied in a post-processing mode.

Least Squares Harmonic Fit

A competitive approach to the polynomial fitting method might be a least squares fit using a harmonic function. Similar to the polynomials, harmonics also result in a continuous and continuously differentiable curve. This method is implemented, as an alternative, for use in the integrated algorithm suggested in Chapter Five. The results of its implementation are discussed in Chapter Eight.

Rolling Quadratic Fit

Variations of the foregoing are also possible in practice, for instance Ridyard (1989), has suggested the use of a 'rolling quadratic' algorithm in which a series of individual quadratics are used to fit a small group of compasses. This algorithm is clearly very effective and this, and similar approaches have been widely adopted within the industry. Whilst they may be very powerful interpolation devices, and whilst they may be very effective in sorting out outliers and highlighting problems, they cannot be easily adopted in the unified approach developed in this study. This is because (as it is the case for the cubic spline) the coefficients of the final curve vary along the length of the cable.

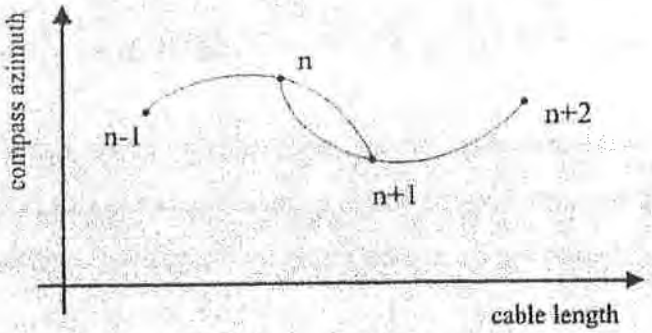

Figure 2.1: The 'rolling quadratic' technique

However, in Section 2.3.2, this algorithm is used to compute the positions for a sample of hydrophone groups for a few shotpoints for the set of data described in Appendix E. These preliminary results are then compared with those derived using a polynomial curve fitting model in order to justify and validate the selection of single polynomials for use in the unified algorithm. Therefore, in the following paragraphs, a more detail description of the 'rolling quadratic' algorithm is provided.

The azimuth value for each group of three compasses n-1, n and n+1, shown in Figure 2.1, it is assumed to be given by a quadratic equation of the form

$$B_i = a_{0_n} + a_{1_n} l_i + a_{2_n} l_i^2 \qquad 2.1$$

where

B_i : is the compass reading
l_i : is the offset of the i-th compass from its reference point
a_{0_n}, a_{1_n}, a_{2_n} : are the quadratic coefficients for compasses n-1, n and n+1

It is assumed that as moving from compass n to compass n+1 a decreasing linear ramped weight is applied to the quadratic curve centered on compass n, i.e. the weight is equal to zero at compasses n-1 and n+1 while in compass n is one. Similarly a rising linear ramped weight is applied to the quadratic curve centered on n+1. Therefore the azimuth value at any offset between compasses n and n+1 is given by

$$B_i = \frac{1-(l_i - l_n)}{l_{n+1} - l_n}\left(a_{0_n} + a_{1_n} l + a_{2_n} l^2\right) + \frac{l_i - l_n}{l_{n+1} - l_n}\left(a_{0_{n+1}} + a_{1_{n+1}} l + a_{2_{n+1}} l^2\right) \quad 2.2$$

The azimuth between each of the ends of the cable and first and last compass respectively is computed by the single quadratic curve at this region. Consequently, the cable position at each region can be found by integrating over the cable offset Equation 2.2.

2.3 POLYNOMIAL APPROXIMATION

In order to justify the selection of the polynomial fitting method from an accuracy point of view a series of tests have been carried out. These tests involved the fitting of series of polynomials, of a variety of orders, to real compass data and comparison of these results with those derived from a rolling quadratic method. The mathematics and the results are described in the next two sections.

2.3.1 Calculation of Cable Positions Using a Polynomial Function

In these tests the only information used is that derived from the magnetic compasses fixed along the length of the cable. In such a case the final accuracy of a streamer position is a function of raw compass data, the local magnetic declination, individual compass corrections and the algorithm used for processing the data. The polynomial equation can be written as

$$B_i = a_0 + a_1 l_i + a_2 l_i^2 + \ldots + a_n l_i^n \qquad 2.3$$

where

B_i : is the compass reading
l_i : is the offset of the i-th compass from its reference point
a : is the polynomial coefficient

The solution of this equation system, using a least squares method, gives the values of the polynomial coefficients. With the polynomial coefficients determined from the compass readings a mathematical transformation is required to transform the tangential azimuths to streamer or Cartesian coordinates. In this study a simplified approach is adopted. A formal description for the determination of an array shape in an analytic form may be found in Egeland (1982), Gilbert (1980), Owsley (1981) and Jakubowicz (1980).

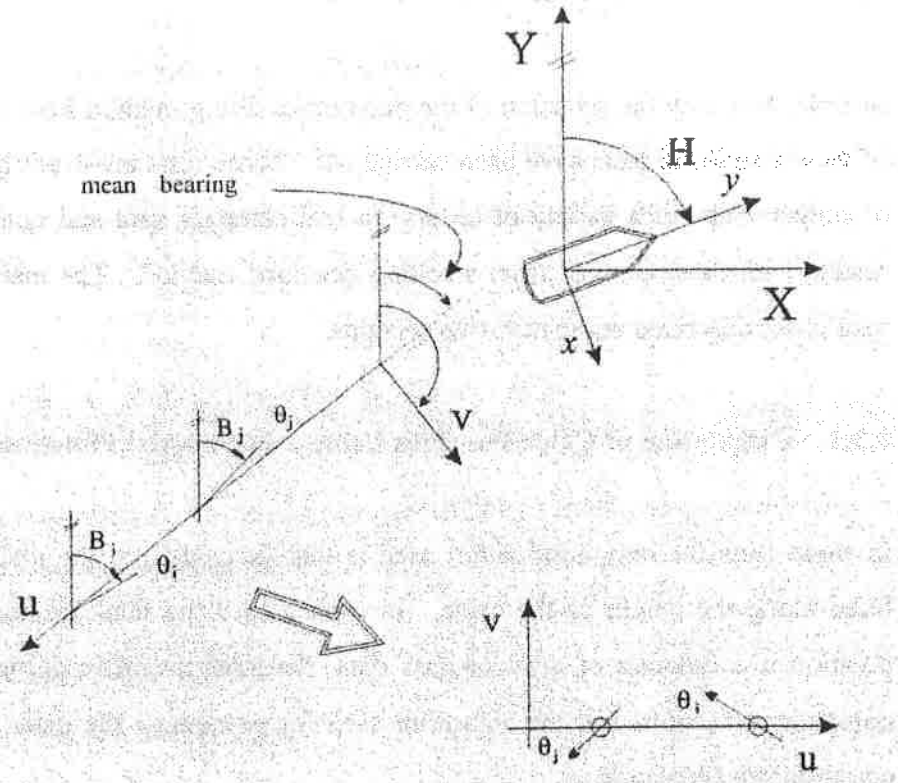

Figure 2.2: Geometrical representation of compass observations

Taking into account the geometrical configuration to be as shown in Figure 2.2 the following expressions can be written

$$\theta_{(rad)} = \text{atan}(dv/du) \cong \text{atan}(dv/dl) \qquad 2.4$$

which for any θ in (-1°, 1°) becomes

$$\theta_{(rad)} \cong \tan\theta = dv/du \cong dv/dl \qquad 2.5$$

Also from the same figure

$$\begin{aligned} B_i > B:\ B_i &= B+\theta = B+(dv/dl) \\ B_i < B:\ B_i &= B-\theta = B+(-dv/dl) \end{aligned} \qquad 2.6$$

Upon substituting Equation 2.3 into Equation 2.6 and integrating the streamer position expressed in local coordinates can be described as

$$\begin{aligned} u &= l \\ v &= c_0 l + c_1 l^2 + \ldots + c_n l^{n+1} \end{aligned} \qquad 2.7$$

where

$$c_0 = B - a_0 \quad \text{and} \quad c_k = a_k / (k+1), \quad \text{for k=1 to n}$$

The final coordinates X, Y can then be estimated by rotating these coordinates to the East, North coordinate system using

$$\begin{aligned} X &= \cos(a)\, l + \sin(a)\, v \\ Y &= \sin(a)\, l - \cos(a)\, v \end{aligned} \qquad 2.8$$

2.3.2 Testing the Method with Real Data

In order to test the feasibility of the polynomial algorithm in terms of correctness and computational efficiency, the foregoing method has been applied to a subset of real compass data. This includes compass measurements derived from two seismic campaigns. A full description of both survey configurations and data sets may be found in Appendix E. Here it is simply mentioned that in the first survey (Gabon, 1992) the network configuration deployed three streamers of 3.1 km length, comprising 13 compasses each. Similarly in the second survey (Irish Sea, 1993) a dual streamer configuration was used consisting of 10 compass units per streamer, deployed in a total length of approximately 2.0 km.

The process was carried out for polynomial orders up to eight for more than one hundred shotpoints for both sets of data. A typical set of results, derived for the first and second data sets, is given in Figures 2.3 and 2.4 respectively. Detailed analysis of tens of such sets of curves has led to the following general conclusions

1. Polynomials of order five or six fit the data extremely well in most cases.

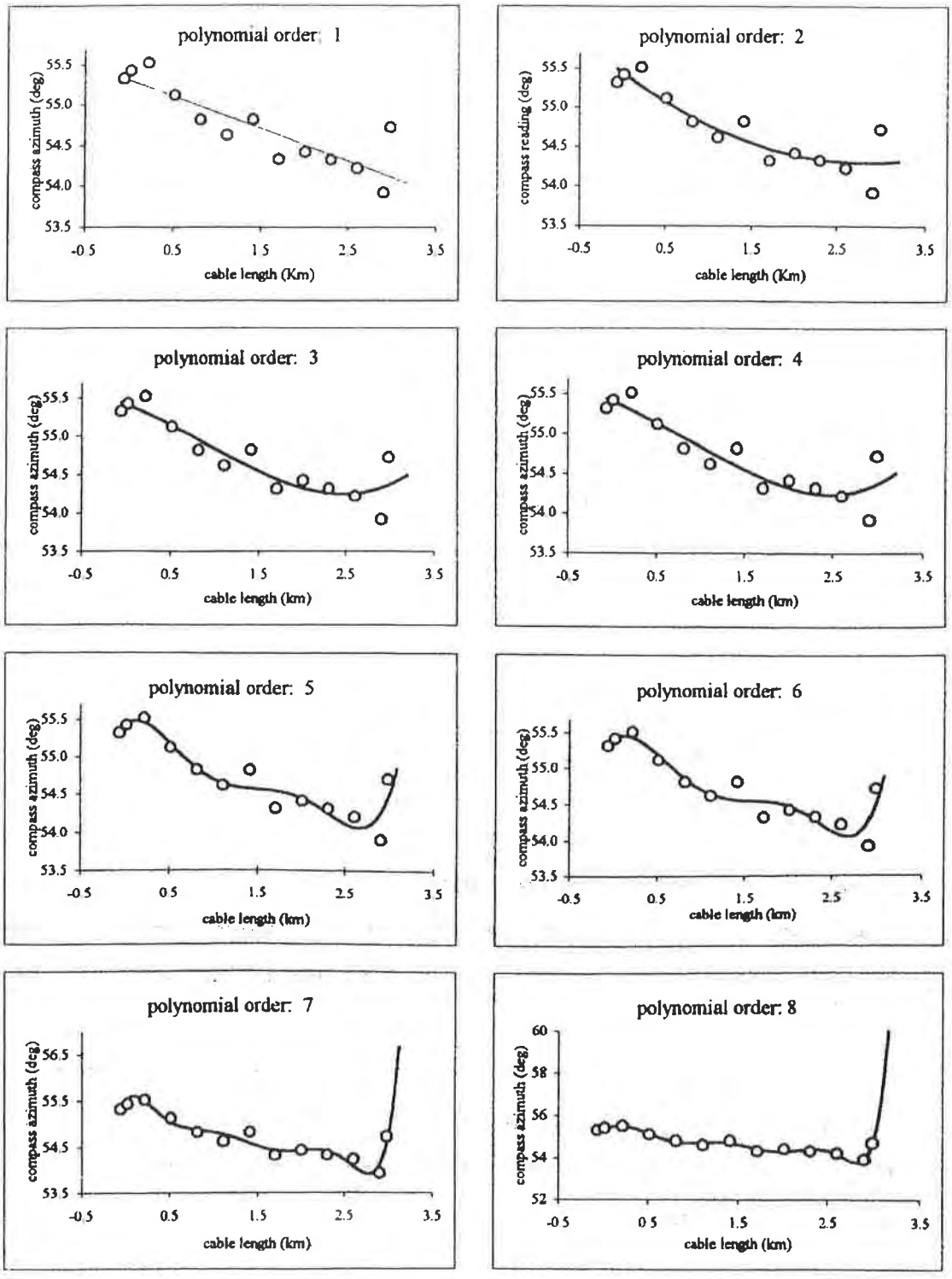

Figure 2.3: Streamer modelling for a single shotpoint based on a least squares polynomial approximation, Gabon 1992

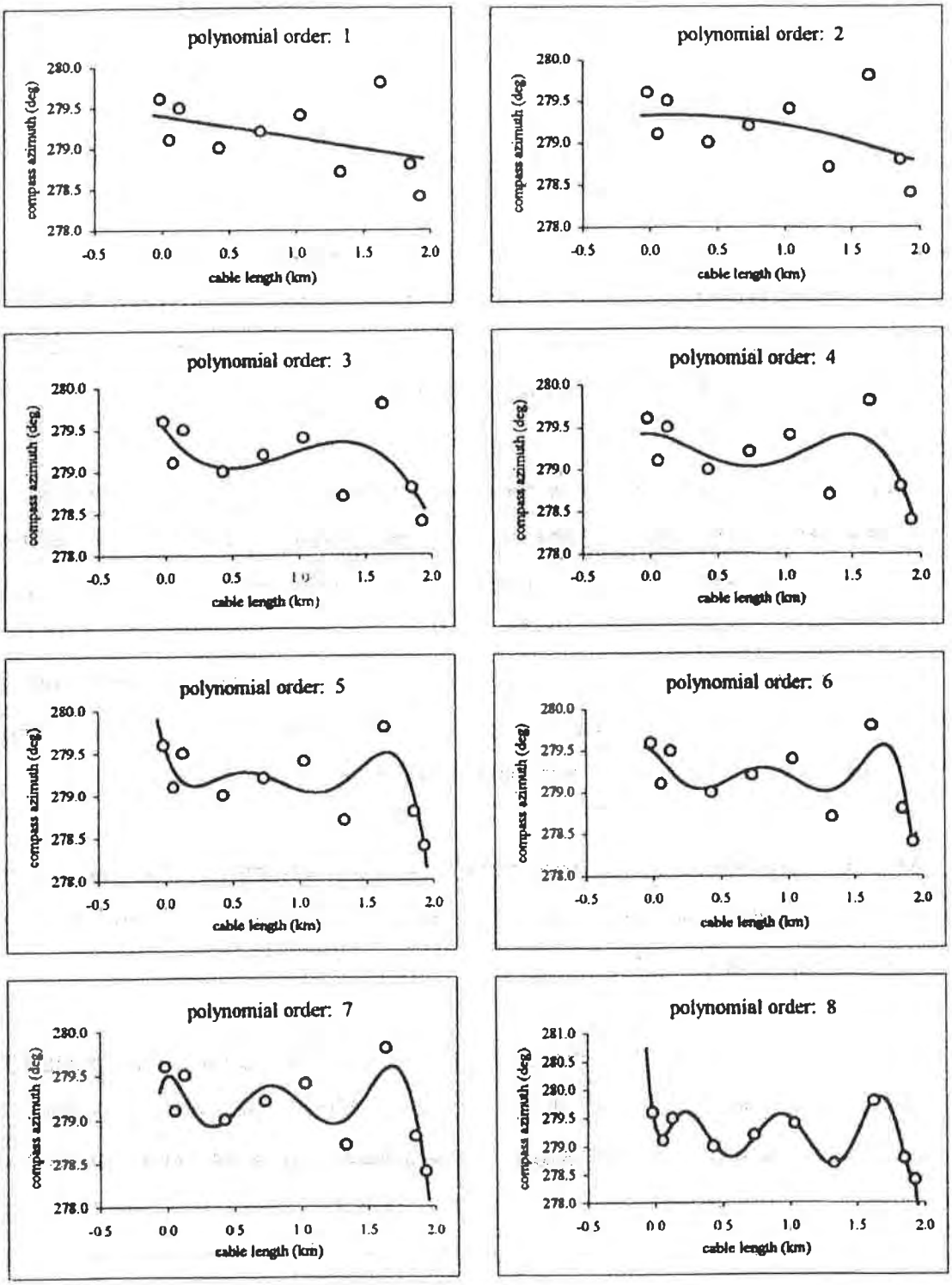

Figure 2.4: Streamer modelling for a single shotpoint based on a least squares polynomial approximation, Irish Sea 1993

2. Polynomials of order four or less do not describe faithfully the observations. In such cases the differences between the actual compass readings and those predicted by the polynomial can (in a few cases) exceed half degree. This might be important given that, in practice, cable compass resolution (but not accuracy) can be as high as 0.1°.
3. Polynomials of order greater than six can sometimes generate curves characterized by steep changes of gradient, which may affect significantly the fidelity of the final coordinates. This phenomenon is particularly noticeable for compasses close to the ends of the streamers.

It should be stressed, however, that these conclusions apply only to these particular sets of observations. For instance, analysis of a small sample of compass readings from another data set indicated that polynomials of order seven or eight can also be used. This discrepancy can be easily justified since in this campaign more compasses were used. In general it is advisable not to use very high order fits since compass observations may contain significant errors. For configurations of ten to fifteen compasses a fifth or sixth order polynomial is suggested.

After the coefficients of the polynomial have been determined, the eastings and northings of the hydrophone positions with respect to the streamer reference point can be computed using Equation 2.8.

As stated in Section 2.2.1 in order to validate the choice of the polynomial method for use in the integrated algorithm described in Chapter Five the differences between these coordinates and those obtained using a 'rolling quadratic' algorithm were computed. It should be noted that, all computations related to the 'rolling quadratic' algorithm have been worked out entirely at the company that provided the positioning data for this project. In fact, only a solution which is related to the first data set is available.

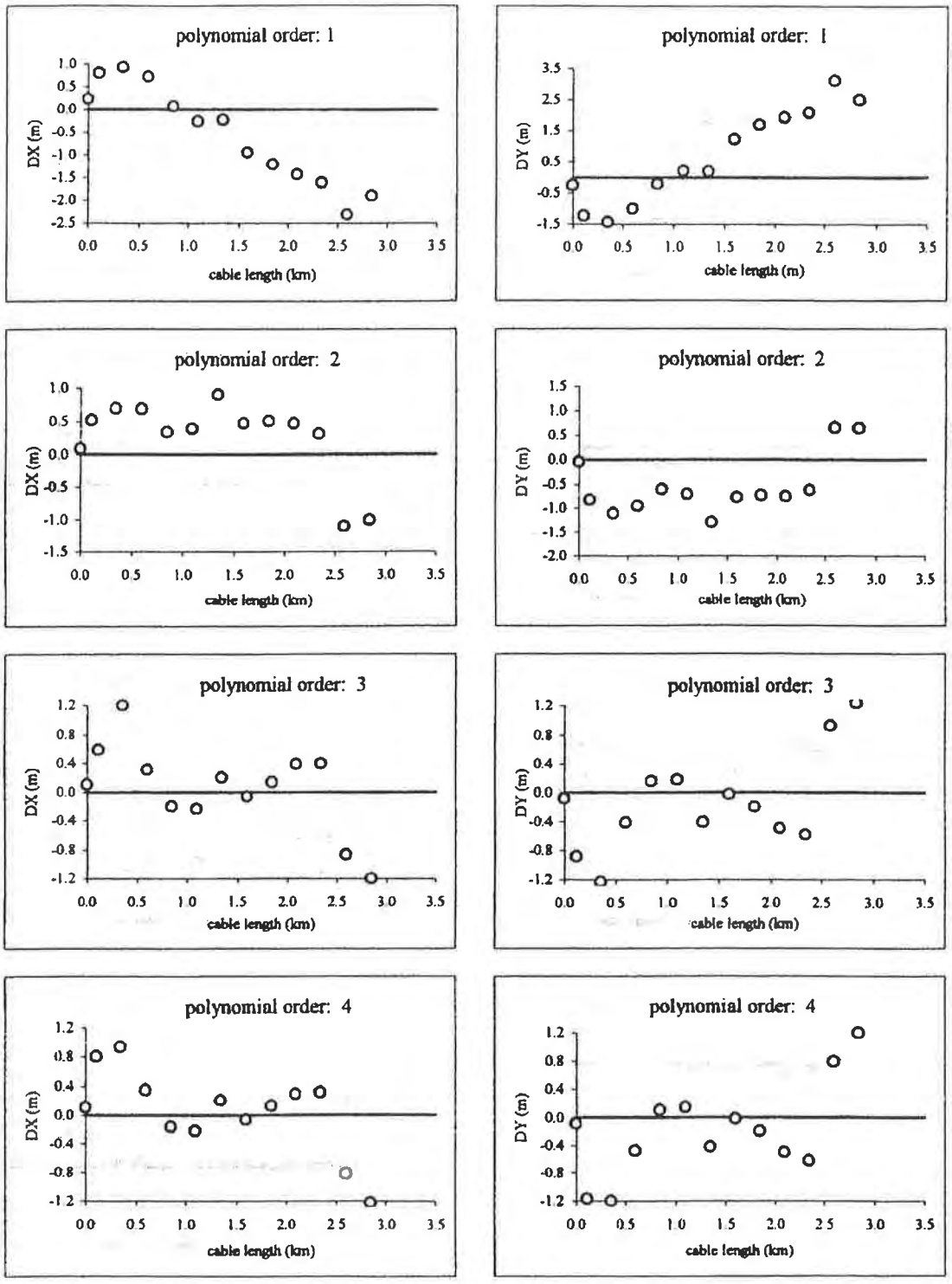
polynomial order: 1
DX (m)
cable length (km)
polynomial order: 1
DY (m)
cable length (m)
polynomial order: 2
DX (m)
cable length (km)
polynomial order: 2
DY (m)
cable length (km)
polynomial order: 3
DX (m)
cable length (km)
polynomial order: 3
DY (m)
cable length (km)
polynomial order: 4
DX (m)
cable length (km)
polynomial order: 4
DY (m)
cable length (km)

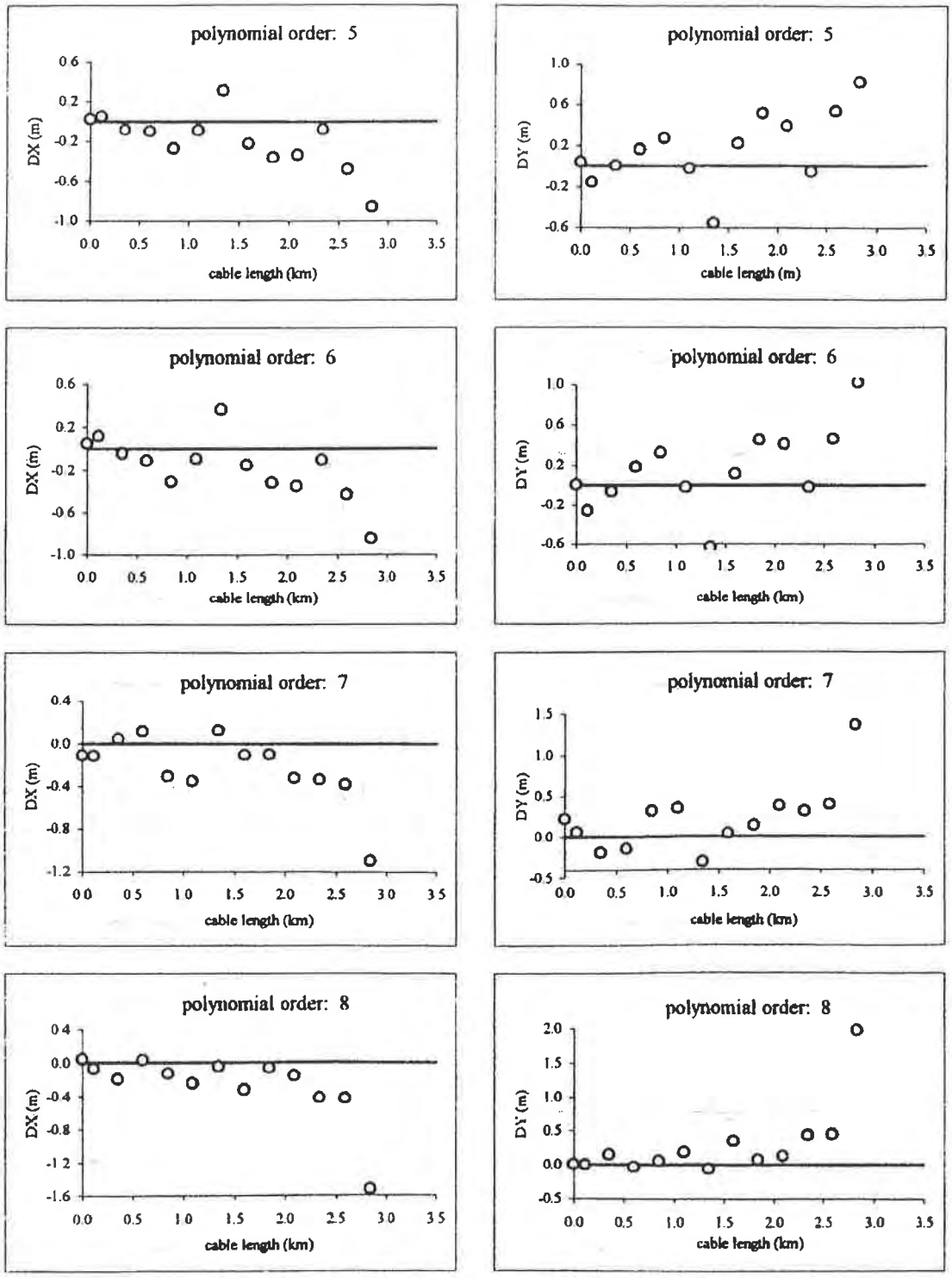

Figure 2.5: Differences in the Cartesian coordinates, of thirteen hydrophone groups, between those derived using a linear up to eight order polynomial fitting model and those derived using a 'rolling quadratic' algorithm for the compass data shown in Figure 2.3, Gabon 1992

Figure 2.5 shows the differences in eastings and northings between the two solutions for the compass readings depicted in Figure 2.3. With only a very limited examination of Figure 2.5 it can be seen that the differences derived using a polynomial of order four or less are more significant than those obtained using polynomials of a higher order. On the contrary if a fifth or sixth order polynomial is used the maximum resultant differences are of the order of one meter - even for the groups of hydrophones in the far end of the cable. Finally, the effect of high risk extrapolations if polynomials of order more than six are used is apparent in the last four plots.

From these tests it is evident that the use of a polynomial approximation is a highly realistic approach to the problem. Moreover, the method has the advantage of being easily incorporated into a Kalman filter model for real time positioning and quality control from mixed data sources. The n-order polynomial has hence been adopted as the primary streamer model in the mathematical system developed in this study.

CHAPTER THREE
THE KALMAN FILTER

3.1 INTRODUCTION

The Kalman filter is probably the best known of the commonly used recursive algorithms for the estimation of the parameters of time-varying systems. It has constituted the framework for a unified and concise treatment of a broad range of filtering problems from electronic engineering to surveying and geodesy. However, usually, the Kalman filter is perceived as a 'black box', into which measurements go in order to be converted into positions, since there still remains a certain amount of ignorance in the hydrographic surveying community with respect to Kalman filtering. Therefore, in the past, it has not proved popular with the offshore community and many offshore operators currently prefer simple and independent 'epoch by epoch' least squares computations. This chapter aims to provide a brief description of the Kalman filter models and algorithms as well as to explain the meaning of the most commonly used terms associated with it.

Kalman filter estimates have the advantage of being least squares estimators. This means, as can be shown (Cross, 1983), that they are the best in the minimum variance sense within the complete class of the linear unbiased estimators. For these reasons they are often referred to as Best Linear Unbiased Estimates (BLUEs). The basic difference between a simple least squares computation and Kalman filtering, is that, the Kalman filter comprises of the specification of a dynamic model in addition to an observation model that to together provide an optimal solution. The use of a dynamic system reveals, somehow, the amount of knowledge with respect to the system dynamics, i.e. the behavior of the system as it varies with time. For instance, in the case of a moving vessel, where its position and velocity are the desired results, the position fix measurements provided by a shore-based or satellite navigation system constitute the

observation model while the dynamic model is expressed by the assumption of constant acceleration between the position fixes.

3.1.1 Predicting, Filtering and Smoothing

Three types of problems constitute the estimation problem associated with Kalman filtering. These are known as prediction, filtering and smoothing, and they are related to the estimation of the state vector parameters x, of a time-varying problem, computed at any instant with respect to the present time.

The step of prediction is related to the computation of the filter estimates x(-), at time of interest t_j that occurs after the last available measurement(s). In this case, only the state estimates and its associated covariance matrix computed from the previous epoch, as well as the dynamics of the system, are used to provide the state vector solution.

Once a new measurement(s) is available the predicted state vector x(-) is used together with the new measurement(s) to solve for the state estimates. In this case, in which the time of the last measurement(s) coincides with the estimation time, the problem is referred to as filtering and the state vector denoted by x(+).

At a post-proccessing stage the state vector parameters can be computed at any time t_j where information for some time interval prior and later to time t_j is used. This part of the problem is known as smoothing and it denoted by x(s). Obviously, a solution of this type can only be available after some delay. Usually, in most real-time surveying applications, only the prediction and filtering steps are implemented since their implementation is straightforward. Although smoothing procedures can be executed in real time they are usually only used in post-processing because they require much more memory space.

These three distinct estimation problems can be defined as

$t_i < t_j$	prediction	x(-)
$t_i = t_j$	filtering	x(+)
$t_i > t_j$	smoothing	x(s)

3.1

The three types of the filtering problem are illustrated in Figure 3.1.

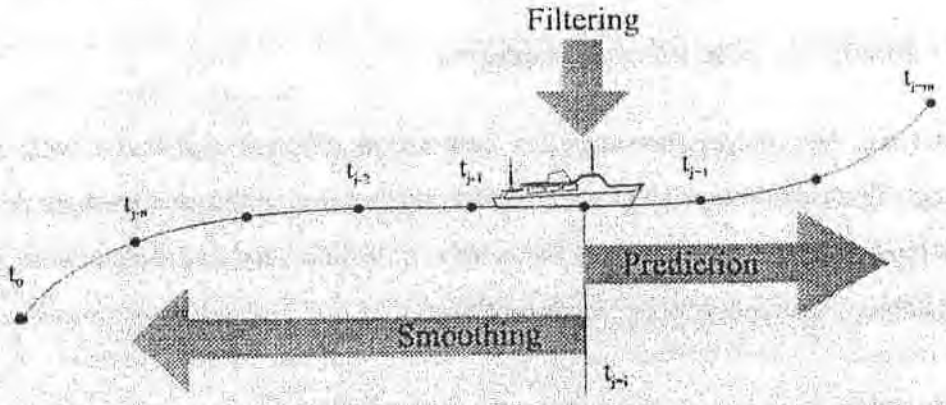

Figure 3.1: Predicting, filtering and smoothing

3.1.2 Kalman filtering versus Simple Least Squares

Kalman filtering has the following specific advantages over simple 'epoch by epoch' least squares and it is in order to exploit these fully that Kalman filtering is selected as the basic stochastic process for most offshore positioning applications.

1. Simple least squares treats each epoch independently. This means that it does not use knowledge of the motion of the system. Often, and especially in seismic work, it is possible to make a very accurate prediction of where the network will be at any epoch using just the previous position and the estimated configuration motion. Not to use this 'knowledge of motion' is effectively throwing away information and must lead to poorer quality results than those obtainable from a properly tuned Kalman filter. In the past (and sometimes today) poorly tuned filters were used and in this case results might be worse - simply because the system motion may have not been well determined and/or not used properly in the estimation process. So simple least squares is a safe option - but it does not have the potential accuracy of Kalman filtering. The challenge, of course, is to tune the filter properly in real time - and the fact that some have failed to do this in the past has led to Kalman filtering gaining a poor reputation in some circles.
2. The use of a Kalman filter for a highly complex seismic configuration enables a rigorous computation of precision and reliability measures such as error ellipses and

marginally detectable errors respectively, (Cross et al, 1994a). If a step-by-step approach is adopted (such as curve fitting the compass data followed by fitting the results to the acoustics and then to the navigation data) it is almost impossible to compute these measures.

3. Due to its ability to predict the network, a Kalman filter is a far more powerful tool than simple least squares for quality control. Much smaller outliers and biases can be found by Kalman filtering than by simple least squares. It is, however, recommended that, where possible, simple least squares also be carried out at every epoch in order to identify (and correct or remove) the larger outliers. This is because Kalman filtering can be rather time-consuming from a computational point of view and any initial cleaning that can be done by other methods will increase its efficiency.
4. Kalman filtering is able to solve for small biases that will remain in the data if only an epoch by epoch method is used - such as drifts in gyros and (C-O)s in terrestrial (shore-based) ranging systems. These look like noise in simple least squares and can easily go undetected. A lot can be learnt by looking at the time variation of the data. Of course, in principle this could be done in simple least squares by analysing time series of residuals but it would be hard to do this in real time - and hard to feed back any findings into the system.
5. Because it can determine and use the system motion, Kalman filtering is able to use observations that do not completely define the system - i.e. GPS data from just two satellites could be used to update a vessel position. Of course, long periods of such data would lead to a significantly degraded result.
6. A Kalman filter can accept data as and when it is measured. With simple least squares, data has to be reduced to a specified epoch. Therefore, a Kalman filter can cope well with data arriving as a more or less continuous stream.
7. The Kalman filter regime is highly suited to the mixing of varied data types. For instance Celik and Cross, (1994) show that when poor satellite geometry leads to poor positions in a DGPS-only solution, the introduction of data from a gyro carried by the vessel can make a major improvement. It would not be possible to combine these data types in simple least squares - because for an individual epoch the gyro does not give any positional information.

3.2 THE KALMAN FILTER MATHEMATICAL MODELS

The implementation of the Kalman filter requires the specification of two mathematical models. The measurement, primary or functional model that relates the state vector parameters to the measurements, and the dynamic, secondary or kinematic model that relates the parameters at epoch t_{i-1} to those at a later epoch t_i.

3.2.1 The Measurement Model

In order to implement a Kalman filter the minimum number of individual and determinable parameters (or unknowns) necessary to describe the complete system must be first defined - this is known as the state vector. The measurement model is nothing but a mathematical representation of the underlying physical and geometric relationships between the measured quantities and the state vector parameters. Therefore, if $\mathbf{l}_1$, $\mathbf{l}_2$, ..., $\mathbf{l}_i$ are denoted as the observation vectors, and $\bar{\mathbf{x}}_1, \bar{\mathbf{x}}_2, \ldots, \bar{\mathbf{x}}_i$ are denoted as the true values of the system parameters at times t_1, t_2, ..., t_i respectively, the measurement model can be written as

$$F_1(\bar{\mathbf{x}}_1) = \bar{\mathbf{l}}_1 \quad \text{at time event } t_1$$
$$F_2(\bar{\mathbf{x}}_2) = \bar{\mathbf{l}}_2 \quad \text{at time event } t_2$$

or more generally

$$F_i(\bar{\mathbf{x}}_i) = \bar{\mathbf{l}}_i \quad \text{at time event } t_i \qquad 3.2$$

In most surveying applications the observation equations, which constitute the measurement model, are not linear functions of the state vector parameters. The linerised form of a non-linear measurement model $F(x) = l$ is given by

$$A_i x_i = b_i + v_i \qquad 3.3$$

where

A_i is the design matrix
x_i is the correction to the provisional value of the filtered state vector, $\tilde{x}_{i(+)}$
b_i is the 'observed - computed' vector, given by $l_i - F_i(\tilde{x}_{i(+)})$
v_i is the state vector residuals

The filtered state vector $\hat{x}_{i(+)}$ is computed iteratively until there is no significant change in the provisional state $\tilde{x}_{i(+)}$.

The measurement model in most surveying problems will not be sufficient to solve for all parameters of the state vector. Usually, in order the system to solve for velocity and acceleration terms the implementation of a dynamic model is required since these are related directly with the dynamics of the system.

3.2.2 The Dynamic Model

The dynamic model describes state changes with time as a result of the system noise. It essentially provides a functional relationship that relates the state vector elements between two subsequent epochs, and hence can be expressed as

$$F_{i-1,i}(\bar{x}_{i-1}, \bar{x}_i, t_{i-1}, t_i) \qquad 3.4$$

where

$\bar{x}_{i-1}$ is the true state vector at time t_{i-1}
$\bar{x}_i$ is the true state vector at time t_i

The discrete linearised form of this expression is given by

$$x_i = M_{i-1}x_{i-1} + y_{i-1} \qquad 3.5$$

where

M_{i-1} is the transition matrix from time t_{i-1} to time t_i

y_{i-1} is the dynamic model noise from time t_{i-1} to time t_i

The vector y_{i-1} it is practically expressed by the product Tg where g consists of the quantities that cause the dynamic model to be incorrect, i.e. the driving noise of the system. T is a coefficient matrix chosen such that the product Tg describes the effect of the driving noise on the state elements. Therefore Equation 3.5 becomes

$$x_i = M_{i-1}x_{i-1} + T_{i-1}g_{i-1} \qquad 3.6$$

3.2.2.1 The Polynomial Dynamic Model

Several different types of dynamic models can be used to represent the dynamics of a system varying with time. For instance Cross and Pritchett (1986) refer to the 'polynomial model', the 'differential model' and the 'model with deterministic forcing function'. However, the first one is the most well known and widely used in offshore positioning applications, and therefore this is discussed here in detail.

It is assumed that x(t) is a continuous process. If x(t) is then expanded using Taylor's theorem, this for a later time $t+\delta t$ reads

$$x(t+\delta t) = x(t) + \dot{x}(t)\delta t + \ddot{x}(t)\delta t^2/2 + \dddot{x}(t)\delta t^3/6 + \cdots \qquad 3.7$$

In this equation the single, double and triple dots represent the first, second and third defferentials of x(t). Application of the Taylor's expansion on the $\dot{x}(t)$ and $\ddot{x}(t)$, assuming that these are also continuous functions of time, yields

$$\dot{x}(t+\delta t) = \dot{x}(t) + \ddot{x}(t)\delta t + \dddot{x}(t)\delta t^2/2 + \cdots \qquad 3.8$$

$$\ddot{x}(t+\delta t) = \ddot{x}(t) + \dddot{x}(t)\delta t + \cdots \qquad 3.9$$

Combining Equations 3.7, 3.8 and 3.9 in a matrix notation can be written as

$$\begin{bmatrix} x \\ \dot{x} \\ \ddot{x} \end{bmatrix}_i = \begin{bmatrix} 1 & \delta t & \delta t^2/2 \\ 0 & 1 & \delta t \\ 0 & 0 & 1 \end{bmatrix} \begin{bmatrix} x \\ \dot{x} \\ \ddot{x} \end{bmatrix}_{i-1} + \begin{bmatrix} \delta t^3/3 \\ \delta t^2/2 \\ \delta t \end{bmatrix} [\dddot{x}]_{i-1} \qquad 3.10$$

In the case when the state vector represents the position and motion elements of a moving vessel, then x(t) denotes the position of the vessel whilst $\dot{x}(t)$ and $\ddot{x}(t)$ represent the velocity and acceleration components. The rate of change of the vessel's acceleration $\dddot{x}(t)$ is then a stochastic quantity representing the driving noise of the model g. The analogy between Equations 3.10 and 3.6 is obvious.

3.2.3 The Stochastic Models

In order to implement a Kalman filter two stochastic models have to be specified. These are invariably in the form of covariance matrices and they describe the precision of the observations C_l and the dynamic model respectively, i.e. they describe the quality of the measurements and how well the model describes reality. For a dynamic model of a polynomial type, the stochastic model can be derived by applying the Gauss' propagation of error law at the second half of Equation 3.6. Therefore the covariance matrix of the dynamic model reads

$$C_y = T C_g T^T \qquad 3.11$$

where C_g is the covariance matrix of the driving noise parameters g - in most cases diagonal.

Hence, from Equations 3.6, 3.10 and 3.11 it follows that the covariance matrix of the dynamic model for the example of a moving vessel can be written as

$$C_y = \begin{bmatrix} \delta t^3/6 & 0 \\ 0 & \delta t^3/6 \\ \delta t^2/2 & 0 \\ 0 & \delta t^2/2 \\ \delta t & 0 \\ 0 & \delta t \end{bmatrix} \begin{bmatrix} \sigma_E^2 & 0 \\ 0 & \sigma_N^2 \end{bmatrix} \begin{bmatrix} \delta t^3/6 & 0 & \delta t^2/2 & 0 & \delta t & 0 \\ 0 & \delta t^3/6 & 0 & \delta t^2/2 & 0 & \delta t \end{bmatrix} \quad 3.12$$

where σ_E and σ_N are the standard deviations of the rate of change of the vessel acceleration's in either direction.

Correct specifications of these stochastic models is essential for both the proper 'tuning' of the filter and its capability to produce accurate quality (precision and reliability) measures (Salzman, 1993). The tuning of the filter refers, in essence, to the relative sizes of the elements of the observation and model covariance matrices. By decreasing the variances (increasing the weights) of the observations, the final filter estimates can be made to fit the observations more closely - but with the danger of small observational errors appearing as obviously impossible vessel manoeuvres. Conversely decreasing the variances of the dynamic model leads to too smooth a final answer and one that cannot react quickly to rapid changes in the true track of the vessel and of the hardware being towed. Such situations are well-known in practice and are evidenced, for instance, by a ship's track continuing to be shown as straight long after all on board are well aware that a turn has been made.

In mixed measurement systems it is also necessary to carefully consider the relative sizes of the elements within the covariance matrix of the observations. For instance, in a 3D seismic network, by selecting the elements appropriately it would be easy, for instance, to make the final results fit the compass data very closely and virtually ignore the acoustics, or vice versa.

Although it is the relative size of these covariance matrices that is critical to the fidelity of the filter, it is their absolute size that drives the computed covariance matrices of the predicted and final filter estimates. Too small covariance matrices will lead to over-

optimistic quality measures, and vice versa. Hence the problem is one of determining both relative and absolute sizes of the elements of the covariance matrices.

The correct practical approach to the solution of this problem is a matter for on-going research in several centre. Celik and Cross (1994), for instance, have suggested an approach whereby the standard deviations of the variance observation types are first determined by independent study (e.g. epoch by epoch network adjustment of acoustic ranges and simple curve fitting to the compasses). These values are then considered 'fixed' and the elements of the covariance matrix of the dynamic model are tuned until (on average) the correct number of rejections is made during the analysis of the innovation sequence. Certain model statistics are then used to scale the overall sizes of both matrices. This approach is relatively straight forward in the case of a seismic spread because the system is so well behaved (vessels sailing straight courses in calm seas). Much more research is, however, still needed in this area.

3.3 THE KALMAN FILTER ALGORITHMS

3.3.1 The Kalman Filter Principles

The derivation of the Kalman filter equations as was initially proposed by Kalman, (1960) is based on the maximum likelihood criterion (Cross, 1983; Mood and Graybill, 1963; Thompson, 1969). However, when observation and dynamic model errors are assumed to be normally distributed, Kalman filter equations can be derived from the standard least squares requirement. Consequently, the Kalman filter can be described as an optimal filter estimator which minimizes the quadratic form of the mean square estimation error given by (Cross, 1987)

$$v_{i-1}^T C_{\hat{x}_{i-1}}^{-1}(+) v_{i-1} + v_i^T C_{l_i}^{-1} v_i + y_{i-1}^T C_{y_{i-1}}^{-1} y_{i-1} \qquad 3.13$$

where $C_{\hat{x}_{i-1}}(+)$ is the covariance matrix of the filtered state vector.

In the 'real world' it is very likely that correlation is present in the Kalman filter models. In practice three different types of correlation can be considered (Roberts, 1993)

A. Correlation between the measurement noise at successive epochs.
B. Correlation between the system disturbances at successive epochs.
C. Correlation between the measurements and the system disturbances over a sample period.

Cases A and B are more likely to prevail in practice due to internal processing mechanism in the measurement systems (case A), and due to inadequate approximation of the system dynamics (case B). These types of correlation is usually referred to as time correlated noise. The third type of correlation refers to the type of correlation between the two models. In certain cases it is possible that the system disturbances have some effect on the measurements, e.g. pitch, roll and heave may have some impact on the observations provided by satellite or terrestrial measurement system. The

interested reader is referred to Salzmann, (1993) for a more detailed discussion of the matter.

In the formulation of the standard Kalman filter equations, a basic assumption is that these three types of correlation are eliminated. Therefore, following this assumption, the statistical models for the Kalman filter can be defined as (Roberts, 1993; Gao et al, 1992)

$$E(v_k v_i) = \begin{cases} C_l & i = k \\ 0 & i \neq k \end{cases} \qquad 3.14$$

$$E(y_k y_i) = \begin{cases} C_y & i = k \\ 0 & i \neq k \end{cases} \qquad 3.15$$

$$E(y_k v_i) = 0 \qquad 3.16$$

3.3.2 The Prediction Equations

In the prediction stage of the estimation process the state vector parameters are computed at a future time at which the states are required without the use of the observations, by the equation

$$\hat{x}_i(-) = M_{i-1}\, \hat{x}_{i-1}(+) \qquad 3.17$$

in which the symbol $\wedge$ denotes an estimated quantity. The symbols (-) and (+) following a vector or matrix denote the value of that vector or matrix at the instant in time before and after a measurement update respectively. In Equation 3.17 the residuals of the dynamic model y_{i-1} do not appear since they are unknown and therefore assumed to be equal to zero.

The covariance matrix of the predicted state vector is obtained by applying the Gauss' error propagation law, and hence

$$C_{\hat{x}_i}(-) = M_{i-1} C_{\hat{x}_{i-1}}(+) M_{i-1}^T + C_{y_{i-1}} \qquad 3.18$$

where matrix $C_{y_{i-1}}$ is computed using Equation 3.11. Both Equations 3.17 and 3.18 require initial values which can be obtained in a rather simple way by applying a least squares approximation or even by a hand computation dependent on the problem. The nearest the initial values to the 'true' ones, the faster the filter will settle down and the solution tend towards optimality.

3.3.3 The Filtering Equations

Filtering refers to estimating the state vector at the current time, based upon all past measurements. At this stage of the filtering problem both observation and dynamic models are combined to provide an optimal solution of the state vector and its uncertainty matrix. The filtered state vector can be computed from the equation

$$\hat{x}_i(+) = \hat{x}_i(-) + G_i(b_i - A_i \hat{x}_i(-)) \qquad 3.19$$

where G_i is the so-called gain matrix which combines observations and system dynamics to balance the effect of both models on the estimation results and can be computed from

$$G_i = C_{\hat{x}_i}(-) A_i^T \left(C_{l_i} + A_i C_{\hat{x}_i}(-) A_i^T \right)^{-1} \qquad 3.20$$

Finally, the covariance matrix of the filtered state vector is given by

$$C_{\hat{x}_i}(+) = (I - G_i A_i) C_{\hat{x}_i}(-) \qquad 3.21$$

or

$$C_{\hat{x}_i}(+) = (I - G_i A_i)\, C_{\hat{x}_i}(-)\, (I - G_i A_i)^T + G_i C_{l_i} G_i^T \qquad 3.22$$

which has been proved to produce a more stable solution while maintaining symmetry.

3.3.4 The Smoothing Equations

The smoothing process refers to the estimation of the state vector parameters at time t_i such that information prior and later to time t_i is used. Therefore, the smoothed states can be expressed as the weighted mean of the estimated states of a Kalman filter applied both forwards and backwards in time (Napier, 1990). Gelb, (1974) suggests that three types of smoothing may be considered

A. Fixed-interval smoothing, in which the initial and final times of the smoothing interval 0 and T are fixed and the smoothed state is computed at every epoch in the time interval [0, T].
B. Fixed-point smoothing, in which the state estimates are computed at a particular time t_j at every epoch for the time interval [0, T].
C. Fixed-lag smoothing, in which the smoothed states are provided at a time that is a constant delay behind the most recent observation.

The basic equations to implement the fixed-lag smoothing technique may be found in Gelb, (1974), and can be summarized as follows.

If the current epoch is denoted by n then it is assumed that for the current epoch the smoothed and filtered solutions are the same, and therefore

$$\hat{x}_n(s) = \hat{x}_n(+) \quad \text{and} \quad C_{\hat{x}_n}(s) = C_{\hat{x}_n}(+) \qquad 3.23$$

Then for any epoch i backwards, the smoothed state vector and its associated covariance matrix can be obtained from

$$\hat{x}_i(s) = \hat{x}_i(+) + S_{i+1}(\hat{x}_{i+1}(s) - \hat{x}_{i+1}(-)) \qquad 3.24$$

$$C_{\hat{x}_i}(s) = C_{\hat{x}_i}(+) + S_{i+1}(C_{\hat{x}_{i+1}}(s) - C_{\hat{x}_{i+1}}(-)) S_{i+1}^T \qquad 3.25$$

where S_{i+1} is the smoothing matrix given by

$$S_{i+1} = C_{\hat{x}_i}(+) M_i^T C^{-1}_{\hat{x}_{i+1}}(-) \qquad 3.26$$

Obviously the implementation of any smoothing process can be only executed at a post-processing level on board ship or at a processing centre. Interested readers are referred to Gelb, (1974) and Merminod, (1989) for a more detailed discussion on the smoothing processes.

3.3.5 Model Non-linearites

In a strict sense the Kalman filter algorithms, and the equivalent least squares solutions, are based on linear measurement and dynamic models. However, in practice in most geodetic applications, non-linear problems are the rule rather than the exception. To overcome this inherent difficulty, the Kalman filter models are usually approximated by a first order Taylor expansion in which iterations are necessary to obtain less biased estimates. Three types of model non-linearities may be considered (Salzmann, 1993)

A. Non-linear measurement model
B. Non-linear dynamic model
C. Combined non-linear measurement and dynamic model

In geodetic practice almost all applications constitute measurement models with non-linear observation equations. The linearised form, shown in Equation 3.3, is used to provide corrections to the provisional values. The complete form for the filtered state

vector computed at epoch i for the k^{th} iteration for a non-linear measurement model is given by

$$\hat{x}_i^k = \hat{x}_{i(-)} + G_i^{k-1}\left[l_i - \text{comp}(\hat{x}_i^{k-1}(+)) - \partial_x A_i^{k-1}\left(\hat{x}_{i(-)} - \hat{x}_i^{k-1}(+)\right)\right] \qquad 3.27$$

where

$\partial_x A_i^{k-1}$ is the Jacobean matrix of the design matrix A_i^{k-1} computed for the k-1 iteration

$l_i - \text{comp}(\hat{x}_i^{k-1}(+))$ is the 'observed - computed' vector b_i^{k-1}.

At the first iteration the provisional state vector $\hat{x}_i^1$ is computed by

$$\hat{x}_i^1 = \hat{x}_{i(-)} + G_i^0\left[l_i - \text{comp}(\hat{x}_i^0(+))\right] = \hat{x}_{i(-)} + G_i^0\left[l_i - \text{comp}(\hat{x}_{i(-)})\right] \qquad 3.28$$

For systems that are not characterized as highly non-linear, it is not necessary to recompute the design matrix A, the 'observed - computed' vector b, and the gain matrix G at every step. Similarly, the number of iterations k is driven by the amount of non-linearity that contributes to the problem.

In the case of a non-linear dynamic model, the predicted state vector and the transition matrix, as well as the covariance matrix of the dynamic model need to be computed at every epoch. For a dynamic model being a first order non-linear differential equation of the form

$$\dot{x}_i = F(x_i, t) \qquad 3.29$$

Cross, (1990) proposes that the predicted residuals, using a numerical integration, may be computed by

$$\hat{x}_{i(-)} = \hat{x}_{i-1(+)} + \int_0^{\Delta t} \dot{x} dt \qquad 3.30$$

the transition matrix from

$$\frac{\partial F}{\partial x} M = \dot{M} \qquad 3.31$$

and finally the covariance matrix of the dynamic model by

$$C_{y_i} = \int_{t_{i-1}}^{t_i} M_{i-1} C_{y_{i-1}} M_{i-1}^T \, dt \qquad 3.32$$

The derivation of the Equations 3.29 to 3.32 may be found in Cross, (1990). Also on the general issue of non-linearity in least squares and Kalman filtering, the interested reader is referred to Teunissen and Knickmeyer, (1988) and Salzmann, (1993) respectively for a more detailed and mathematically rigorous discussion.

3.4 OTHER FILTERS AND TERMINOLOGY

3.4.1 The Bayes Filter

The Kalman filter algorithms are not the only optimal (in the least squares sense) mathematical procedure used to solve for the state parameters of time-varying problems. Another, slightly less well known, set of equations known as the Bayes filter can be used to produce absolutely identical results to those of the Kalman filter. The only difference between them is in the manner in which the so-called gain matrix is computed. For the derivation of the gain matrix equation involved in the Bayes filter algorithm, the following procedure may be adopted (Gelb, 1974).

Upon substituting Equation 3.20 to 3.21 the covariance matrix of the filtered state vector reads

$$C_{x_i}(+) = C_{x_i}(-) - C_{x_i}(-)\,A_i^T\left(C_{l_i} + A_i C_{x_i}(-) A_i^T\right)^{-1} A_i\, C_{x_i}(-) \qquad 3.33$$

In this expression there is a matrix inversion relationship which states that $C_{x_i}^{-1}(+)$ can be written as

$$C_{x_i}^{-1}(+) = C_{x_i}^{-1}(-) + A_i^T C_{l_i}^{-1} A_i \qquad 3.34$$

The previous expression can be verified by showing that $C_{x_i}(+)\,C_{x_i}^{-1}(+) = I$. Therefore using this result Equation 3.20 becomes

$$\begin{aligned} G_i &= \left(C_{\hat{x}_i}(+)\,C_{\hat{x}_i}^{-1}(+)\right) C_{\hat{x}_i}(-)\,A_i^T\left(C_{l_i} + A_i C_{\hat{x}_i}(-) A_i^T\right)^{-1} \\ &= C_{\hat{x}_i}(+)\left(C_{\hat{x}_i}^{-1}(-) + A_i^T C_{l_i}^{-1} A_i\right) C_{\hat{x}_i}(-)\,A_i^T\left(C_{l_i} + A_i C_{\hat{x}_i}(-) A_i^T\right)^{-1} \end{aligned}$$

Expanding and collecting terms yields

$$G_i = C_{\hat{x}_i}(+)\, A_i^T \left(I + C_{l_i}^{-1} A_i C_{\hat{x}_i}(-) A_i^T\right) \left(C_{l_i} + A_i C_{\hat{x}_i}(-) A_i^T\right)^{-1}$$

and finally

$$G_i = C_{\hat{x}_i}(+)\, A_i^T\, C_{l_i}^{-1} \qquad 3.35$$

Expression 3.35 provides the gain matrix for the Bayes filter algorithm while the covariance matrix of the filtered state vector can be obtained directly from Equation 3.34

$$C_{\hat{x}_i}(+) = \left(C_{\hat{x}_i}^{-1}(-) + A_i^T C_{l_i}^{-1} A_i\right)^{-1} \qquad 3.36$$

The computation of the gain matrix in the Bayes filter involves an inversion of a matrix whose size is equal to the number of parameters in the state vector, whilst in the Kalman form an inversion of a matrix whose size is equal to the number of observations is required. Therefore, if a large number of observations (more than the number of states) are involved within a computation process then it is more convenient to use the Bayes filter than the Kalman form and vice versa. Positioning of 3D marine seismic surveys is a typical example where the Bayes filter proves more efficient since observations from mixed data sources contribute to a relatively small number of states.

3.4.2 Alternative Forms of Kalman Filters

In the previous sections two different Kalman filter algorithms were presented, the Kalman and the Bayesian forms, which are equivalent and produce identical results. However, alternative forms of these standard equations can be obtained depending on the way they are implemented, and on the models particular characteristics, i.e. whether they are linear and/or correlated. Some of these alternative forms are listed

- *Linearised Kalman filter* - For a non-linear measurement model if no iterations are performed and the value $\hat{x}_1^0(+)$ in Equation 3.28 is equal to $\overline{x}_1$, where $\overline{x}_1$ an externally provided approximate state, the filter is called a linearised Kalman filter.
- *Extended Kalman filter* - For a non-linear measurement model if no iterations are performed and the value $\hat{x}_1^0(+)$ in Equation 3.28 is equal to $\hat{x}_i(-)$ the filter is called an extended Kalman filter.
- *Iterated extended Kalman filter* - For a non-linear measurement model if iterations are performed and the value $\hat{x}_1^0(+)$ in Equation 3.28 is equal to $\hat{x}_i(-)$ the filter is called an iterated extended Kalman filter.
- *Sequential Kalman filter* - If the measurement errors are uncorrelated then the inverse operation involved within the computations may be eliminated by processing the observations sequentially in blocks or one at a time. This technique of filtering is referred as sequential Kalman filtering (Brown and Hwang, 1992).
- *Augmented Kalman filter* - When the observations are time correlated, one way to model the biases that are common to several observations is to include additional states in the functional model. The resultant filter is called an augmented Kalman filter. An orthogonalization approach may be used as an alternative to derive a filter algorithm for time correlated observations (Salzmann, 1993).
- *Adaptive Kalman filter* - An adaptive Kalman filter is one in which a statistical testing procedure is applied in order to eliminate the effect on the state estimates caused by biases in the measurements. This procedure refers to the quality control of the system, and is discussed in Chapter Four.

CHAPTER FOUR

QUALITY MEASURES IN OFFSHORE POSITIONING

4.1 INTRODUCTION

4.1.1 Introduction to Quality Assessment

In any measurement process all observations will invariably be erroneous, however sophisticated their measurement technology might be. Competent sensor calibration and careful measuring procedures are a first defense against observational errors that will further reduce these but not completely eliminate them. Therefore, it is essential to establish how 'good' the measurements are, in order to assess the quality of the results of an estimation process, i.e. to assess the size and nature of any undetected errors that might remain in these. The characteristic nature of the observational errors is usually described as being either random, or biased.

Random errors are by definition unpredictable and unavoidable, caused by small fluctuations in the physical factors that constitute the measurement process (Cross et al, 1994b). Random errors, that are usually small in size, are described by statistics and it can be shown, via the so-called central limit theorem (Cramer, 1946), that they are from a normally distributed population which allows statistical hypothesis to be tested.

Biases can take the form of gross errors, known also as blunders or outliers, and systematic errors. Gross errors (often large in size) are due to erroneous observations on the part of the observer resulting of carelessness or confusion. Systematic errors refer to model misspecifications that follow some physical law and can be described by a mathematical function. This kind of errors can be eliminated by careful sensor calibration and design of the functional and dynamic models.

The term quality measures in surveying is used to determine the correctness and usefulness of a position fix or the overall quality of geodetic network. This encompasses measures of precision and measures of reliability.

Measures of precision are used to indicate the quality of positions with respect to random errors by describing the populations that it is assumed the errors come from. The information that it is used to generate precision analysis is contained in the covariance matrix of the unknown parameters resulting from the implementation of the least square processes. Measures of precision are discussed in this unit in Section 4.2.

As well as being vital to establish how good the results of an estimation process are, it is also necessary to estimate the effect that any undetected bias (here gross error) will have upon the estimated parameters and any quantities derived from them. Measures of reliability are used to determine the presence of outliers in the data. In general reliability is measured by stating the size of the error that might remain undetected with a specified probability (Cross et al, 1994b). Measures of reliability are discussed in detail in Section 4.4.

4.1.2 The Kalman Filter Predicted Residuals

An important role in the process of model testing is played by the predicted residuals or the so-called innovation sequence. The predicted residuals are computed from the difference between the measurements at a particular time and the measured quantities computed from the predicted state of the system. Under normal conditions predicted residuals are 'small' in size and correspond the random fluctuations in the output since all systematic trends are eliminated by the model (Teunissen and Salzmann, 1988). It can be seen that if the model is valid predicted residuals are zero mean Gaussian distributed (Kailath, 1968). The predicted residuals at epoch t_i are computed by

$$\hat{v}_i(-) = b_i - A_i\hat{x}_i(-) \qquad 4.1$$

with a covariance matrix given by

$$C\hat{v}_i(-) = Cl_i + A_i C\hat{x}_i(-)A_i^T \qquad 4.2$$

In the case of a non-linear system, which is not rare in surveying, the predicted residuals are given by the initial 'observed - computed' values held in vector b_i.

4.2 MEASURES OF PRECISION

4.2.1 Design Parameters that Effect Measures of Precision

Precision is without doubt the best known and most widely used criterion to describe the quality of position in navigation applications. The covariance matrices of the predicted and filtered state vectors of a Kalman filter computation are themselves measures of precision. Application of the Gauss's propagation of error law to any functions of the state vector estimators is used to provide the precision of the positions or any other parameters of interest.

From the Kalman filter algorithms it is directly evident that measures of precision are dependent on the functional and stochastic models. Changes in the geometrical configuration and the system redundancy (e.g. usually more observations lead to better precision) can affect drastically the precision of the state estimators. Although difficult to quantify, any changes in the dynamic model (e.g. revision of the assumption of a vessel moving with constant acceleration) do have an impact on the estimated precision. Similarly, any changes in the stochastic models have a direct impact on the precision of the state estimates. Improving the precision of the stochastic model of the observations and/or the stochastic model of the dynamic model leads to the precision of the Kalman filter estimators also being improved.

However, it should be stressed, that in most cases it is very difficult to establish a relationship to quantify the effect of any changes in the functional and stochastic models on the precision of the estimation results. This is because, in reality, navigation errors are complex functions of time, with variations in geometry, propagation paths, atmospheric conditions, time of day, instrumentation and other factors (Chevron Training Course, 1992). Moreover, all precision measures assume 'normality' for their associated probability statements. Obviously this assumption is entirely valid only if all biases have been removed from the raw data. This point is, however, detailed in Sections 4.3 and 4.4.

4.2.2 Classification of Precision Measures

A number of different ways have been used to express uncertainty in navigation. In the following sections the most frequently used ways are classified and discussed.

4.2.2.1 Simple Precision Measures

At least two measured lines of position (LOP) are required as a minimum to position a point using terrestrial navigation systems, i.e. Syledis. This can be achieved in several ways, e.g. by making two distance observations, or two angle observations, or a distance and an angle observation, or by measuring two distance differences. The angle of cut between two LOP's is very important because it determines the shape of the probable area where the position fix will occur (Figure 4.1). This principle applies for example to acoustic networks used in 3D seismic surveys. The in-line separation of the acoustic units should be a function of the cable separation. If the in-line separation is insufficient the angles of cut of the acoustic positions will produce distorted error diamonds which in turn degrades the quality of the position fix of the acoustic nodes.

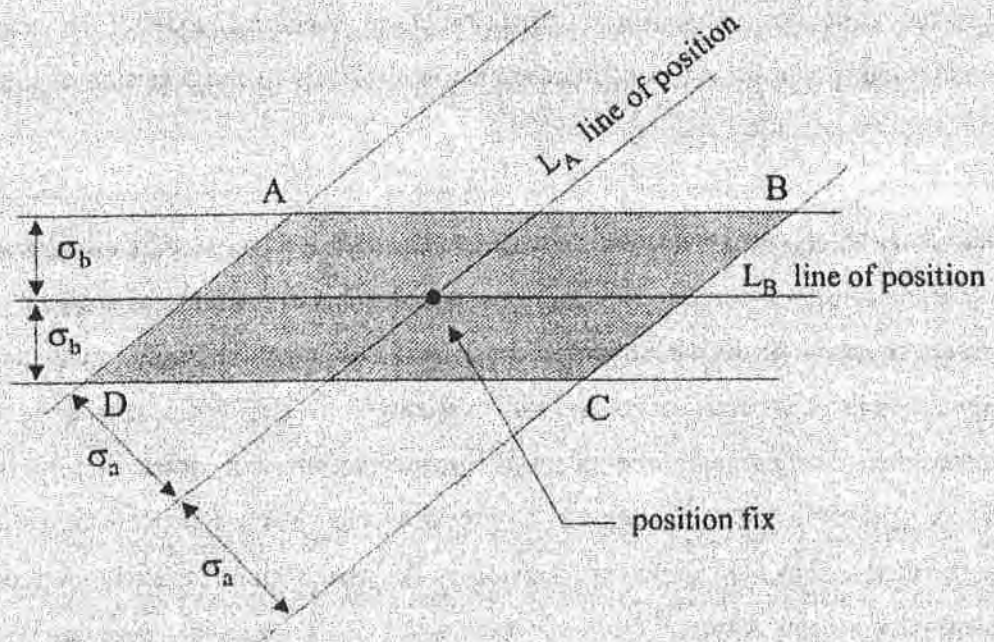

Figure 4.1: The error diamond

4.2.2.2 Measures Based on the Covariance Matrix

Following a Kalman filter computation there are several covariance matrices that can be estimated, from which precision information can be obtained. Various authors, including Cross (1983), describe the useful information that can be derived from the covariance matrix of the state vector parameters $C_{\hat{x}}$, in which the diagonal elements represent the variances and the off-diagonal elements the covariances. The covariance matrix of a n-dimensional position fix is then computed using the Gauss' propagation of error law, unless the unknown parameters themselves represent the estimated positions.

Standard deviation

Commonly the precision of a position fix is measured in terms of a standard deviation. This can be simply derived by taking the square root of the diagonal elements of the covariance matrix of the associated positions. Standard deviation describes the spread of the random errors remaining in any component of a position. When a normal distribution is adopted as a reference, standard deviation represents probability of *one sigma* or a 68% confidence level. In order to determine the 95% confidence level these values must be multiplied by 1.96. It is important to understand that standard deviation refer to one-dimensional errors, such as latitude or longitude, and therefore it should be carefully used when it represents the n-dimensional problem (Mertikas, 1985).

Distance root-mean-square error or drms

The distance root-mean error for a two-dimensional position fix is defined as the square root of the sum of its positional variances, that is

$$d_{rms} = \sqrt{\sigma_x^2 + \sigma_y^2} \qquad 4.3$$

The probability associated with $1\,d_{rms}$ value ranges between 63.2% and 68.3% while for $2\,d_{rms}$ it ranges between 95.4% and 98.2%. The degree of confidence that can be placed on it depends on the correlation between the elements of the covariance matrix

(Forssel, 1991). Although d_{rms} has the advantage of representing a range of confidence with a single value the correlation information available is ignored.

Root-mean-square error or ε_{rms}

This is a measure of an average linear error, which for a single point is given by

$$\varepsilon_{rms} = \sqrt{\frac{\sigma_x^2 + \sigma_y^2}{2}} \qquad 4.4$$

Similar to d_{rms}, the probability associated with ε_{rms} depends on the correlation between the variances of the position fix and the appropriateness of the Gaussian distribution.

Error ellipse

It is very often necessary to know how the errors are distributed in directions other than those obtained from the covariance matrix of a position fix, usually northings and eastings. The horizontal error ellipse is very often used for this purpose.

The horizontal error ellipse is computed from the rotated covariance matrix of the covariance elements given usually in a local topographic system, based on the equation

$$\begin{bmatrix} p \\ q \end{bmatrix} = \begin{bmatrix} \cos\psi & \sin\psi \\ -\sin\psi & \cos\psi \end{bmatrix} \begin{bmatrix} x \\ y \end{bmatrix} \qquad 4.5$$

where ψ determines the orientation of the two axes of the ellipse, given by

$$\psi = \frac{1}{2}\tan^{-1}\left(\frac{2\sigma_{xy}}{\sigma_x^2 - \sigma_y^2}\right) \qquad 4.6$$

Application of the Gauss's propagation of error law to Equation 4.5 leads to the following equations which describe the maximum and minimum variances of the position fix in the directions p and q respectively.

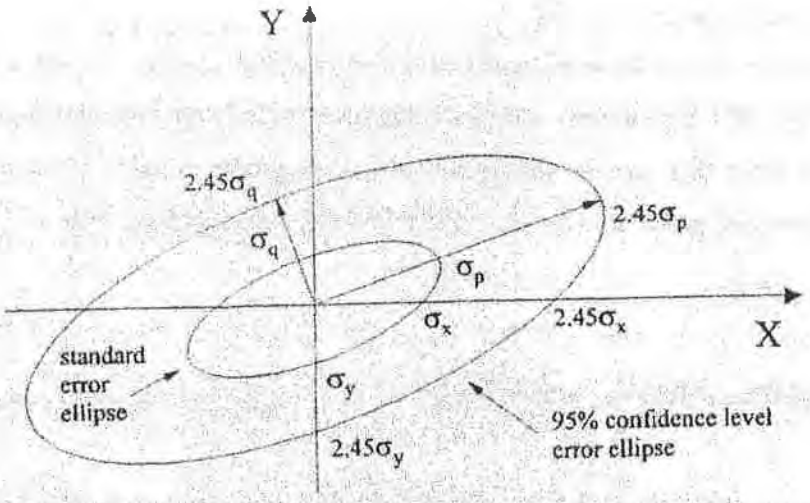

Figure 4.2: Standard error ellipse (one sigma) and 95% error ellipse

$$\sigma_p^2 = \cos^2\psi\,\sigma_x^2 + \sin^2\psi\,\sigma_y^2 + 2\cos\psi\,\sin\psi\,\sigma_{xy} \qquad 4.7$$
$$\sigma_q^2 = \sin^2\psi\,\sigma_x^2 + \cos^2\psi\,\sigma_y^2 - 2\cos\psi\,\sin\psi\,\sigma_{xy}$$

The square root of these values represent the length of the semi-major and semi-minor axes of the ellipse, i.e. the directions of the lowest precision (highest deviation) and the highest precision (lowest deviation) respectively. The estimates given by Equation 4.7 describe the one sigma error ellipse at confidence level 39.4%. The UKOOA recommendation requires positional standard ellipses at the 95% confidence level (Cross et al, 1994a). To obtain the error ellipse at a 95% precision level these values should be multiplied by a factor of 2.447 (Figure 4.2).

4.2.2.3 Radial Precision Measures

In many applications it is more convenient to use circles, instead of ellipses, with particular probability confidence levels to quantify precision. This practice originated from military applications in bombing (Mertikas, 1985; Zacks and Solomon, 1975). The most common of these used in navigation applications are discussed here.

Circle Error Probable or CEP

Circular error probable refers to the radius of the circle inside of which there is a 50% probability of being located, that is, the radius of a circle containing 50% of all possible position fixes that can be obtained with a navigation system. The most accurate approximation given to compute CEP, for σ_p / σ_q greater than 0.3, is given by (Forssel, 1991)

$$CEP_{0.5} = 0.615\sigma_q + 0.562\sigma_p \qquad 4.8$$

In order to obtain the radius of error probability at a different level of confidence the equation is

$$CEP_\alpha = CEP_{0.5}\sqrt{\frac{-\ln(1-\alpha)}{\ln 2}} \qquad 4.9$$

Although circles are more easily understood it is becoming prevalent to use $2\,d_{rms}$ rather than $CEP_{0.5}$ because the probability of 50% attached to CEP is too small.

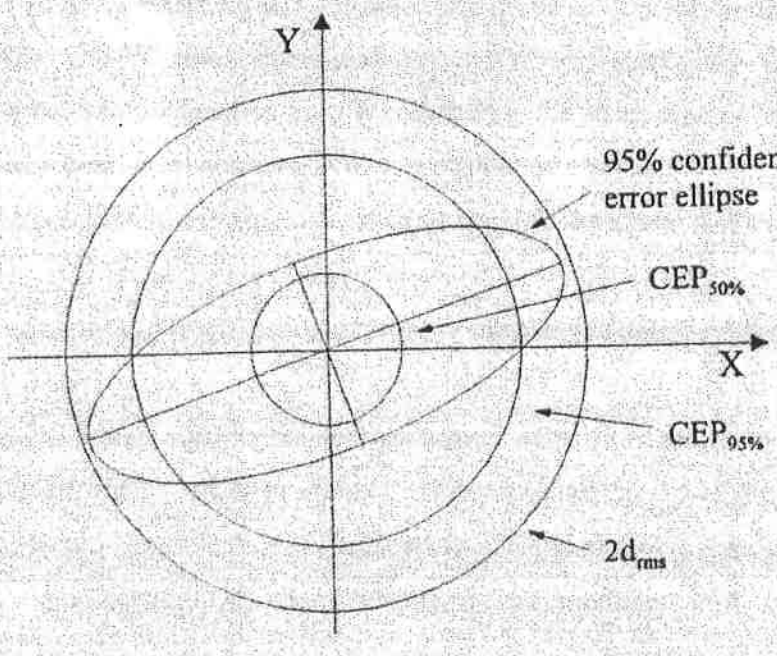

Figure 4.3: The error ellipse and circles of equivalent probability

Geometric Mean Error or GME

Geometric mean error is defined as the radius of a circle by assuming that the circle of radius GME has the same area as the 50% error ellipse (Mertikas, 1985). Similarly, circles of radius GME at a different level of confidence can defined.

Obviously, all these estimates of precision can be extended to a three dimensional position fix. Figure 4.3 provides a geometrical representation of several precision measures referred to a single position fix in two dimensions.

4.3 STATISTICAL ANALYSIS TO QUANTIFY KALMAN FILTER ESTIMATED PARAMETERS

Kalman filter estimates have the advantage of being least squares estimators, which can be shown (Cross, 1983) to be the best (in the minimum variance sense) within the complete class of linear unbiased estimators. It is important to realize, however, that any biases in the observations will invalidate the estimation results and, therefore, any conclusions based on them. Hence, there is a real need to have ways to confirm that the functional and stochastic models used to compute the precision and reliability measures are indeed correct. Statistical testing procedures are used to determine whether or not the assumptions made in the quality assessment process are correct. However, it should be stressed that test statistics are not quality measures and therefore statistical testing is not formally part of the quality assessment process (Cross et al, 1994a).

A simple statistical hypothesis is a statement about the probability distribution of a set of parameters. The term null hypothesis H_o, is generally used to describe the hypothesis that is to be tested, for example, the statement that the probability distribution of random errors is normal. Tested against the null hypothesis is an alternative hypothesis which takes the completely opposite view. Therefore, in the above mentioned example the statement is, the random errors do not belong, or cannot be explained by, the normal distribution.

When performing a statistical test, it is possible that one of two kinds of error may be made (Cross, 1983)

1. The null hypothesis can be rejected when it should be accepted. This is termed as a Type I Error, and the probability of making such an error is called level of significance of the test and is often assigned the Greek letter α.
2. The null hypothesis can be accepted when it should be rejected. This is termed as a Type II Error, and the probability of it occurring is usually denoted by the Greek letter β. The quantity $1-\beta$ is usually referred as the power of the test.

In practice truly random errors follow certain rules. In surveying it is assumed that all random errors are from a normally distributed population. An illustration of the two-sided probability α, of rejecting good data derived from a population following a standard normal distribution with zero mean, and the one-sided probability of accepting outlying data β, derived from a population following a standard normal distribution with no zero mean, is given in Figure 4.4. Choices of α and β are arbitrary. Varying α will affect the amount of data accepted and therefore the results obtained. In contrast the choice of β is related with the chance to accept bad data, and therefore, affects only any statement that can be made regarding the quality of the data and not the estimation result. Choices of 1% and 20% for α and β respectively are commonplace in offshore positioning practice (Cross et al, 1994a), however, a more detailed discussion on the choices of α and β may be found in Salzmann, (1993).

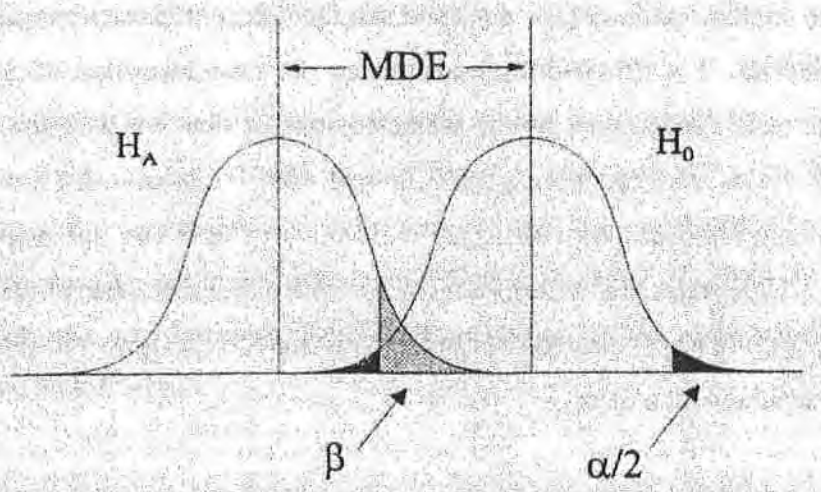

Figure 4.4: Probability of type I and II errors under the null H_0 and alternative hypothesis H_A for a normal distribution.

As pointed out in Section 4.1.2, the predicted residual naturally presents itself as a tool for model validation of the Kalman filter due to its well defined statistical properties under the null hypothesis, and therefore it forms the basis for all statistical testing. The only uniform approach that can be used for the statistical testing of the Kalman filter is that developed by the Delft Geodetic Computing Centre. This is based on the so-called B-method, a testing procedure for geodetic networks developed by Baarda (1968). The

procedures are for the detection, identification and adaptation (DIA) of the overall model (Salzmann, 1995). These can be described as

1. The detection step of the DIA procedure concerns in checking the overall validity of the null hypothesis. Therefore the tests associated with this phase are used for detecting possible unspecified biases in H_o.
2. If the null hypothesis is rejected in the detection step, i.e. a bias is detected, then in the identification step various alternative hypotheses are examined to identify the most likely error source, i.e. identify the outlying observation(s).
3. If a bias is detected and identified, the real time operation of the filter requires that corrective action is taken immediately. The adaptation phase of the DIA procedure is meant to eliminate the effect on the state estimates caused by a bias identified in the previous step.

In the implementation of the detection and identification phases two kind of tests can be considered. Local model tests are carried out on information of a particular epoch. These tests depend only on the predicted state at time equal to the time of incoming observations and can be executed in real time. Global tests are used to test for unmodelled global trends that may build up with time and not detected by the local tests. These tests are performed using information of a number of epochs. In this case better results may expected since smoothing is involved, however, global tests can only be executed with a delay.

Further details regarding the specific tests for the detection and identification of biases are given in Appendix B. However, readers interested for a more concise discussion are referred to Salzmann (1995), Teunissen (1990a and 1990b), Teunissen and Salzmann (1988) and Xiang (1995).

4.4 MEASURES OF RELIABILITY

Reliability analysis is used to determine the presence of blunders in the raw data. It is a measure of the ease with which outliers can detected and identified. Moreover reliability is used to determine what is the effect of any undetected outlying observations on the estimation results, i.e. the state vector elements and position-fix coordinates.

4.4.1 Internal Reliability

The sensitivity of a position fix to detecting outliers was defined by Baarda as internal reliability. This is quantified by means of a statistical quantity called the Marginally Detectable Error.

4.4.1.1 The Marginally Detectable Error

Suppose that at epoch i the vector of m observations used in a Kalman filter computation is denoted by l_i. Then the measurement model is given by

$$l_i = A_i x_i + \varepsilon_i \qquad 4.10$$

The null hypothesis for observations with normally distributed errors ε_i can be specified as

$$H_0: \; l_i \sim N(A_i x_i, C_{l_i}) \qquad 4.11$$

If one of the observations is assumed to be biased, of size ∇_i, the alternative hypothesis can be specified as

$$H_A: \; l_i \sim N(A_i x_i + e_i \nabla_i, C_{l_i}) \qquad 4.12$$

where $e_i = [0\ 0\ 0\ \cdots\ 1\ \cdots\ 0\ 0\ 0]^T$, is the vector defining the assumed bias in the observations at epoch i, and therefore the biased elements of vector e_i equal unity; the remaining are zero.

Based on the predicted residuals the null and alternative hypothesis can be written as

$$\begin{aligned} H_0 &: \ v_i \sim N(0, Cv_i) \\ H_A &: \ v_i \sim N(e_i \nabla_i, Cv_i) \end{aligned} \qquad 4.13$$

where the symbol (-) following the matrices and vectors computed at the predicted step is omitted for simplicity. The appropriate test statistic for testing H_0 against H_A (Salzmann, 1993) is given by the expression

$$\underline{T}_i = \underline{v}_i^T C_{v_i}^{-1} e_i \left(e_i^T C_{v_i}^{-1} e_i \right)^{-1} e_i^T C_{v_i}^{-1} \underline{v}_i \qquad 4.14$$

which can be interpreted as reject H_0 in favour of H_A if $T \geq k_a$, where k_a is the critical value. The critical value of the test can be obtained from the distribution of the test statistic given by Equation 4.14 which can be shown that follows a X^2 distribution. Equation 4.14 under the alternative hypothesis H_A, i.e. $\underline{v}_i = e_i \nabla_i$, becomes

$$\underline{T}_i = \left(\nabla_i^T e_i^T \right) C_{v_i}^{-1} e_i \left(e_i^T C_{v_i}^{-1} e_i \right)^{-1} e_i^T C_{v_i}^{-1} \left(e_i \nabla_i \right) \qquad 4.15$$

and finally

$$\underline{T}_i = \nabla_i^T e_i^T C_{v_i}^{-1} e_i \nabla_i \qquad 4.16$$

The product in Equation 4.16, the so-called noncentrality parameter, is by definition of the test statistic, equal to the square root of the amount that the mean of the population of the normal distribution of the 'good data' (not outlying) is shifted under the alternative hypothesis H_A. Inversely, for a given set of values of the significance of the

test α, and power of the test 1-β the non-centrality parameter $\underline{T}$ (or δ^2 dependent on the notation) is fixed, and the measure of the bias that can be detected in the observation is given by the equation

$$\nabla_i = \frac{\delta}{\sqrt{e_i^T C_{v_i}^{-1} e_i}} \qquad 4.17$$

A MDE is defined as the size of the bias given by Equation 4.17, viz. it is the error in the observation that can be detected by a statistical test for a certain level of significance and power of the test. MDE is used as a measure of internal reliability.

Equation 4.17 is associated with a test at time k for a model misspecification with time of occurrence also k. In the case that only one outlier occurs at time k in observation j Equation 4.17 becomes

$$\nabla_i = \frac{\delta}{\sqrt{C_{v_i}^{-1}[j,j]}} \qquad 4.18$$

To compute Equation 4.18 it is necessary to form the inverse of the covariance matrix of the predicted residuals at every epoch. Zinn and Rapatz, (1995) suggest a simpler form in which it is assumed that the predicted residuals are uncorrelated and therefore C_v becomes diagonal matrix. Under this assumption Equation 4.18 can be written

$$\nabla_i = \delta \sigma_{v_i}[j,j] \qquad 4.19$$

where $\sigma_{v_i}[j,j]$ is the standard deviation of the innovation of observation j at epoch i.

4.4.1.2 Design Parameters that Effect Internal Reliability

Internal reliability is a hypothetical measure defined by the significance and power of the test statistic, the geometrical set-up and the stochastic models of the system. Therefore, since it does not depend on actual data, the MDE can be used as a design tool in the same way that the covariance matrix of the estimated parameters, derived from a conventional least squares computation, it is used for network optimization.

More specifically, changes in any one of the following parameters affect the size of the MDE

- *Functional model* - The functional model consists of the measurement model and the dynamic model. Any changes in the number or type of sensors used to compute the network, or changes in the geometry configuration constitute changes in the measurement model. Generally, by increasing the number of sensors the MDEs decrease because the system redundancy is improved. Similarly the better the observational geometry, e.g. not very small or large angles of cut between LOP's, the smaller the MDEs. On the contrary, the effect of changes in the dynamic model is not as easy to predict.
- *Stochastic model* - This is invariably in the form of covariance matrices that describe the precision of the observations and the precision of the dynamic model: the smaller the observational standard deviations, the smaller the MDEs. Similarly, lower system noise results in smaller MDEs.
- *Testing parameters* - It can be seen from Equation 4.17 that an MDE is a function of the non-centrality parameter δ. The value of δ depends on the selection of the values of the testing parameters, i.e. the significance of the test α, and the power of the test $1-\beta$. By increasing α the non-centrality parameter δ decreases and therefore the MDEs decrease. In contrast, by increasing the power of the test $1-\beta$ the non-centrality parameter δ increases and consequently the MDEs increase.

4.4.2 External Reliability

Although internal reliability is important, it is often more practically useful to know what is the effect of any undetected outliers of the size of MDEs on the unknown parameters. From Equation 3.19 and 4.1 it follows that

$$\hat{x}_i(+) = \hat{x}_i(-) + K_i v_i(-) \qquad 4.20$$

Therefore the effect in the state estimates caused by an outlier ∇_{ij}, of the size of the MDE in observation j at epoch i reads

$$\Delta\hat{x}_{ij} = K_i e_{ij} \nabla_{ij} \qquad 4.21$$

where K_i and e_{ij} are the gain matrix and the vector defining the assumed bias in observation j at epoch i. The computation shown in Equation 4.21 is done as many times as there are the observations. $\Delta\hat{x}_i$ are then vectors measures of external reliability. The vector with elements of the largest size is then can be used as a measure of maximum external reliability.

In many cases the state estimates from a Kalman filter computation are used to calculate a vector of parameters $\hat{g}$, i.e. final coordinates or parameters of interest, which is a function of the state estimates $\hat{x}$ of the form

$$\hat{g} = f(\hat{x}) \qquad 4.22$$

The effect of a marginally detectable error in the j^{th} observation on $\hat{g}$ is then given by

$$\Delta\hat{g}_{ij} = J_i \Delta\hat{x}_{ij} \qquad 4.23$$

where J_i is the Jacobean matrix describing the model shown in Equation 4.22 at epoch i.

CHAPTER FIVE

AN INTEGRATED KALMAN FILTER ALGORITHM FOR POSITIONING 3D MARINE SEISMIC NETWORKS

5.1 INTRODUCTION

In Chapter One the various methods and associated problems of positioning a marine seismic network in real-time were discussed. In particular, discussion showed that, due to the demand of better positioning accuracies offshore, driven by the geophysical requirements of the implementation of the 3D method, and due to the expansion of the type and quantity of the survey data collected, integrated positioning systems are coming more and more into use. Moreover, it is evident that the computations of these systems, in order to exploit fully the peculiarities of the dynamic environment in which they operate, are usually performed by means of a Kalman filter.

Chapter Five describes the mathematical basis of a Kalman filter that can, in principle, handle any number of vessels, streamers and guns and any set of observations to produce either real-time or post-processed positions and quality (precision and reliability) measures. It is a filter that can also be used prior to data collection to test the suitability of a proposed set of measurements to meet the positioning quality specifications necessary for the design of new systems.

In the past, the challenge of integrated positioning offshore seismic networks has been discussed rather rarely (Houtenbos, 1989), and only a very limited number of seismic operators have implemented integrated systems into use (Zinn and Rapatz, 1995). Though in all approaches the main objective is the same, i.e. real-time positioning and QC throughout the spread, the proposed algorithm differs from other approaches.

The chapter starts with some definitions related to the various elements involved in a seismic spread and a few remarks about the coordinate systems that are used. Then, what follows is a review of the functional and stochastic models needed for such an approach. Finally, the formulae that were used to compute precision and reliability measures, modified where necessary so that they meet the model requirements, are discussed.

5.2 COORDINATE SYSTEMS

Within a typical seismic configuration there are several sub-systems that are able to move independently of each other, and of the vessel. These include every single float (gun array or any auxiliary reference station) and each streamer (Houtenbos, 1989). Each sub-system must therefore have its own parameters and coordinate system - which must, in turn, be linked by the mathematical model in order to determine the complete configuration. Before defining the various state vector parameters for each one of the configuration subsystems it is necessary to describe their different coordinate systems.

An earth fixed geodetic system, involving latitude and longitude or a map projection system, is used to describe the final positions of all of the points of interest. The vessel and tailbuoys absolute positions, derived by GPS/DGPS or a radio positioning system, will, of course, naturally be in this system but it is not especially convenient for describing the rest of the spread.

For this it is more convenient to use a local topographic coordinate system. This system has its origin at the vessel navigation reference point with the X-axis aligned with the east direction and Y-axis aligned northwards. When necessary the Z-axis is defined as being perpendicular to the XY plane (i.e. upwards) such that the resultant coordinate system is right handed, as in Figure 5.1. It is obvious that this system moves with respect to a geodetic earth system as the vessel's position changes. Also it is clear that, given the relatively short distances (a few kilometre) involved within the network, there will be minimal error in working with the computed distances and azimuths in the XY (horizontal) plane and then using a direct geodetic formulation to determine the coordinates (latitude and longitude) of the points of interest - i.e. the earth is effectively considered to be flat within the region of the seismic spread.

Some of the available observations are made relative to devices fixed on the vessel. For this reason it is necessary to define another coordinate system that is attached to the vessel. The origin of this coordinate system coincides with the navigation reference point. Its y axis is aligned with the vessel's bow-stern direction. Its x axis (starboard)

is in the horizontal plane and perpendicular to the y axis whilst z axis is defined to be perpendicular to xy plane (upwards) - see Figure 5.1.

Finally, in order to estimate the position of any point on each of the streamers, taking into account its distance from the streamer head, l, as a parameter, it is necessary to introduce another local coordinate frame for each streamer in the spread. A set of three dimensional coordinate systems (u, v, z) is therefore defined. Each has its origin at the head of the first active section of the streamer, or any other point of known offset, its u axis aligned with the base course of the cable (as results from the Kalman filter computations) and its v axis perpendicular to the u-axis and pointing to the port side. The z axis is defined such that the resultant coordinate system is right-handed (Figure 5.1).

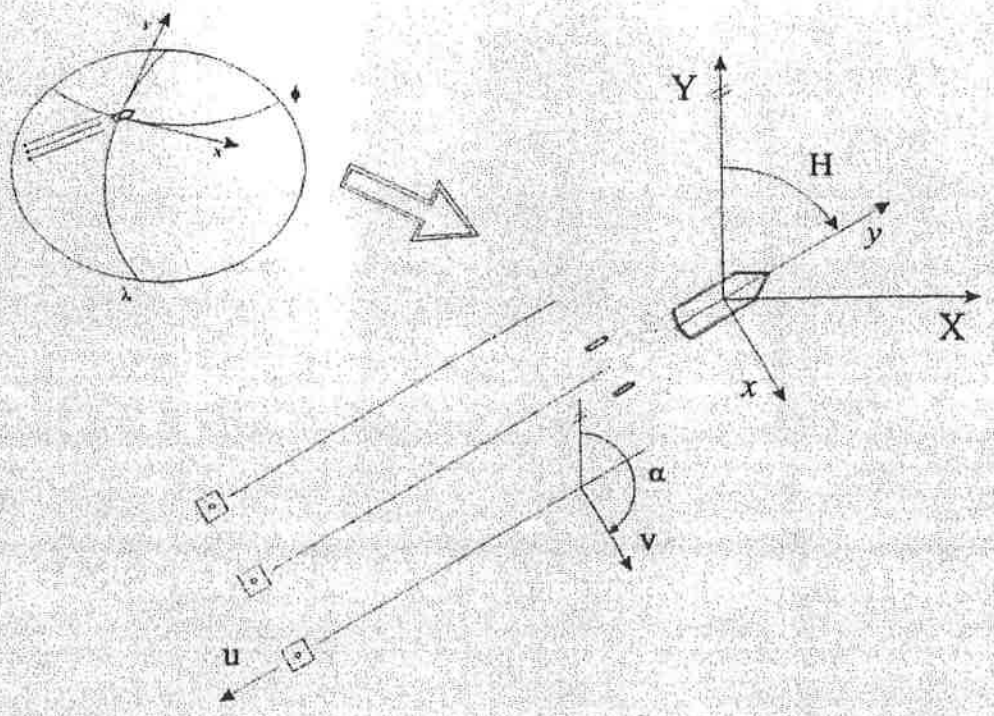

Figure 5.1: Coordinate systems involved in positioning marine seismic networks

In most cases the float nodes involved in a seismic network are not very large structures, towed at relatively small distances from the vessel's stern. Therefore, it is assumed that their orientation coincides with the vessel's heading. As a result, the position of any device fixed on them is reduced to the centre of the float using its nominal coordinates with respect to the centre of the float and the vessel's heading. However, it should be noted that, in an utterly rigorous approach the orientation of each float should be placed in the state vector. In this case there is a need to define another coordinate system such that its origin coincides with the centre of the float and its y axis points to the instantaneous orientation of the float.

5.3 KALMAN FILTER FUNCTIONAL MODELS

5.3.1 State Vector

In Chapter Three it has been shown that the state vector consists, in general terms, of the minimum number of individual (and determinable) parameters (or unknowns) necessary to describe the complete system. In the case of an offshore seismic network the unknowns consist of those which describe the vessel's position and the motion and those which describe the position and motion of each subsystem. In the following, the unknown parameters are classified by subsystem.

Vessel unknowns

The unknown parameters that describe the vessel position and motion are defined to be the instantaneous values of the following elements

φ, λ	the geodetic 'ellipsoidal' coordinates of the ship reference point
$\dot{\varphi}, \dot{\lambda}$	the instantaneous velocity of this point
c	the crab angle, i.e. angle between course made good and vessel's heading (Figure 5.2)

Note that for many navigation applications it would also be necessary to define the acceleration of the vessel in the state vector but the almost straight line motion associated with seismic surveying makes it unnecessary in this case.

Float unknowns

The unknown parameters for any tow points attached to the vessel are also included in the state vector. Tow point positions are defined as position vectors expressed in X, Y coordinates along with their velocity components $\dot{X}$, $\dot{Y}$ with respect to the local topographic coordinate system. It should be stressed here that to date the filter has only been implemented in the XY (horizontal) plane. The (known) Z coordinates of all components, are taken into account by making geometrical 'corrections' to the observations, i.e. observations are corrected to the values they would have had the

whole system been in the XY plane. Also, it is important to note that the unknown coordinates X, Y refer to the centre of the floating arrays. It will usually be necessary to correct observations to these centre points.

Streamer unknowns

The streamer unknown parameters must clearly refer directly to the streamer model. For the purposes of this study a polynomial model has been adopted. Hence, the u, v coordinates of any point on a streamer are given by the following equations

$$u = l \qquad 5.1$$

$$v = c_2 l^2 + c_3 l^3 + \ldots + c_n l^n \qquad 5.2$$

Testing of the integrated algorithm using real data showed that (perhaps not surprisingly) coefficients c_0 and c_1 should be ignored. The polynomial coefficient c_0 must be null since, by definition, v is zero at the head of the cable (i.e. when $l = 0$). Also the c_1 coefficient (which is directly related to the overall orientation of the streamer) is redundant in the state vector since the orientation of the u, v system, the direction angle α, in Figures 5.1 and 5.2, is considered to be an unknown in the system. Therefore, the streamer parameters consist of the polynomial coefficients c_i, the direction angle α of the u axis and the streamer's coordinate reference system origin X, Y along with its velocity components $\dot{X}$, $\dot{Y}$.

The total complete state vector is summarised in Table 5.1. It is evident that the number of states to be estimated for every shotpoint depends on the number of floats and streamers that are utilised throughout the spread as well as on the polynomial order of the streamer model. Hence, for a configuration that consists of m_1 floats, m_2 streamers and for a n-order polynomial, the state vector dimension will be equal to $5 + 4(m_1 + m_2) + nm_2$, which for a typical spread of two sources and three streamers is equal to forty elements. The Kalman filter algorithms can easily provide a solution for a state vector of this size since within typical modern seismic configurations the total number of available observations is well over a hundred per shotpoint.

It is worth noting at this stage that the tailbuoy position does not form part of the state vector. This is because the tailbuoy is treated as a simple extension of the streamer. It would be quite possible to include the tailbuoy in the system as an independent point but it would not then be able to fulfill its primary role of providing overall orientation and scale control for the cable.

As noted in Chapter Two, at the implementation stage of this study, a different streamer model based on a harmonic function has also been considered and tested. The particular characteristics of the selected function as well as the incorporation of this model into the algorithm are given in Chapter Eight.

VESSEL	1	ϕ λ $\dot{\phi}$ $\dot{\lambda}$ c		STREAMER	1	ORIGIN	X_{s1} Y_{s1} $\dot{X}_{s1}$ $\dot{Y}_{s1}$
						ORIENTATION	α_{s1}
						POLYNOMIAL COEFFICIENTS	c_{s11} ⋮ c_{s1n-1}
FLOAT	1	ORIGIN	X_{f1} Y_{f1} $\dot{X}_{f1}$ $\dot{Y}_{f1}$		⋮		
	⋮				m2	ORIGIN	X_{sm2} Y_{sm2} $\dot{X}_{sm2}$ $\dot{Y}_{sm2}$
	m1	ORIGIN	X_{fm1} Y_{fm1} $\dot{X}_{fm1}$ $\dot{Y}_{fm1}$			ORIENTATION	α_{sm2}
						POLYNOMIAL COEFFICIENTS	c_{sm21} ⋮ c_{sm2n-1}

Table 5.1: Unknown parameters - state vector- for one vessel, m1 floats and m2 streamers configuration

5.3.2 Observations

As has already been stated in Chapter One, in a modern marine seismic survey several measurement devices are employed to position the various points of interest throughout the spread. The most commonly used devices include magnetic compasses, laser systems, long, short or ultra short baseline acoustic devices, terrestrial radio ranging systems (e.g. Syledis, Hyperfix, ARGO) and differential navigation systems as GPS

(Chevron Training Course, 1992 and N.C. Kelland, 1994). Regardless of whether the actual observations are measured time or phase differences between any two devices in the network or between any device and any shore or satellite station, basic observation types in this study reduce to slope ranges, bearings and bearing differences and the absolute geodetic position of certain nodes in the network. In particular, observation equations are formed for the following measurements

1. Vessel geodetic position.
2. Vessel gyro.
3. Slant acoustic and laser ranges between vessel, sources, streamers and miscellaneous hardware.
4. Directions between vessel, sources, streamers and other auxiliary assemblies.
5. Float and tailbuoy absolute position.
6. Compass bearings along the streamer.

A more detailed discussion on the devices used and the observations made to locate a marine seismic network may be found in Chapter One.

5.3.3 Observation Equations

Once the different observation types have been specified and the state vector parameters have been explicitly defined, the measurement functional model can be set up in the form of the observation equations. As mentioned in Chapter Three, observation equations are simply mathematical representations of the underlying physical and geometric relationships between the measured quantities and the parameters. Note that this stage of the process is crucial in the sense that any mistakes in the formulation of these equations, even seemingly small, will lead to an incorrect design matrix (the matrix A in Equation 3.3) and small errors in the final solution that, in general will not be easy to detect. Bearing in mind that for the purposes of this study local topographic coordinates have been selected for the computational model, the observation equations for each measurement discussed in Section 5.3.2 can now be presented.

Vessel geodetic position

Since the vessel's geodetic position is itself an unknown, the observation equation can be written as

$$\begin{aligned} \phi_v &= \phi + v_\phi \\ \lambda_v &= \lambda + v_\lambda \end{aligned} \qquad 5.3$$

where

ϕ_v, λ_v are the unknown ellipsoidal coordinates
ϕ, λ are the observed ellipsoidal coordinates of the vessel
v_ϕ, v_λ are the measurement residuals

However, it should be noted that, if the sensor that provides the vessel's position is located sufficiently far away of the navigation reference point it will be necessary to correct the observation to this point using the general formula that given by Equations 5.9, 5.10 and 5.14.

Vessel gyro

The output from the vessel's gyro is essentially the azimuth of the vessel and it can be related, through Figure 5.2, to the velocity of the vessel via the crab angle, c, as follows

$$\tan^{-1}\left[\frac{\dot{E}}{\dot{N}}\right] + c = H + v_H \qquad 5.4$$

or

$$\tan^{-1}\left[\frac{\nu \cos(\phi)\,\dot{\lambda}_v}{\rho\,\dot{\phi}_v}\right] + c = H + v_H \qquad 5.5$$

where

H is the gyro measurement
$\dot{E}$ is the instantaneous easterly velocity of the vessel
$\dot{N}$ is the instantaneous northerly velocity of the vessel
c is the crab angle of the vessel
v_H is the measurement residual of the gyro

and

$$\nu = \frac{a}{\left[1 - e^2 \sin^2(\phi)\right]^{1/2}}, \quad \rho = \frac{a(1-e^2)}{\left[1 - e^2 \sin^2(\phi)\right]^{3/2}}, \quad e^2 = \frac{a^2 - b^2}{a^2} \qquad 5.6$$

with

a is the semi-major axis of the reference ellipsoid
b is the semi-minor axis of the reference ellipsoid

Slant ranges and bearings

The standard observation equations for a measured distance and azimuth between any two nodes, i and j, in the network are given by the following expressions

$$\sqrt{(X_j - X_i)^2 + (Y_j - Y_i)^2 + (Z_j - Z_i)^2} = D_{ij} + v_{D_{ij}} \qquad 5.7$$

$$\tan^{-1}\left[\frac{X_j - X_i}{Y_j - Y_i}\right] = A_{ij} + v_{A_{ij}} \qquad 5.8$$

where

X_i, X_j are the easting components of stations i and j
Y_i, Y_j are the northing components of stations i and j
Z_i, Z_j are the distances of stations i and j from the XY plane.
D_{ij} is the measured distance between stations i and j
A_{ij} is the measured or reduced azimuth between stations i and j

The Cartesian coordinates of the stations i and j are expressed in a different form in accordance to the subsystem to which they refer. Three different cases are considered here (Figure 5.2).

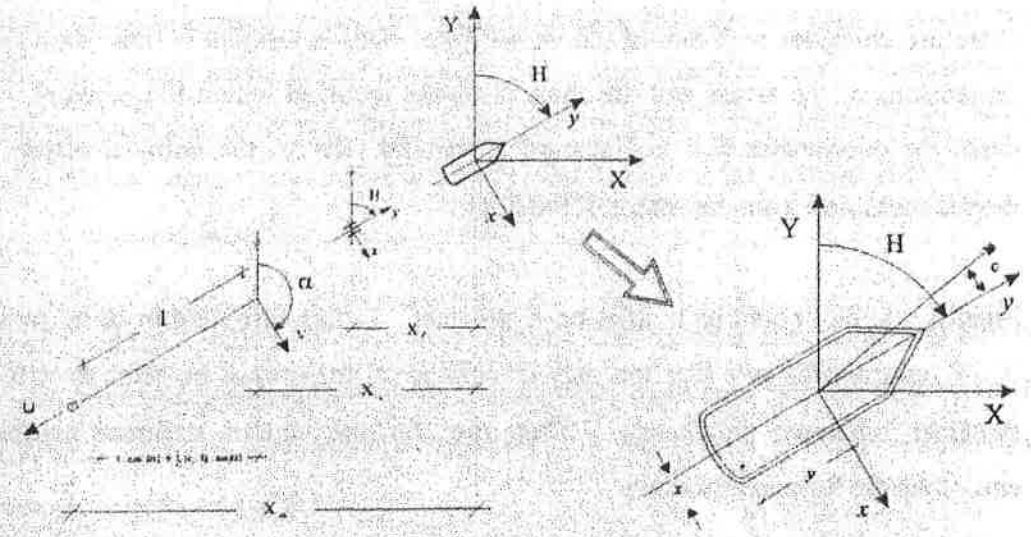

Figure 5.2: Relation between the state and geometry of the system components

If a station i is a point on the vessel (sonardyne, laser device, etc.) then

$$\begin{aligned} X_i &= x\cos(H)+y\sin(H) \\ Y_i &= -x\sin(H)+y\cos(H) \end{aligned} \qquad 5.9$$

where

x, y are the coordinates of the device fixed on the vessel
H is the vessel's heading

Given that, the vessel's heading, H, is not considered to be an unknown in the system it must be substituted in Equation 5.9 by

$$H = \tan^{-1}\left[\frac{\nu\cos(\phi_v)\dot{\lambda}}{\rho\dot{\phi}_v}\right] + c \qquad 5.10$$

so that the observation relates only to unknown parameters.

Similarly, if a station i is a device on a float array (gun, towfish, buoy etc.) the observation should first be corrected to the centre of the array using Equations 5.9 and

5.10. In such a case it would be usual to assume that the orientation of any float structure coincides with that of the vessel gyro. This is justified by the relatively small dimensions of the arrays and the short distances involved within the network. In this case, the coordinates x, y in Equation 5.9 would refer to the nominal offsets of the device measured from the centre of the float.

Finally, station i could be a point on a streamer. In this case, and in order to express X_i, Y_i coordinates as a function only of unknowns, these must be refer directly to the streamer unknown parameters. Therefore, for the chosen streamer model these equations are formed as follows

$$\begin{aligned} X_i &= X_s + l\cos(\alpha) + \sum_{k=2}^{n}\left[c_k l^k\right]\sin(\alpha) \\ Y_i &= Y_s - l\sin(\alpha) + \sum_{k=2}^{n}\left[c_k l^k\right]\cos(\alpha) \end{aligned} \qquad 5.11$$

where

- X_s, Y_s are the Cartesian coordinates of the streamer's reference point in the XY coordinate system
- α is the instantaneous orientation of the streamer coordinate system u,v
- c_k are the polynomial coefficients
- n is the polynomial order
- l is the offset of station i from the streamer's reference point

In fact several different equations can be written, for both distance and azimuth observations, depending upon the subsystems to which stations i and j refer. Hence, and for example, the observation equation for a measured azimuth from the vessel's laser to a laser reflector fixed on a streamer is given by the following equation, (Equation 5.12)

$$\tan^{-1}\left[\frac{X_s + l\cos(\alpha) + \sum_{k=2}^{n}\left[c_k l^k\right]\sin(\alpha) - \left\{x\cos\left[\tan^{-1}\left(\frac{v\cos(\phi_v)\dot{\lambda}_v}{\rho\dot{\phi}_v}\right)+c\right] + y\sin\left[\tan^{-1}\left(\frac{v\cos(\phi_v)\dot{\lambda}_v}{\rho\dot{\phi}_v}\right)+c\right]\right\}}{Y_s - l\sin(\alpha) + \sum_{k=2}^{n}\left[c_k l^k\right]\cos(\alpha) - \left\{-x\sin\left[\tan^{-1}\left(\frac{v\cos(\phi_v)\dot{\lambda}_v}{\rho\dot{\phi}_v}\right)+c\right] + y\cos\left[\tan^{-1}\left(\frac{v\cos(\phi_v)\dot{\lambda}_v}{\rho\dot{\phi}_v}\right)+c\right]\right\}}\right] = A_{ij} + v_{A_{ij}}$$

Similarly, the observation equation for a measured range between two acoustic devices i and j located on streamers 1 and 2 respectively, can be formed as

$$\sqrt{\Delta X_{ij}^2 + \Delta Y_{ij}^2 + \Delta Z_{ij}^2} = D_{ij} + v_{D_{ij}} \qquad 5.13$$

where

$$\Delta X_{ij} = X_{S_1} + l_i\cos(\alpha_1) + \sum_{k=2}^{n}\left[c_{1_k} l_i^k\right]\sin(\alpha_1) - \left\{X_{S_2} + l_j\cos(\alpha_2) + \sum_{k=2}^{n}\left[c_{2_k} l_j^k\right]\sin(\alpha_2)\right\}$$

$$\Delta Y_{ij} = Y_{S_1} - l_i\sin(\alpha_1) + \sum_{k=2}^{n}\left[c_{1_k} l_i^k\right]\cos(\alpha_1) - \left\{Y_{S_2} - l_j\sin(\alpha_2) + \sum_{k=2}^{n}\left[c_{2_k} l_j^k\right]\cos(\alpha_2)\right\}$$

$$\Delta Z_{ij} = Z_i - Z_j$$

It is important to note, that, in the case of any observed direction the measurement should be first reduced to an azimuth (bearing) and then be corrected for grid convergence before the observation equation is formed.

Float and tailbuoy geodetic position

For any floating body towed by the vessel, except for the tailbuoys, geodetic position observation equations can be formed (Figure 5.2) as follows

$$\begin{aligned} \phi_v + \frac{Y_f}{\rho} &= \phi_f + v_{\phi_f} \\ \lambda_v + \frac{X_f}{\nu\cos(\phi_v)} &= \lambda_f + v_{\lambda_f} \end{aligned} \qquad 5.14$$

where

X_f, Y_f are the unknown Cartesian coordinates of the float
ϕ_v, λ_v are the unknown ellipsoidal coordinates of the vessel
ϕ_f, λ_f are the observed geodetic coordinates of the float
$v_{\phi_f}, v_{\lambda_f}$ are the measurement residuals

Note that these equations make the (entirely reasonable) assumption that the radius of curvature in the plane of the meridian ρ, and the prime vertical ν, throughout the spread are equal to those for the reference navigation point.

Tailbuoy position observation equations differ slightly from the equations given above because, as explained in Section 5.3.1, tailbuoy coordinates are not parameters of the system, i.e. they are not in the state vector. A streamer's parameters are therefore required in order to obtain its tailbuoy position. Substituting Equation 5.11 into Equation 5.14 leads to

$$\begin{aligned} \phi_v + \frac{Y_s - l\sin(\alpha) + \sum_{k=2}^{n}\left[c_k l^k\right]\cos(\alpha)}{\rho} &= \phi_{tb} + v_{\phi_{tb}} \\ \lambda_v + \frac{X_s + l\cos(\alpha) + \sum_{k=2}^{n}\left[c_k l^k\right]\sin(\alpha)}{\nu\cos(\phi_v)} &= \lambda_{tb} + v_{\lambda_{tb}} \end{aligned} \qquad 5.15$$

where

ϕ_{tb}, λ_{tb}	are the tailbuoy measured geodetic coordinates
$v_{\phi_{tb}}, v_{\lambda_{tb}}$	are the measurement residuals

Compass bearings

To form a compass bearing equation it is necessary to consider the geometry of the configuration as shown in Figure 5.3. The observation equation for a compass of offset l , measured from the streamer reference point, is then formed as follows

$$\alpha - \left[\tan^{-1}\left(\frac{dv}{du}\right) + \frac{\pi}{2}\right] = B_{comp} + v_{B_{comp}} \qquad 5.16$$

where

α	is the instantaneous orientation of the streamer coordinate system u,v
B_{comp}	is the observed compass bearing
$v_{B_{comp}}$	is the measurement residual

and

$$\frac{dv}{du} = \frac{d\left(\sum_{k=2}^{n} c_k l^k\right)}{dl} = \sum_{k=2}^{n}\left[k c_k l^{k-1}\right] \qquad 5.17$$

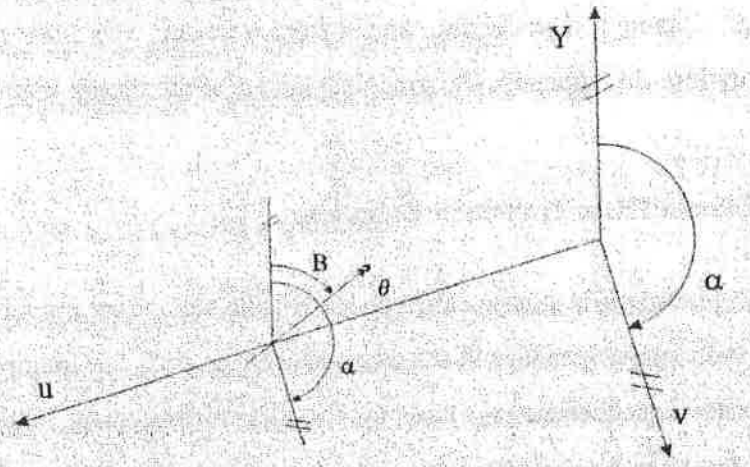

Figure 5.3: Compass azimuth observations

Compass observations should be reduced to the grid before they are incorporated into the Kalman filter process. This is done by correcting them for magnetic declination, magnetic deviation and grid convergence according to the following equation

$$B_{comp} = B + mag\_decl + mag\_dev + grid\_conv \qquad 5.18$$

Therefore, by combining Equations 5.16, 5.17 and 5.18 the complete form can be obtained from

$$\alpha - \left[\tan^{-1}\left(\sum_{k=2}^{n}\left[k c_k l^{k-1}\right]\right) + \frac{\pi}{2}\right] - mag\_decl - mag\_dev - grid\_conv = B + v_B \qquad 5.19$$

Note that, in principle, magnetic declination and magnetic deviation could be placed in the state vector and recovered from the measurements along with all of the other parameters. This has not been done in the work reported here but the fact that it is possible is another advantage of this unified approach.

The foregoing observation equations are given in their original, and mostly non-linear, form. To determine the design matrix (matrix A in Equation 3.3) it is necessary to linearise these equations by applying the Taylor series expansion as far as first differentials. Because of the large number of unknown parameters contributing to the system and the complicated nature of some of the equations, many of these differentials are better obtained numerically, and where relevant this has been done in this implementation. In Appendix C a graphical layout of the design matrix A is provided.

5.3.4 Kalman Filter Transition Equations

In Kalman filtering it is a basic assumption that the secondary model is able to describe perfectly the system dynamics in the mean sense, i.e. such that model errors are limited to white noise sequences v_i and y_i for the measurement and dynamic models respectively. Here a simple Taylor's expansion of the state vector elements (polynomial dynamic model discussed in Section 3.2.2.1) is used for this purpose

$$x = x_0 + \dot{x}_0 t + \tfrac{1}{2}\ddot{x}_0 t^2 + \ldots \qquad 5.20$$

As has already been explained the stable nature of seismic exploration surveys (calm seas and straight line tracks) has led to the state vector only including zero and first order terms (no acceleration or higher order terms). Consequently, and using Equation 5.20, the dynamics of a seismic vessel and any other floating body (source, streamer reference point, etc.) is described, for a short period of time, by the following equations

$$\begin{aligned} X_i &= X_{i-1} + \dot{X}_{i-1}dt + \tfrac{1}{2}a_X dt^2 \\ Y_i &= Y_{i-1} + \dot{Y}_{i-1}dt + \tfrac{1}{2}a_Y dt^2 \\ \dot{X}_i &= \dot{X}_{i-1} + a_X dt \\ \dot{Y}_i &= \dot{Y}_{i-1} + a_Y dt \end{aligned} \qquad 5.21$$

where a_X and a_Y, the average acceleration components for the time interval dt, are treated as white noise (Houtenbos, 1982).

The remaining elements of the state vector, i.e. the crab angle c, the orientation of each streamer coordinate system α and the polynomial coefficients can be modelled in a simpler way because they are not expected to vary significantly with time. Therefore these states are modelled as a linear function of time according to the equation

$$d_i = d_{i-1} + \dot{d}_{i-1}dt \qquad 5.22$$

where

d is the state vector element
$\dot{d}$ is the rate of change of d

5.4 STOCHASTIC MODELS

As stated in Chapter Three the implementation of the Kalman filter requires the specification of two stochastic models. The measurement noise stochastic model that reflects how good the observations are, and the driving noise stochastic model which describes the differences between the dynamic system and reality. In this study the standard Kalman filter algorithms are implemented, and therefore, these two models are assumed to be totally uncorrelated - see also Section 3.3.1.

The stochastic model of the observations is described by their covariance matrix C_l. The various observation types that the system has been designed to cope with are given in Section 5.3.2. In practice these are assumed to be uncorrelated and independent of one another, and therefore, the covariance matrix C_l is taken to be diagonal with its elements representing the variances of the observations. However, the Kalman filter algorithms can, in principle, deal with full matrices for the case when correlation among the measurements exists. The observation variances are a function of the random errors of the observations. Minimum values of the inherent accuracy of the sensor units are provided by the manufacturer specifications. Nevertheless, the final accuracy of an observation depends on other factors as well. For instance, the *a priori* standard deviation of an acoustically measured distance depends on the precision of the acoustic signal velocity propagation. Observational variances can be considered to be fixed for an entire line or dynamically estimated. The design of the model, by itself, can cope in both circumstances. Further details on the implementation of these alternatives are given in Chapters Six and Ten.

The stochastic model of the dynamic model is in the form of the covariance matrix of the dynamic model C_y given by

$$C_y = TC_gT^T \qquad 5.23$$

where C_g is the covariance matrix of the driving noise g. The matrix T models the effect of the noise on the state vector. Its elements consist of the components of the Taylor's

series detailed in Section 5.3.4. In this application the noise is assumed to be uncorrelated and white, and therefore has a random distribution. More specifically, the off-diagonal elements of matrix C_g are assumed to be zero whereas the diagonal elements are given in Table 5.2.

standard deviations of the driving noise										
vessel			float		streamer					
σ_{a_φ}	σ_{a_λ}	σ_{crab}	$\sigma_{\ddot{x}_F}$	$\sigma_{\ddot{y}_F}$	$\sigma_{\ddot{x}_s}$	$\sigma_{\ddot{y}_s}$	$\sigma_{\dot{\alpha}}$	$\sigma_{\dot{c}_2}$	...	$\sigma_{\dot{c}_n}$

Table 5.2: Driving noise uncertainties for the three basic elements of a marine seismic network

As mentioned before, it is assumed that seismic surveys are carried out in calm seas while the vessel sails in almost straight lines. Therefore, under these circumstances, it is not very difficult to assign standard deviation values for the vessel, float nodes and streamer reference points acceleration. It is not, however equally easy to adopt values for the uncertainties of the rate of change of the streamer direction angle α, and the streamer model coefficients c_i.

It is important to note that the role of the stochastic models takes a big share in the computation of the filter estimates and the quality of the final results. The rather complicated structure of the proposed algorithm and the large number of observations involved in the system make this point extremely important, and therefore, particular attention has been paid to this point. The effect of the stochastic models on the results of the filter computations and their quality are explicitly discussed in Chapters Eight and Nine.

5.5 SEISMIC SOURCES AND HYDROPHONES POSITIONING AND QUALITY MEASURES

5.5.1 Positioning the Seismic Sources and Hydrophones

It has been stated in Section 5.1 that the significant innovation of the proposed method is centred upon its ability to provide the position of any point of interest throughout the spread, (essentially the positions of the gun nodes and hydrophone groups) along with its associated quality measures in a straightforward manner, i.e. there is no need for any additional interpolations as in most other methods.

The implementation of the unified Kalman filter algorithm solves at every epoch for the state vector elements $\hat{x}_{(+)}$, and their covariance matrix $C_{\hat{x}(+)}$. The position elements of the centre of the energy sources relative to the vessel are themselves states of the system, and therefore this information is obtained directly with no need for any further computations.

Each hydrophone group is deployed at the network at a known offset, l, from the head of the streamer, or the tow point, or some other point. Hence, in order to locate a hydrophone, i, with respect to the local topographic system originating at the vessel's NRP, the following equations are used

$$\begin{aligned} X_i &= X_s + l_i \cos(\alpha) + \sum_{k=2}^{n} \left[c_k l_i^k \right] \sin(\alpha) \\ Y_i &= Y_s - l_i \sin(\alpha) + \sum_{k=2}^{n} \left[c_k l_i^k \right] \cos(\alpha) \end{aligned} \qquad 5.24$$

where both the state vector elements and the receiver's offset are known.

Having computed the positions of the seismic sources and hydrophone groups with respect to the vessel, the position of the vessel is used to transform these in a global

reference system by applying a direct geodetic formulation. Finally, in most cases, these positions are then expressed in other coordinate frames to simplify the binning processes.

5.5.2 Measures of Precision

Since the positions of the seismic sources are states of the system their uncertainty values form a direct by-product of the Kalman filter process and are held in the filtered covariance matrix of the state vector. In fact, this information is associated with the standard deviations of probability of one sigma given in two directions, namely northings and eastings.

To compute the same estimates for the hydrophone group positions the formulae that relate the receiver positions to the state vector elements are used, viz. Equations 5.24. Hence, the covariance matrix of the receiver positions is computed by applying the Gauss' propagation of error law on these equations recursively for each receiver. In this computation only part of the information held in $C_{\hat{x}(+)}$ is used, i.e. the sub-matrix which refers to the states that contribute in positioning hydrophone groups.

This information is then used to express nodal uncertainty in other ways such as drms, CEP and error ellipses. The appropriate formulae may be found in Chapter Four.

5.5.3 Measures of Reliability

Measures of reliability are computed only for individual biases (gross errors) in the observations. Therefore all observations are tested, in turn, for biases at every single epoch and measures of internal and external reliability are produced. The testing procedure involves an examination of the predicted residual of each observation for every shotpoint. In fact the relative size of the predicted residual is compared to the *a priori* observational error at a level of probability of usually three sigma. This check is simply to identify (and probably reject) outlying observations. Suggestions for rigorous statistical testing are given in Chapter Ten.

Internal reliability computations rely on Equation 4.18, which is reproduced here

$$\nabla_i = \frac{\delta}{\sqrt{C_{v_i}^{-1}[j\mathbf{I}j]}} \qquad 5.25$$

This operation involves an inversion of a matrix whose size is equal to the number of observations at every epoch, and therefore, in order to reduce processing time and the computations complexity the simplified formula given by Equation 4.19 was initially implemented. However, analysis proved that this formula cannot be used because this expression leads to relatively big values for the marginally detectable errors in many observations - especially for those observations made at the rear end of the spread. It is very likely that the polynomial streamer model assumption produces, somehow, correlation among the predicted residuals of the observations, and hence, the off-diagonal elements of matrix $C_{v(-)}$ cannot be ignored.

External reliability in positioning marine seismic networks is computed in several sequential steps in a rather more complicated manner. In the first place the impact on the state vector parameters due to observational errors of the size of MDE's (computed at the previous stage of internal reliability) is estimated, in turn, for all observations using Equation 4.21, which is rewritten here

$$\Delta\hat{x}_{ij} = K_i e_{ij} \nabla_{i_j} \qquad 5.26$$

Since the hydrophone positions do not form states in the system the effect on the receiver positions (horizontal shift) is computed for each vector $\Delta\hat{x}$ using Equation 4.23 which reads

$$\Delta\hat{g}_{i_j} = J_i \, \Delta\hat{x}_{i_j} \qquad 5.27$$

where J is Jacobean matrix of the Equation System 5.24. This computation is done as many times as there are the observations. Therefore if m observations are used to

measure the network at epoch i, with r receivers involved in the spread, m $\Delta\hat{g}$ vectors are computed the size of which are 2r - horizontal shift in two directions, i.e. northings and eastings.

Maximum external reliability at an epoch is defined as the maximum horizontal shift (resultant horizontal displacement) computed at any node in the network for all observations. Nevertheless, in practice, maximum external reliability (maximum horizontal shift) is specified in terms of HMP rather than nodal shift (source and receiver). Nowadays the decision whether or not survey quality specifications are being met is mostly based on diagrams of HMP maximum external reliability assessed at the end of each line. Interested readers are recommended to study Zinn and Rapatz, (1995) and Zinn and Humbert (1994) for a detailed discussion and implementation of reliability during towed streamer surveys.

CHAPTER SIX

SOFTWARE IMPLEMENTATION

6.1 INTRODUCTION

The proposed model described in Chapter Five is not a technically complete solution as it needs a certain amount of testing using real data. The reason is twofold. Firstly in order to verify the correctness of the mathematics involved in the model, and secondly to test the feasibility of the associated algorithms in terms of convergence, solubility and computational efficiency. Obviously, to achieve this objective, the development of a series of computer software routines that can, ideally, be grouped together to analyse and process a complete set of raw positioning seismic data is essential.

The algorithm has been implemented in a piece of software known as NewCastLe NETwork (NCL_NET) program. Because of the broad acceptance in these times of the C programming environment as a common industry standard, the software has been designed and written in the C programming language to run under the UNIX operating system. All source code was compiled using the *C-89 compiler*, always adhering to the ANSI C standard, in a standard Hewlett-Packard 9000/710 machine with processing speed 12 megaflops at 24-Mbytes RAM.

The suite of software comprises many subroutines that have been written to implement the various steps of the processes described in Chapter Five. This chapter is intended to provide a description of the internal architecture of the software and to detail the program various features and capacities as well as the restrictions and limitations associated with it.

6.2 SYSTEM CONFIGURATION

The NCL_NET program has been designed to provide real-time positioning of the energy sources and hydrophones, along with their associated quality measures, involved in marine seismic surveys. The general communication layout of the program is illustrated in Figure 6.1. As detailed in Chapter One, the computational flow line involves a field navigation system that provides the positioning algorithm with the raw measurement data and header information. The processed data, i.e. positions and their quality measures, are then passed into an on-board processing system for real-time binning.

Figure 6.1: NCL_NET system communications

The UKOOA P2/91 format, discussed in Chapter One, has been generally accepted by the offshore exploration industry as the standard format for the exchange of raw marine positioning data. However, many seismic contractors still use (at least in certain stages of the process) their own in-house formats to specify and record all output data from the measurement systems. The NCL_NET program acquires its measurement data in ASCII form generated by the TBV (Trust But Verify) quality control and analysis of positioning data software package developed by QC Tools, Inc. A set of subroutines was written to read the raw positioning data and feed the NCL_NET positioning algorithm. Similarly, another set of subroutines was written to store the output information, namely vessel, float, receiver and tailbuoy positions and their quality measures. These are also in ASCII format which can be used as input information (after they have converted in an appropriate format) for use by an on-board or office binning system.

6.3 THE NCL_NET PROGRAM STRUCTURE

6.3.1 Overview

At an early stage of this project it was agreed that a principal requirement of the NCL_NET program should be a well designed, powerful and flexible experimental piece of software rather than a fully operational software package. The reason is twofold.

Firstly, as mentioned earlier, the primary objective of this study is simply to test the suggested method for positioning a modern seismic network offshore. However, due to the extremely complicated structure of a completely general marine seismic spread (number of floats, streamers, devices, etc.;) the development of a fully operational software becomes rather a pure computing problem, which is out of the scope of this study. Moreover, for the same reasons, a complete user interface (at this stage of the implementation) is not a major requirement.

Therefore, the software at this stage has been designed basically as a research and development tool but flexible enough to cope with certain modifications in the source code in order to be able to test alternative hypotheses regarding the observation data and the functional and stochastic models.

Nevertheless, it should be stressed that the suggested algorithm described in Chapter Five is a completely general one, able to describe the geometry of any likely practical set-up. Also, the trials performed using NCL_NET program cover all possible combinations of the major available observation types involved within modern multi-streamer operations and therefore, the testing of the model and the conclusions made from the analysis can be treated as general.

A general, introductory design specification of the I/O functions for positioning 3D seismic surveys software, that may help as a starting point in the development of a multi-purpose commercial software package, is provided in Appendix D.

6.3.2 Main Computational Sections

The complete software development is subdivided into six basic areas. A schematic representation of these areas is illustrated in Figure 6.2. In summary, these can be described as follows

- *Control* - This part of the software is split into several subareas that are intended to provide the system with all the requisite information necessary to define the survey/navigation configuration, geometry network configuration, nominal offset values, and *a priori* quality measures.
- *State* - Approximate values for the state vector elements are required to initiate the system. At the end of every cycle of computations these values are updated and used as input information to the mathematical processes for the next time event computations.

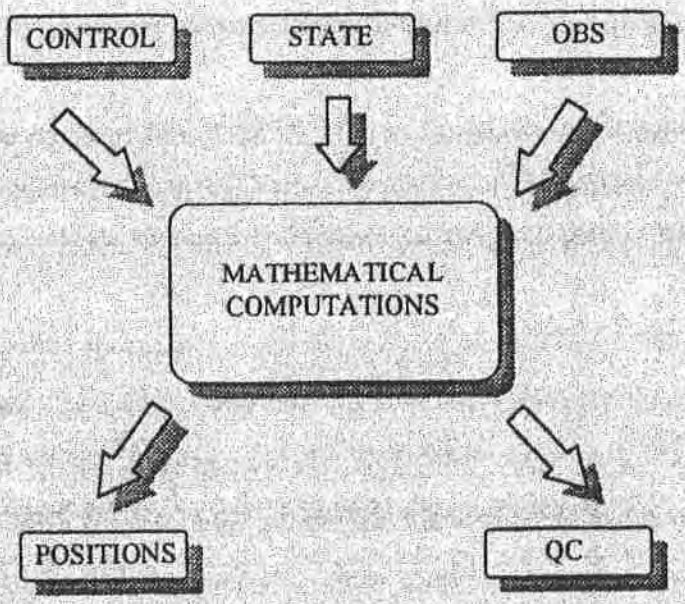

Figure 6.2: NCL_NET program main computational sections

- *Observations* - At every time event, usually shotpoint, a vector containing all available raw positioning data is formed. This information is then passed to the

mathematical computations subroutines to update the network positions and their quality.

- *Mathematical computations* - This is the 'core' of the software where the actual positioning algorithm is implemented. It consists of the processes needed to form the design matrix, the 'computed-observed' vector (functional model) and the transition matrix (dynamic model). These are then used to implement the filtering algorithms in order to solve for the state vector and its uncertainty matrix.
- *Positioning* - At this stage of the computations the filter solution is used to generate and store the positions of the points of interest. These include the vessel, float nodes (energy sources and auxiliary stations), hydrophone groups and the tailbuoys.
- *Quality measures* - This is the last step of the sequence of computations, executed at every time event. Precision and reliability measures are computed to describe the quality of the estimation results for each node deployed in the spread and at the network level.

6.3.3 Working Principle and Mathematical Processes of NCL_NET

It is a fundamental requirement that NLC_NET, as a research and development tool, to be as far as possible well-structured, understandable and simple. The main steps of its computational flow line are summarized in Figure 6.3 and are explained as follows.

The system is initiated by creating a directory where all estimation results are stored. Also, at this stage NCL_NET reads all configuration measurements and opens and names the output files. Thereafter, the system requires the file names of the vessel navigation data and the network positioning data. An initialization file is used to assign approximate values for the state vector elements and their uncertainties in order to start the Kalman filter.

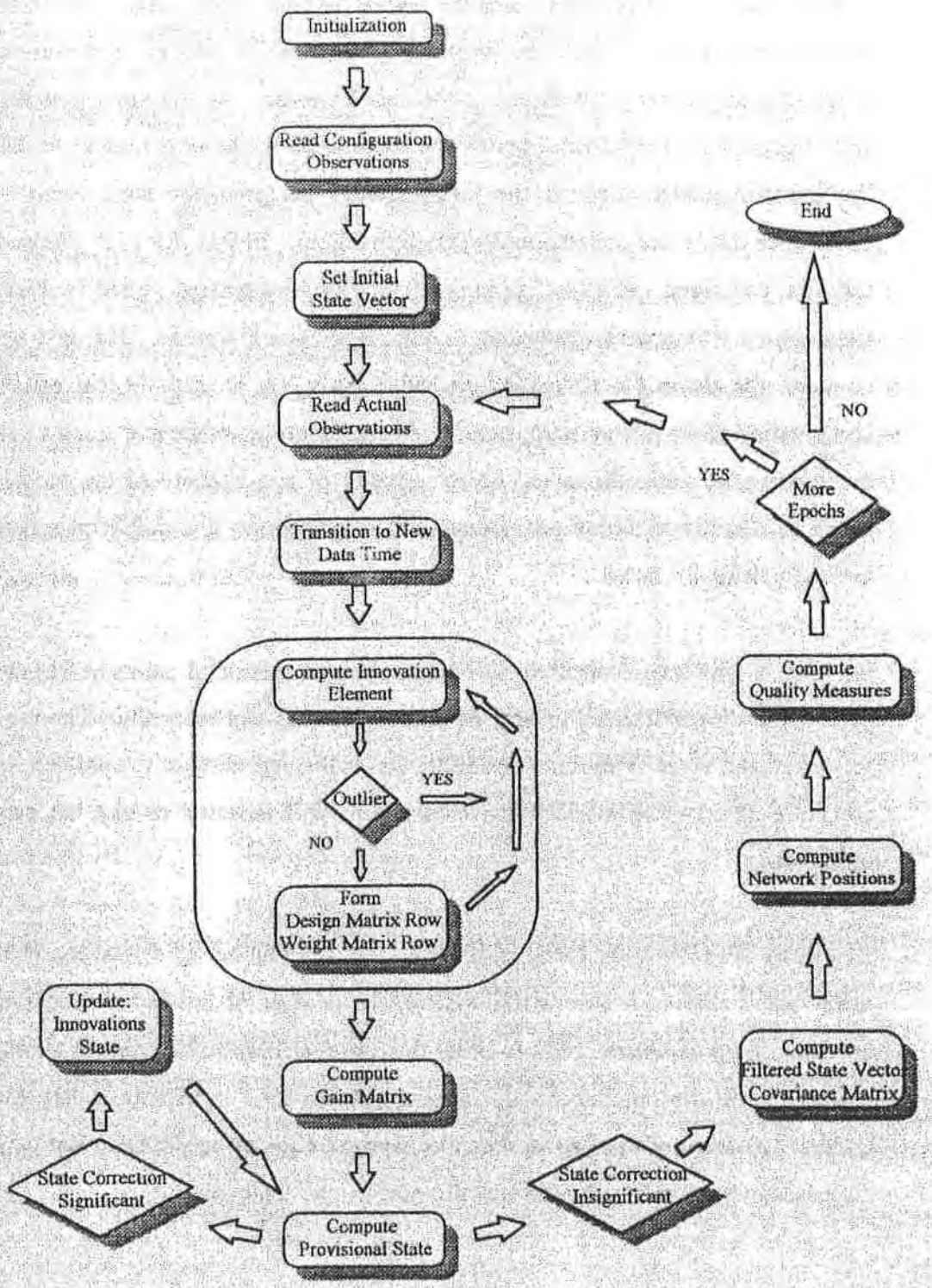

Figure 6.3: Computational flowchart of NCL_NET software

After initialization, NCL_NET reads the raw observation values which are available for the first time event. Using the provisional state vector and the observations both prediction and filtering processes are then implemented. At the prediction phase the state vector and its covariance matrix are transmitted to the next time event based on the dynamic model, while at the filtering stage the predicted state vector and its covariance matrix are updated using the observations. In fact, for each observation in turn, its 'computed - observed' or innovation value is calculated, tested for biases, and the design matrix row corresponding to this observation is formed. The next step is to compute the Bayes (or Kalman) filter gain matrix. It is possible that prior to the computation of the filtered state vector it is necessary to compute and correct iteratively the provisional states depending on the amount of non-linearity of the model which basically depends on the adopted streamer model function - e.g. polynomial, harmonics and the polynomial order.

Finally, the filter solution is used to compute the positions of all points of interest in the spread and their associated quality measures, precision and reliability. The results are formatted and saved in the output files created at the beginning of the process. If there are more observations available the complete loop is repeated or else the process is terminated.

Obviously the processing speed is dependent on the number of states, the number of observations that contribute to the system, the number of internal iterations and the capacity of the hardware used. In order that the algorithm to be efficient enough, it is crucial in real-time operations that the processing time is kept less than one shot interval. Analysis of two sets of data (see Appendix E), using the hardware equipment discussed in Section 6.1, showed that this goal can be achieved.

6.4 FUNCTIONAL OVERVIEW

The NCL_NET program consists of a number of functional groups of subroutines that may be classified in groups according to their operation. The main features of each group are discussed in the following paragraphs.

6.4.1 Main Function

The main function is the master function which aims at coordinating all groups of functions, i.e. it has overall control of the software operations, with the basic tasks to perform being

1. Call the initialization files in order to assign provisional values for the system states and their uncertainties.
2. Assign values for the *a priori* standard deviations of the observations and the driving noise.
3. Open all input and output files that NCL_NET requires in order to operate.
4. Read the survey and geometry configuration information held in the header files.

Also, at every cycle of computations (time event) the main function has been set to call the submaster functions to perform the various model computational operations described in Section 6.4.3.

6.4.2 Input/Output Functions

A set of subroutines was written to perform all necessary reading and writing operations. In particular, for each observation type one function, or a set of functions, was developed in order to

1. Read the raw measurement values.
2. Allocate them in dynamically defined arrays.

3. Assign a number of flags necessary to describe certain attributes related to each measurement such as serial number, observation type, connecting nodes, nominal offsets, etc.;

The program has been designed to accept raw data for four basic observation types. These are laser and acoustically derived slant ranges, compass azimuths, vessel and tailbuoy geodetic positions and vessel gyro. Particular attention was paid to the basic structure in order that the system can easily incorporate new observation types. Similarly, the software is flexible enough to produce a solution simultaneously involving all observations or, for analysis and testing purposes, just some of them. However, it should be noted that these functions were built specifically to read the sets of data provided to test the model, and therefore they need to be modified in order to accept data from other standard input formats.

The computation results consist of those containing the state vector solution and those containing the positions of the nodes involved in a seismic network and their quality measures. These results are classified in eleven types of files, each file containing the following information

- *l_nav* - Filtered values of the vessel NRP geodetic position and the vessel crab angle.
- *l_sup* - Filtered solution for the streamer unknown parameters namely, positions of their reference points, orientation angle and streamer model coefficients.
- *l_fpv* - Filtered values of the positions and velocities of the centre of the floats involved in the network.
- *l_hp* - Filtered positions of all hydrophone groups (or a sample of them) deployed in the network.
- *l_tb* - Filtered positions of the tailbuoy nodes.
- *l_mp* - Measures of precision for all float and tailbuoy points and for a sample of receivers for each streamer. The precision of these nodes is expressed in drms, 50%CEP and 95% error ellipses.

- *l_ir* - Marginally detectable errors for each observation. Disabled and rejected observations are denoted by -1, and -2 to be easily identified from 'healthy' observations.
- *l_er* - Horizontal shift for every float in the network and for a sample of receivers per streamer for every processed observation.
- *l_mhs* - Maximum horizontal shift at any node in the network derived for all observations - this is a single value computed at every event time and is used to describe the whole network.
- *l_pr* - Observational predicted residual values ('computed - observed' values) for all processed observations.
- *l_sie* - This is a flag file used to identify which observations are used, are disabled and rejected. These are denoted by 1, -1 and -2 respectively.

The above information is obtained for every time event. All nodal positions refer to the local topographic coordinate system originating at the vessel NRP or, in order to aid interpretation, are rotated to the mean along-track and cross-track directions and expressed in meters. Only the position of the vessel is given in degrees. All node velocities are produced in meters per second.

6.4.3 Model Computational Functions

This group of functions split into the following five areas

Functional Model - At this stage of the process the innovation vector and the design matrix for the current event time are formed. For each observation in turn, one of the so-called observation equation routines is run, depending on the observation type and the observation attributes, in order to compute its innovation value and the design matrix elements (see Appendix C) with respect to this observation.

Dynamic Model - The Kalman filter transition equations and the covariance matrix of the driving noise are implemented to form the transition matrix M, and the covariance matrix of the dynamic model C_y. Both M and C_y matrices are only functions of time t.

Therefore, this computation is repeated at every epoch since the time interval between observations (usually the shot interval) is not fixed.

Filtering Computations - The functions involved in this area are meant to implement the Kalman filter computations as they are detailed in Chapter Three. The overall control of all filtering operations is carried out in one master function that coordinates the several steps involved in the process and transmits the input and output information to the main function. The input information necessary for the filtering processes consists of the design matrix, the innovation vector, the transition matrix and the stochastic models for the current time event, and the filter solution derived from the previous time event. The filtered state vector and its covariance matrix form the output results.

Positioning - This part is intended to compute the hydrophone and tailbuoy positions using their offset nominal values. The position of the vessel NRP and the float nodes is a direct output of the filter computation since they are states in the system.

Quality Measures - Three subroutines are involved in this final stage of the computations. In the first one the covariance matrix of the filtered state vector used to produce measures of precision for the float points and the receiver groups. In the second one the full covariance matrix of the predicted residuals is used to compute measures of internal reliability (MDE) which are transmitted to the third function to produce external reliability measures (horizontal shift).

6.4.4 General Functions and Header Files

The group of this type of functions consists of functional subgroups of routines; math library, dynamic memory allocation and check or trial subroutines.

1. The math library contains all necessary functions that required to perform the mathematical operations, mainly matrix algebra operations and coordinate system transformations.

2. Memory allocation functions are used to dynamically allocate matrices and vectors of different types.
3. Check or trials routines are functions especially built to perform specific tests used in order to assess the correctness of the estimation results. The tests that were performed are discussed in Section 7.5.

Finally, the following types of information which is common to all functions is held in header files

1. General definitions and survey datum and projection parameters.
2. External variables definitions, structure declarations and function prototypes.
3. Configuration observations. These include
   - the nominal coordinates of all navigation sensors fixed on the vessel, the floats, the streamers and the tailbuoys with respect to the vessel and float coordinate systems and the streamer reference points respectively.
   - the nominal coordinates of the energy sources with respect to the centre of the floats and the hydrophone offsets from the streamer reference points.

6.5 PERFORMANCE IMPROVEMENT AND ASSOCIATED PROBLEMS

Approximate states - Approximate values for the state vector elements and their uncertainties are supplied to the system using an initialization file. These values are based on simple hand computations that express the geometry configuration at the starting time. The accuracy of the initial coordinates is sufficient if it is within a few metre. The starting values for the vessel crab angle, the polynomial coefficients and the velocities of the float nodes and the streamer reference points are taken to be equal to zero. Analysis showed that under these circumstances it takes only several epochs the for filter to settle.

Design matrix preparation - As detailed in Chapter Five the measurement model of the proposed algorithm is a non-linear one. Moreover, due to the complicated nature of most of the observation equations, an analytical approach to their differentiation seemed not to be the best solution to the problem. Therefore the design matrix is computed numerically as shown in Appendix C. Implementation of the method using real data has led to the following conclusions

1. The size of the small amount, δ x, needed to apply the method is very important to the correct estimation of the design matrix elements and consequently to the final estimation results. More specifically, because the method is an approximate one, if large values are selected the design matrix elements would be significantly incorrect, while choices of very small values may cause numerical problems in the computational procedure. Therefore, the size of values δ x for a given level of precision for the design matrix elements, (though this is not always easy to evaluate, especially for the streamer model coefficients) is computed iteratively testing a set of δ x values until the difference in the size of the design matrix elements is less than the required accuracy.
2. Although it is the absolute size of δ x that is critical to the fidelity of the design matrix A, the relative size of δ x (i.e. the relative size of δ x between different states) affects also part of the estimation results. In particular it seems that measures of reliability are influenced while the final coordinates and their uncertainties seem not to change. For instance, the relative sizes of the small

amounts $d\dot{\varphi}$ and $d\dot{\lambda}$ required to differentiate the vessel gyro observation equation have an impact on the size of the MDE of the gyro observations. From the analysis so far it is evident that very small errors in the design matrix A are propagated to the covariance matrix of the predicted residuals $C_{v(-)}$ (Equation 4.2). In fact the problem becomes visible in the MDE values since their computation requires this matrix to be inverted (Equation 4.17). However, much more research still needed in this area.

3. A third point to consider, associated with the design matrix preparation, is the structure of the design matrix itself. This concerns possible numerical problems that may be caused due to the relative sizes of the element values. In other words it is possible the mathematical operations between columns of very large elements (those computed with respect to the polynomial coefficients) may cause numerical problems. Some sort of scaling of the design matrix could be a first idea to prevent any numerical problems that may arise for a rather complicated or uncommon geometry configuration.

State vector iterative computation - Because of the non-linear nature of the measurement model the filtered state vector is computed iteratively. To serve this purpose a routine was written in order to implement the algorithm given by Equation 3.27. Separate subroutines were written to recompute the design matrix A, the gain matrix G, and the 'observed - computed' vector b. The process is designed to terminate after the provisional states have been computed for a certain (fixed) number of iterations or, after the differences in (some of) the state vector estimates between two successively loops of computations are insignificant.

However, analysis using real data proved that no significant differences occur in the state vector solution (and therefore in the final source and receiver positions) if this is computed iteratively. Also, analysis proved that it is more likely that iterations are required only when a polynomial streamer model of a high order is used. Alternatively, if no iterations are implemented, the filtered state vector is computed using Equation 3.28 which is the case of an extended Bayes (Kalman) filter.

Streamer model finalization - The overall analysis and preliminary tests of the individual compass measurements discussed in Chapter Two were carried out using a polynomial function of the form

$$B_i = a_0 + a_1 l_i + a_2 l_i^2 + \ldots + a_n l_i^n \qquad 6.1$$

and the coordinates of any point on the streamer (see Section 2.3.1) were computed using equations

$$\begin{aligned} u &= l \\ v &= c_1 l + c_2 l^2 + \ldots + c_{n+1} l^{n+1} \end{aligned} \qquad 6.2$$

where the zero order coefficient is eliminated after integration. Similarly, in the integrated algorithm a polynomial function of the form shown in Equation 6.2 was initially implemented. However, analysis of this type of function revealed that the streamer's baseline orientation is significantly affected by a constant rotation factor faking the final coordinates, and therefore the first order coefficient c_1 is found to be redundant in the state vector. In fact this result is not entirely surprising since the first order coefficient expresses the first derivative of the streamer, namely the direction of the tangent of the streamer which is considered to be state in the system that takes the form of the direction angle α. Therefore it has been decided to eliminate also coefficient c_1 resulting in an equation of the form

$$v = c_2 l^2 + \ldots + c_{n+1} l^{n+1} \qquad 6.3$$

Similarly, in the case of the harmonics streamer model, an attempt was made to select a function that does not cause redundancy in the state vector (see also Section 8.2.1.2).

CHAPTER SEVEN

TESTING THE ALGORITHM FOR CORRECTNESS AND COMPUTATIONAL EFFICIENCY

7.1 INTRODUCTION

In Chapter Five an integrated Kalman filter algorithm for positioning 3D seismic networks offshore was discussed in detail. In particular, the first part of the chapter concentrated on the design of the functional and the stochastic models necessary for the implementation of such an approach. In Chapter Six, the basic characteristics and options of the software development that was written to perform the computations were described.

This chapter deals with the implementation of the software using real offshore data. The overall aim is to assess the algorithm and performance of the software in terms of correctness and computational efficiency. In other words the main objective of this chapter is to test and to assure that the observation and the dynamic models are correct, and that they are correctly implemented. However, no attempt is made to examine the effect of the functional and stochastic models on the filter solution, i.e. use of a different streamer model and tuning of the filter. These questions are discussed in detail in Chapter Eight.

Three different methods of assessment have been adopted in order to analyse the results that have been derived from the processing of the data sets described in Appendix E. These are

- Analysis of the state vector elements and receiver positions.
- Assessment of the predicted residuals of the observations.

- Independent checks.

In order to aid interpretation, the analyses of the results of both data sets are examined jointly for each method of assessment. Also, for the same reason, all coordinate values in eastings and northings, that were computed with respect to the vessel local topographic coordinate system, were rotated into their along-track and cross-track components. For the first data set (survey in Gabon, 1992) a rotation angle of 58.2 degrees was accepted while for the second one (survey in Irish Sea, 1993) 272.5 degrees - both based on the vessel gyro observations. The determination of approximate state values, necessary to initiate the filter, were computed using the nominal offset and separation values of the various devices deployed in the spread. The initial orientation of the network was based on the vessel gyro value given for the starting time of the line.

Before the results of the aforementioned analyses are discussed, it is necessary to make some remarks on the functional and stochastic model parameters adopted for this part of the analysis. These are given in the following section.

7.2 FUNCTIONAL AND STOCHASTIC MODELS

Both data sets were processed using a fifth order polynomial streamer model. This choice was based on the conclusions that are related to the preliminary compass fitting tests, demonstrated in Chapter Two. Nevertheless, the implementation of a streamer model of a different polynomial order is discussed in Chapter Eight.

Tables 7.1 and 7.2 summarize the standard deviations used to develop the stochastic models that were adopted for these tests, for the first and second data sets. It should be noted that, the observation uncertainty values accepted for these tests are based on the device specifications and on contractors recommendations, as well as on previous experience (Houston, 1987; Naylor, 1990; van Zeelst, 1991; Zinn and Rapatz, 1995). Since seismic surveys are usually carried out in calm seas, quite small values have been set for the standard deviations of the vessel, float and streamer reference point accelerations. Moreover, all measurements were assumed to be uncorrelated. Similarly, the correlation between northings and eastings accelerations has been assumed to be zero (Houtenbos, 1989).

standard deviations of the observations		
	data I	data II
vessel position	3.0 m	3.0 m
vessel gyro	0.5 deg	1.0 deg
acoustic ranges	2.0 m	2.0 m
laser ranges	1.5 m	1.5 m
laser bearings	0.5 deg	-
compass azimuths	0.5 deg	0.7 deg
tailbuoy positions	3.0 m	3.0 m

Table 7.1: Stochastic model of the observations, data I - Gabon 1992, and data II - Irish Sea 1993

As a seismic network is a system that is well behaved with time, the choice of standard deviation values for the vessel and other node accelerations is not a very hard task. On the contrary, the choice of standard deviations that can be used for the streamer

orientation angle and especially for the polynomial coefficients driving noise is not such a straight forward process - it is not easy to interpret their real physical effect. Here, it is simply mentioned that for the second set of data, a set of one order lower standard deviation values was adopted for the polynomial coefficient states than the values accepted for the first data set. Given that, in the second survey most of the rear end compasses seem to be quite noisy (possibly due to sea state) and that acoustic data are only available at every other shotpoint, the lower system noise allows the filter the flexibility to react to any abrupt changes of the observations.

standard deviations of the driving noise			
		data I	data II
vessel acceleration		0.01 m/sec^2	0.01 m/sec^2
crab angle rate		0.04 deg/sec	0.01 deg/sec
float and streamer reference point accelerations		0.01 m/sec^2	0.01 m/sec^2
streamer base line's orientation rate		0.01 deg/sec	0.01 deg/sec
streamer polynomial coefficients	data I	c_0	0.5 E-7 m/m^2/sec
		c_1	0.5 E-10 m/m^3/sec
		c_2	0.5 E-13 m/m^4/sec
		c_3	0.5 E-16 m/m^5/sec
	data II	c_0	0.5 E-8 m/m^2/sec
		c_1	0.5 E-11 m/m^3/sec
		c_2	0.5 E-14 m/m^4/sec
		c_3	0.5 E-17 m/m^5/sec

Table 7.2: Stochastic model of the dynamic model, data I - Gabon 1992, and data II - Irish Sea 1993

7.3 LOCATING THE SEISMIC SPREAD ELEMENTS

As detailed in Section 5.3.1 the optimal estimates of the minimum number of individual parameters necessary to locate any point of interest in the spread in real time, are held in the state vector. The filtered state, and its covariance matrix, that is effectively the weighted mean of the predicted state and the state that best fits the measurements at that epoch, is a direct product of the filter computations. Detailed analysis of its element values provides a first idea as to whether both functional and stochastic models are correct and the filter is properly tuned. Also, these estimates can be used as a means of quickly identifying areas of problems or areas which might require particular attention. In the following sections, the results derived for the state vector solution are classified and discussed in groups as formulated in Section 5.3.1.

7.3.1 Vessel Positioning and Heading

It has already been stated in Section 5.3.1 that the vessel's geodetic position and velocity are themselves unknowns of the system. However, in this section only the filtered time series plots of the vessel velocity are being examined. This is because measures of velocity are expected to be much more sensitive to any model misspecifications than measures of position. Figure 7.1 shows the time series in northings and eastings of the vessel velocity in metre per second for the first and second sets of data.

From these plots it can be clearly seen that the velocity values are almost randomly distributed around a mean value with no substantial peaks occurring in at any component in either data sets. More specifically, it should be noted that, during the time interval between shotpoints 700-740, for the analysis of the first data set, the vessel's velocity seems to change rather faster than it does for the rest of the line. It is obvious that this phenomenon is related with the variation in vessel's gyro values - see Figure 7.2. There is clear evidence that the filter solution follows the gyro trends - a sign verifying that the model has been designed and implemented correctly.

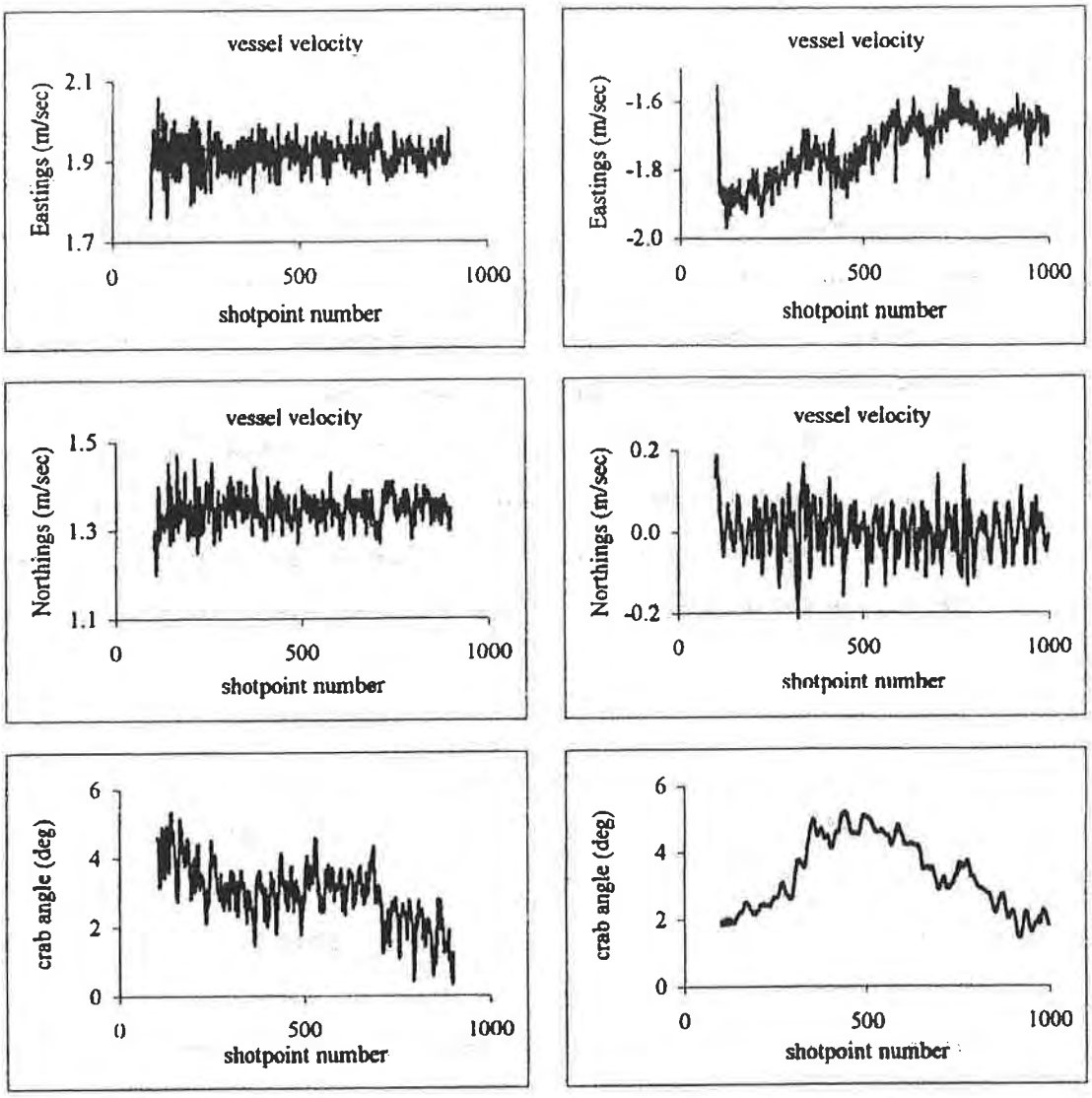

Figure 7.1: Vessel velocity and crab angle, Gabon 1992 (left) and Irish Sea 1993 (right)

In the second data set, as it is reasonable to expect, analysis of the velocity values in northings shows that they are approximately equal to zero, since the vessel's course was due west. Moreover these values seem to be quite noisy, compared with the velocity values derived in eastings - possibly due to substantially noisy gyro values. Also, it should be pointed out that examination of the velocity values by chronological order reveals a slight decrease in the vessel's resultant velocity.

The plots which are displayed at the bottom of Figure 7.1 depict the filter solution for the vessel crab angle. These plots allow the following conclusions to be drawn.

For the solution of the first data set a strong link between the crab angle values and the raw gyro measurements can be observed. The top plot of Figure 7.2 shows clearly that as gyro values decrease with shotpoint the crab angle values also do so. This similarity in trends is much more distinct during the time period about shotpoint 700. The same phenomenon can be also noticed in the second data set by examining the corresponding plots of Figures 7.1 and 7.3. However, here, this phenomenon is not immediately evident due to the very noisy raw gyro. Because of the noisy gyro, a lower standard deviation has been used for the crab angle acceleration (Table 7.2) resulting in a much smoother curve than the one derived for the first data set. In Chapter Eight it will be shown that the vessel crab angle time series pattern is highly dependent on its standard deviation driving noise value, i.e. the dynamic model.

7.3.2 Streamer Base Line Orientation and Reference Point Location

In this section the results of the analysis for the state vector elements that are related to the streamer unknowns are discussed. These parameters consist of the polynomial coefficients, the streamer orientation angle and the streamer's coordinate reference system origin along with its velocity components. The last three will be discussed here in more detail. For the polynomial coefficients it is simply mentioned that analysis proved that coefficients of a low order, namely third or fourth, are of bigger magnitude in absolute terms, than coefficients of a higher order. Moreover, it seems that all coefficients do not change very fast with time, especially those of a low order. A more detailed discussion of their role and effect on the receivers position and precision is given in Chapters Eight and Nine.

Figure 7.2 illustrates the filter solution for the direction angle α for each one of the three cables for the data set derived from the survey in Gabon while Figure 7.3 depicts the same estimate for the analysis of the second set of data - the Irish Sea campaign.

The first thing to note from Figure 7.2 is that the results for all three streamers are comparable. This excellent consistency in magnitude and trends reveals that all cables seem to react in the same way to external forces and to any changes in the vessel's

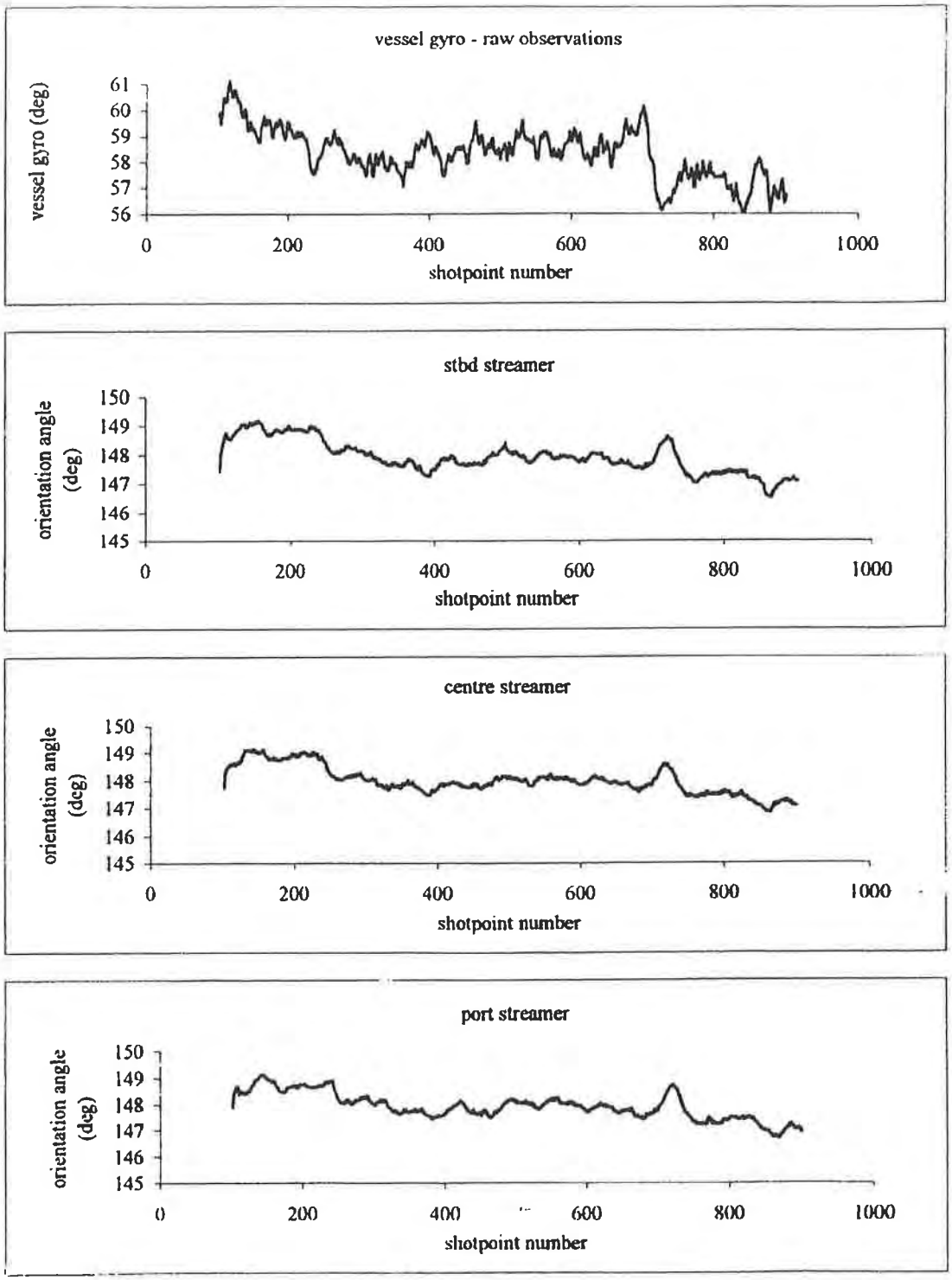

Figure 7.2: Raw gyro measurements and streamer orientation angle, Gabon 1992

course. Moreover, similar conclusions to those derived for the vessel's crab angle can be also drawn for the orientation angle of each streamer. Again, the variations of angle α follow very closely the variations of the vessel's gyro values. Of course, the main criterion, on which how fast angle α is expected to change with time, depends on the choice of the driving noise standard deviation of α, i.e. the stochastic model of the dynamic model. However, this point is discussed in more detail in Chapter Eight.

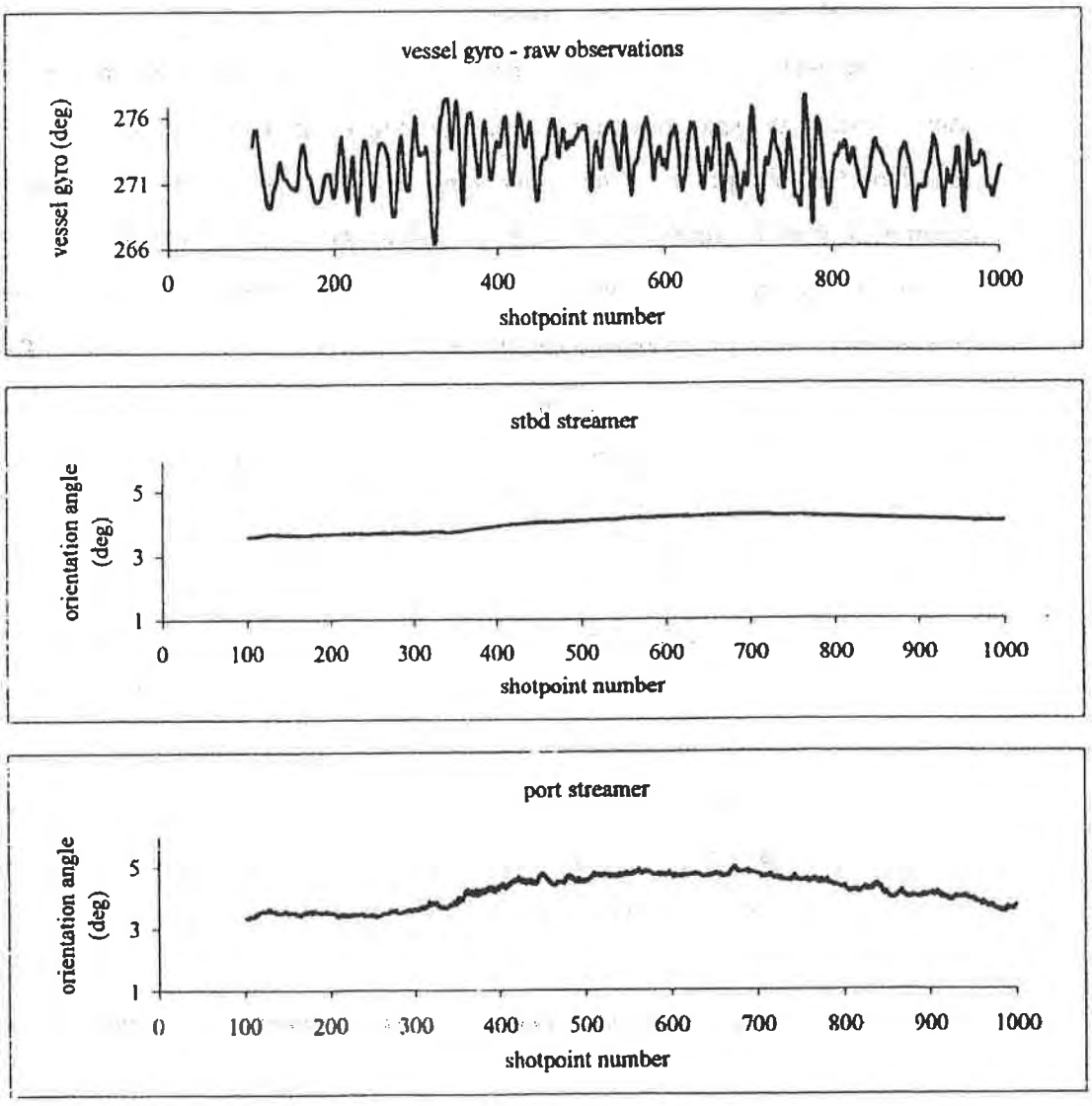

Figure 7.3: Raw gyro measurements and streamer orientation angle, Irish Sea 1993

From Figure 7.3 it is evident, almost just at a glance, that these conclusions can also apply for the results derived from the analysis of the second data set. Nevertheless, a few differences can be observed with the following points being of interest.

Although analysis showed very similar patterns for angle α for both starboard and port streamers, the variations with time for the port streamer seem to be much more noisy than for the starboard one for some reason which is not discernible from the analysis so far. Nevertheless, it should be stressed that the same input values for the stochastic model parameters have been set for both cables. Moreover, given that both streamers point at almost the same direction at the beginning of the line, it is surprising that after a period of 500 shotpoints - about one hour of survey - the mean orientation of the streamers differs by almost 0.8 degrees - a radial separation of about 28.0 metre at the rear end of the cables. However in reality it is reasonable to expect the separation between streamers not to change significantly with time - as angle α does. This can be easily seen by examining the receiver positioning time series plots given in the following section. It is possible that the polynomial coefficients shoulder the task of restoring this discrepancy, and shift back the streamer to its 'true' position.

The streamers' coordinate reference system origin and its velocity components is the last group of the state vector elements to be discussed in this section. Analysis of the results of both data sets lead to similar conclusions. Note that in order to aid interpretation the along-track differences are plotted at a different scale to the cross-track ones. This also applies for some of the plots shown in the following sections. The points to notice from these diagrams are

1. Figures 7.4 and 7.5 demonstrate that the maximum variations in the location of the head point of any streamer range from approximately 6.0 metre in the in-line direction to approximately 15.0 metre in the cross-track direction. This applies throughout the line with only a very few shotpoints exceeding these marginal values.
2. The cross-track coordinates show similar patterns for all streamers in each line. On the contrary, the variations in the along-track direction indicate a symmetrical effect

between the starboard and port streamers. Only the centre streamer coordinates suggest no significant variations with time.

3. Figure 7.6 illustrates the velocity estimates of each streamer reference point with respect to the vessel navigation reference point. Analysis of these diagrams shows that the velocity values for all these points follow an approximately white noise pattern with no substantial peaks occurring - suggesting that there is no need at all to model acceleration terms.

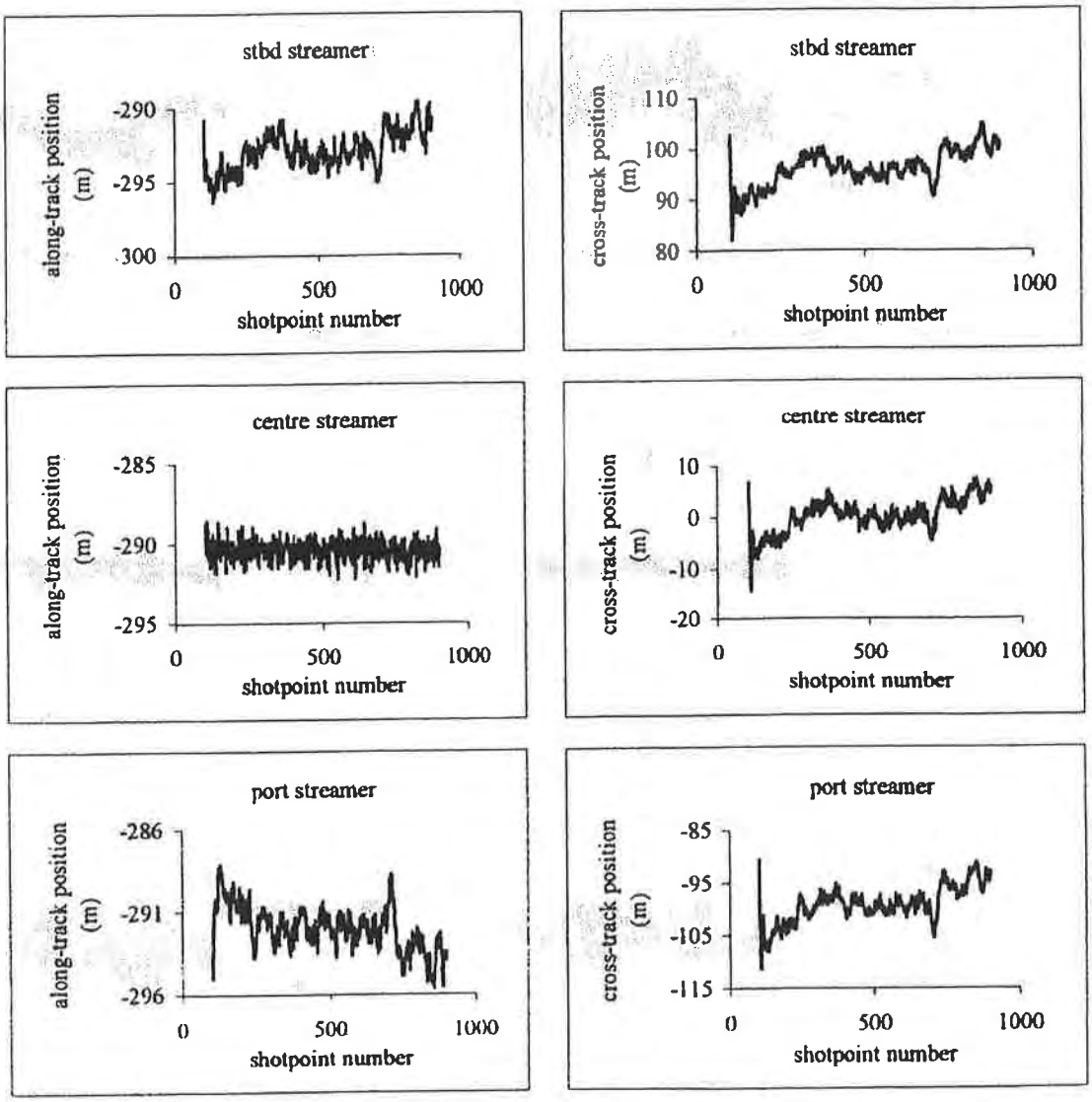

Figure 7.4: Streamer reference point location, Gabon 1992

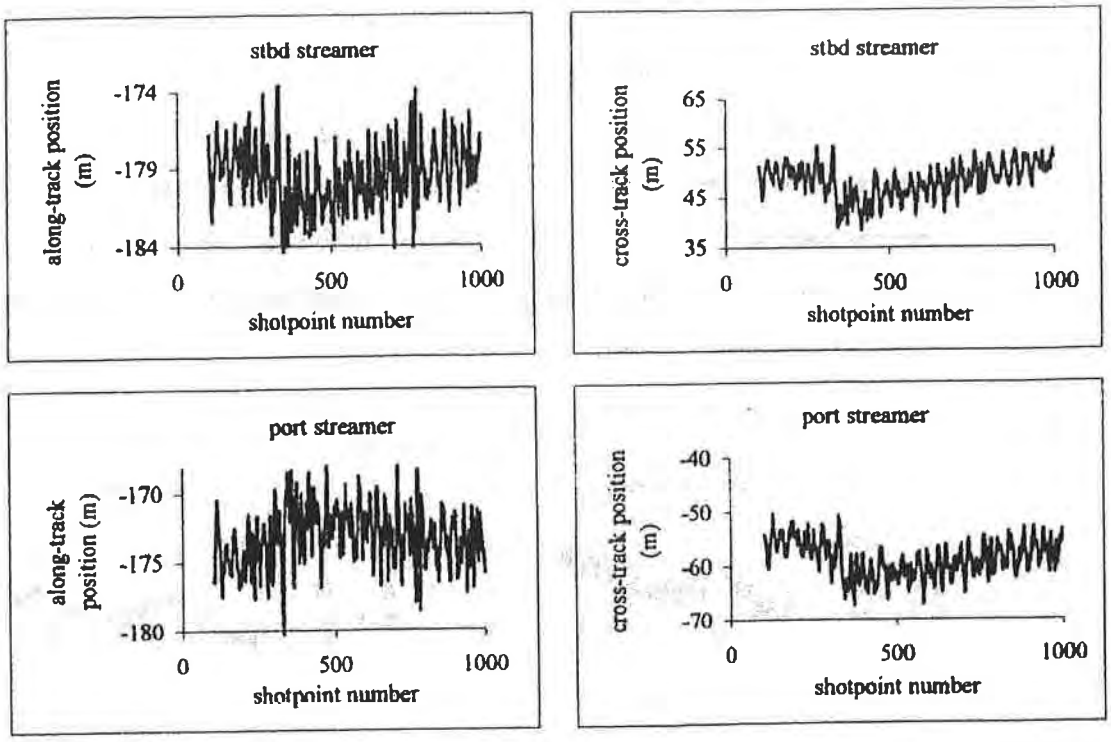

Figure 7.5: Streamer reference point location, Irish Sea 1993

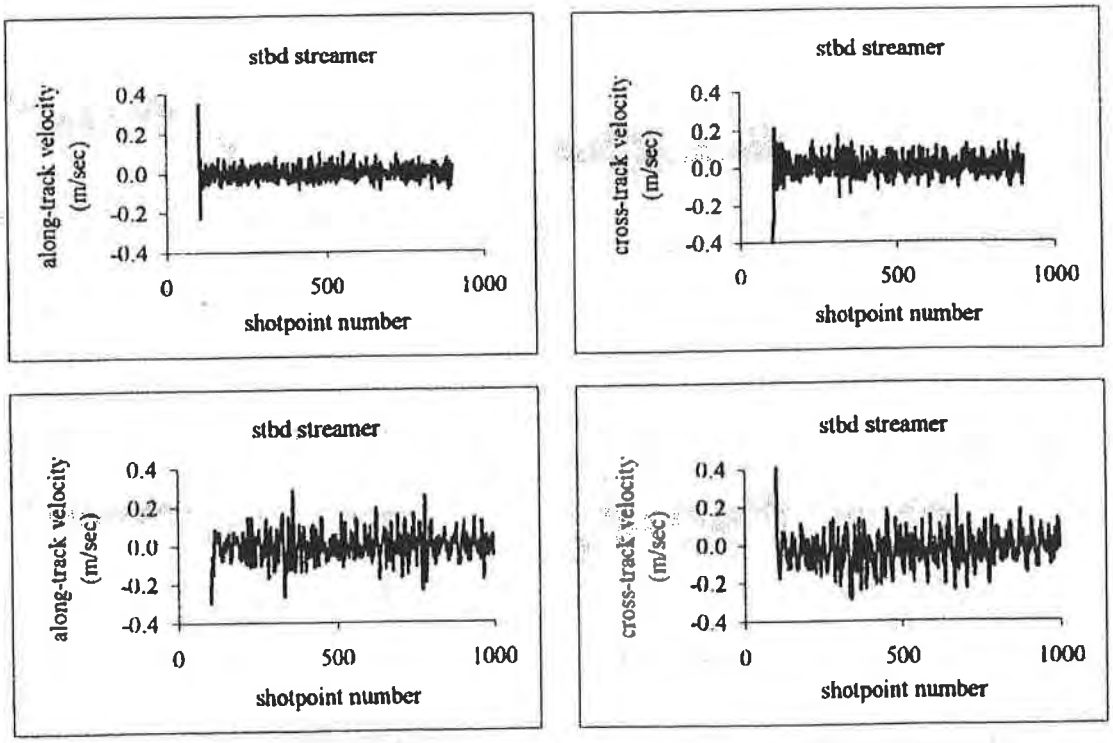

Figure 7.6: Velocity components of the starboard streamer reference point, Gabon 1992 (top), and Irish Sea 1993 (bottom)

7.3.3 Float Nodes and Hydrophone Groups Positioning

'Offshore operators are today specifying acceptable seismic navigation results in terms of seismic bin size and the HMP' (Zinn and Rapatz, 1995). As stated in Section 1.2.1 a HMP is defined as the average of the positions of a source node and a streamer receiver. Therefore, source and hydrophone positions are doubtless the estimates of the greatest importance of all parameters that are being discussed in this section. To compute the hydrophone positions the filtered values of the state vector, that relate to streamer modeling are used, while source locations are themselves states in the system. The results that relate to float positions are illustrated first in the following discussion.

As mentioned in Appendix E, a configuration comprising a dual source and six float deployments (four sources and two towfish) was used in the first and second surveys respectively. Nevertheless, here, only the results of four of these units are discussed. This is because analysis of the time series coordinates of each individual source has led to similar conclusions for each data set. The points to note from the analyses of the first data set are

1. Figure 7.7 indicates a consistency in magnitude and trends in the along and cross-track positions for the starboard and port source units. However, the occurrence of quite a few peaks, of the order of 1.5 metre, in the along-track coordinates of the starboard gun, suggests that, the observed ranges from/to this unit from/to the various connecting nodes in the front end network are noisy, e.g. acoustic range 13 at the front-end network - see Appendix E1.
2. If Figure 7.7 is examined in combination with Figure 7.4, it is apparent that, there appears to be considerable evidence to support the idea that all nodes in the front end of the spread react in a similar way to any changes in the vessel's course or to any external forces - representing a strong argument that the model is correctly designed and implemented.
3. Again, similar to the streamer reference points, the velocity components of these units reveal an approximately zero mean pattern in the along and cross-track directions.

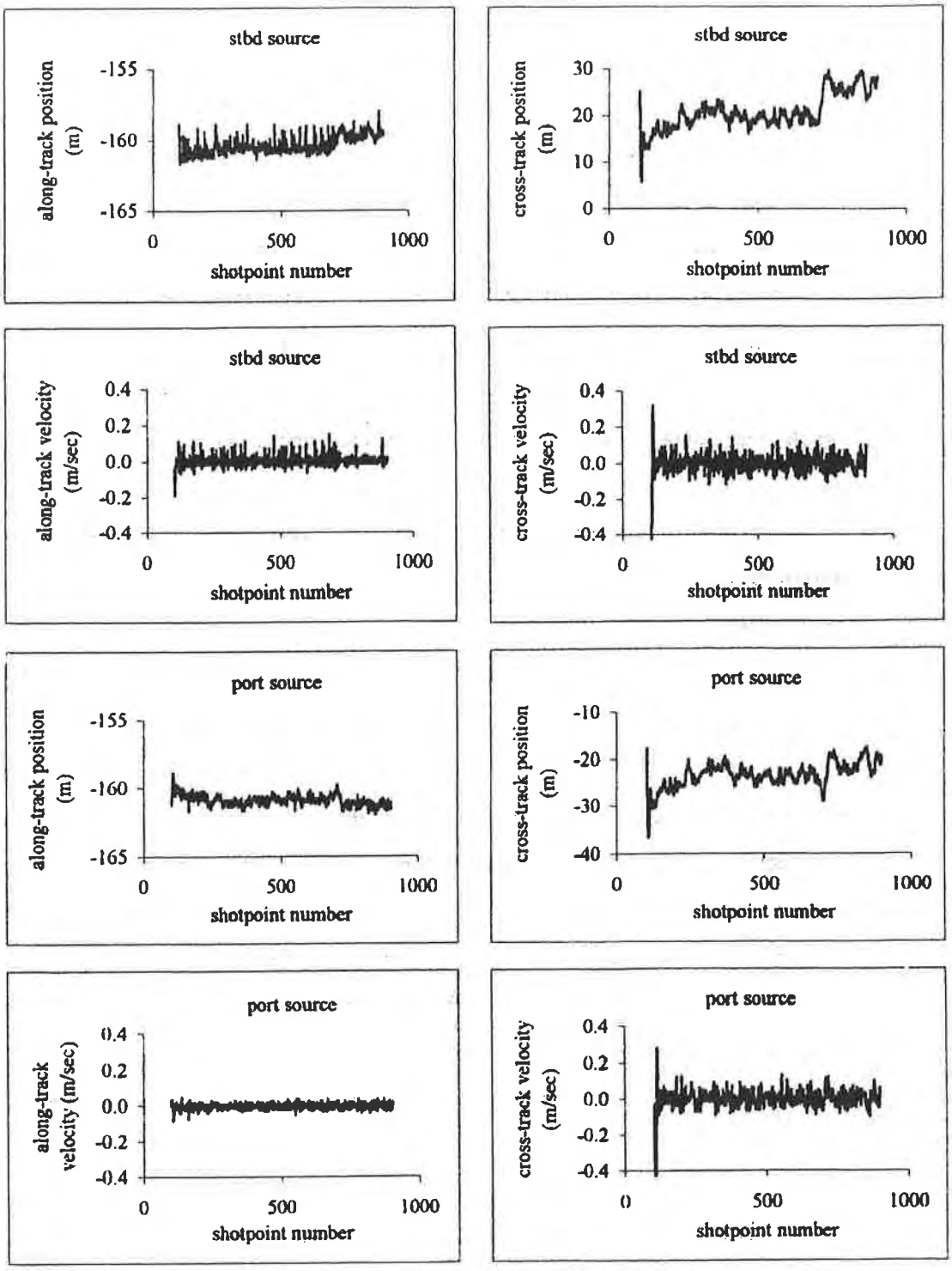

Figure 7.7: Location and velocity components of the source points, Gabon 1992

Analysis of the results of the processing of the second set of data leads to similar conclusions. Here, only the plots that are related to the port outer gun and starboard towfish are given in Figures 7.8 and 7.9 respectively. In addition to the previous conclusions the following points should be noted.

Figure 7.9 indicates more insignificant variations in both along and cross-track coordinates, notably in the cross-track direction, for the starboard towfish than for any other floating body for this data set. Any change of the vessel's speed and any fluctuation in the waves generated by the vessel could be a partial explanation of this phenomenon. This is because the guns are towed right behind the vessel, while towfish deployments have been designed to float a few metre on each side of the vessel. The second point to note is that due to lack of adequate observations from/to the port towfish the filter has proved itself unable to locate this node - see also Section 7.4.1.

Though float and receiver positions are both equally critical in locating the HMP between these two targets, the computation of float and receiver positions is not an equally simple task. The real challenge is how to locate correctly and accurately the receiver groups. Figures 7.10 through 7.12 depict the results of the analyses of the processing of both data sets.

In the first survey the network configuration deployed three streamers comprising 240 hydrophones, each in total length of about 3100 metre. Here, for reasons of clarity, only the positions for three receiver groups fixed on the starboard streamer for each survey are depicted in Figure 7.10. In order to cover the geometry, these have been selected as, one unit from the near-end groups, the second from the rear-end groups, and the third one fixed somewhere midway along the cable.

Figure 7.10 shows similar trends in pattern and magnitude for all three hydrophones. In particular, from these plots there is considerable evidence that the three receivers move, more or less, as a rigid body in the in-line direction. By examining the plots that relate to the first survey, shown on the left, in more detail, only a relative displacement of the order of 0.30 metre can be observed between the first and last receiver for the time

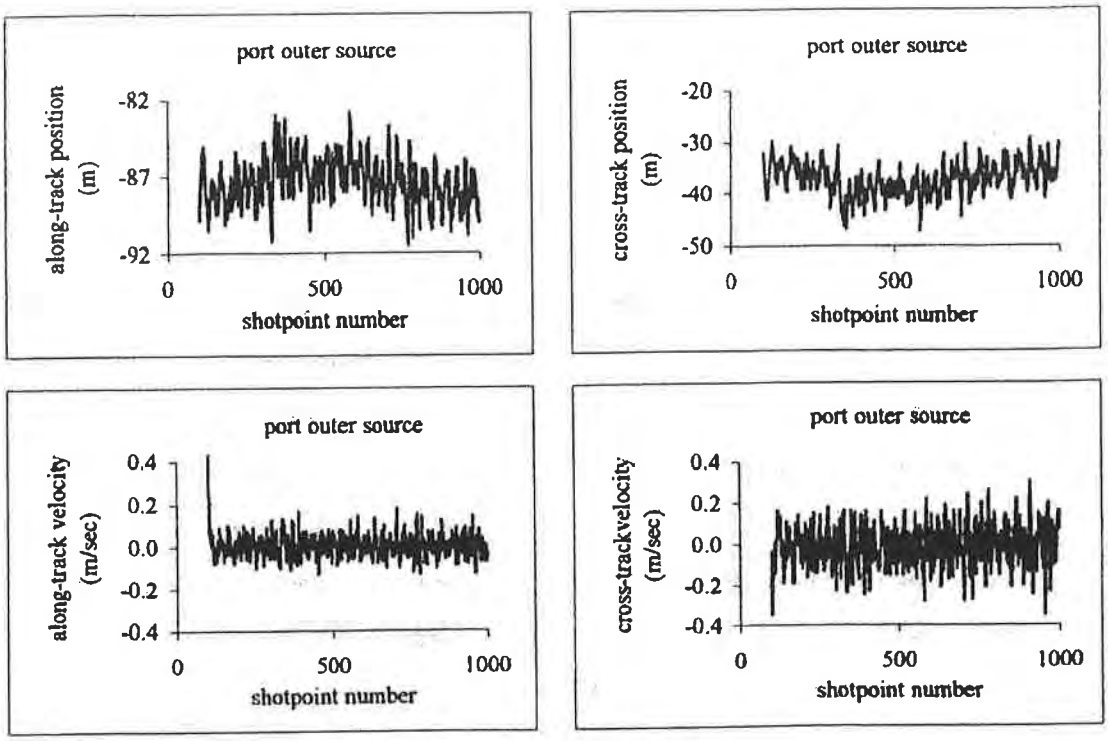

Figure 7.8: Location and velocity components of the port outer source point, Irish Sea 1993

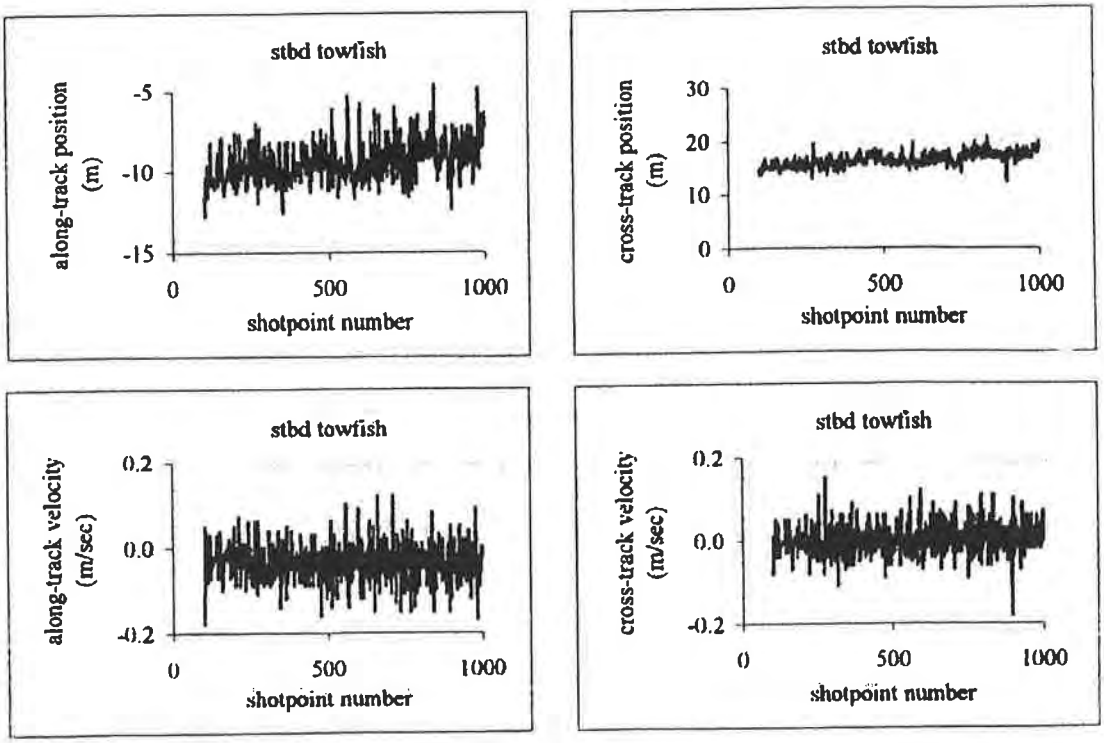

Figure 7.9: Location and velocity components of the starboard towfish point, Irish Sea 1993

interval between shotpoints 200 and 700. Fluctuations in cable stretch could be a valid reason for a variation of this magnitude. Nevertheless, any absolute variation (with respect to the vessel) in the in-line positions, is basically due to the movement of the head of the streamer (movement of the whole streamer) with respect to the vessel navigation reference point - see also Figure 7.4.

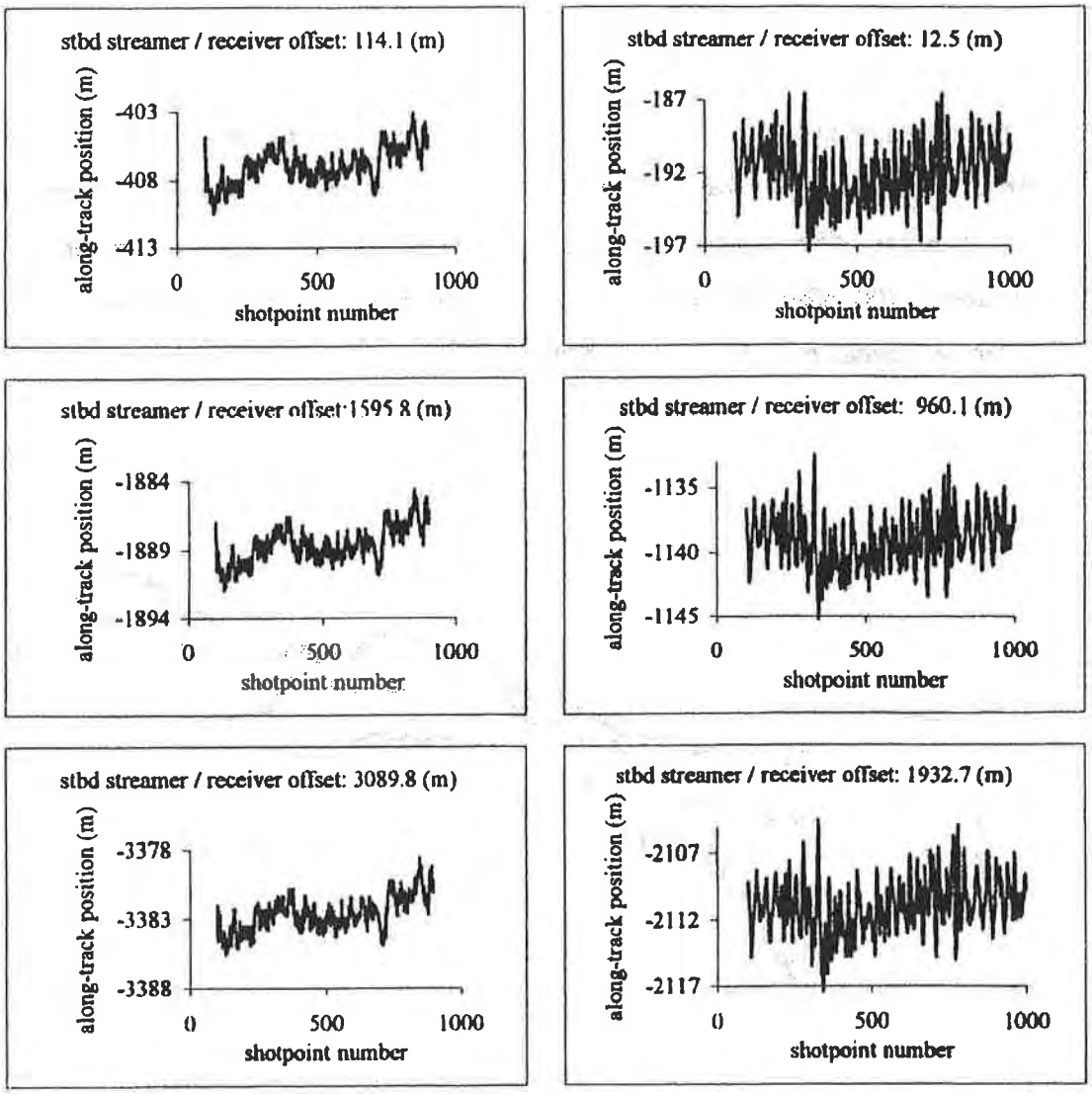

Figure 7.10: Along-track location components for three hydrophone groups, Gabon 1992 (left), and Irish Sea 1993 (right)

Cross-track coordinates, given in Figure 7.11, show an apparent movement to the starboard, especially for the receiver which is located at the rear end of the cable. The following explanation could account for this phenomenon. As mentioned at the very beginning of this chapter, cross-track and along-track coordinates are computed with

respect to a fixed gyro value. Therefore, as the vessel's gyro and streamer orientation angle α decrease with time (Figure 7.2), it seems that the receiver positions move to the starboard; along-track and cross-track positions are not related to instantaneous gyro values. This phenomenon is more distinct for the far end groups because they are a long distance from the vessel, i.e. the origin of the along-track and cross-track coordinate system.

The second point to note is that the variation with time of the rear end receiver seem to be slightly more noisy than the variations of the hydrophone placed at the front end of the streamer. Also, again, any abrupt variations in the vessel's gyro and angle α, about shotpoint 700, affect the receiver cross-track positions, in particular those for devices which are deployed at the tail end of the network.

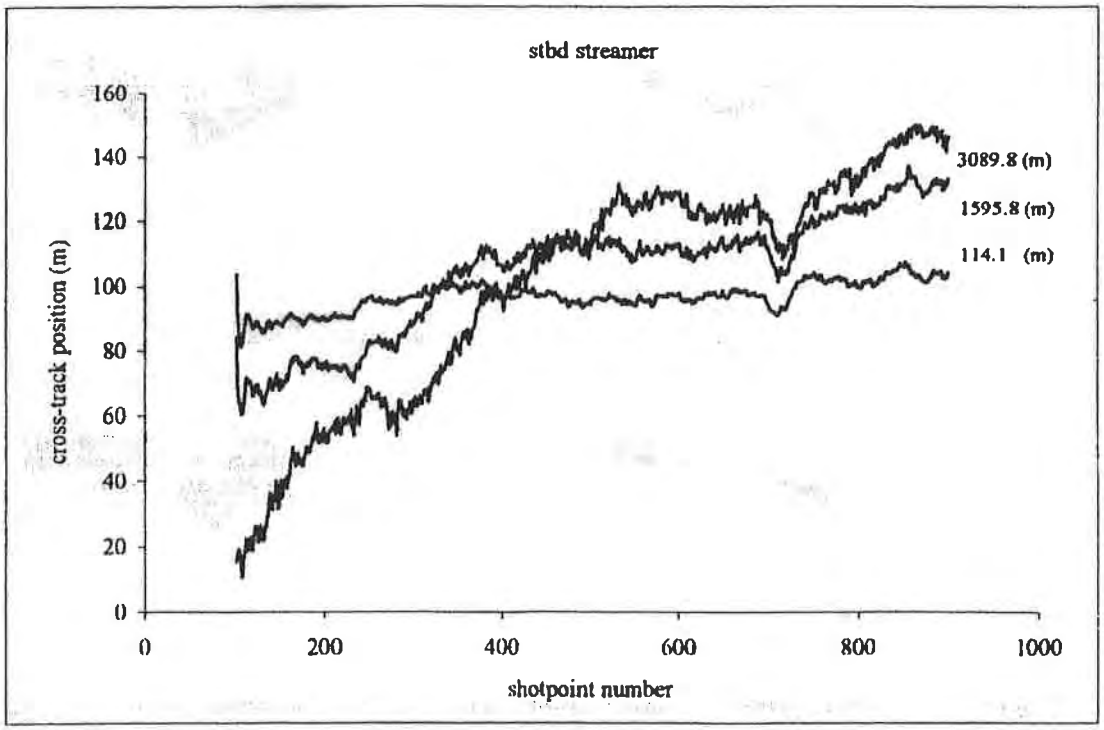

Figure 7.11: Cross-track location components for three hydrophone groups located on the starboard streamer, Gabon 1992

Similar conclusions can also be drawn from the analysis related to the second survey. Figure 7.12 depicts the same estimates as for the first data set, for three receivers fixed on the starboard streamer. Once more, the only point to stress here, is the potential of

the interdependence of an integrated network. Any variations (improvements) to tailbuoy positioning, can affect (improve) the positions of the front end receivers. The variations to the starboard tailbuoy positioning between shotpoints 310 and 340 and shotpoints 760 and 780, shown in Appendix E2, affect the position of all the receivers.

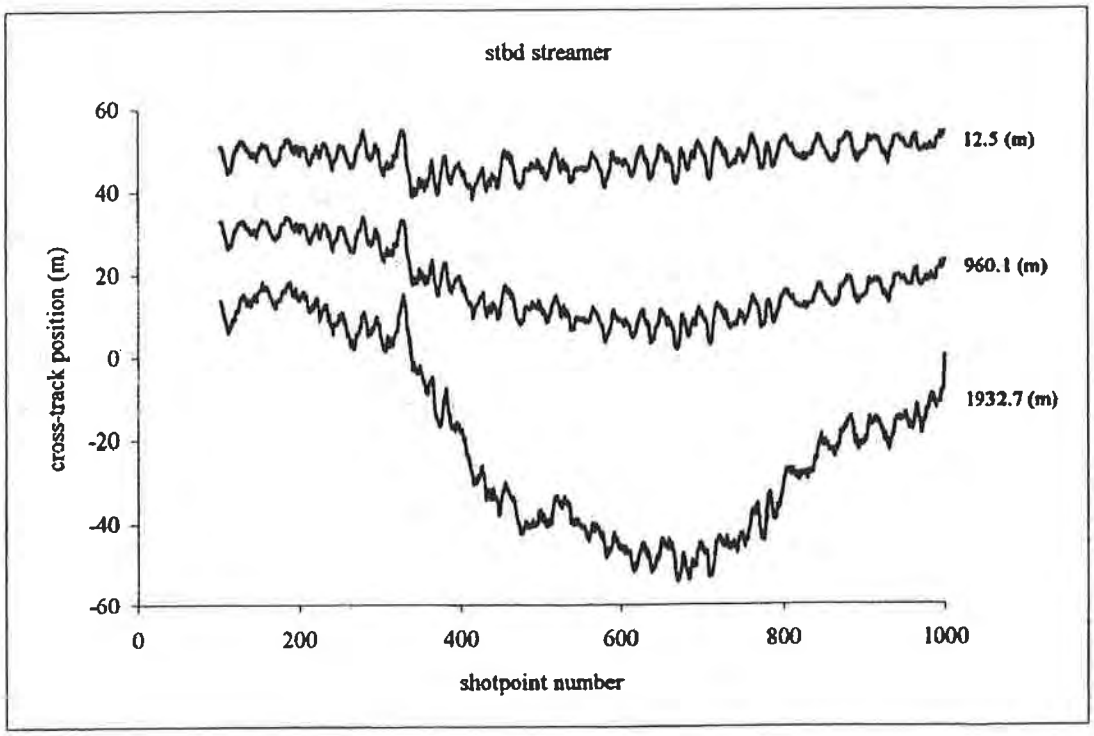

Figure 7.12: Cross-track location components for three hydrophone groups located on the starboard streamer, Irish Sea 1993

7.4 ASSESSMENT OF THE PREDICTED RESIDUALS OF THE OBSERVATIONS

As stated in Section 4.1.2 a predicted residual is computed from the difference between a measurement at a particular time (usually a shotpoint) and the measured quantity computed from the predicted state of the system. Predicted residuals, also known as the innovation sequence, are an excellent way to assess the performance of a system. Predicted residuals that are, overall, unbiased (i.e. zero mean) and commensurate in size with the expected observation errors, show that the observation and dynamic models are correct, that they are correctly implemented, and that the filter is properly tuned.

In the following section an attempt is made to evaluate the innovation sequence results derived for each single measurement classified by observation type. These include predicted residual values for all the acoustic and laser ranges, compass azimuths as well as predicted residuals of points of known 'absolute' position, i.e. Syledis or GPS stations.

7.4.1 Acoustic and Laser Range and Bearing Observations

As detailed in Appendix E, part of the survey configuration in the first campaign consisted of an acoustic and laser ranges observation network as well as of a few laser bearings, a total number of 56 observations at the front end, while 29 acoustic ranges were observed at the tail end of the spread. In the second survey, front end positioning utilized an acoustic network consisting of 10 Sonardyne acoustic units. In addition, a full-length MultiTRAK acoustic system was used to provide total cable positioning, all together 68 observations - see Appendices E1 and E2.

Around 800 continuous shotpoints from the first survey and 900 shotpoints from the second (spanning a total period of time 105 and 120 minutes respectively) have been processed and a number of the analyses of the predicted residuals of the observations have been performed. These results are depicted in Figures 7.13 through 7.18. In the following sections the part of the analysis that is related to the first data set is discussed first.

Figure 7.13 and the plots on the left of Figure 7.14 contain the mean values and standard deviations of the observation residuals as well as the number of rejected measurements for each observation computed from all 800 shotpoints. These include the acoustic ranges (observations 1-45), laser ranges (observations 46-49) and laser bearings (observations 1-7) at the front end of the spread and all acoustic ranges observed at the tail end network (observations 1-29). Given that the *a priori* standard deviations of the acoustic ranges, laser ranges and laser bearings have been set to be 2.0 metre, 1.5 metre and 0.5 degrees respectively, these results are really extremely encouraging.

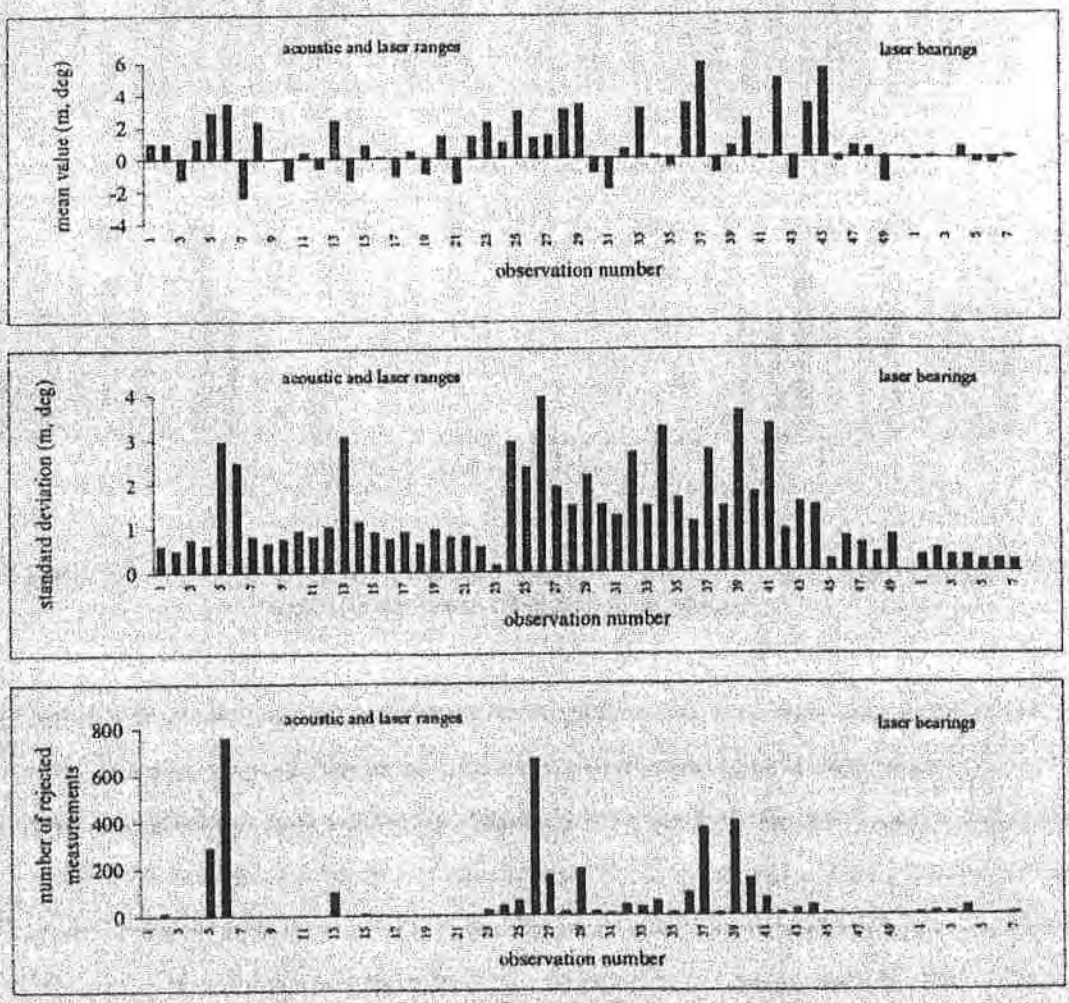

Figure 7.13: Statistics of the predicted residuals - front end acoustic and laser networks, Gabon 1992

As can be seen from these histograms the mean values for most of the acoustic ranges are less than three standard deviations. Examination of Figures 7.13 and 7.14 in more

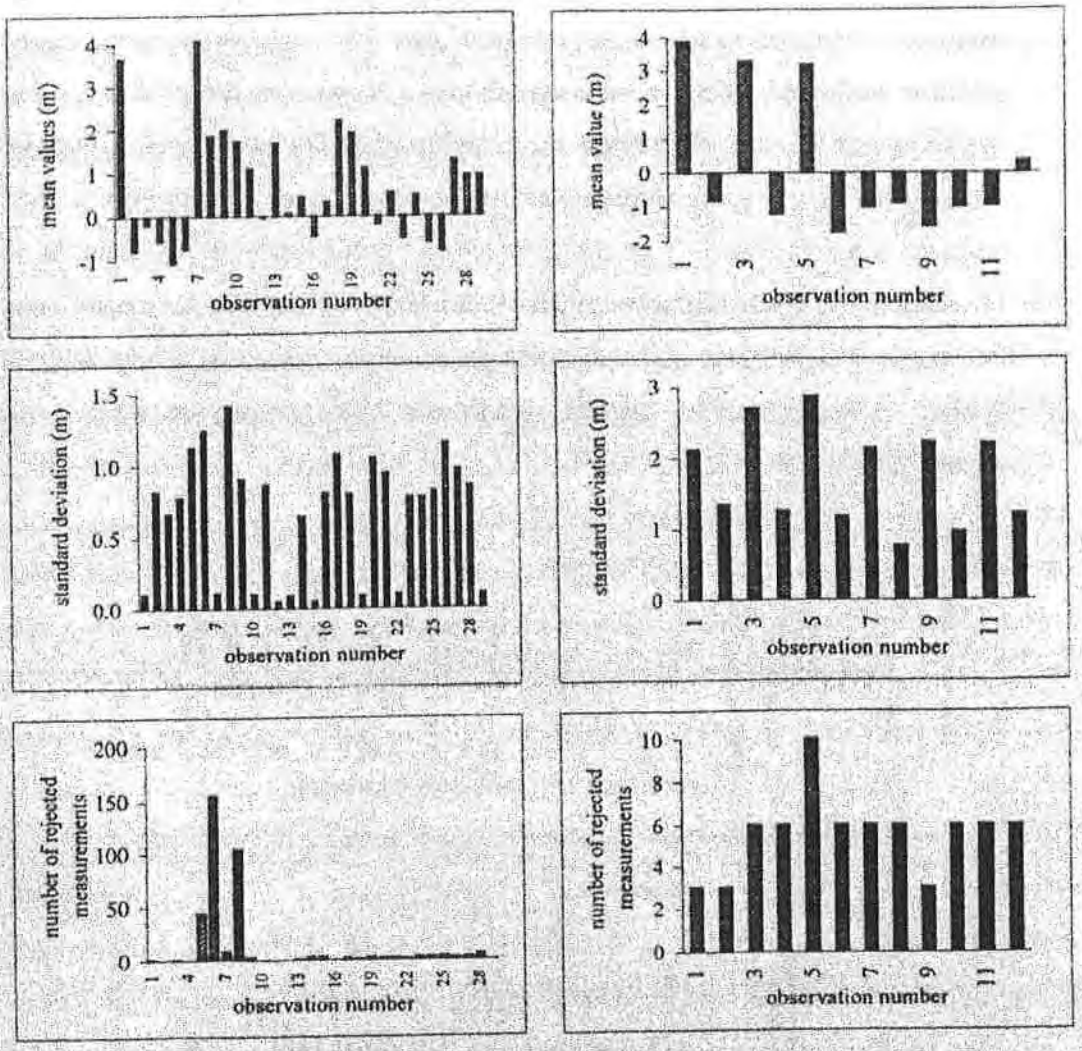

Figure 7.14: Statistics of the predicted residuals - tail end acoustic network, Gabon 1992 (left) and front end laser network, Irish Sea 1993 (right)

detail shows that ranges for which a large number of shotpoints has been rejected present bigger standard deviations. This is to be expected as the contribution of these observations to the final solution is smaller (there are less of them) - see plots 7.13 centre, 7.13 bottom and plots 7.14 centre left, 7.14 bottom left. This phenomenon is more distinct for ranges 5, 6, 13, 26, 37 and 39 in the front end network and for ranges 5, 6 and 8 in the rear end network. Moreover, these results can be explained by examining these diagrams in combination with the corresponding raw measurement time series plots given in Appendix E1. From these graphs it can be clearly seen that these observations are the most noisy. Hence, it can be concluded that the filter is correctly

identifying the outlying observations. However, it should be mentioned here, as detailed in Section 5.5.3, that the only criterion that the filter uses in order to detect and reject a measurement depends solely on its predicted residual - a very simple procedure for identifying and removing outliers has been adopted here.

Also, from the same histograms the following three points can be concluded. Firstly, observations 1-22, i.e. any range observed between the vessel and any node at the front end, - except for observations 5, 6 and 13 as discussed earlier on - present much smaller standard deviations, of the order of 1.0 metre, than those made between any devices fixed both on streamers. This conclusion is consistent with the raw observation time series plots - see Appendix E1. The second point to note, is that, the standard deviation values for almost all ranges observed between points located on the same streamer are very small and of similar magnitude. This is well justified since the system is expected to be much more stronger in the along-track direction. However, this phenomenon may reveal, somehow, an unknown model effect on these observations - possibly due to the assumption of polynomial fitting model. Such observations are ranges 23, 42, and 45 in the front end network and observations 1, 7, 10 and 12 in the rear end network (see configuration diagrams in Appendix E1). Finally, all predicted residuals and standard deviations that relate to laser ranges and bearings are within the limits in which they are expected to vary, i.e. their *a priori* observation errors.

If Figure 7.15 is examined in combination with the corresponding raw observation time series diagrams, it is immediately evident that most of the conclusions drawn for the first set of data, in the foregoing sections, apply for the second data set as well. Therefore, in the text that follows only conclusions that are related to special characteristics of the second survey, such as observation quality and geometry configuration features, are discussed.

The points to notice from the histograms shown in Figure 7.15 are

1. Ranges 1 and 7 were observed between devices 1 and 2, which are both fixed on the vessel, i.e. they are configuration measurements. Therefore, these observations are

not included in the filter solution and do not appear on the corresponding histograms.

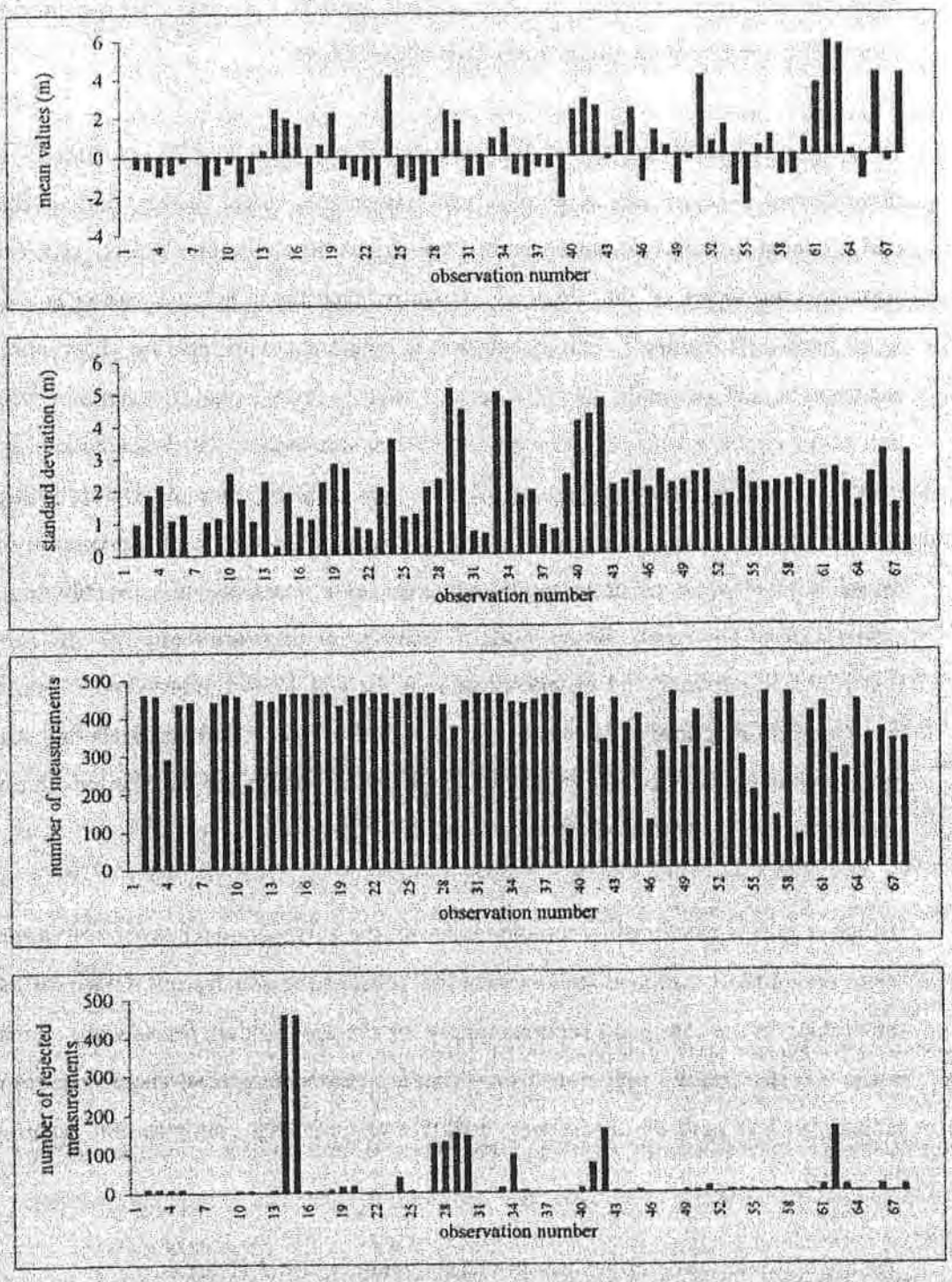

Figure 7.15: Statistics of the predicted residuals - Sonardyne and MultiTRAK acoustic networks, Irish Sea 1993

2. Although the data files consist of 900 continuous shotpoints, acoustic measurements are only available for less than 450 shotpoints for most of the observations. This is because ranging data was collected at approximately every other shotpoint location, i.e. every 25.0 metre or 14 seconds. Moreover, for the same observations, it should be pointed out that 14 out of 66 ranges are available for less than 350 epochs and some of them are available for much less than 200 epochs - on average every 4.5 shotpoints. Examination of the third histogram in Figure 7.15 in more detail reveals that acoustics 39, 46, 55, 57 and 59 present the lowest number of measurements. Bearing this in mind, it is fairly easy to note from the survey configuration diagrams (Appendix E2) that these ranges are related to units 27 and 68. Therefore, it can be concluded that devices 27 and 68 were unusable for quite long time throughout the line for some unforeseen reason.
3. The bottom plot of Figure 7.15 shows that observations 14 and 15 have been rejected for almost every shotpoint though they are not especially noisy - see Appendix E2. However, this is not entirely surprising since observations 14 and 15 are the only measurements to locate the port towfish float - there are no redundant measurements. Hence, it is possible to assume that even small variations in these measurements cause the filter to diverge, resulting in sequential rejections of these observations, and therefore, inability to locate this node.
4. The last point to note is that observations 27 through 30, which have been rejected for a large number of epochs, are all ranges observed from/towards device 8 (see Appendix E2). Therefore, it is possible to conclude that this unit did not operate properly.

The last observation type to be examined in this section is laser ranges. Before an attempt is made to assess the predicted residual measures of these observations it should be pointed out that these observations are not 'real' measurements. These values represent northings and eastings of the actual laser observations made from the vessel to the various nodes in the front end network. Moreover, since the line direction is 270 degrees (east-west), northings represent cross-track coordinates while eastings represent along-track coordinates.

Two points are immediately evident to the histograms given on the right of Figure 7.14

1. All observation components in northings present much bigger mean and standard deviation values than in eastings. As expected the system is much more sensitive in northings, (almost in the cross-line direction), than in eastings, (almost in the in-line direction).
2. Also, all measurements in northings that have been observed towards the port sources and streamer (observations 1, 3 and 5) present bigger values than those observed towards the starboard elements. This implies some sort of cooperative behavior. Its origin is currently unknown and under investigation.

7.4.2 Compass Azimuths

In the first campaign a configuration of 13 compass units per streamer, spaced at intervals of approximately 300 metre, was utilized to provide total cable orientation. Similarly, in the second survey 10 compass units were deployed at intervals also of 300 metre along the length of each of the cables in this twin streamer configuration. The uncertainties of the raw compass observations adopted for the purpose of this analysis are given in Table 7.1.

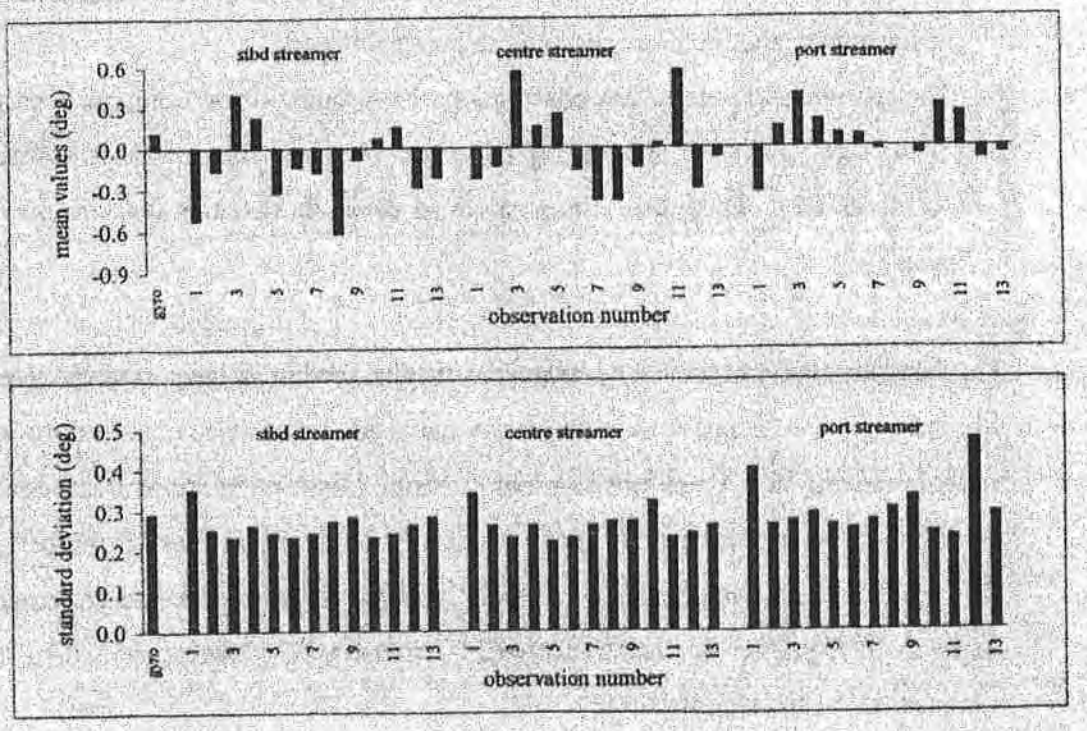

Figure 7.16: Statistics of the predicted residuals - compass azimuths, Gabon 1992

Similar to the previous section, the results of the analysis related to the first set of data are discussed fist. These results are presented in Figure 7.16 and allow the following conclusions to be drawn

1. It is important to note that the mean values for all compasses are less than 0.6 degrees given that the *a priori* standard deviations of these measurements have been set to be 0.5 degrees. Also, they follow an approximately white noise pattern strongly supporting the use of the polynomial cable shape model.
2. All compass standard deviation as well as vessel gyro values are of the same low magnitude. Moreover, they show similar trends in the three streamers.

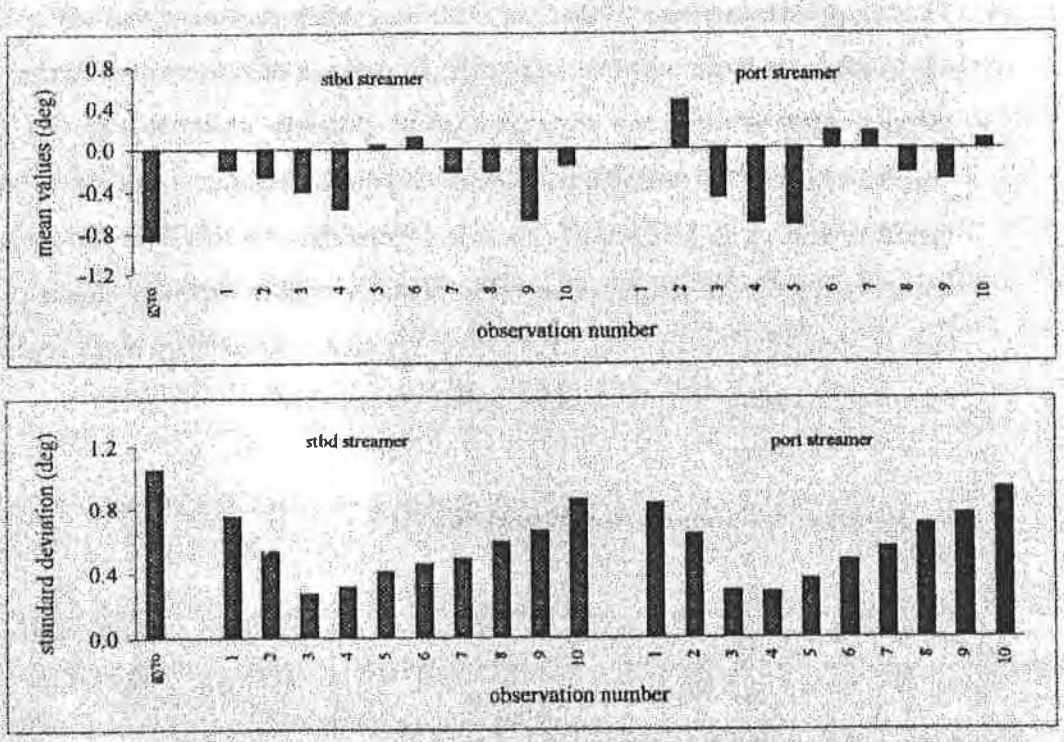

Figure 7.17: Statistics of the predicted residuals - compass azimuths, Irish Sea 1993

In contrast to these conclusions, the results derived from the processing of the second data set seem not to be especially encouraging. From Figure 7.17 it can be seen that

1. The magnitude of both mean and standard deviation values has slightly increased, notably the standard deviation values, compared with the results derived from analysis of the first data set. However, this trend seems to be consistent with the corresponding raw observation time series plots and the conclusions drawn for the

last one of the independent checks discussed in section 7.5.3. Moreover, it should be noted that the *a priori* standard deviation values which have been accepted to process this data set are somewhat higher than to those adopted for the first one.

2. Although the mean values derived for the starboard streamer are, on average, the same in magnitude as they are for the port one, a small systematic bias seems to appear in the starboard cable - the values are not randomly distributed. Moreover, an apparent bias seems to be present in both streamer standard deviation values - much bigger values can be observed for all compasses placed in the front and tail ends of the cables compared to those fixed midway the streamers. The origin of these discrepancies is currently unknown.
3. The last point to mention, is that, for both data sets a very small number of compass observations has been rejected. This phenomenon is directly related to the window length which is used for detection (and possibly rejection) of an outlying observation, i.e. the maximum accepted predicted residual value in order for a measurement not to be rejected. For the second data set this limit has set to be six times the standard deviation value. Note that if a smaller window value is selected a large a number of compass observations is rejected - obviously a more sophisticated approach of testing the raw data for outliers is required.

7.4.3 Vessel and Tailbuoy Absolute Positions

In this section the results of the analyses based on the predicted residual values for the 'absolute position' measurements are discussed. These include the vessel and tailbuoys Syledis. These results are depicted in Figure 7.18.

From these figures it is apparent that the mean values of the predicted residuals of the vessel geodetic positions are of about the same magnitude and of the order of the *a priori* standard deviations (Table 7.1) of these observations in both data sets and in both components. Similar conclusions to these can also be drawn for the standard deviation values of these estimates.

Whilst the mean values of the predicted residuals of the tailbuoy positions reveal the same sort of trends and further analysis is not required, a more detailed analysis of the standard deviation plots of these estimates shows that standard deviations for the first set of data are much bigger than those for the second one, although the same *a priori* uncertainty values have been adopted - see Table 7.1. The second point to note from these figures is that all latitude uncertainties are larger than the longitude ones. From the analysis so far it is unclear what is causing the problem.

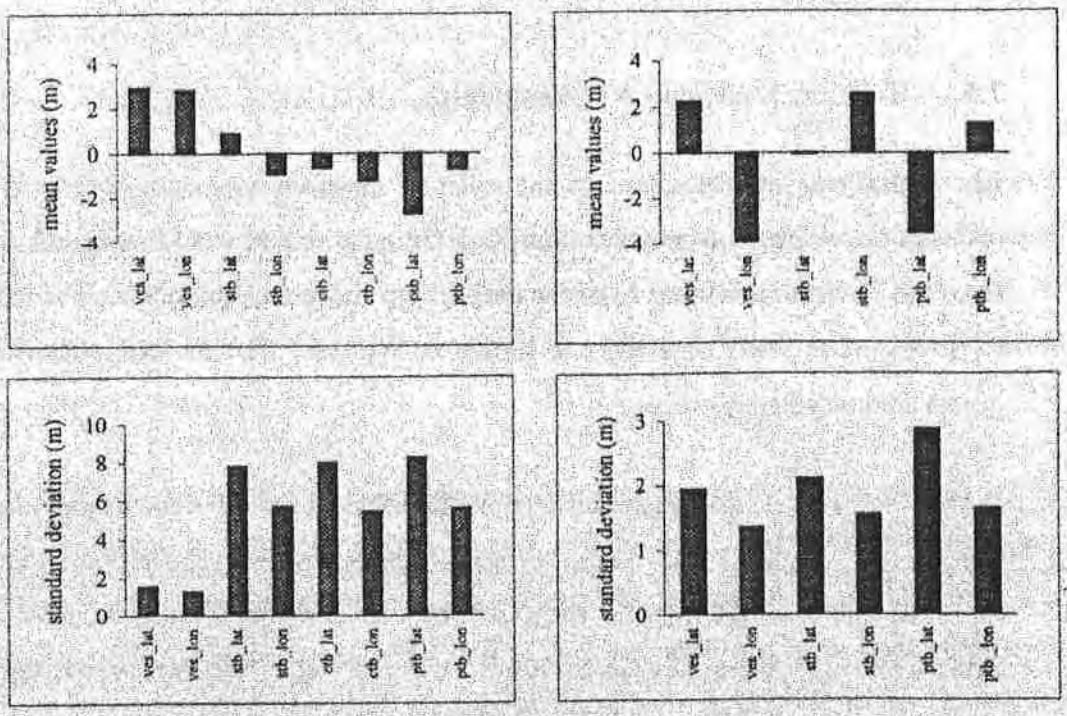

Figure 7.18: Statistics of the predicted residuals - vessel and tailbuoys Syledis observations, Gabon 1992 (left) and Irish Sea 1993 (right)

7.5 INDEPENDENT CHECKS

Another way to ascertain the correctness and effectiveness of both functional and stochastic models is to carry out completely independent checks. Such checks are concerned with the comparison of identical quantities computed using completely different data. These tests are of great importance because they can be used to detect gross and systematic bias in the raw data, such as in magnetic declination. Three such tests have been carried out based on both data sets.

7.5.1 Tailbuoy Location - A Control Point

In the first test two estimates of the tailbuoy positions were compared. The first estimate came directly from the tailbuoy Syledis measurements and the second one came from the Kalman filter using all of the data except those measurements. The results for all streamers for both data sets are shown in Figures 7.19 and 7.20. The following points are immediately evident.

In the first data set, the differences in each direction are of the same magnitude for the three cables - Figure 7.19. Also, they show similar trends with shotpoint. However, there is a significant difference in the two directional components in each streamer. The along-track differences vary up to 10.0-12.0 metre, while the cross-track differences vary up to 20.0-25.0 metre. This disparity is easily to understood as the along-track differences are cable-length related and the cross-track differences are cable-orientation related - clearly in this uncontrolled manner (the filter has no tailbuoy positioning) it is not surprising that the larger errors are orientation related.

The errors are of course the sum of several components including the unknown behavior of the tailbuoy tether and errors in the 'check', i.e. the Syledis positions. They are, however, still not large. A maximum 20.0 metre cross-track error over a 3 km cable represents a maximum overall orientation error of less than 0.5 degrees - and the mean error is clearly very much smaller than this - of the order of 5.0 metre or 0.1 degrees.

This marked rotation systematic bias could also be caused by a small error in the magnetic declination. To validate this hypothesis data from several lines in opposite directions should be analyzed. If the mean differences for each line are of the same magnitude but their sign depends on the line's direction, there is a strong indication of an error in magnetic declination.

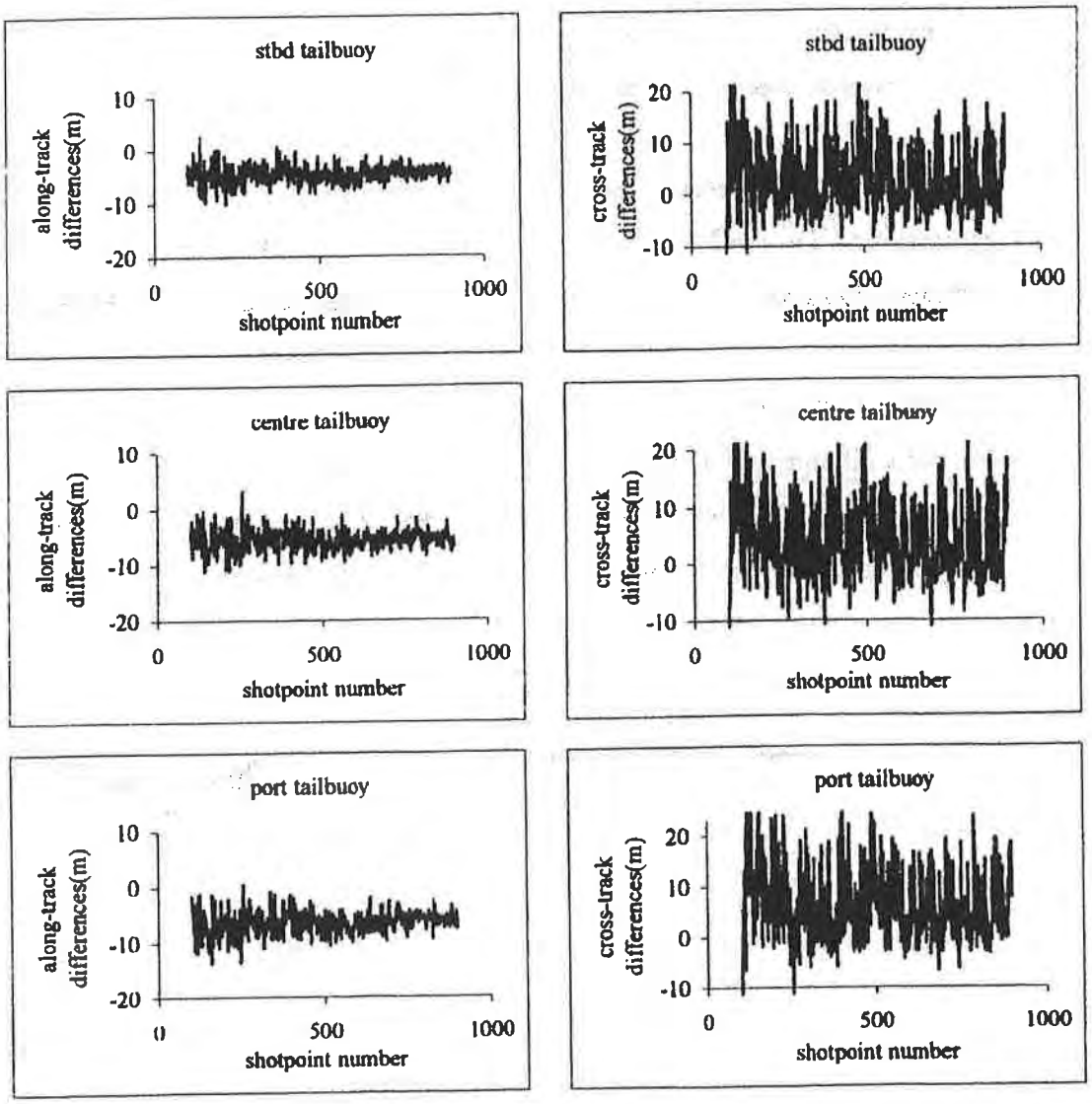

Figure 7.19: Differences between Syledis (observed) and filter derived tailbuoy location (not including tailbuoy Syledis observations), Gabon 1992

Also, from the same figure, it can be seen that the along-track differences for the three tailbuoys show a mean displacement of almost 5.0 metre. This discrepancy in the in-line position is difficult to resolve. Perhaps the most marked reason for this, is due to

incorrect positioning of the nodes at the front end of the streamers, and in part, due to errors in the 'check', i.e. the Syledis positions.

The same sort of conclusions are also observed for the second set of data - Figure 7.20. However, a better examination of this figure shows that the cross-track differences are considerable, up to 45.0 metre radial difference for a limited number of shotpoints. Moreover, detailed examination of the same figure on a larger scale - not shown here - reveals considerable fluctuations from shotpoint to shotpoint.

To resolve these questions, the cross-track differences were separated based on their original data, i.e. the Syledis raw observations and the filter computed positions, and redrawn. Diagram 7.21 depicts the period of the biggest separation for the starboard tailbuoy, which is for the part of the survey between shotpoints 300 and 400. From this diagram it is apparent that the Syledis derived latitudes, i.e. the cross-track coordinates, present a difference of almost 34.0 metre between shotpoints 330 and 360, i.e. a rate of 8.5 metre/min. The filter has proved itself unable to follow these abrupt changes in the Syledis positions, possibly due to the dynamic model standard deviation estimates.

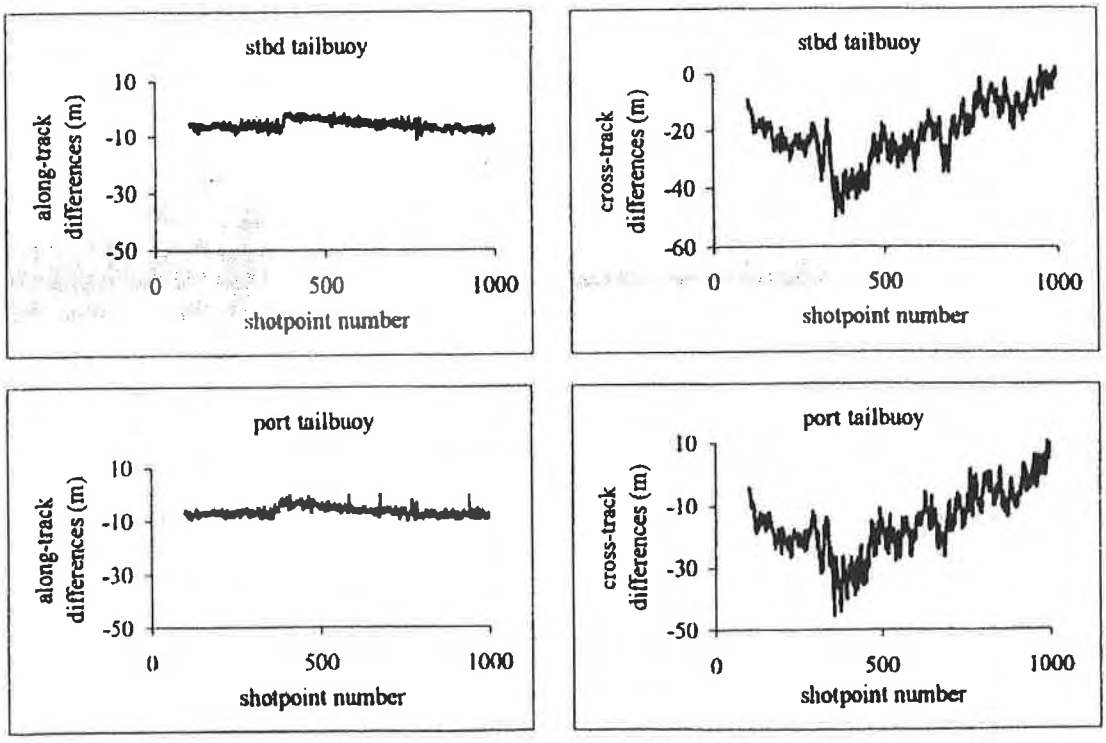

Figure 7.20: Differences between Syledis (observed) and filter derived tailbuoy location (not including tailbuoy Syledis observations), Irish Sea 1993

To answer the second question, the shot to shot changes for both estimates have been assessed. The Syledis data show variations of about one metre between consecutive shotpoints confirming that this estimate is not responsible for this phenomenon. On the contrary, the filtered values reveal variations of the order of 2.0-4.0 metre and in certain cases 6.0 metre variations. These figures are not entirely surprising given that the high variation in the rear end raw compass azimuths - see Appendix E1. Inaccurate positioning of the front end of the spread and improper tuning of the filter may also contribute to this phenomenon.

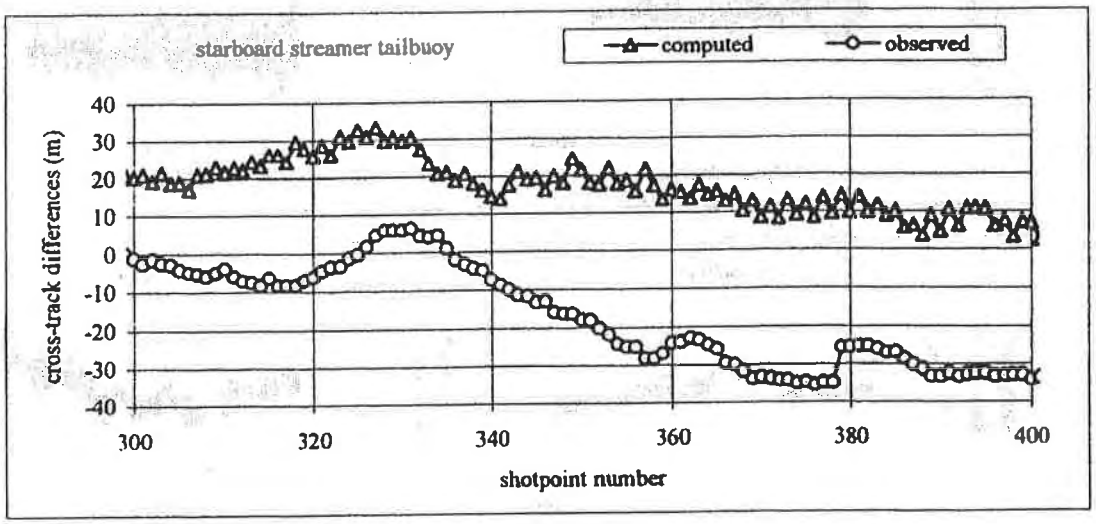

Figure 7.21: Differences between starboard tailbuoy Syledis (observed) and filter derived tailbuoy location (not including tailbuoy Syledis observations) for shotpoints between 300 and 400, Gabon 1992

To illustrate the effect of the absence of active tailbuoys on the tail ends positioning, and hence on the positions of the rear end receivers, it is imperative to examine Figures 7.19 and 7.20 in conjunction with Figure 7.22. Figure 7.22 graphs the differences between the tailbuoy Syledis measurements and the Kalman filter solution derived using all data including the Syledis observations.

In the first data set if active tailbuoys are used (Figure 7.22 top) the differences in the cross-track direction , in almost every case, are less than 10.0 metre with a mean value very close to zero. As expected, the differences in the along-track coordinates are not significantly affected of the presence of tailbuoy data. Similarly, the cross-track misclosure for the second data set are reduced from 45.0 metre - the worst case if the

tailbuoys are disabled - down to 20.0 metre if all measurements are used - see Figure 7.22 bottom. Of course, it should be stressed that the mean difference is clearly much smaller, of the order of 5.0 metre. Again, differences in the along-track direction are not significantly affected. These conclusions are consistent for all streamers in both data sets.

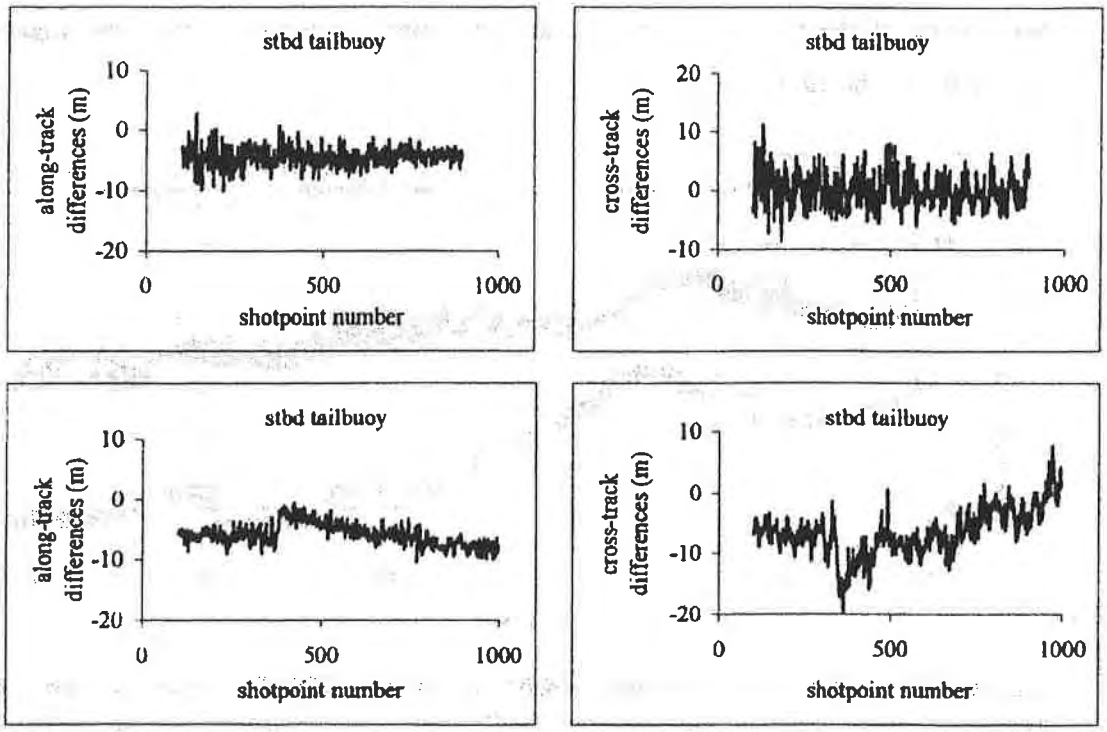

Figure 7.22: Differences between starboard tailbuoy Syledis (observed) and filter derived tailbuoy location (including tailbuoy Syledis observations), Gabon 1992 (top) and Irish Sea 1993 (bottom)

7.5.2 Computation of Acoustically Observed Ranges

In this 'independent' test the state vector parameters were used, at every shotpoint, to compute the coordinates of two acoustic or laser devices located on a streamer, source or on the vessel. The computed distance between these points was directly compared with the acoustically or laser observed value. Obviously, as in the first test, and in order the test to be independent, this observation was not included in the filter solution.

Detailed analysis of a number of such checks, using data from both surveys, has led to similar conclusions. In the following sections four of these tests are discussed. The first

two are based on the processing of the first data set while the latter two on the second one.

To make the check more powerful, a range observed in the tail end network was chosen for the first test. This is basically because when the position of a device that is located at the rear end of the cable is computed, the entire state vector contributes - including the polynomial coefficient and streamer orientation unknowns. Hence, in this test the coordinates of two acoustic devices were computed, one located on the starboard streamer (device F1T1) and the other located on the port streamer (device S3T4) - see Appendix E1, acoustic 21 in the tail end network. In the second check, in order to examine the behavior of the sources in the system, a range between two devices, one located on the port source (device G2T1) and the other at the front end of the port streamer (device S3T2) was tested - acoustic 22 in the front end network. Accordingly from the second set of data, the range that was observed between the vessel fore hull pinger (device 1) and the head of the port streamer (device 10), as well as the range between devices 72 and 32 that were fixed close to the starboard and port tailbuoys respectively were selected and tested - acoustics 2 and 68 respectively. The resulting differences are shown in Figures 7.23 and 7.24.

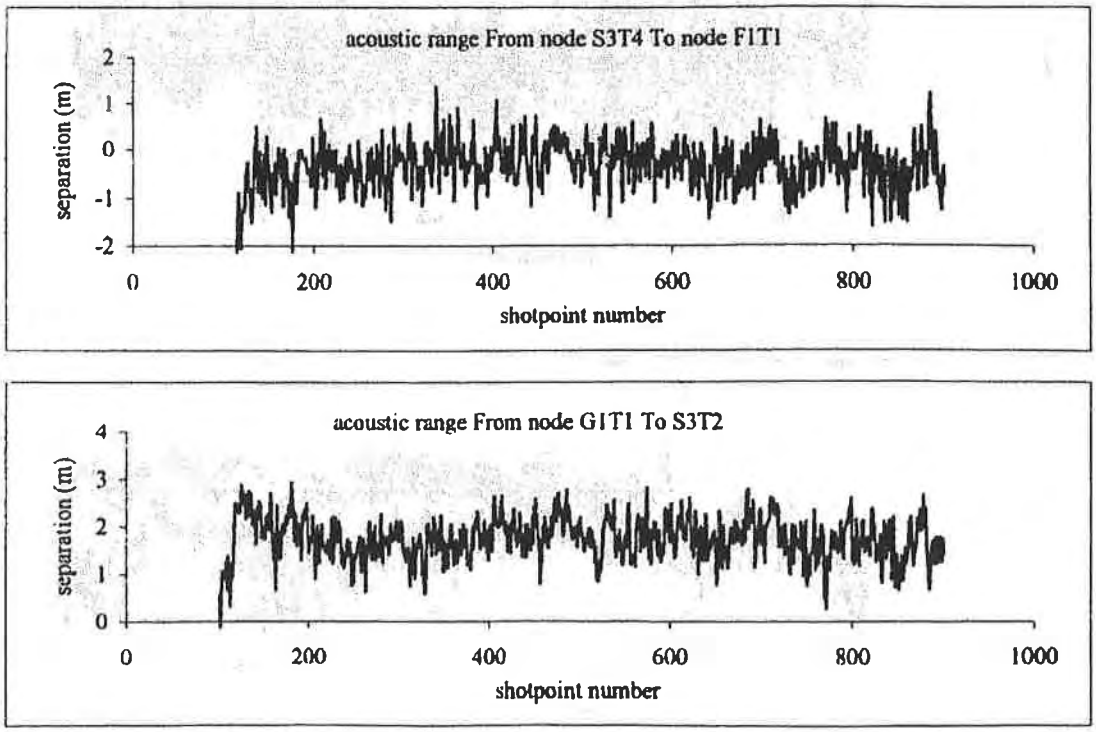

Figure 7.23: Differences for two acoustic ranges between the observed values and those derived from the Kalman filter (not including the observation), Gabon 1992

The points to notice from these analyses are

1. In the second data set, as stated earlier, acoustic data is only available at every other shotpoint or at even longer intervals. To make this visible, the plots in Figure 7.26 depict both the observed and computed values rather than only differences.
2. The mean differences in all tests range between ±5.0 metre and for three of them are much smaller, less than ±2.0 metre. Moreover, it is important to note that these figures are commensurate in size with the predicted residuals of these observations - see corresponding Figures in Section 7.3.1. This represents another strong argument that the model is correct.
3. Most of the separation values lie within a 2.0 metre band for the ranges from the first data set and within 6.0 metre for the ranges derived from the second data set. These trends in magnitude can easily be justified by examining the time series plots of these observations - Appendix E. Also, the similarities in variation between the separation values and the raw data time series add further confirmation that the model and its implementation are correct.

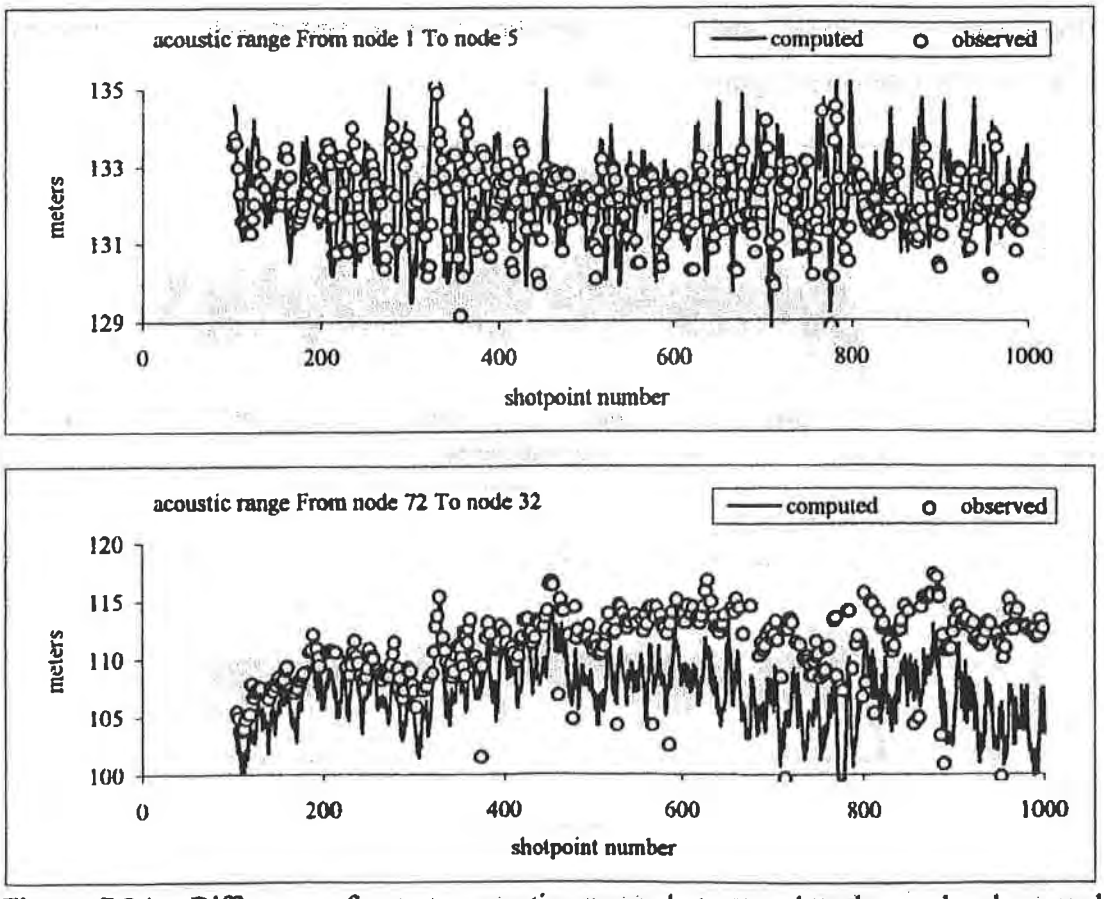

Figure 7.24: Differences for two acoustic ranges between the observed values and those that derived from the Kalman filter (not including the observation), Irish Sea 1993

7.5.3 Computation of Compass Observed Azimuths

In the last of this series of checks an estimate of the direction of the tangent of the streamer, at several offsets, equal to those at which compass units were deployed, was computed. This computation was based on Equation 5.19 using the filtered values of the state vector solution. Of course, as stated earlier on, the corresponding compass observations were not included in the filter solution. Then, these estimates were directly compared with the raw compass azimuths.

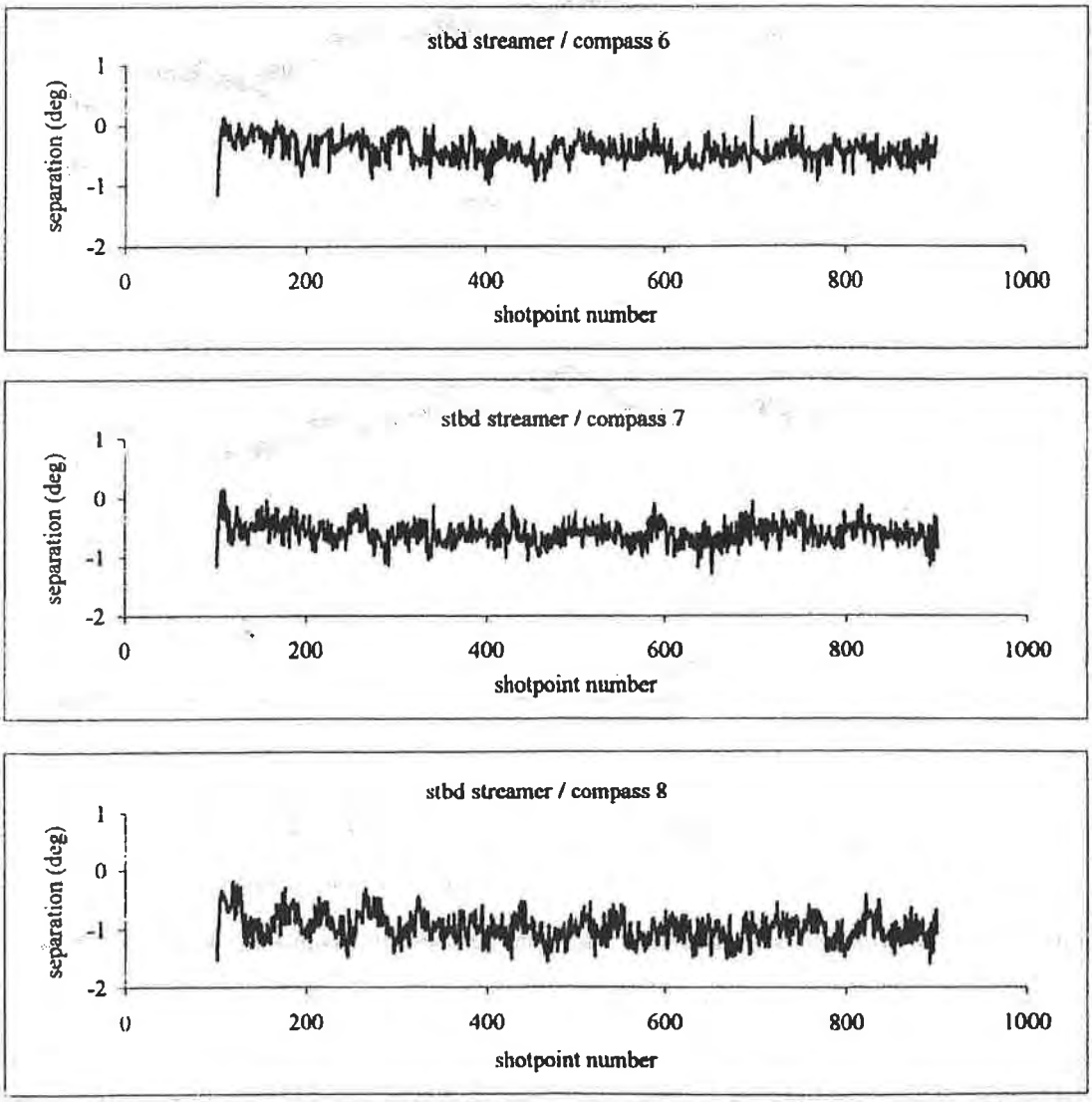

Figure 7.25: Differences for three compass azimuths between the observed compass azimuths and those that derived from the Kalman filter (not including the observations), Gabon 1992

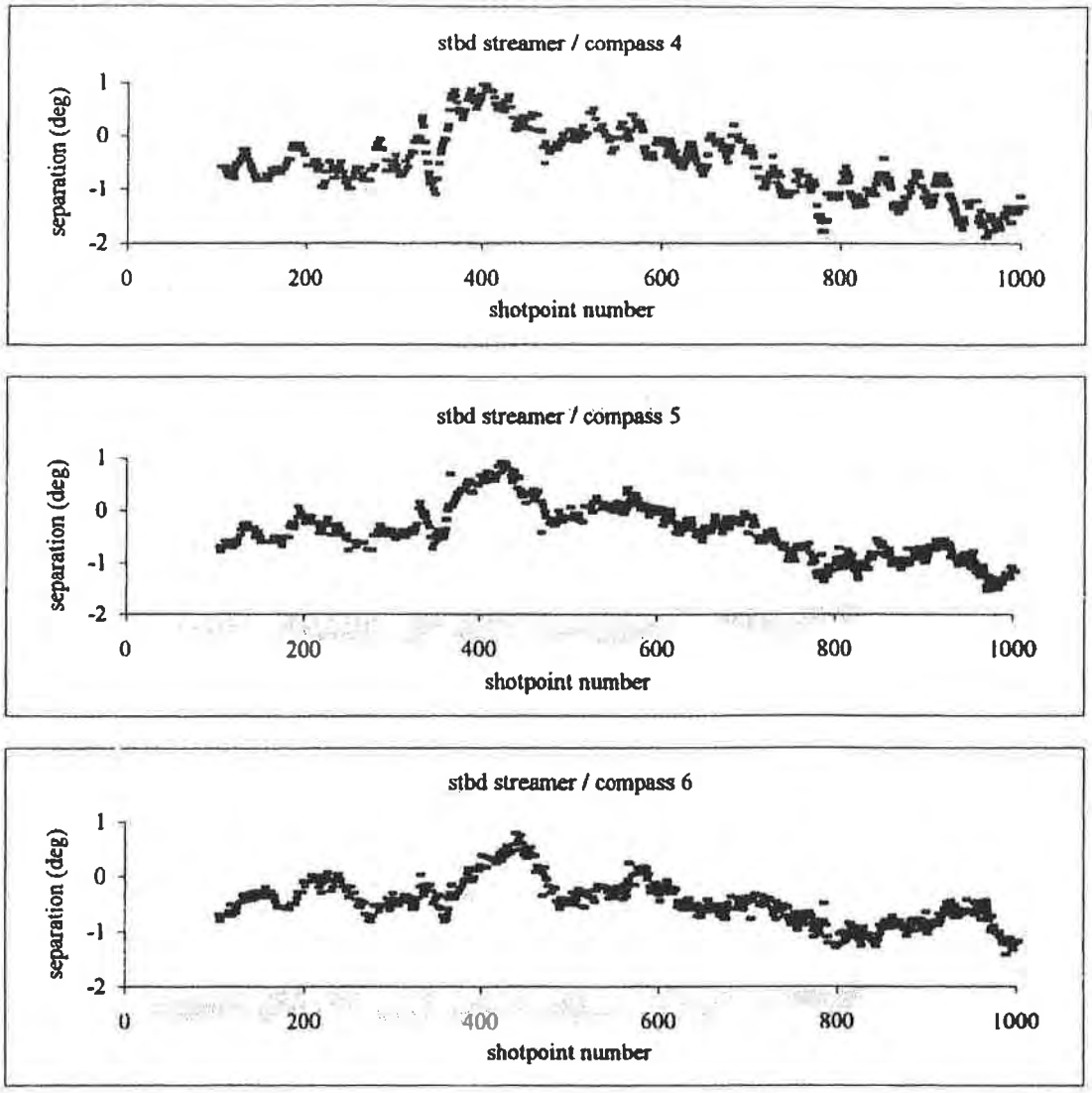

Figure 7.26: Differences for three compass azimuths between the observed directions and those derived from the Kalman filter (not including the observations), Irish Sea 1993

Two such tests have been carried out, one for each set of data, under the following circumstances. In the first test, compasses 6, 7 and 8 of the starboard streamer were eliminated, while in the second one it has been decided to disable compasses 4, 5 and 6 of the starboard streamer again. The choice of compass groups lying mid way along the streamers was made in order to assist in identifying problems and trends more effectively, since this part of the network is the one with the poorest redundancy. The results of these analyses are shown in Figures 7.25 and 7.26 with the points of interest being

1. The first point to note is that the mean separation value for each graph is very close to the mean value of the predicted residual the observation - see corresponding Figures in Section 7.3.2.
2. The resulting differences scatter over a range of half degree about the mean value for the analysis related to the first data set, while in the second trial the variations are of the order of one degree. It should be noted that these patterns are consistent with the raw observation time series plots - see Appendix E.

7.6 CONCLUSIONS

The results from the preliminary testing of the integrated algorithm using real offshore positioning data allow a number of conclusions. These may be summarized as follows

1. The results derived from the analyses of the first data set (Gabon, 1992) seem to more consistent in magnitude and trends than those derived from the analysis of the second set of data (Irish Sea, 1993). This marked discrepancy is shouted to be mainly due to the raw data. As pointed out in Section 7.4. the Irish Sea data include more noisy, outlying and missing observations.
2. Although the primary interest of this study lies on the positioning of the seismic sources and hydrophones with respect to the vessel, the filter also solves (for navigation purposes) for the vessel position and velocity as well as the vessel crab angle. Analysis of these results reveals no peaks to occur in the time series of the vessel position while velocity analysis indicates zero mean and random distributed values. Moreover, as expected (see the gyro observation equation - Section 5.3.3), the vessel velocity as well as the vessel crab angle patterns seem to follow the general trends of gyro.
3. In accordance to the previous conclusion the streamer baseline orientation follows the gyro trends. Clearly, as it is reasonable to expect, this effect is not that distinct as it is for the vessel crab angle since the streamer baseline orientation do not directly correlated with gyro. Also, the time series of the orientation of the streamer baseline indicate the same sort of behavior in all streamers at each survey.
4. The position and velocity of the reference point of the streamers and the centre of the seismic sources are states in the system. Analysis of the these results leads to the conclusion that all nodes at the front-end of the network show almost the same variations in magnitude and trends. This consistency reveals that all cables seem to react in the same way to external forces and to any changes in the vessel's course. Furthermore, the variations in position along-track are significantly smaller (of the order of 6.0 metre) than those derived across-track (of the order of 15.0 metre) throughout the recording lines.
5. The mean values of the predicted residuals of all observations are zero-mean and commensurate in size with the *a priori* observation errors. Analysis also proved that

observations that present predicted residual with large standard deviation and high rate of rejection are the most noisy ones - a sign that the filter correctly identifies the outlying observations. Moreover, as it is reasonable to expect observations between devices fixed on the same streamer present smaller mean and standard deviation values. However, the relatively higher mean standard deviation values of the compass observations of the second data set and the mean values of the tailbuoy observations of the first data set require further research.

6. Finally, the relatively small discrepancies between observed quantities and the same ones derived from the filter solution (independent checks) add further confirmation that the observation and dynamic models are correct and correctly implemented. However, in accordance to the previous conclusions the differences derived from the analysis of the Irish sea survey seem to be more significant than those obtained from the analysis of the first data set.

CHAPTER EIGHT

THE EFFECT OF FUNCTIONAL AND STOCHASTIC MODELS ON POSITION AND PRECISION

8.1 INTRODUCTION

The assessment of the overall quality of a particular design, and therefore its performance in real time operation, is dependent on the quality criteria discussed in Chapter Four, namely precision and reliability. In other words the quality of a system (and of the dynamic system discussed in this study) is assured only if the results of the estimation procedure can meet the preset quality requirements specified in terms of precision and reliability.

The design options or parameters that the quality of a system depends on, consist of the functional and stochastic models as well as the testing procedure that is used for bias identification. Moreover, use of real or simulated data assists in evaluating the results of different filter solutions (estimation result) and their quality measures, which are based on different combinations and assumptions related to these parameters. It is important to note that the quality of the design is independent of actual data, whereas the quality of the estimation result is not.

Throughout Chapter Seven, all tests and trials that have been carried out to assess the structure of the algorithm and performance of the software relied upon the assumption of fixed functional and stochastic models. Furthermore the analysis of the results has been confined to a general valuation of the model, i.e. to check whether or not the model is fundamentally correct and correctly implemented.

The results of the analyses discussed in the present chapter come as a sequence of the preliminary results detailed in Chapter Seven. During the following discussion an attempt is made to evaluate the effect of both the functional and stochastic models on the results of the filter computations and their quality using the data sets described in Appendix E. These include those based on the statistics of the predicted residuals of the observations, analysis of the filter states time series, assessment of the source and receiver positions and tests of precision. The part of the analysis that is related to reliability assessment is discussed separately in Chapter Nine.

In particular the effect of the streamer model on position and precision is examined in great detail. This is because the mathematical representation that is used to determine the shape of streamer forms the fundamental assumption in the design of the observation model. Polynomial functions of different orders and a function based on a harmonic series of the streamer length are two alternative curve fitting models that were adopted for the purpose of this analysis. Also, in order to study the impact of the observation geometry on the filter output, selected sensors or groups of sensors were eliminated and the data were reprocessed.

The second half of the chapter attempts to investigate the role of the stochastic models in the estimation process and its results. This concerns the stochastic model of the observations and the stochastic model of the dynamic model. Particular attention was paid to the examination of the role of the polynomial coefficients, namely the stochastic model of their disturbances.

As stated in Chapter Seven, the procedure that was adopted for testing the raw data for potential outliers is based on examination of the predicted residual of the observations and no further analysis is undertaken within the scope of this study. Much more research, however, is still needed in this area. The benefit of the implementation of a rigorous statistical testing procedure, and some special modifications in order that such a procedure meets this model requirements are discussed in Chapters Four and Ten. Finally, the chapter concludes with a brief overview of the results derived from the analyses of all trials discussed throughout the chapter.

8.2 THE FUNCTIONAL MODEL

In Chapter Three is explained in detail that the functional model of a system consists of the measurement or observation model and the dynamic model. The measurement model depends on the number of observations, the observation types, and the geometry configuration of the measurement setup, as well as on any arbitrary model assumptions such as the 'model curve' adopted in this study to represent the shape of the streamer. The role of these parameters is discussed in the following sections, although no attempt is made to examine any modifications related to the dynamic model described in Section 5.3.4. It is assumed that the actual dynamics of the system underlie the dynamic model, and hence this model cannot be changed at will. Moreover, here, this point takes on a special importance because of the stable nature of the conditions during seismic exploration surveys.

8.2.1 The Streamer Model

8.2.1.1 Polynomial Functions of a Different Order

It is shown in Chapter Two that an n-order polynomial has been adopted as the streamer model in the mathematical system developed for the purpose of this study. To justify this choice, a series of tests have been carried out. These tests involved the fitting of a series of polynomials, of a variety of orders, to real compass data.

In this section the estimation results derived from the implementation of the unified algorithm using polynomial functions of different orders are discussed. Particularly, polynomial models of fourth, fifth and sixth order are being tested. The standard deviations that were adopted to describe the stochastic models of both observation and dynamic models are the same with those given in Table 7.1. In addition, the standard deviations of the driving noise of the polynomial coefficients adopted for these tests are summarized in Table 8.1.

In the following paragraphs the results related to the positioning of the seismic spread are discussed first whilst the precision of these estimates is discussed in the second half of this section.

Figure 8.1 shows the cross-track coordinates of the starboard tailbuoy antenna for the three polynomial models derived for both data sets - see Appendix E. Figure 8.2 depicts the same estimates for a hydrophone group located somewhere midway along the streamer in both networks. The points to note from these plots are

1. Use of a polynomial model of a fourth, fifth or a sixth degree results in almost the same cross-track coordinates for the streamer tailbuoys for the first series of data - Gabon 1992. In contrast with this conclusion the results derived from the processing of the second data set - Irish Sea 1993 - show that if a polynomial of order six is used the estimated positions of the tailbuoy node are more consistent with the raw observations than those derived from a lower order polynomial. However, the differences between the solutions derived for a fifth and a sixth order rarely exceed 4.0 metre.

	Polynomial Order 4	
	data I	data II
c_0	0.5 E-7 $m/m^2/sec$	0.5 E-8 $m/m^2/sec$
c_1	0.5 E-10 $m/m^2/sec$	0.5 E-11 $m/m^2/sec$
c_2	0.5 E-13 $m/m^2/sec$	0.5 E-14 $m/m^2/sec$
	Polynomial Order 6	
	data I	data II
c_0	0.5 E-7 $m/m^2/sec$	0.5 E-8 $m/m^2/sec$
c_1	0.5 E-10 $m/m^2/sec$	0.5 E-11 $m/m^2/sec$
c_2	0.5 E-13 $m/m^2/sec$	0.5 E-14 $m/m^2/sec$
c_3	0.5 E-16 $m/m^2/sec$	0.5 E-17 $m/m^2/sec$
c_4	0.5 E-19 $m/m^2/sec$	0.5 E-20 $m/m^2/sec$

Table 8.1: Stochastic model for the dynamic model of the polynomial coefficients for models of order four and six, Gabon 1992 (left) and Irish Sea 1993 (right)

2. Examination of the results derived for the receiver groups fixed at the front end and middle of the network leads to similar conclusions (Figure 8.2). Particularly, these results have a great weight for the middle part of the cables since the network in this area is less redundant (the only available observations are compass azimuths), and hence the role of the streamer model becomes crucial. Moreover these figures suggest that the results based on a fifth or a sixth order are more consistent for both sets of data irrespective of the receiver offset than those based on a model of a lower degree.

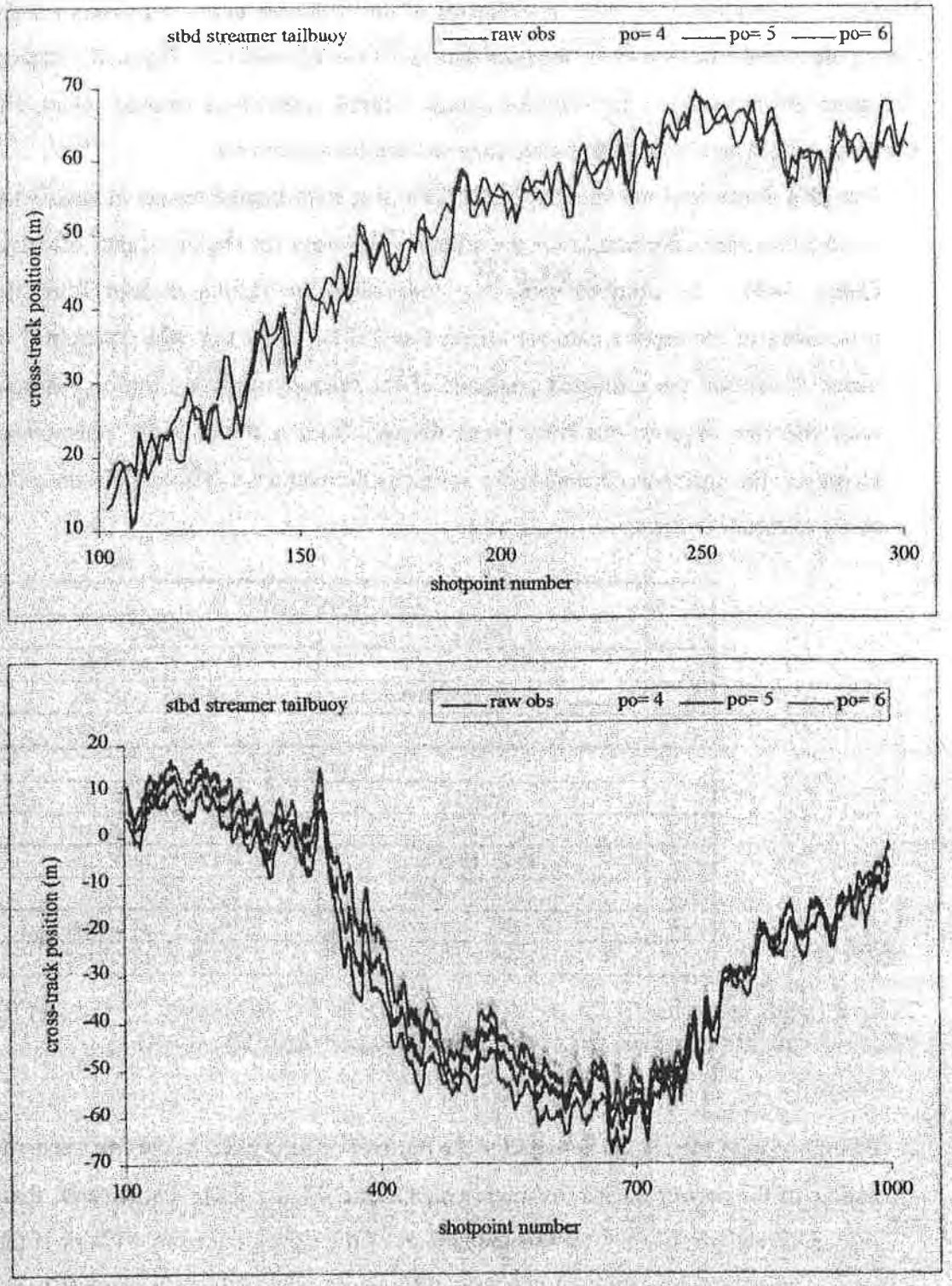

Figure 8.1: Cross-track tailbuoy coordinates computed for three different polynomial orders, Gabon 1992 (top) and Irish Sea 1993 (bottom)

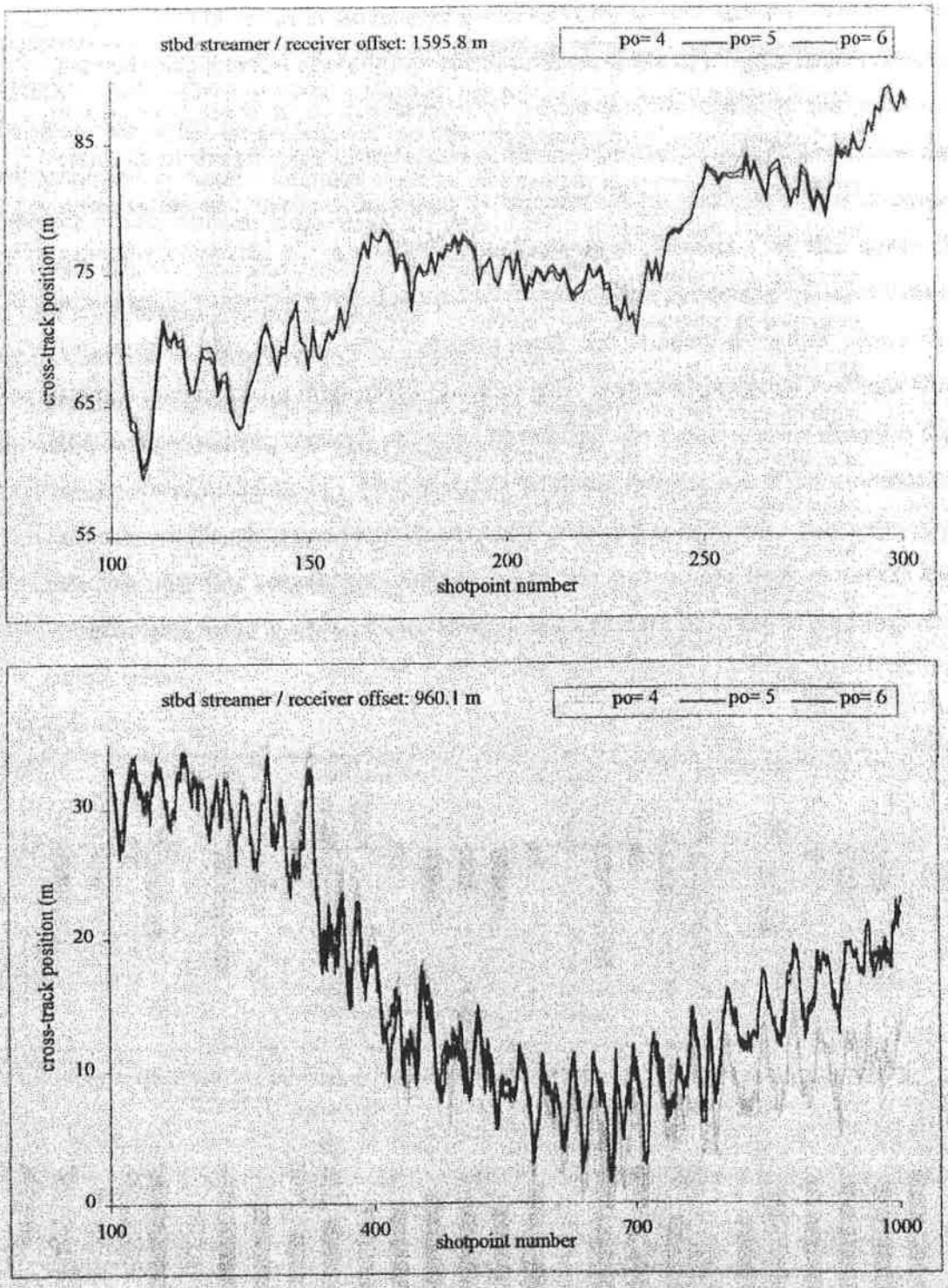

Figure 8.2: Cross-track coordinates of a hydrophone group located midway along the cable computed for three different polynomial orders, Gabon 1992 (top) and Irish Sea 1993 (bottom)

3. The disparity observed in the receiver positions in the second data set between those derived using a model of order four and those for a model of a higher degree (Figure 8.2 bottom) seems to be consistent with the conclusions related to the predicted residuals of the compass observations of these solutions. Figure 8.3 contains the mean values and standard deviations of the observation residuals of the compass azimuths computed for a fourth degree polynomial function. If this figure is examined in conjunction with Figure 7.17 (solution for a polynomial of order five) it can be seen that the magnitude of both mean and standard deviation values has slightly increased and their pattern has changed. Increased predicted residuals (for the same stochastic models) probably means that the model cannot describe the observations as faithfully. Also, it should be noted that the use of polynomials of order more than six seem to result in similar problematic solutions. It is important to note that this remark, for polynomials of too low or too high an order, has already been made in Chapter Two where a first approach to streamer modeling was undertaken.

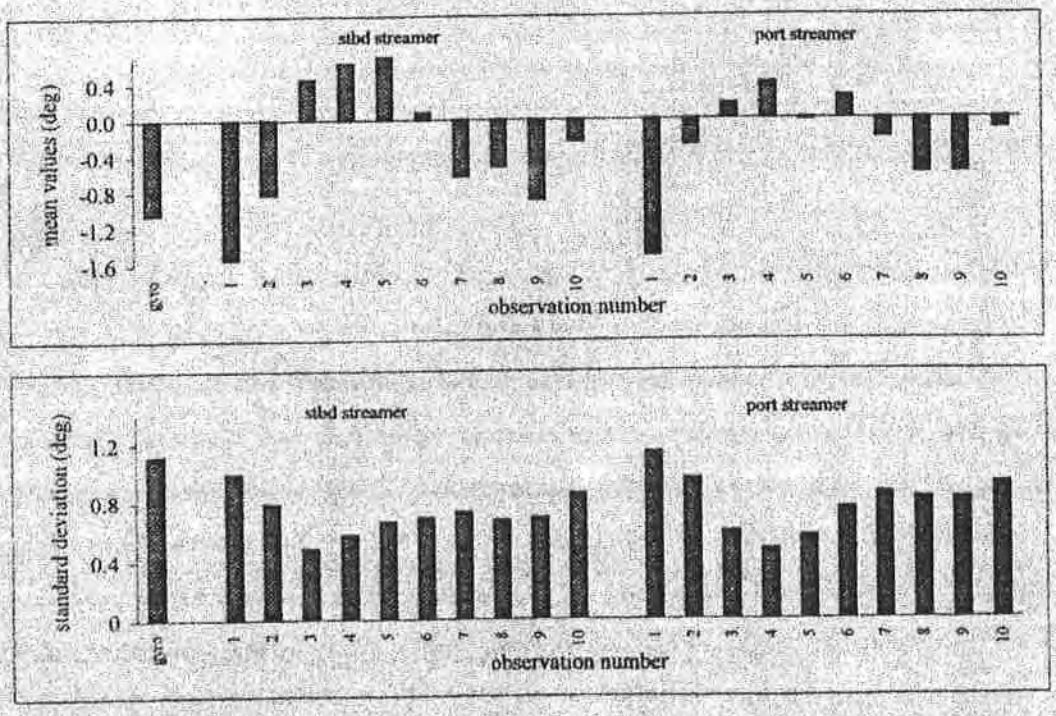

Figure 8.3: Statistics of the predicted residuals computed for a fourth order polynomial model - compass azimuths, Irish Sea 1993

As expected the streamer model does not significantly affect the along-track coordinates of the receiver positions. Figure 8.4 illustrates this estimate for the receivers examined in Figure 8.2. From these plots it is immediately evident that the differences in the in-line positions for any combination of polynomial orders do not exceed 0.5 metre, almost in any case, for both data sets.

Finally, it should be mentioned that analysis has proved that changes in the polynomial order of the streamer model do not significantly affect the positioning of the float nodes.

System	Node	95% Error Ellipse			2drms	50% CEP
		σ_{max}	σ_{min}	ψ_{max}		
vessel	NRP	2.6	2.6	52.23	3.0	1.3
float	stbd source	1.9	1.7	13.11	2.1	0.9
	port source	1.9	1.7	109.67	2.1	0.9
streamer	114.1	2.0	1.4	136.88	2.0	0.8
	599.8	3.2	1.5	145.13	2.9	1.1
	1097.8	4.6	1.5	147.17	3.9	1.4
position relative	1595.8	5.4	1.5	148.01	4.5	1.6
tow point	2093.8	5.3	1.5	148.60	4.5	1.6
	2591.8	4.7	1.5	148.85	4.0	1.5
	3089.8	3.8	1.5	146.74	3.4	1.3

Table 8.2: Measures of precision computed for a fifth order polynomial streamer model, Gabon 1992

It has already been mentioned that the greatest single asset of the suggested method is its ability to provide a rigorous measure of precision throughout the seismic spread. Implementation of the integrated algorithm using polynomials of different orders has led to similar figures of precision for the vessel navigation reference point (NRP) and float positions. Therefore, in the following paragraphs only the precision results for the hydrophone positions of the aforementioned analyses are discussed. However, before this discussion a more detailed assessment of the precision of the whole seismic spread is given. This is based on the solution derived for a fifth degree polynomial for both first and second data sets.

The formulae used to compute precision measures are those provided in Chapter Four. Typical 95% error ellipses were computed for the vessel NRP, the centre of each float

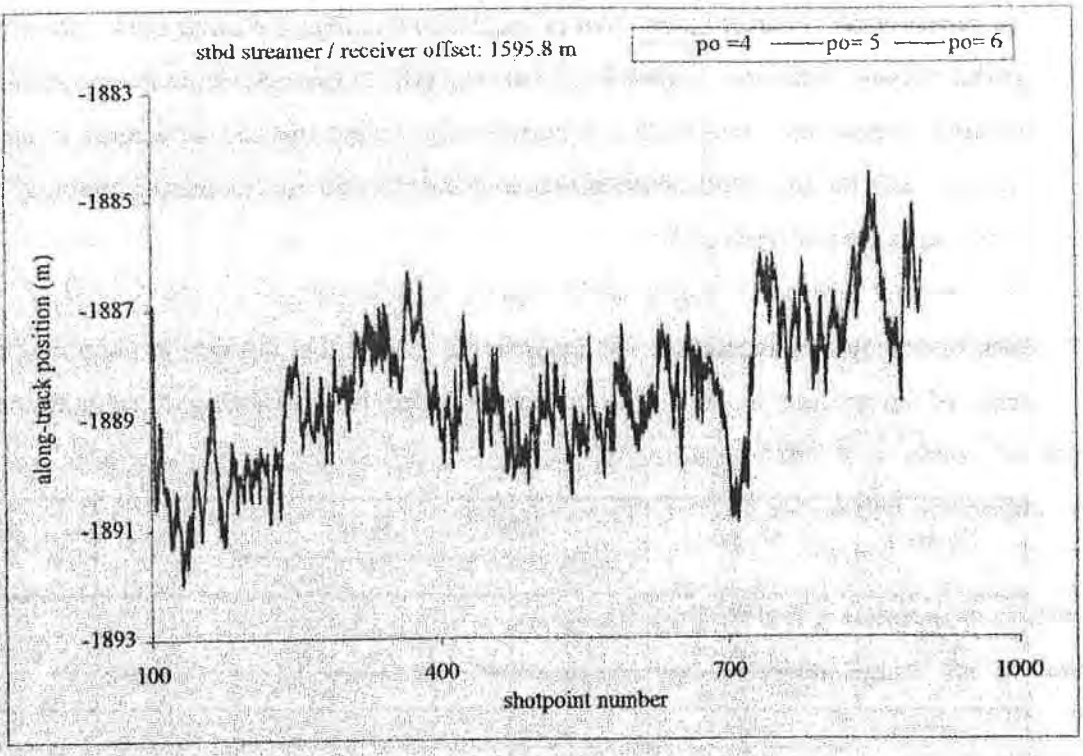

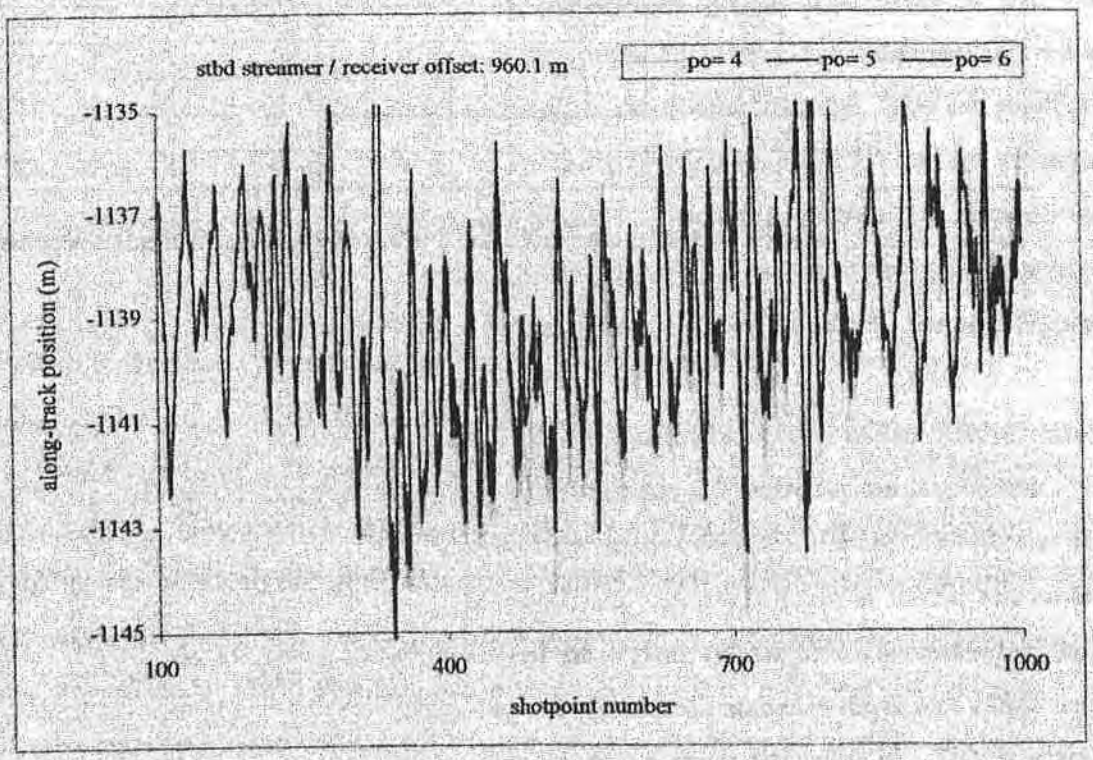

Figure 8.4: Along-track coordinates of a hydrophone group located midway along the cable computed for three different polynomial orders, Gabon 1992 (top) and Irish Sea 1993 (bottom)

and a sample of receivers fixed along the cables. In addition to these estimates, given that among the seismic industry precision is not rarely expressed in drms, a 2drms value is computed for each node in the spread as well. Also, precision is specified and illustrated at a 50% level of circular error probability (CEP).

Tables 8.2 and 8.3 summarize the results of the precision analysis for the 'standard' solution (polynomial order five) for both seismic networks. These results allow the following conclusions to be drawn

1. The precision of the estimated position of the vessel NRP is of about the same magnitude in all directions for the data files of both first and second campaigns, and of the order of its *a priori* standard deviation.
2. Analysis of the precision estimates derived for the float nodes indicates an excellent consistency in magnitude in both maximum and minimum figures for all units deployed in the first and second networks.
3. For the precision estimates of the hydrophone groups it is apparent that the maximum error occurs, as expected, approximately in the cross-track direction while the minimum error occurs approximately in the in-line direction. This can easily be verified by comparing the values ψ_{max}, shown in Tables 8.2 and 8.3 and the streamer orientation values given in Figures 7.2 and 7.3. In fact the differences between the direction of minimum error and the cables' baselines, i.e. the angle α, as computed from the filter, are no more than 3.0 degrees in most of the cases - see also Figures 7.2 and 7.3.
4. The in-line deviations are of the same magnitude irrespective of the receiver offset and of about 1.5 metre for the first set of data and 2.2 metre for the second one.
5. In Table 8.2 the cross-track standard deviations range from about 2.0 metre at the front end, reach 5.4 metre in the middle and about 4.0 metre at the far end of the cables. On the contrary, the results of the analysis related to the second set of data, summarized in Table 8.3, show that the cross-track standard deviations range from about 2.5 metre at the front end increasing towards the tailbuoy. This is mainly because in this latter configuration a full-length acoustic network was used, in addition with compass measurements. This of course improves the precision as well as observation redundancy and hence reliability in this part of the network.

However, as detailed in Section 8.3.2, the magnitude of these estimates is significantly influenced by the values that are used to build the stochastic models.

System	Node	95% Error Ellipse			2drms	50% CEP
		σ_{max}	σ_{min}	ψ_{max}		
vessel	NRP	2.7	2.4	130.34	3.0	1.3
float	stbd towfish	3.3	2.5	150.53	3.4	1.4
	port towfish	-	-	-	-	-
	stbd outer source	3.2	2.0	156.61	3.1	1.2
	stbd inner source	3.2	2.6	153.03	3.3	1.4
	port inner source	3.0	2.1	21.67	3.0	1.2
	port outer source	3.0	1.9	26.87	2.9	1.2
streamer	171.3	2.6	2.2	178.82	2.8	1.2
	514.0	2.7	2.2	179.62	2.8	1.2
	856.6	2.8	2.2	0.54	2.9	1.2
position relative	1199.2	2.9	2.2	1.20	3.0	1.2
tow point	1541.8	3.0	2.2	1.37	3.0	1.2
	1884.4	4.3	2.2	1.76	4.0	1.6
	2116.6	3.2	2.2	2.82	3.7	1.5

Table 8.3: Measures of precision computed for a fifth order polynomial streamer model, Irish Sea 1993

It should be stressed that although these results, as well as those given in the following sections, were based on the analysis for a single shotpoint (time event 150) these estimates do not change very fast with time, and therefore, can be considered more or less as typical values for the whole line for both data sets. Note that the maximum differences from these values are of the order of 1.0 metre occurring in the cross-track direction for the receivers located at the rear end of the cables. Finally, analysis proved that these results are consistent in all streamers in both surveys.

Tables 8.4 and 8.5 detail the results for the analyses obtained from the processing of both data sets using polynomials of different orders. From these tables it can be clearly seen that the precision estimates are hardly influenced by changing the order of the polynomial function. A more detailed analysis of these results shows that precision in the along-track direction is not affected at all in both surveys. Cross-track deviations are only effected in the middle of the cable for the first data set and at the far end of the streamers for the second set of data by almost 0.5 metre. However, if a polynomial of a

higher order is used, viz. seven or higher, the receiver positions and their quality are significantly distorted.

Hydrophone position relative tow point	95% Error Ellipse			2drms	50% CEP
	σ_{max}	σ_{min}	ψ_{max}		
114.1	2.0	1.5	137.24	2.0	0.8
599.8	3.1	1.5	145.23	2.8	1.1
1097.8	4.2	1.5	147.19	3.6	1.3
1595.8	4.9	1.5	147.96	4.2	1.5
2093.8	5.0	1.5	148.39	4.3	1.5
2591.8	4.3	1.5	148.27	3.7	1.4
3089.8	3.8	1.5	146.56	3.3	1.3
114.1	2.0	1.5	136.66	2.0	0.8
599.8	3.3	1.5	145.01	2.9	1.1
1097.8	4.7	1.5	147.10	4.0	1.4
1595.8	5.6	1.5	147.95	4.7	1.6
2093.8	5.5	1.5	148.54	4.6	1.6
2591.8	4.8	1.5	149.01	4.1	1.5
3089.8	3.9	1.5	146.96	3.4	1.3

Table 8.4: Measures of precision computed for polynomial streamer model of order four (top) and six (bottom), Gabon 1992

Hydrophone position relative tow point	95% Error Ellipse			2drms	50% CEP
	σ_{max}	σ_{min}	ψ_{max}		
171.3	2.6	2.2	177.74	2.8	1.1
514.0	2.6	2.2	178.54	2.8	1.2
856.6	2.7	2.2	179.36	2.8	1.2
1199.2	2.7	2.2	179.75	2.9	1.2
1541.8	2.8	2.2	179.77	2.9	1.2
1884.4	3.9	2.2	2.48	3.4	1.4
2116.6	3.0	2.2	2.22	3.1	1.3
171.3	2.7	2.2	178.96	2.8	1.2
514.0	2.7	2.2	179.72	2.9	1.2
856.6	2.8	2.2	0.55	2.9	1.2
1199.2	2.9	2.2	1.14	3.0	1.2
1541.8	3.0	2.2	1.33	3.1	1.2
1884.4	4.8	2.2	2.89	4.3	1.6
2116.6	3.4	2.2	1.95	3.3	1.3

Table 8.5: Measures of precision computed for a polynomial streamer model of order four (top) and six (bottom), Irish Sea 1993

8.2.1.2 Harmonic Function

Incorporation of the Harmonic Function into the Algorithm

The results derived from the implementation of the integrated algorithm based on a polynomial streamer model has proved rather successful. Nevertheless, as stated in Section 2.2.1, alternative fitting models ought to be considered to simulate the shape of the streamer. It has also been pointed out that in order for any alternative model to be easily incorporated in an integrated recurrent process, as the algorithm developed in Chapter Five, a single and continuous function is required.

A function that contains a summation of different sinusoidal components, i.e. a harmonic function, fulfills these conditions. Harmonic functions have been used widely in fields such as electrical engineering and geophysics to analyse time series functions. Here, the overall aim behind this idea is to define a harmonic function as a series of the streamer length such that the frequency and amplitude elements of the sinusoidal components are states in the system - similar to polynomial coefficients. It is believed that the Kalman filter will shoulder the task of estimating values for these parameters so that the resultant shape of the streamer will be optimal. The function that was selected for the purpose of this analysis consist of the summation of two sine terms, and therefore the u,v coordinates of any point on a streamer are given by the following equations

$$u = l$$
$$v = \sum_{k=2,2}^{4} \left[c_k \sin(c_{k+1} l) \right] \qquad 8.1$$

These equations are equivalent to Equations 5.1 and 5.2 for a polynomial fitting model. Also, note that this function consists only of sine terms - no cosine terms are included. This is because by definition v must be zero at the head of the cable i.e., for zero offset.

Hence, for the chosen streamer model the easting and northing components of a point on a streamer can be described by the expressions

$$X_i = X_S + l_i \cos(\alpha) + \left(\sum_{k=2,2}^{4} \left[c_k \sin(c_{k+1} l_i) \right] \right) \sin(\alpha)$$

$$Y_i = Y_S - l_i \sin(\alpha) + \left(\sum_{k=2,2}^{4} \left[c_k \sin(c_{k+1} l_i) \right] \right) \cos(\alpha)$$

8.2

Similarly the foregoing equations are equivalent to Expression 5.11 for a polynomial streamer model. Finally, the equivalent of Equation 5.17, that is used to describe the direction of the tangent of the streamer at a point of offset l, is given by

$$\frac{dv}{du} = \frac{d\left(\sum_{k=2,2}^{4} \left[c_k \sin(c_{k+1} l) \right] \right)}{dl} \qquad 8.3$$

In the following section the conclusions of the assessment of the results derived from the implementation of the model using the same data that were used to test the polynomial streamer model are discussed.

	Harmonics Model	
	data I	data II
c_0	0.5 E-8 m/sec	0.5 E-8 m/sec
c_1	0.5 E-9 m/m^2/sec	0.5 E-9 m/m^2/sec
c_2	0.5 E-8 m/sec	0.5 E-8 m/sec
c_3	0.5 E-9 m/m^2/sec	0.5 E-9 m/m^2/sec

Table 8.6: Stochastic model of the dynamic model of the parameters of a harmonic streamer model, Gabon 1992 (left) and Irish Sea 1993 (right)

Implementation of the Method

In order to aid comparison in the assessment between the results derived using a polynomial and a harmonic streamer model the same *a priori* standard deviations have been used to describe the precision of the observations as well as the dynamic model. Of course, the standard deviations used to describe the disturbances of the harmonic function parameters cannot be the same as those accepted for the polynomial coefficients. Table 8.6 outlines the standard deviation values accepted for these

parameters. It is important to note that although several sets of similar values have been tested only values of this order of magnitude seem to provide a solution that is overall acceptable. It has been mentioned before that it is extremely difficult to build up that part of the stochastic model related to these parameters of the dynamic model. One suggested approach to the solution of this problem has been discussed in Section 3.2.3. Here, examination of the Kalman filter products, and especially the covariance matrix of the predicted residuals of the observations which tends to more sensitive to any changes in the stochastic models, helps in making decisions.

The most important points to conclude from the implementation of the aforementioned method are discussed in the following paragraphs.

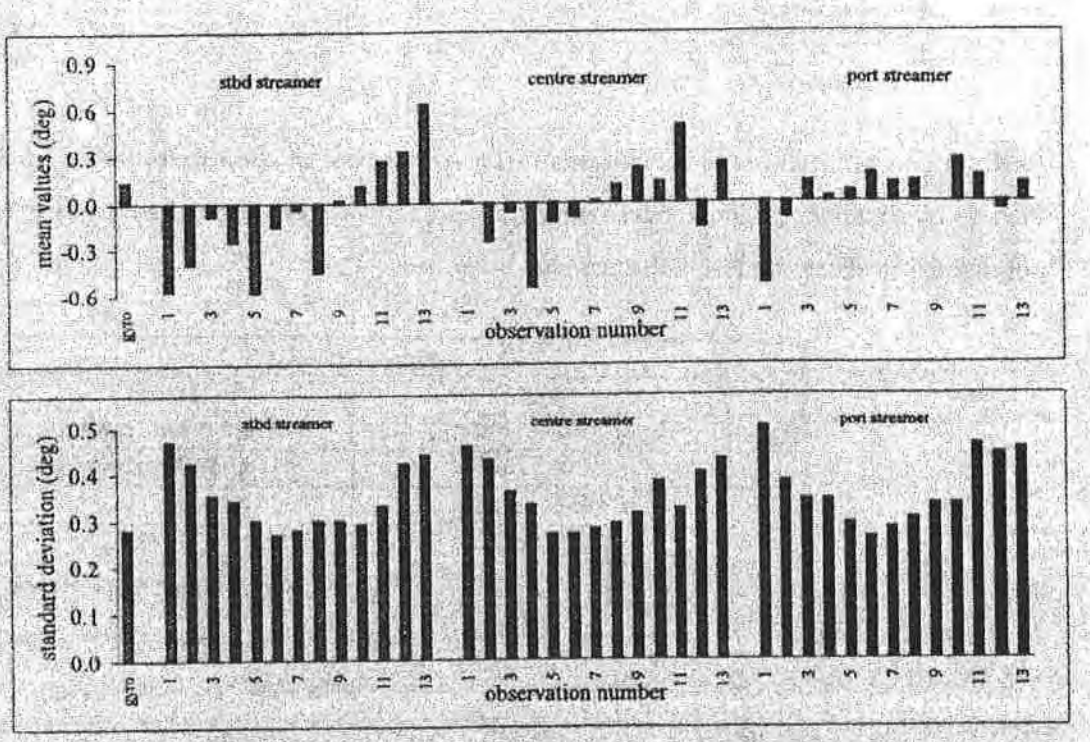

Figure 8.5: Statistics of the predicted residuals of the compass azimuths computed for a harmonic streamer model, Gabon 1992

The first point to note is that the predicted residual values for all observation types, except those for the compasses and tailbuoys, are hardly affected by this modification in the streamer model. In particular only the predicted residual values for the acoustic ranges observed in the middle of the network for the second survey present differences

of about 0.5 metre on average compared with those obtained using a fifth order polynomial function. On the contrary, the results derived from the analysis of the first set of data show only slight differences compared with those based on a polynomial streamer model.

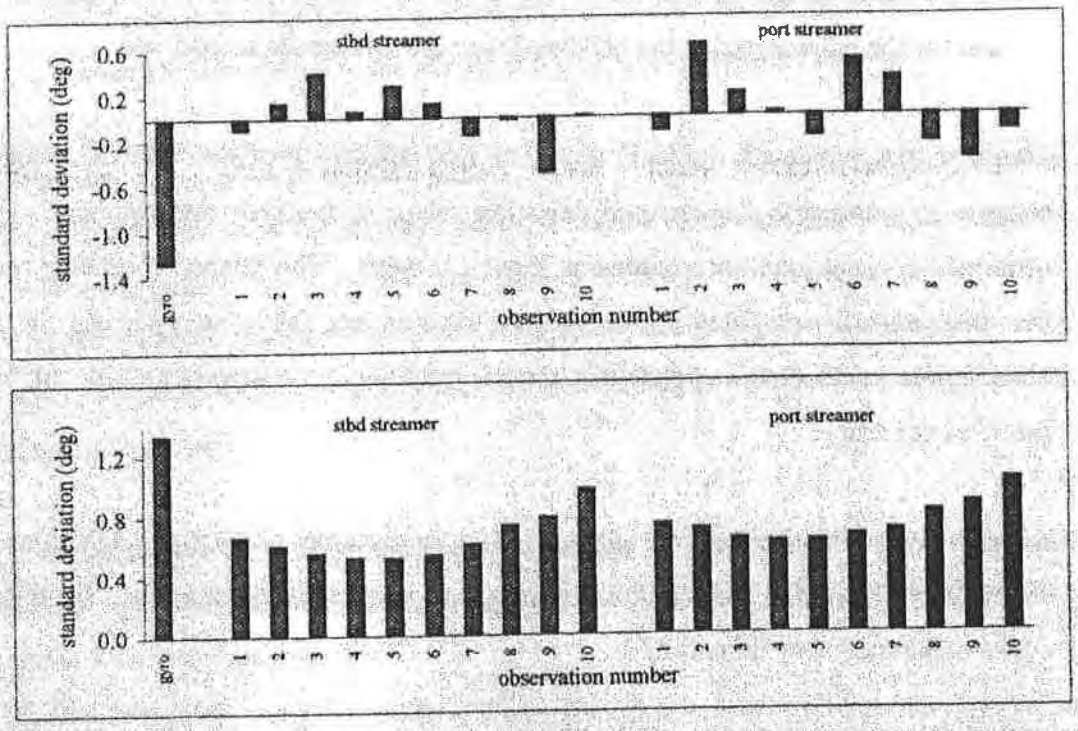

Figure 8.6: Statistics of the predicted residuals of the compass azimuths computed for a harmonic streamer model, Irish Sea 1993

From these results there appears to be considerable evidence to support the idea that the relative position of the streamers in each survey seem not to be affected by the streamer model. However, their absolute position (with respect to the vessel) is affected as can be seen from the tailbuoys and compass predicted residuals as well as from the analysis that follows.

The histograms shown in Figures 8.5 and 8.6 depict the mean values and standard deviations of the predicted residuals for the compass observations. Examination of these figures in conjunction with Figures 7.16 and 7.17 allow the following conclusions to be drawn

1. The mean values follow an approximately white noise pattern, although they are different from those derived for a polynomial streamer model, in both data sets. Also, their magnitude ranges within the limits derived for a polynomial model, shown in Figures 7.16 and 7.17.
2. Analysis of the standard deviation values indicates an increase of about 0.2 degrees for the compasses located at the front and rear ends of the cables for the first survey, and for the units placed in the middle of the network for the second one.

Similarly, the predicted residual values of the tailbuoy geodetic derived positions suggest an increase in the standard deviation values of the predicted residuals of the order of 0.5 metre, and in certain cases about 1.0 metre. This phenomenon may reveal that the positions computed by the Kalman filter do not follow very closely the raw observations (as those for a polynomial model) resulting in a relatively smooth curve for the streamer shape.

Another point to notice from the analysis is that the streamer orientation angle does not follow very closely the changes in the gyro values suggesting again a relatively smooth curve with time - see Figure 8.7.

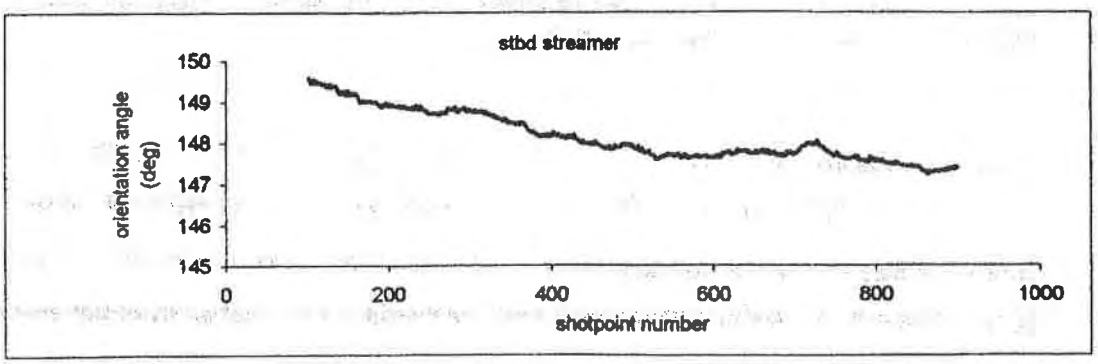

Figure 8.7: Streamer orientation angle time series computed for a harmonic function streamer model, Gabon 1992

Although analysis of estimates such as predicted residuals and the filter states helps in identifying trends and highlighting problems in the raw data, the final product, i.e. source and hydrophone positions, are the estimates of greatest importance.

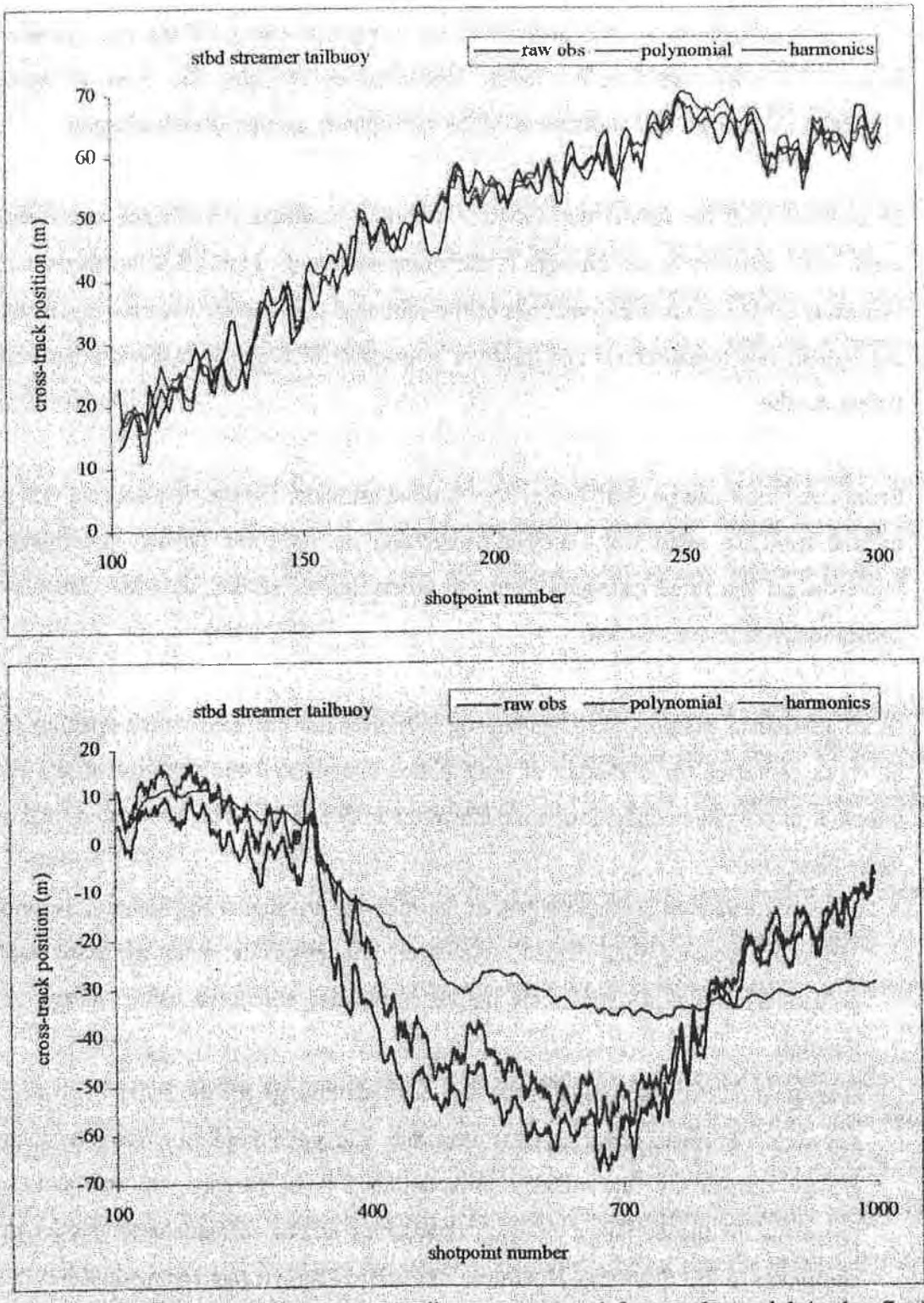

Figure 8.8: Cross-track tailbuoy coordinates computed for a polynomial (order five) and a harmonic function streamer model, Gabon 1992 (top) and Irish Sea 1993 (bottom)

As it is reasonable to expect, analysis of the computed values of the float positions proved that these estimates are hardly influenced by changing the streamer model. Similarly, the along-track coordinates of the hydrophone groups are not affected.

In contrast with the results derived for the in-line positions, cross-track coordinates seem to be sensitive to any changes in the streamer model. Figure 8.8 illustrates three estimates for the cross-track positions of the starboard tailbuoy for each survey, namely the Syledis raw measurement and the filter estimation for a polynomial and a harmonic fitting model.

From this plot it can be clearly seen that all three estimates for the first data set (shown on the top) are quite well-matching suggesting no need for further investigation. Nevertheless the same estimates from the processing of second data set result in a substantially different solution.

In an attempt to examine this phenomenon in more detail the cross-track positions for all three estimates for a sample of hydrophone groups and the tailbuoy of the port streamer of the same configuration are illustrated in Figure 8.9 The points to note from these plots are

1. The results derived for the first half of the streamer are similar for both a polynomial and a harmonic fitting model. However, the positions obtained based on a polynomial model are apparently noisier than those computed using a harmonic function.
2. It is apparent that the results of the two methods diverge for the second half of the streamer. Furthermore it is clear that only the polynomial solution can follow closely enough the raw tailbuoy observations. It is, perhaps, the mathematical properties of the harmonic function themselves and/or the stochastic model that contribute to this disparity. However, taking into account that the method has been successfully implemented for the first set of data it is possible to support the idea that this discrepancy should be sought in the raw data. This point has been partially discussed in Section 7.5.1. Much more research, however, is still needed in this

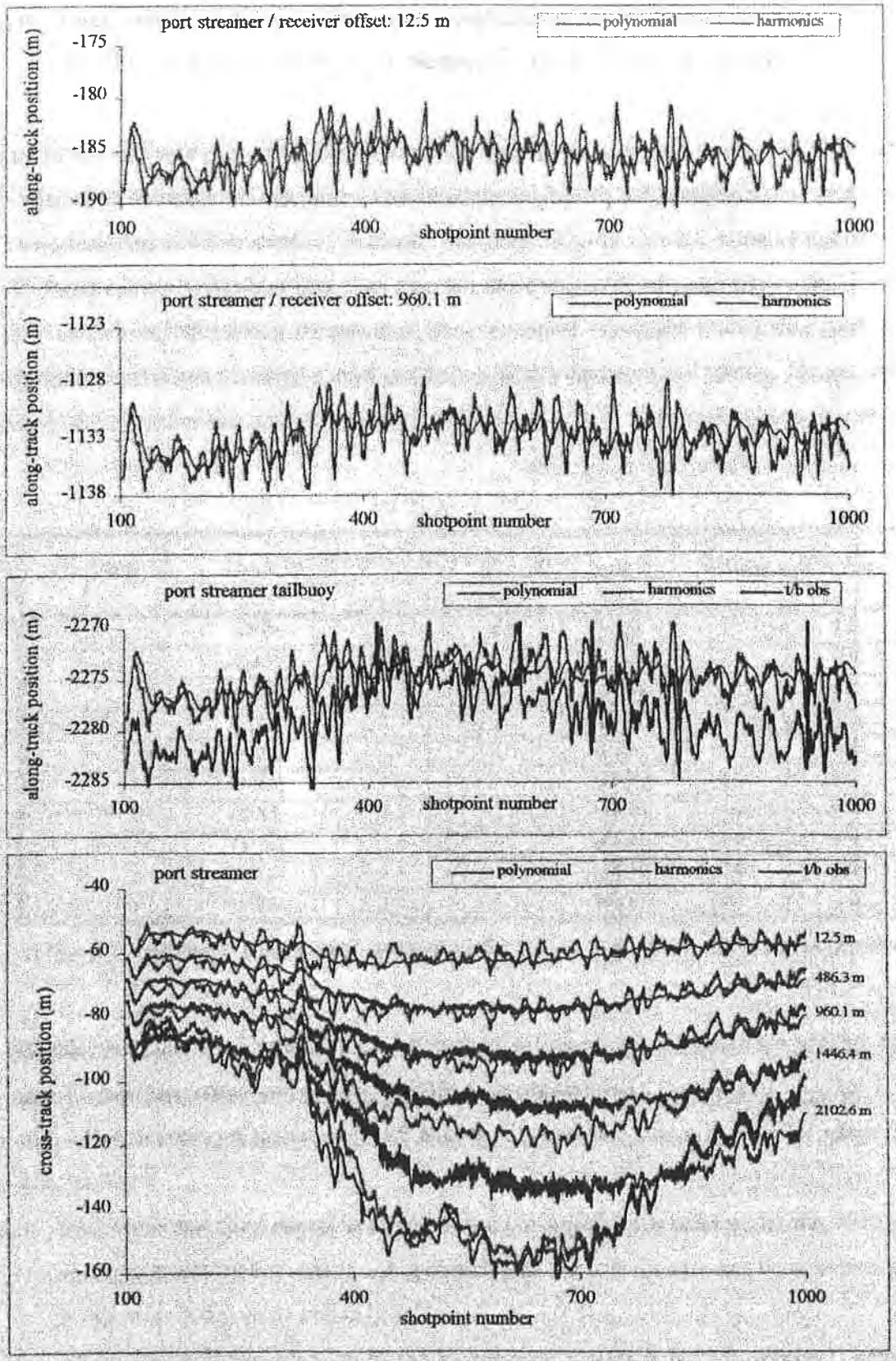

Figure 8.9: Along and cross-track hydrophone and tailbuoy coordinates computed for a polynomial (order five) and a harmonic function streamer model, Irish Sea 1993

area. Testing of the same data based on slightly modified functional and stochastic models may help to resolve the problem.

Analysis of the along-track positions of the same devices, shown at the top of Figure 8.9, indicates again that the polynomial derived coordinates are substantially noisier than those computed for a harmonic function. However, a more detailed examination of the tailbuoy position (the third plot from the top) can assist in clearing up this point. From this plot it is immediately evident that the polynomial computed coordinates and the Syledis derived ones present similar patterns in both magnitude and trends. Hence, this is a strong indication that the stochastic models used to implement the polynomial method have been properly tuned.

System	Node	95% Error Ellipse			2drms	50% CEP
		σ_{max}	σ_{min}	ψ_{max}		
vessel	NRP	2.8	2.6	52.34	3.2	1.3
float	stbd source	1.9	1.7	13.26	2.1	0.9
	port source	1.9	1.7	109.69	2.1	0.9
streamer	114.1	1.8	1.5	133.57	1.9	0.8
	599.8	1.8	1.4	129.45	1.9	0.8
	1097.8	1.9	1.5	134.79	2.0	0.8
position relative	1595.8	2.2	1.5	140.33	2.1	0.9
tow point	2093.8	2.6	1.5	143.47	2.4	1.0
	2591.8	3.1	1.5	145.19	2.8	1.1
	3089.8	3.6	1.5	146.21	3.1	1.2

Table 8.7: Measures of precision computed for a harmonic function streamer model, Gabon 1992

Finally, in order this discussion to be complete, a few remarks should be made on the precision of the estimation results from the implementation of the method. Tables 8.7 and 8.8 outline the precision results for both first and second data sets with the points of interest being

1. The vessel and float precision estimates are not significantly affected by this change in the streamer model. Maximum differences of about 0.5 metre can be observed in some units in the second configuration.
2. The increase in the precision of the hydrophone groups is hard to resolve. More specifically it can be seen that the maximum error for the receivers deployed in the

middle of the cable decreases by about 2.5 metre and 1.0 metre for the first and second sets of data respectively. This clear disparity from the polynomial model solution adds further confirmation that more research is required in this area.

System	Node	95% Error Ellipse			2drms	50% CEP
		σ_{max}	σ_{min}	ψ_{max}		
vessel	NRP	2.9	2.2	130.78	2.9	1.2
float	stbd towfish	3.1	2.5	151.58	3.2	1.3
	port towfish	-	-	-	-	-
	stbd outer source	2.6	2.0	142.81	2.6	1.1
	stbd inner source	2.8	2.3	114.71	3.0	1.2
	port inner source	2.4	2.0	32.63	2.6	1.1
	port outer source	2.4	1.9	38.47	2.5	1.0
streamer position relative tow point	171.3	1.1	1.0	15.36	1.2	0.5
	514.0	1.2	1.0	13.31	1.2	0.5
	856.6	1.4	1.0	9.42	1.3	0.5
	1199.2	1.6	1.0	7.14	1.5	0.6
	1541.8	1.9	1.0	5.92	1.7	0.7
	1884.4	2.5	1.0	4.92	2.2	0.8
	2116.6	2.3	1.0	5.23	2.0	0.8

Table 8.8: Measures of precision computed for a harmonic function streamer model, Irish Sea 1993

8.2.2 The Effect of Measurement Geometry and an Allusion to the Design of Seismic Networks

In the introduction of this chapter it has been pointed out that the geometry configuration of the measurement setup is one of the design parameters that the functional model depends on. In the present section an attempt is made to assess the effect of different geometry configurations on position and precision of the seismic spreads processed in this study, and consequentially, if possible, to draw some conclusions related to the design of new systems.

However it should be stressed that the design of new systems, and especially of integrated dynamic systems such as the one developed in Chapter Five, is a rather compound and complicated problem. In the design phase of a system the precision and

reliability requirements have to be reconciled with limiting conditions such as cost, available hardware, computer power, personnel, and time schedules (Salzmann, 1993). This approach is limited to aspects of precision, discussed in this section, and reliability discussed in Chapter Nine. Finally it should be noted that this discussion is just a first approach to the problem. Suggestions for further analysis under this topic are provided in Chapter Ten.

To study the design of a system no actual data are required since the quality of the design is independent of actual data. It is only the observation matrix of the measurement model, the stochastic models and the testing strategy that the quality of a system depends on. Nevertheless, in the following tests both first and second sets of data are processed, so that the quality of the estimation result is what is being assessed - not the quality of the design. These results are then evaluated in combination with the results derived in section 8.2.1.1, i.e. the 'standard' solution.

The data files from the first survey (Gabon 1992) were used to study the effect of measurement geometry under three different circumstances. The three tested configurations were

(a) all observations except the Syledis derived tailbuoy position of the starboard streamer.

(b) all observations except the Syledis derived tailbuoy position of the starboard streamer and all the tail end acoustic ranges from/to starboard streamer.

(c) all observations except the Syledis derived tailbuoy position of the starboard streamer, all the tail end acoustic ranges from/to starboard streamer, and the two compass units deployed at the tail end of the starboard cable.

Of course, it is apparent that it is almost impossible to experience such a configuration in reality, i.e. to build a system like this, or for all these sensors located at the rear end of the network to fail simultaneously. In fact this trial is an attempt to test the impact of a 'worst case scenario', besides testing the operation of the algorithm under such unexpected geometry.

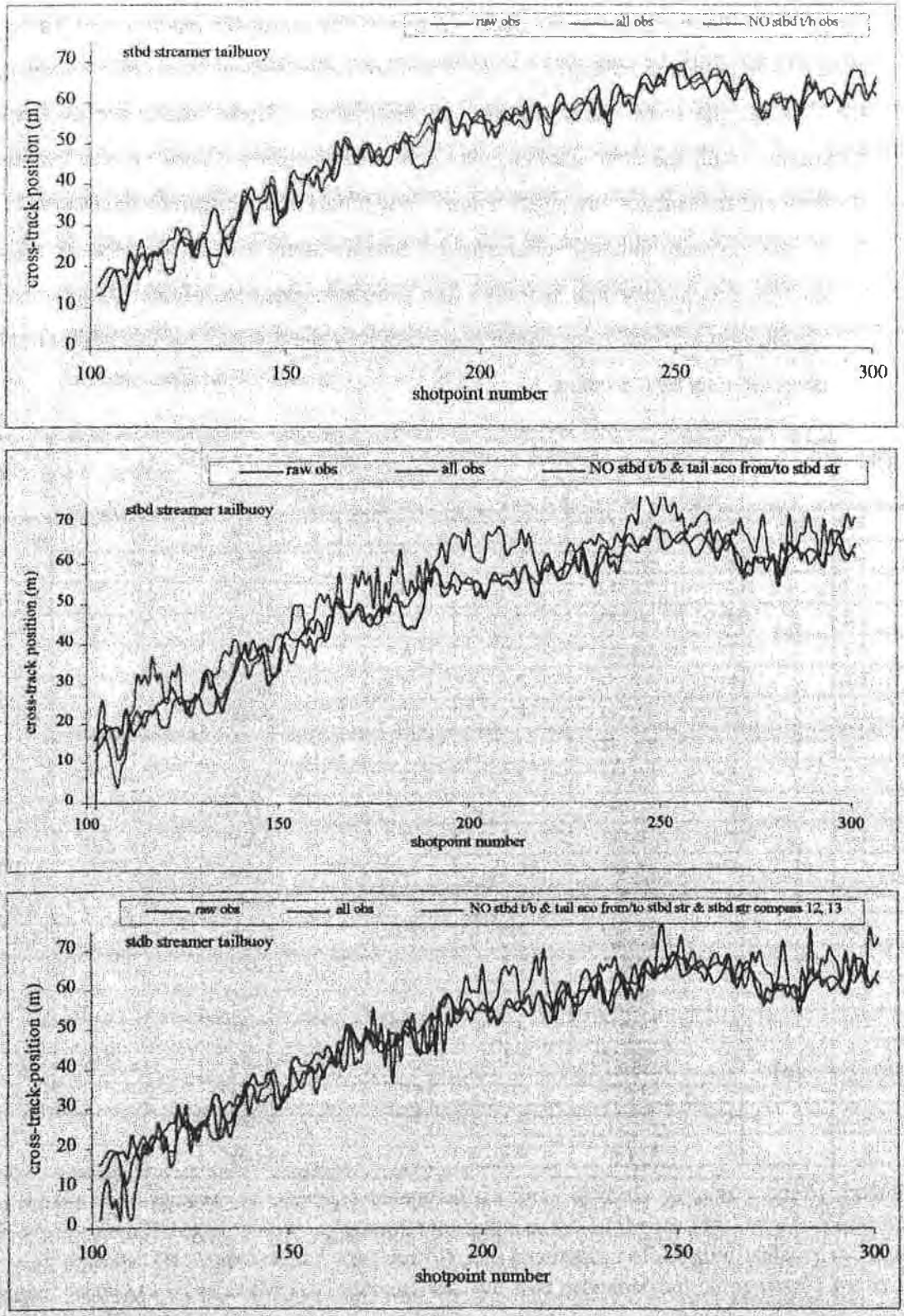

Figure 8.10: Cross-track tailbuoy coordinates computed for three different geometry configurations, elimination of the stbd tailbuoy location (a), elimination of the stbd tailbuoy location and tail acoustics from/to stbd streamer (b), and elimination of the stbd tailbuoy location, tail acoustics from/to the stbd streamer and the stbd tail-end compasses 12 and 13 (c), Gabon 1992

Figure 8.10 illustrates the cross-track position of the starboard tailbuoy and Table 8.9 outlines the precision measures for the starboard cable derived from the processing of the data for the three aforementioned configurations. These results are assessed in comparison with the filter solution, where all observations are used i.e. the 'standard' solution and the tailbuoy raw observations. The points to note from these results are

1. If the starboard tailbuoy is not used (or fails for some reason) the network still has enough redundancy and therefore the estimated position of the tailbuoy is not significantly affected (plot on the top). Similarly the precision of this node seems to decrease only by 0.5 metre.

	Hydrophone position relative tow point	95% Error Ellipse			2drms	50% CEP
		σ_{max}	σ_{min}	ψ_{max}		
(a)	114.1	2.0	1.5	136.98	2.0	0.8
	599.8	3.2	1.5	145.23	2.9	1.1
	1097.8	4.6	1.5	147.22	4.0	1.4
	1595.8	5.3	1.5	148.06	4.5	1.6
	2093.8	5.4	1.5	148.68	4.5	1.6
	2591.8	4.8	1.5	149.04	4.0	1.5
	3089.8	4.2	1.5	147.58	3.6	1.3
(b)	114.1	2.1	1.6	131.58	2.1	0.9
	599.8	3.6	1.6	144.38	3.2	1.2
	1097.8	5.6	1.6	146.87	4.8	1.7
	1595.8	7.8	1.6	147.81	6.5	2.2
	2093.8	10.4	1.6	148.38	8.7	2.5
	2591.8	13.5	1.6	148.70	11.1	3.5
	3089.8	15.8	1.6	148.84	12.9	4.0
(c)	114.1	2.1	1.6	131.60	2.1	0.9
	599.8	3.6	1.6	144.43	3.3	1.2
	1097.8	5.7	1.6	146.92	4.1	1.7
	1595.8	7.9	1.6	147.88	6.6	2.2
	2093.8	10.8	1.6	148.43	8.9	2.9
	2591.8	13.9	1.6	148.72	11.4	3.6
	3089.8	22.5	1.6	148.98	18.5	5.6

Table 8.9: Measures of precision computed for three different geometry configurations, elimination of the stbd tailbuoy location (a), elimination of the stbd tailbuoy location and tail acoustics from/to the stbd streamer (b), and elimination of the stbd tailbuoy location, tail acoustics from/to the stbd tailbuoy and the stbd streamer tail compasses 12 and 13 (c), Gabon 1992

2. Under the second scenario, it is apparent that the tailbuoy's position and precision is significantly influenced. No link with the centre and port streamers practically

means no use of their tailbuoy Syledis observations, extremely important information in order to locate the receivers fixed at the rear end of the spread. The effect on the hydrophone positions is enormous. Though the receivers placed at the front end are very little affected, the maximum error (almost cross-track) reach 15.0 metre at the far end of the cable.

3. Finally, under scenario three, although the resultant differences range more or less within the same limits, some changes in trends are obvious. The tailbuoy cross-track position jumps up and down with reference to the 'standard' solution possibly due to lack of the rear end compasses. Again, the precision of the front end groups hardly alters while for the tail end groups exceeds 22.0 metre. The minimum error (almost in-line) is only very little affected in all three trials.

In the second series of tests discussed in this section the second set of data was used to perform two more trials. In the former one the data were processed assuming that no acoustic ranges were observed at the middle of the spread. Obviously this test aims to assess the importance of a full length acoustic network. More specifically the acoustics denoted by observations 43, 44, 45, 46, 47, 48, 54, 55, 56, 57, 58 and 59, a total number of twelve observations were eliminated and the data reprocessed (Appendix E). Table 8.10 (top) outlines the precision results derived for the starboard streamer receivers.

Examination of this table in combination with Table 8.3 shows that the minimum error (almost in-line) is very little affected irrespective of the receiver offset. However, significant changes can be noticed in the maximum error (almost cross-track). As expected the error of the receivers placed at the front end of the network increases only by 0.5 metre, possibly due to the very strong front network, while the error of the receivers deployed at the rear end of the cables is influenced by almost 2.5 metre and reach 5.7 metre. It is the middle of the cables, however, that suffers more when mid acoustics are omitted. The error of these groups reach 7.0 metre, i.e. an increase of more than 3.0 metre.

As stated in Section 7.4.2, in the second survey a configuration of 10 compass units per streamer, spaced at intervals of approximately 300 metre, was used to provide total

cable orientation. However, as can be seen in Appendix E, compasses 1, 2, 3 and 9, 10, that were deployed at the front and rear ends of the network respectively, are fixed only 75.0 metre apart - may be because nonlinearity is greatest in these areas (Cotton et al, 1985).

	Hydrophone position relative tow point	95% Error Ellipse			2drms	50% CEP
		σ_{max}	σ_{min}	Ψ_{max}		
(a)	171.3	3.0	2.4	165.97	3.1	1.3
	514.0	3.2	2.4	172.57	3.3	1.3
	856.6	4.1	2.4	1.45	3.9	1.5
	1199.2	5.6	2.4	4.46	5.0	1.9
	1541.8	6.9	2.4	5.12	6.0	2.2
	1884.4	5.8	2.4	5.6	5.2	1.9
	2116.6	6.7	2.4	2.78	5.9	2.1
(b)	171.3	2.8	2.2	179.86	2.9	1.2
	514.0	3.0	2.2	1.93	3.0	1.2
	856.6	3.6	2.2	3.71	3.5	1.4
	1199.2	4.7	2.2	4.05	4.3	1.6
	1541.8	5.8	2.2	3.90	5.0	1.9
	1884.4	5.3	2.2	3.35	4.7	1.8
	2116.6	6.5	2.2	2.79	5.6	2.1

Table 8.10: Measures of precision for a sample of hydrophones computed for two different geometry configurations - elimination of mid acoustics (a), and elimination of compasses 1, 3 and 9 (b), Irish Sea 1993

In the second trial it has been decided to eliminate compasses 1, 3 and 9, so that all active compasses are now almost 300 metre apart, and reprocess the data as if these units had never existed. Table 8.10 (bottom) summarizes the precision results for the starboard streamer hydrophone groups derived under this assumption. Two points are immediately evident from this analysis

1. The precision of the vessel and float positions - not shown here - hardly alters.
2. It is reasonable to expect that loss of compasses 1, 3, and 9 would effect the front and far ends of the cable. Nevertheless analysis proved that the precision of every single receiver changes - a sign confirming the potential of the interdependence of an integrated network.

It is the geophysicist who is going to evaluate the absolute size of these differences in the quality, and therefore decide whether or not they induce a significant impact on the

final geophysical product. Of course, as stated earlier on, such a decision has to be reconciled with other limiting parameters such as cost in order to achieve the best possible result.

However, it should be stressed once more, that the results discussed in this section refer only to the data sets described in Appendix E and the values that were used to build the stochastic models for this application, and therefore it is rather risky to draw general conclusions. In fact the design of new seismic configurations based (even partially) on the model developed in Chapter Five is an objective that imperatively calls for further research.

8.3 THE STOCHASTIC MODELS

The implementation of the Kalman filter algorithms relies upon the combination of a dynamic and a measurement model together to create an optimal solution. In order to do this, both models must be given an appropriate weighting which is expressed by their stochastic models, that is to say their covariance matrices.

In the following sections the influence of the precision of the observations on the filter estimates and their quality is being examined and a number of these analyses is performed. Then the precision of the observations is kept fixed and the impact of the quality of the dynamic model (covariance matrix of the dynamic model) on the estimation result and its precision is discussed.

8.3.1 The Stochastic Model of the Observation Model

All the results and conclusions that were derived in the preceding analyses have been relied on the stochastic models given in Table 7.1. A brief reference to the justification of the assumptions made behind this choice has been provided in Section 7.2.

In the present section an attempt is made to evaluate the sensitivity of the integrated algorithm to any changes in the precision of the observations. In order to aid interpretation, the results of the analyses derived in this section are assessed in combination with the 'standard' solution discussed in Chapter Seven. Given that the model comprises a peculiarly complicated mixed measurement system the observations are split and classified by observation type and the analysis of the results is performed respectively. These include acoustic and laser ranges, compass azimuths, as well as measurements of 'absolute positions', such as vessel and tailbuoy Syledis or GPS derived locations. In the following paragraphs the role of the acoustic and laser observations is examined first.

In all previous trials the acoustic and laser ranges have been processed assuming *a priori* standard deviations of 2.0 metre and 1.5 metre for these observations respectively

- see Table 7.1. In the analysis that follows these values have been scaled down by half. The points to notice from the results derived under this assumption are

1. The mean values and standard deviations of the predicted residuals of all observation types are very slightly affected (decreased) due to this change in the stochastic model. Similarly, very slightly the state vector elements affected. However, analysis reveals a more noisy pattern with time for some of these estimates. A typical example of these results is given in Figure 8.11 - this figure corresponds to Figure 7.2 for the 'standard' solution.

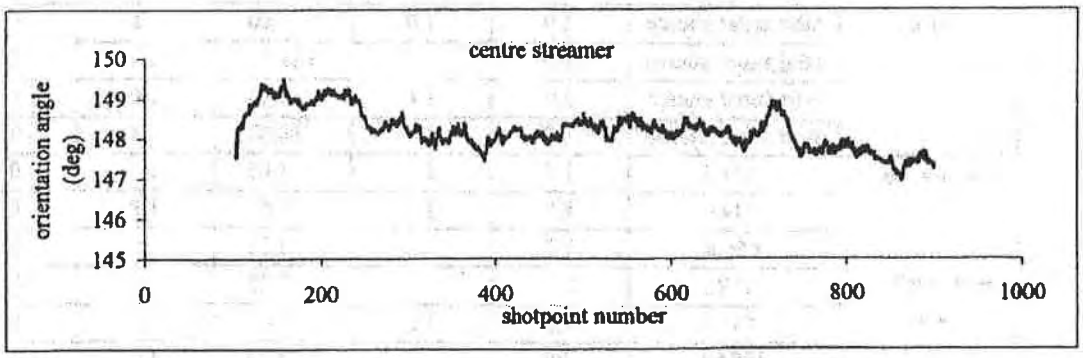

Figure 8.11: Streamer orientation angle computed assuming *a priori* standard deviations of 1.0 and 1.5 metre for the acoustic and laser ranges respectively, Gabon 1992

2. Though the positioning of the seismic spread is not significantly affected, on the contrary, measures of precision are affected. Table 8.11 outlines the results obtained for the second set of data. From this table it is evident, almost at a glance, that float maximum deviations have decreased by 1.0 - 1.5 metre and the minimum values, on average, by 1.0 metre. These results can easily be explained since the float positions, in both surveys, are determined only by means of acoustic and laser observations.
3. Hydrophone minimum (almost along-track) deviations are scaled down almost by half for any offset. Maximum (almost cross-track) deviations decrease by almost 1.0 metre at the front end and drop off to 0.5 metre at the far end of the cable.
4. These results seemed consistent for all streamers in both data sets.

The conclusions derived from the analysis of the results which consist of changes in the stochastic model of the compass azimuths seem to be more prominent. For the purpose

of this trial the observational standard deviations of the compass units have been set to be 1.0 degree, i.e. they have been increased by 0.3 degrees. A sample of these results is demonstrated in Figure 8.12 as well as in Table 8.12. The points of greatest importance can be summarized as follows

System	Node	95% Error Ellipse			2drms	50% CEP
		σ_{max}	σ_{min}	ψ_{max}		
vessel	NRP	2.7	2.4	130.28	2.9	1.2
float	stbd towfish	1.8	1.4	151.03	1.8	0.8
	port towfish	-	-	-	-	-
	stbd outer source	2.0	1.0	160.80	1.8	0.7
	stbd inner source	1.9	1.1	161.11	2.0	0.8
	port inner source	2.0	1.4	8.91	2.0	0.7
	port outer source	2.0	1.1	24.52	1.8	0.7
streamer position relative tow point	171.3	1.7	1.2	1.05	1.7	0.7
	514.0	1.8	1.2	1.61	1.8	0.7
	856.6	1.9	1.2	2.11	1.8	0.7
	1199.2	2.1	1.2	2.25	2.0	0.8
	1541.8	2.3	1.2	1.87	2.1	0.8
	1884.4	3.9	1.2	2.23	3.4	1.2
	2116.6	2.8	1.2	1.56	2.5	1.0

Table 8.11: Measures of precision computed assuming *a priori* standard deviations of 1.0 and 1.5 metre for the acoustic and laser ranges respectively, Irish Sea 1993

1. The predicted residuals of all observation types seem not to be affected by this change in the stochastic model except those for the compass observations shown in Figure 8.12. More specifically, if these results are assessed in comparison with those based on the 'standard' solution, shown in Figure 7.16, it can be clearly seen that their mean values have almost been doubled in magnitude. Moreover these results indicate no significant changes occurring in their patterns. Finally, a small increase can be noticed in their standard deviation values.
2. Again, as noted for the previous group of trials, the filter states time series as well as the positioning of the seismic elements are hardly altered.
3. As expected the estimated precision of the vessel and float nodes does not change (Table 8.12).
4. From the same table it is also apparent that the minimum (almost along-track) precision of the seismic receivers does not change at all. This result can be easily

understood as the compass observations reflect the direction of the tangent of the streamer and therefore these estimates are only cable-orientation related.

5. In contrast with the previous remark the maximum (almost cross-track) deviations are strongly influenced by changing the precision of compass observations. Although the precision of the hydrophone groups fixed at the front and rear ends of the cable decreases only by 0.5 metre, the precision of the receivers deployed in the middle of the streamer decreases more than 2.0 metre. This disparity in magnitude is somewhat not entirely surprising given that the precision of the network in the middle depends mainly on the presence of the compass measurements.

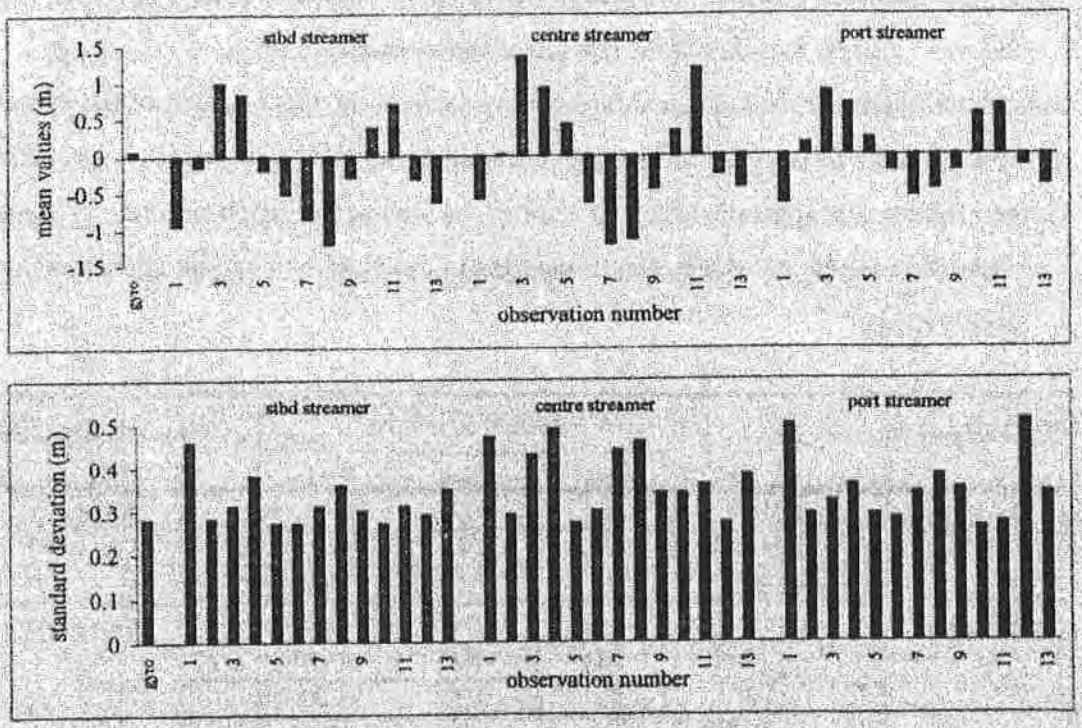

Figure 8.12: Statistics of the predicted residuals of the compass azimuths. These estimates were computed assuming *a priori* standard deviations of 1.0 degree for all compasses deployed in the network, Gabon 1992

The Syledis derived tailbuoy locations is the last observation type to be considered in this section. Two different scenarios were implemented in order to study the influence of the precision of these observations. In the first scenario standard deviations of 5.0 metre were accepted for the Syledis derived tailbuoy positions for the entire line, for both first and second data sets, while in the second one deviations of only 1.0 metre

were adopted and tested. Analysis of the results has led up to similar conclusions for both sets of data. In Figure 8.13 and Tables 8.13 and 8.14 only a small sample of these results are given. The main points to note from these analyses are

1. By decreasing the variances of the tailbuoy observations the predicted residuals of the acoustic, laser, compass, gyro and vessel Syledis observations are not influenced. Only the mean values of the predicted residuals of the tailbuoy measurements are affected, in fact decreasing by factor two. Such an example is given in the left plot of Figure 8.13. The corresponding plot derived for the 'standard' solution is given in Figure 7.18.
2. Similarly, by increasing the variances of the tailbuoy measurements the mean values of the predicted residuals of these measurements increase almost by factor two. Figures 7.18 and 8.13 depict the results for the second data set.
3. The last point to mention is that only the precision of the rear end part of the seismic spread seems to be affected by these changes in the stochastic model. The better precision at this area under the first scenario as well as the bigger uncertainty values under the second are clearly due to changes in the stochastic model of the tailbuoy observations.

System	Node	95% Error Ellipse			2drms	50% CEP
		σ_{max}	σ_{min}	ψ_{max}		
vessel	NRP	2.7	2.6	52.67	3.1	1.3
float	stbd source	1.9	1.8	12.35	2.1	0.9
	port source	1.9	1.7	110.51	2.1	0.9
streamer	114.1	2.1	1.4	137.20	2.1	0.9
	599.8	4.0	1.5	145.74	3.5	1.3
	1097.8	6.1	1.5	147.68	5.1	1.8
position relative tow point	1595.8	7.3	1.5	148.61	6.1	2.1
	2093.8	7.4	1.5	149.35	6.1	2.1
	2591.8	6.1	1.5	149.92	5.1	1.8
	3089.8	4.2	1.5	146.69	3.7	1.3

Table 8.12: Measures of precision computed assuming *a priori* standard deviations of 1.0 degree for the compass azimuths, Gabon 1992

In the foregoing analyses a number of tests have been carried out to study the effect of the stochastic model of the observations on the estimation result and its precision. In fact these tests consist of changes in the values of certain elements of the covariance

matrix of the observations. Also, it is important to note that these changes have been applied to each single measurement of the observation type tested - depending on the trial - for the entire data file. However, in reality, it is not possible for all observations to be of the same the accuracy, especially for a long period of time - some of them are more noisy than others and/or some sensors do not operate properly. Obviously a more sophisticated approach to the determination of the observational standard deviations is required. One suggested approach is whereby the standard deviation of each observation is determined in real time mode by independent assessment of the observation, and possibly its predicted residual, time series values. A brief outline for the implementation of the method is given in Chapter Ten.

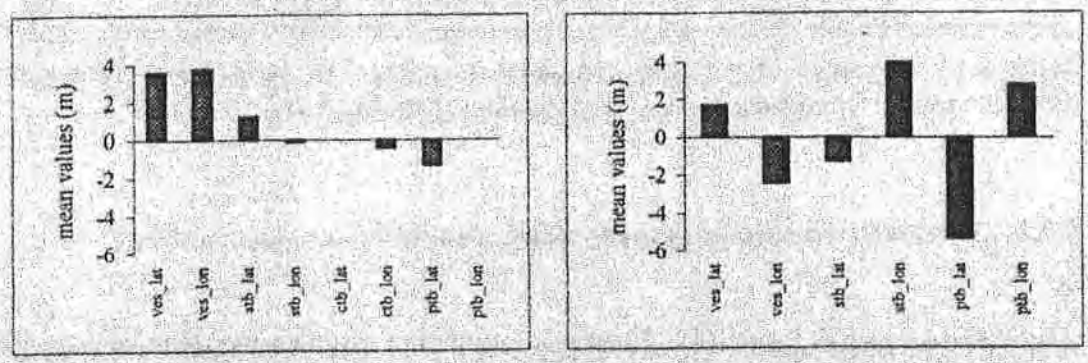

Figure 8.13: Statistics of the predicted residuals of the vessel and tailbuoy Syledis derived locations. These estimates were computed assuming 1.0 and 5.0 metre *a priori* standard deviations for the tailbuoy observations for the surveys in Gabon 1993 (left) and Irish Sea 1993 (right) respectively

System	Node	95% Error Ellipse			2drms	50% CEP
		σ_{max}	σ_{min}	ψ_{max}		
vessel	NRP	2.4	2.1	52.35	2.6	1.1
float	stbd source	1.9	1.7	14.70	2.1	0.9
	port source	1.9	1.7	108.69	2.1	0.9
streamer	114.1	2.0	1.4	136.66	2.0	0.8
	599.8	3.2	1.5	144.98	2.9	1.1
	1097.8	4.5	1.5	147.13	3.9	1.4
position relative	1595.8	5.3	1.5	147.98	4.5	1.6
tow point	2093.8	5.2	1.5	148.56	4.4	1.6
	2591.8	4.4	1.5	148.71	3.8	1.4
	3089.8	3.1	1.5	143.46	2.8	1.1

Table 8.13: Measures of precision computed assuming 1.0 metre *a priori* standard deviation for the Syledis derived tailbuoy locations, Gabon 1993

System	Node	95% Error Ellipse			2drms	50% CEP
		σ_{max}	σ_{min}	ψ_{max}		
vessel	NRP	3.1	2.4	130.69	3.2	1.3
float	stbd towfish	3.3	2.5	150.24	3.4	1.4
	port towfish	-	-	-	-	-
	stbd outer source	3.2	2.0	156.73	3.1	1.2
	stbd inner source	3.2	2.6	153.70	3.4	1.4
	port inner source	3.1	2.0	21.24	3.0	1.2
	port outer source	3.1	2.0	26.40	3.0	1.2
streamer	171.3	2.7	2.2	177.63	2.9	1.2
	514.0	2.8	2.2	178.00	2.9	1.2
	856.6	2.9	2.2	179.44	3.0	1.2
position relative	1199.2	3.0	2.2	0.15	3.1	1.3
tow point	1541.8	3.2	2.2	0.34	3.2	1.3
	1884.4	4.3	2.2	1.01	4.0	1.6
	2116.6	5.2	2.2	2.24	4.6	1.8

Table 8.14: Measures of precision computed assuming 5.0 metre *a priori* standard deviation for the Syledis derived tailbuoy locations, Irish Sea 1992

8.3.2 The Stochastic Model of the Dynamic Model

It has been detailed in Section 3.2.2 that the dynamics of a system represent its behavior as it varies with time. Consequently, the stochastic model of the dynamics of a system indicates how well the model describes reality. This is invariably in the form of the covariance matrix of the driving noise of the system.

The dynamics of the integrated algorithm developed in Chapter Five are described by Equations 5.3.4. The velocity or acceleration terms appearing in these expressions represent the driving noise of this system with their standard deviations being the main information that was used to build its covariance matrix.

In the following discussion, in order to aid interpretation, the driving noise parameters are spilt and classified in three groups. Vessel acceleration and vessel crab angle velocity form the first one. Acceleration of the positions of the float nodes refers to the second group, while the third one consists of the acceleration of the streamer reference point position as well as of the rate of change of the cable's orientation angle and polynomial

coefficients. It is, mainly, the role of the polynomial coefficients that is going to be discussed in more detail in the following paragraphs. Analysis proved that changes of their driving noise could influence, in certain cases substantially, the estimation result and its quality.

Due to the stable nature of seismic exploration surveys any small change in vessel acceleration and crab angle velocity deviations do not have a great impact on the positioning of the seismic spread. For example by changing the standard deviation of the velocity of the vessel crab angle from 0.01 degrees/sec to 0.04 degrees/sec only the filtered values of this estimate change. The results derived from the processing of the second data set are depicted in Figures 7.1 and 8.14 respectively. Examination of these results leads to the following conclusions

1. The curve shown in Figure 8.14 is substantially noisier than the one given in Figure 7.1. This phenomenon is not difficult to resolve given that in the second trial (shown in Figure 8.14) the filter relies more on the observations than in the first one - it is believed that the system dynamics describe the model better in the former test.
2. The second point to note is that the crab angle estimates for the second test start from zero, however, within a few shotpoints time they reach the values derived in the first trial. Simply, in the first experiment the initial value for the vessel crab angle has been set to be equal to the difference between the vessel gyro and course made good values (as given by the contractor), while in the second one equal to zero. It is apparent that the filter identifies and restores this discrepancy easily.

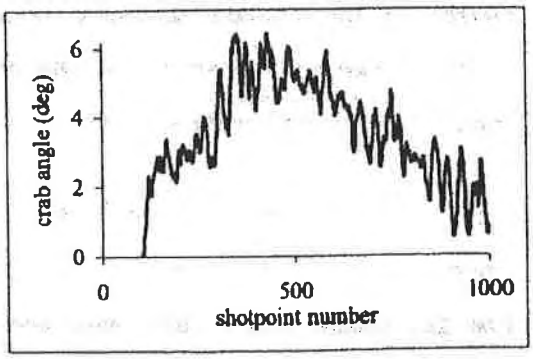

Figure 8.14: Vessel crab angle time series computed assuming a drift rate of 0.04 degrees/sec for the vessel crab angle, Irish Sea 1993

Again, it is due to the intended straight lines and constant sailing speed that small changes in the standard deviation values of the float and streamer head points drive the filter in similar ways. If the deviations of the driving noise of these estimates are set to be 0.1m/sec^2, only the position and velocity of the corresponding states seem to be affected. In fact, both in-line and cross-line coordinates of the float nodes seem to be more noisy and their maximum velocity values increase from 0.2 m/sec to 0.4-0.5 m/sec. In contrast to this conclusion, it should be stressed that if bigger standard deviations are used these positions can change significantly.

System	Node	95% Error Ellipse			2drms	50% CEP
		σ_{max}	σ_{min}	ψ_{max}		
vessel	NRP	2.7	2.4	130.12	3.0	1.2
float	stbd towfish	3.7	3.1	134.55	3.9	1.6
	port towfish	-	-	-	-	-
	stbd outer source	4.8	2.4	160.90	4.4	1.7
	stbd inner source	4.0	3.5	137.29	4.3	1.8
	port inner source	4.3	2.4	16.48	4.1	1.6
	port outer source	4.0	2.2	23.80	3.8	1.5

Table 8.15: Measures of precision of the vessel NRP and float nodes computed assuming a standard deviation of 0.1 m/sec^2 for the float nodes acceleration, Irish Sea 1993

By contrast with the results related to the positioning of the spread, the precision of the float nodes and the receiver groups change. Table 8.15 outlines the results derived for the float positions based on the processing of the second set of data. From this table it is apparent that the worst scenario is for the maximum error is to be increased by 1.6 metre while the minimum value by 0.9 metre. Finally it should be noted that this change in the stochastic model affects only the precision of the receivers deployed at the front end of the cable and by the same factor of magnitude as for the floats.

Figure 8.15 and Table 8.16 depict some of the results that consist of changes in the stochastic model of the streamer orientation angle driving noise. More specifically both first and second sets of data have been processed again assuming an error of 0.1 degrees/sec for the driving noise of angle α. Comparison between these results and those derived for the 'standard' solution (error in the rate of change of α equal to 0.01 degrees/sec) could help the following conclusions to be drawn

1. As can be seen from Figure 8.15 the filter solution for the streamer orientation angle α ranges within the same limits as for the 'standard' solution shown in Figure 7.2. However, Figure 8.15 shows the filtered values to be slightly noisier due to the high standard deviation 0.1 degrees/sec being input.
2. The positions of all nodes (float and receivers) located at the front end of the network seem not to be influenced by increasing the deviation of rate of α. Only the cross-track coordinates of the receivers fixed at the middle and rear end of the network seem to be slightly noisier.

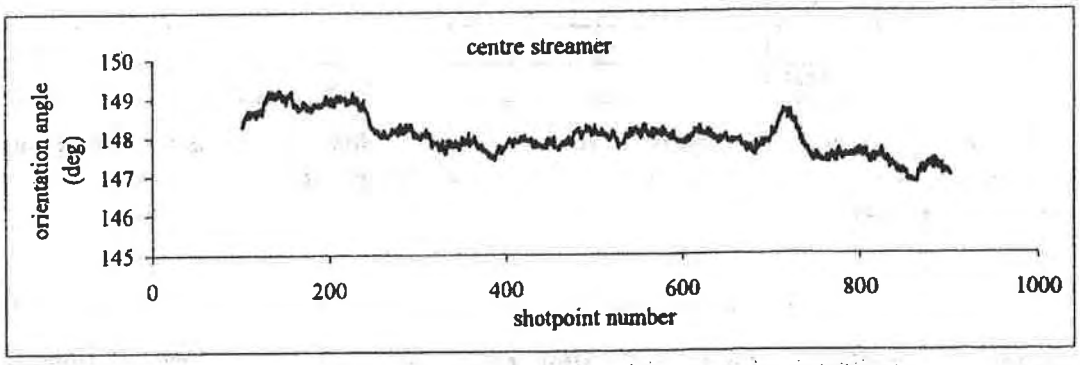

Figure 8.15: Streamer orientation angle time series computed assuming a standard deviation of 0.1 degrees/sec for the streamer orientation angle driving noise, Gabon 1992

3. As it is reasonable to expect, the precision of the vessel NRP and the float nodes is hardly affected. This conclusion applies also for the minimum error (almost along-track) for all hydrophone groups. On the contrary an increase of the order of 1.3 metre can be noticed in the maximum (almost cross-track) error for the receivers located at the middle of the cable. The precision of all nodes at the front and rear ends of the network seem not to be changed. It is, perhaps, the presence of the tailbuoy observations that helps the precision of the rear end receivers not to be increased.

It has been emphasized in the previous paragraphs that the role of the stochastic model of the polynomial coefficients will be discussed in more detail than the role of any other parameter. The reason is twofold. Firstly because it is not easy to interpret their physical meaning (as it is, for instance, for the driving noise of the vessel acceleration),

and therefore difficult to assign values for their standard deviations. Secondly, because the filter results (positions of the receivers and their precision), are strongly dependent on the stochastic model of these states.

Hydrophone position relative tow point	95% Error Ellipse			2drms	50% CEP
	σ_{max}	σ_{min}	ψ_{max}		
114.1	2.1	1.5	137.74	2.1	0.8
599.8	4.0	1.5	146.17	3.5	1.3
1097.8	5.9	1.5	147.57	5.0	1.7
1595.8	6.7	1.5	148.07	5.7	1.9
2093.8	6.3	1.5	148.41	5.3	1.8
2591.8	5.1	1.5	148.64	4.3	1.5
3089.8	3.9	1.5	146.72	3.4	1.3

Table 8.16: Measures of precision for a sample of hydrophone groups computed assuming a standard deviation of 0.1 degrees/sec for the streamer orientation angle driving noise, Gabon 1992

Several scenarios have been adopted to study the effect of the driving noise of the polynomial coefficients on the estimation result and its quality. Two of them are discussed here in more detail. The standard deviation values adopted for these tests for the first and second data sets are summarized in Table 8.17. In fact these tables show that the values used to build the stochastic model of the dynamic model have been decreased by order of magnitude two (model I), and increased by order of magnitude two (model II), compared with the stochastic model used to obtain the 'standard' solution (Tables 7.1 and 7.2).

The discussion of the results of the trials described in the following paragraphs are split into three parts. First an attempt is made to evaluate the filter solution, i.e. the state vector elements, while in the second and third parts the results related to the hydrophone groups positions and their quality are assessed.

The most important of the conclusions related to the system states are

1. The filter results in very similar solutions for the vessel position and velocity as well as for the vessel crab angle irrespective of which scenario is used. Similarly, the position and velocity values of the float and streamer reference points hardly alter.

2. Analysis of the streamer orientation time series plots indicates that if a model of a low system noise is used the angle α is heavily filtered, whereas a model for a high system noise results in a rather noisy curve. This phenomenon is more distinct for the results obtained from the processing of the second data set. Figure 8.16 depicts the filter solution for the orientation angle derived for the port streamer using model II. From this graph, the consistency in trends between the time series of angle α and the vessel gyro (Figure 7.3) is apparent.
3. Analysis of the solution for the polynomial coefficients time series proved that coefficients of a low order, namely third or fourth, are of bigger magnitude in absolute terms, than coefficients of a higher order. Also analysis proved that coefficients of a high order change faster with time than those of a low order. Finally, as expected, for a low system noise the filter results in relatively smoother curves for these estimates than for a system of a high noise.

	Model I	
	data I	data II
c_0	0.5 E-9 $m/m^2/sec$	0.5 E-10 $m/m^2/sec$
c_1	0.5 E-13 $m/m^2/sec$	0.5 E-13 $m/m^2/sec$
c_2	0.5 E-16 $m/m^2/sec$	0.5 E-16 $m/m^2/sec$
c_3	0.5 E-19 $m/m^2/sec$	0.5 E-19 $m/m^2/sec$
	Model II	
	data I	data II
c_0	0.5 E-5 $m/m^2/sec$	0.5 E-6 $m/m^2/sec$
c_1	0.5 E-8 $m/m^2/sec$	0.5 E-9 $m/m^2/sec$
c_2	0.5 E-11 $m/m^2/sec$	0.5 E-12 $m/m^2/sec$
c_3	0.5 E-14 $m/m^2/sec$	0.5 E-15 $m/m^2/sec$

Table 8.17: Testing of the stochastic model for the dynamic model of the polynomial coefficients, Gabon 1992 (left) and Irish Sea 1993 (right)

The vessel and float positions, as well as their precision estimates, are hardly influenced by these changes in the stochastic model of the polynomial coefficients. On the contrary the receiver positions are affected, especially those derived in the cross-track direction. Figure 8.17 illustrates the cross-line coordinates of the starboard streamer tailbuoy for both sets of data under three different circumstances. The three tested stochastic models are

(a) the stochastic model shown in Table 8.17, denoted by 'model I' (low system noise).

(b) the stochastic model adopted for the 'standard' solution, depicted in Table 7.2.

(c) the stochastic model given in Table 8.17, denoted by 'model II' (high system noise).

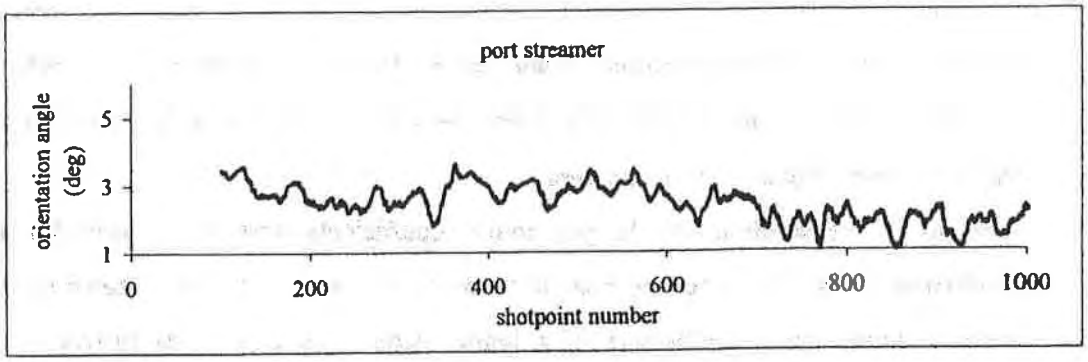

Figure 8.16: Streamer orientation angle computed for the stochastic model 'model II' shown in Table 8.17, Irish Sea 1993

Processing of the data under these three hypotheses results in the curves, shown in Figures 8.17 and 8.18, that are denoted by the figures 1, 2 and 3 respectively. Analysis of these results helps the following conclusions to be drawn

1. The first point to note from these plots is that the results derived from the analysis of the first data set (shown on the top) are much more consistent in trends and magnitude than those derived from the processing of the second one (shown on the bottom). This disparity between the two surveys has been already discussed in previous sections. Perhaps the most marked reason for this, is due to the differences in the quality, distribution and redundancy of the raw data between the two data sets. A partial explanation of this phenomenon has been given in Chapter Seven. However a full description and assessment of the tested data is provided in Appendix E.
2. From the results related to the survey conducted in Irish Sea (shown on the bottom) it can be seen that the differences between the solutions that were based on the low (curve 1) and high (curve 3) system noise exceed 20.0 metre , for almost half of the line, while the solutions derived under the hypotheses (b) and (c) (curves 2 and 3 respectively) led up to similar results. Very low system noise does not allow the polynomial coefficients to change fast enough and therefore to follow the variations of the observations. Analysis of the predicted residuals of the observations adds

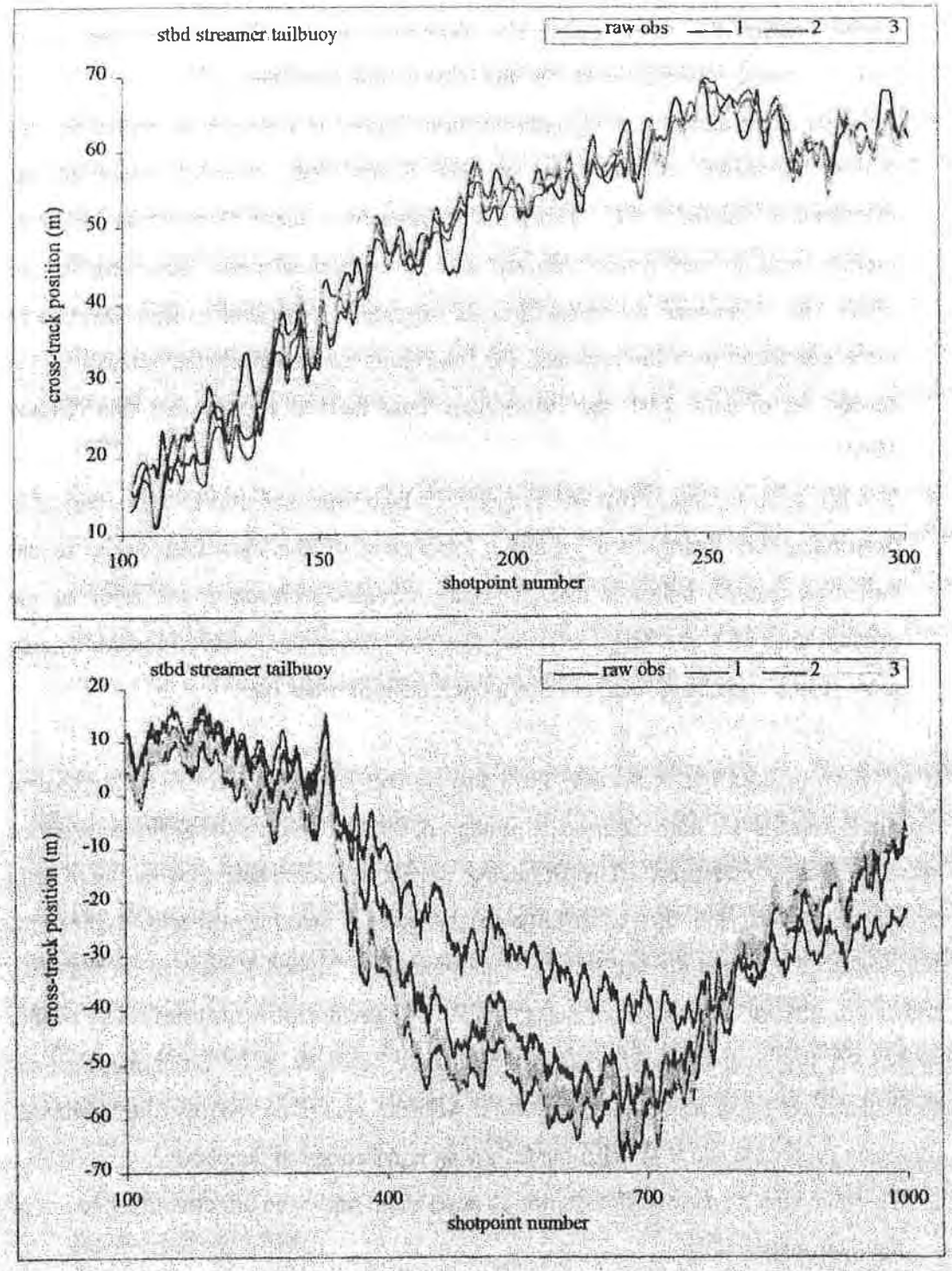

Figure 8.17: Cross-track tailbuoy coordinates computed for three different stochastic models of the polynomial coefficients dynamic model: curves 1 and 3 correspond to models "model I" and "model II" respectively shown in Table 8.17, and curve 2 corresponds to the "standard solution" - Table 7.2, Gabon 1992 (top) and Irish Sea 1993 (bottom)

further confirmation to this assumption since for a system of low noise, mean values were increased, especially those for the tailbuoy measurements.

3. Analysis of the along-track tailbuoy positions, shown in Figure 8.18, reconfirms the almost 5.0 metre difference between the filtered and observed values already discussed in Section 7.5.1. The point to note from these plots is that all three models result in very similar patterns with no substantial peaks occurring for the whole line. However, the fluctuations in magnitude from shot to shot seem to be more consistent with the raw data for the results derived from the analysis of the second set of data (Irish sea 1993) than those derived for the first one (Gabon 1992).
4. The last point to note is that coefficients of a high order seem to be more critical in positioning the hydrophone groups. Processing of the data files using similar stochastic models indicates that, the same increase/decrease in the error of the driving noise of a coefficient of order five will change the receiver positions much more than if this change is applied to a coefficient of order two.

It has been pointed out in Section 3.2.3 that correct specifications of the stochastic models is essential for both the proper 'tuning ' of the filter and its capability to produce accurate quality measures. The following results, in combination with the results already discussed, add further validity to this note. More specifically Table 8.18 summarizes the results derived for a low system noise, 'model I' (shown on the top), and the results for a high system noise, model II (shown on the bottom). The results related to the second set of data are given in Table 8.19 in the same manner. Examination of these results in combination with the results derived for the 'standard' solution (Tables 8.2 and 8.3) helps the following conclusions to be made

1. The minimum deviation (almost along-track) seem not to be affected irrespective of the hydrophone offset.
2. Low system noise results in smaller values (compared with those derived for the 'standard' solution) for the maximum error of the receiver positions. In fact in this case the filter solution is driven from the dynamic model with the measurement model having a very little effect.

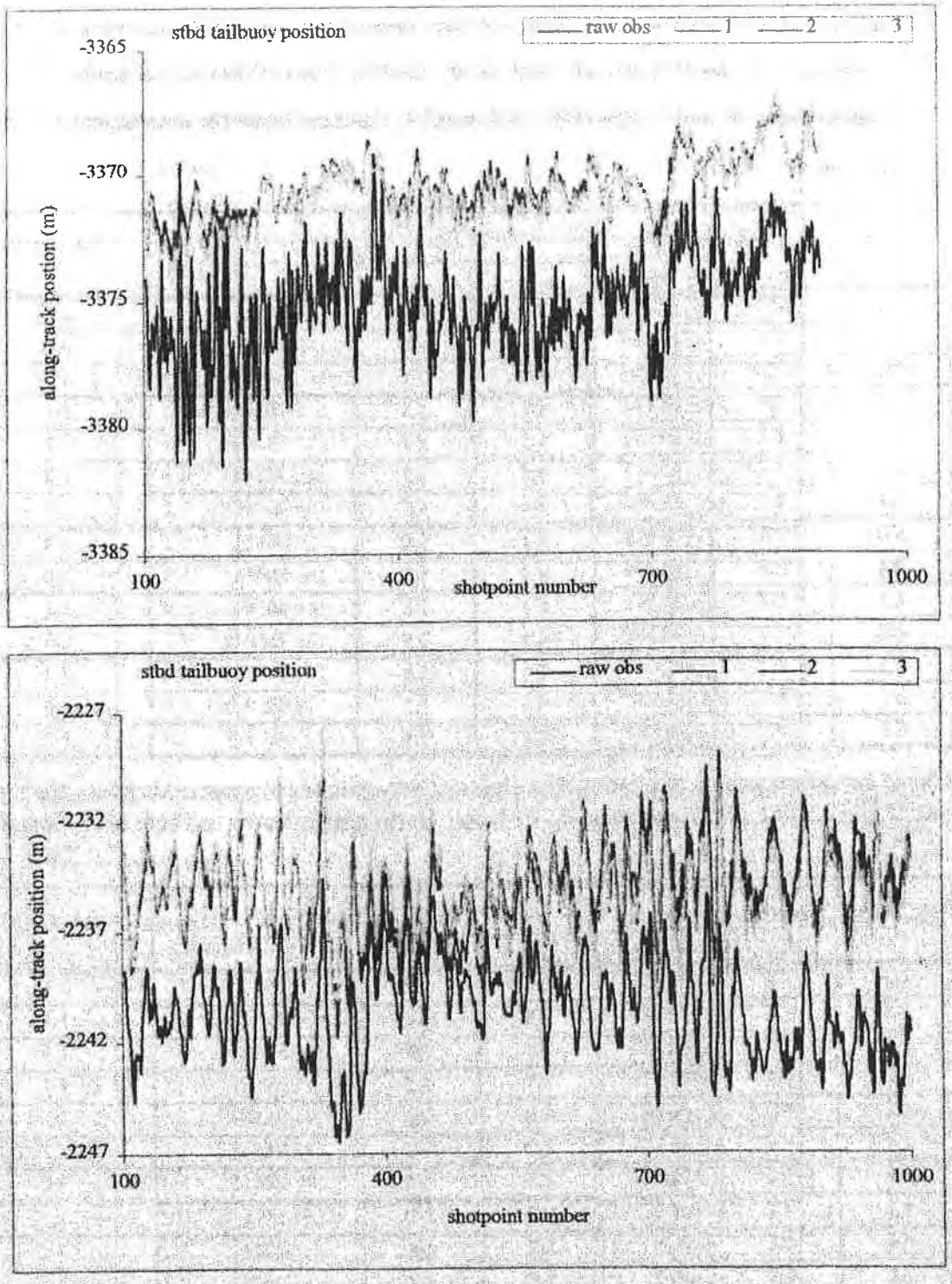

Figure 8.18: Along-track tailbuoy coordinates computed for three different stochastic models of the polynomial coefficients dynamic model: curve 1 and 3 correspond to models 'model I' and 'model II' respectively shown in Table 8.17, and curve 2 corresponds to the 'standard solution' - Table 7.2, Gabon 1992 (top) and Irish Sea 1993 (bottom)

3. If a system of a high noise is used then the error of the hydrophone group positions increases too much, especially for those fixed in the middle of the cable. This phenomenon is more distinct for the results obtained from the processing of the second data set.

Hydrophone position relative tow point	95% Error Ellipse			2drms	50% CEP
	σ_{max}	σ_{min}	ψ_{max}		
114.1	1.8	1.5	136.81	2.0	0.8
599.8	2.1	1.5	143.51	2.1	0.9
1097.8	2.7	1.5	145.09	2.5	1.0
1595.8	3.3	1.5	146.57	3.0	1.1
2093.8	3.6	1.5	147.01	3.2	1.2
2591.8	3.5	1.5	146.71	3.1	1.2
3089.8	3.6	1.5	146.25	3.2	1.2
114.1	2.1	1.5	137.07	2.1	0.9
599.8	4.5	1.5	146.88	3.9	1.0
1097.8	7.7	1.5	148.45	6.4	2.1
1595.8	9.2	1.5	148.93	7.7	2.5
2093.8	8.3	1.5	149.21	6.8	2.3
2591.8	5.3	1.5	149.32	4.5	1.6
3089.8	3.9	1.5	147.09	3.4	1.3

Table 8.18: Measures of precision for a sample of hydrophone groups computed for the stochastic models 'model I' (top) and 'model II' (bottom) shown in Table 8.17, Gabon 1992

Hydrophone position relative tow point	95% Error Ellipse			2drms	50% CEP
	σ_{max}	σ_{min}	ψ_{max}		
171.3	2.5	2.2	173.96	2.7	1.1
514.0	2.5	2.2	174.01	2.7	1.1
856.6	2.5	2.2	174.54	2.7	1.1
1199.2	2.6	2.2	175.38	2.8	1.1
1541.8	2.6	2.2	176.36	2.8	1.2
1884.4	2.7	2.2	177.34	2.8	1.2
2116.6	2.7	2.2	177.97	2.8	1.2
171.3	2.8	2.2	179.10	2.9	1.2
514.0	4.6	2.2	5.37	3.2	1.6
856.6	8.7	2.2	5.04	7.3	2.1
1199.2	11.5	2.2	4.61	9.6	3.2
1541.8	12.0	2.2	4.32	10.0	3.3
1884.4	8.5	2.2	4.02	7.2	2.5
2116.6	7.3	2.2	2.56	6.2	2.2

Table 8.19: Measures of precision for a sample of hydrophone groups computed for the stochastic models 'model I' (top) and 'model II' (bottom) shown in Table 8.17, Irish Sea 1993

8.4 CONCLUSIONS

In summary, the tests and trials of the analyses related to the functional and stochastic models of the integrated algorithm have resulted in a number of conclusions

1. Similar to the conclusions drawn in Chapter Seven, the results derived from the analysis of the first data set (Gabon, 1992) seem to be much more consistent in magnitude and trends than those derived from the analysis of the 'Irish Sea' survey.
2. Polynomial fitting models of orders four, five or six have led into relatively (especially those of order five and six) similar results in positions and precisions confirming the conclusions that were derived from the analysis of the preliminary curve fitting tests described in Chapter Two. Also analysis showed that polynomials of order higher than six result in overall problematic solutions for both sets of data.
3. The implementation of a harmonics function to simulate the streamer shape proved, in principle, to be successful. However, the results relating to the second data set reveal that much more research is still required in this area especially in the stochastic model of the driving noise of the harmonics model parameters.
4. Changes in the geometry configuration of the measurement setup have indicated that the model has been correctly designed and correctly implemented. Moreover these trials demonstrated the potential of the interdependence of an integrated network, i.e. how certain modifications affect the position and quality of each one sensor deployed in the network.
5. Analysis of the results relating to the stochastic model of the observations have shown that changes in the standard deviations of the acoustic and laser ranges mainly affect the precision of the float, and the front and rear end receivers. These tests have also shown that the precision of the receivers deployed in the middle of the network are very sensitive to any changes in the stochastic model of the compass observations and therefore particular attention should be paid in the determination of their *a priori* estimates.
6. Processing of both sets of data have shown that the stochastic model for the dynamic model of the polynomial coefficients can significantly affect the filter results. Very low system noise results in relatively smoothed curves while high system noise results in a rather distorted streamer shape, particularly at the middle of the cable.

CHAPTER NINE

RELIABILITY COMPUTATIONS

9.1 INTRODUCTION

It has been correctly pointed out that internal and external reliability are the 'ribbons and bow' on an algorithm's 'package' of positional error assessment (Zinn and Rapatz, 1995). The expansion of the type and quantity of the navigation data collected and the principal requirement for real-time processing, driven by the geophysical requirements of the implementation of the 3-D method, is today rather common practice in the offshore seismic industry. On such operations, the customer requires that the quality of the navigation data and the estimated positions is assured and that corrective action is taken when misspecifications in the positioning data are noticed.

The mathematical basis of the content of reliability in geodesy, and particularly in the case of dynamic systems, is explicitly discussed in Chapter Four. The specific characteristics and the procedure required in order to compute measures of reliability for a seismic network, based on the algorithm developed in this study, are given Chapter Five.

In the present chapter an attempt is made to evaluate the performance of the integrated algorithm by assessing the reliability results obtained using the data sets described in Appendix E - already analyzed in Chapters Seven and Eight. These results consist in computing and assessing the marginally detectable errors of the observations (MDE) and the maximum horizontal nodal (source and hydrophone) shift. Nevertheless, it should be stressed that this discussion is only a first approach to the subject, i.e. it does not so much aim to provide full cover of the subject as to spark off further research.

Section 9.2 summarizes the basic assumptions underlying the testing and system model parameters adopted for this part of the analysis. The results of the reliability computations as well as the effect of the geometry configuration, observation distribution and redundancy are considered in Section 9.3. Some concluding remarks are given in Section 9.4.

9.2 STREAMER MODEL AND TESTING PARAMETERS

It has been detailed in Section 8.1 that the quality of a system depends on the design options or parameters, namely the functional and stochastic models as well as the testing procedure that it is used to test the data for potential outliers and their effect on the estimation result.

All tests presented in this chapter have been carried out for the same functional and stochastic models that were used to derive the 'standard' solution discussed in Chapter Seven for both first and second sets of data, i.e., a polynomial streamer model of order five and the stochastic models outlined in Tables 7.1 and 7.2. However, in Section 9.3.3 a few remarks derived from the analysis of the same data based on different streamer and stochastic models are summarized.

For the reliability computations the two-sided probability of rejecting good data or the level of significance is set at $\alpha = 0.01$. The power of the tests is $\beta = 80\%$. These choices result in a noncentrality parameter $\gamma = 3.42$. This figure can be interpreted as the number of innovation standard deviations between the mean of the population of good data and the mean of the nearest population of outlying data. The choice of the values of the testing parameters is rather an arbitrary decision. Values of $\alpha = 1\%$ and $\beta = 80\%$ are commonplace in geodetic applications (Cross et all, 1994b; Salzmann, 1993; Zinn and Rapatz, 1995) - see also Section 4.3.

The window length of the tests has been set to zero, i.e. all trials are associated with a test at time t_o for an outlier with time of occurrence also t_o - no slips are considered. Moreover it is assumed that only one observation is biased at a time - no relative biases are considered to occur.

9.3 RELIABILITY ANALYSIS COMPUTATIONS

9.3.1 Internal Reliability

To compute measures of internal reliability the full statistical properties of the seismic network are required, i.e. the covariance matrix of the state vector elements and the covariance matrix of the predicted residuals of the observations. The formulae that were used to compute measures of internal reliability for the purpose of this chapter are those provided in Section 4.3.1.1 for systems operating in a dynamic environment. It should be noted that the aspect of internal reliability in this study is analyzed only by investigating the detectability of the system for potential outliers by making use of the MDE (Equation 4.18). The separability between alternative hypotheses, which is expressed by means of the correlation coefficient is not examined in this analysis.

Figures 9.1 and 9.2 depict the marginally detectable errors, in either meters or degrees, derived from the analysis of the first (Gabon 1992) and second (Irish Sea 1993) data sets respectively. Similar to the precision results these estimates are based on the analysis of a single shotpoint (time event 150). Nevertheless, analysis proved that these values they do not change very fast with time, and therefore, they can be considered more or less as typical values for the whole line in both data sets. Also it should be noted that all negative values appearing on these histograms refer to observations that have been rejected depending upon their predicted residual values. The main points to note from these analyses are

1. The results obtained from the analyses of both data sets seem to be comparable in both magnitude and trends.
2. The size of MDE for any acoustic range in both sets of data ranges between 6.0 - 8.0 meters with no substantial peaks occurring. This practically means that in order for an outlying observation to be detected a bias of at least 6.0 - 8.0 meters should be present. Obviously the size of a MDE depends on the choice of the observational standard deviation. All laser ranges, especially those in the first data set present smaller MDE values because smaller *a priori* uncertainties have been chosen for these measurements than for the acoustics - see Tables 7.1 and 7.2.

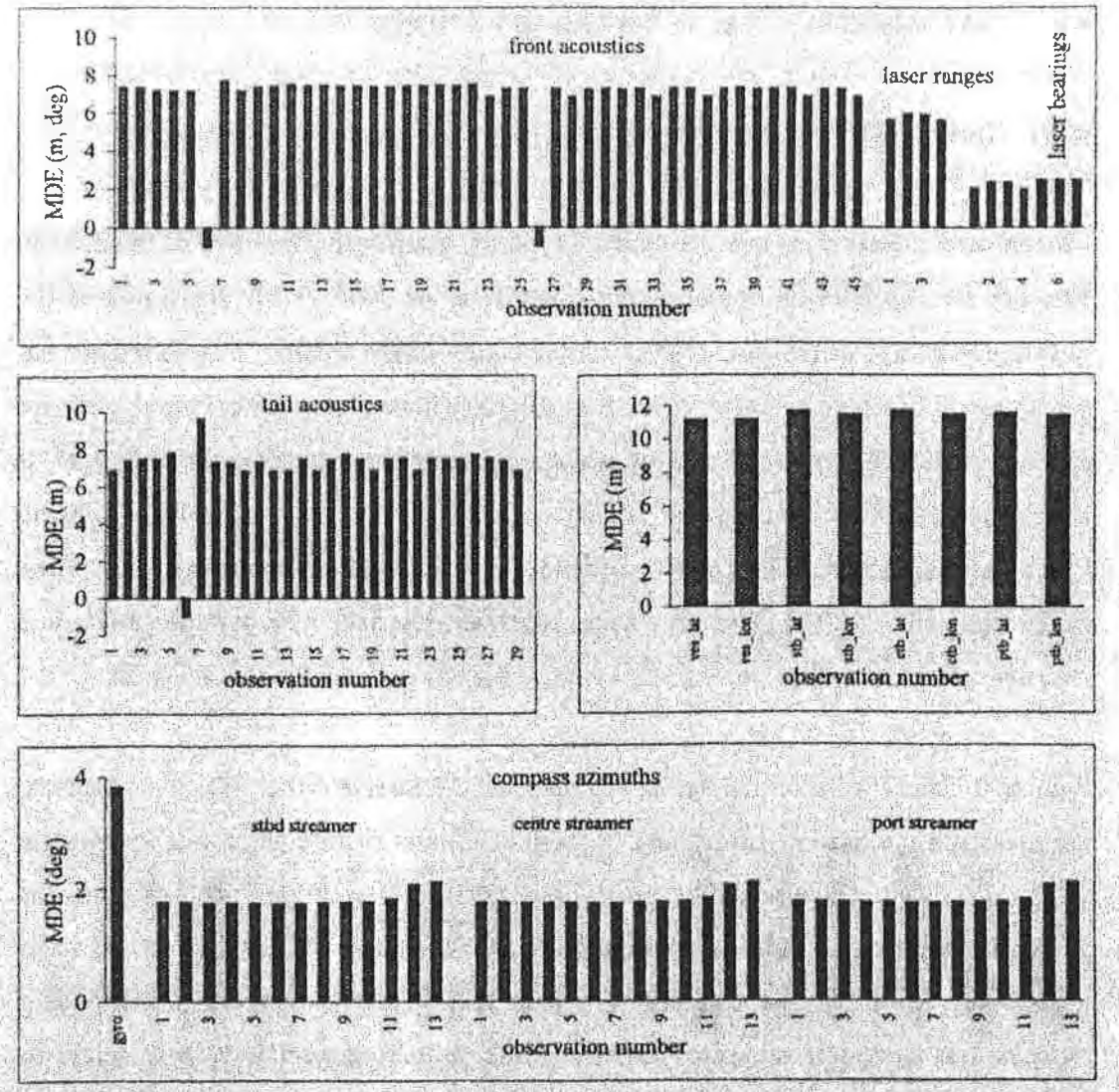

Figure 9.1: Internal reliability measures for all observations in the network, Gabon 1992

3. All vessel and tailbuoy observation MDEs are of the order of 11.0 meters since the same observational *a priori* standard deviations have been adopted for the analyses of both data sets. However it should be noticed that these values seem to be much bigger compared with those derived for the acoustics. This practically means that an error in an acoustic observation will be detected much more easily than an error in the vessel or tailbuoy positions.
4. From Figure 9.1 it is immediately evident that the results derived for the compass azimuths show an excellent consistency for all three streamers. The size of their MDEs is about 2.0 degrees with only the compasses deployed at the rear end of the

cables resulting in slightly larger values. Similar to the first data set the size of the MDEs for the compass measurements of the second set of data increases towards the tailbuoys (Figure 9.2). However, it is worthwhile to note that they are of bigger magnitude, compared with those derived for the first one, possibly due to the higher *a priori* standard deviations.

5. Finally, vessel gyro observations present much bigger MDEs than the compass azimuths - see Tables 7.1 and 7.2.

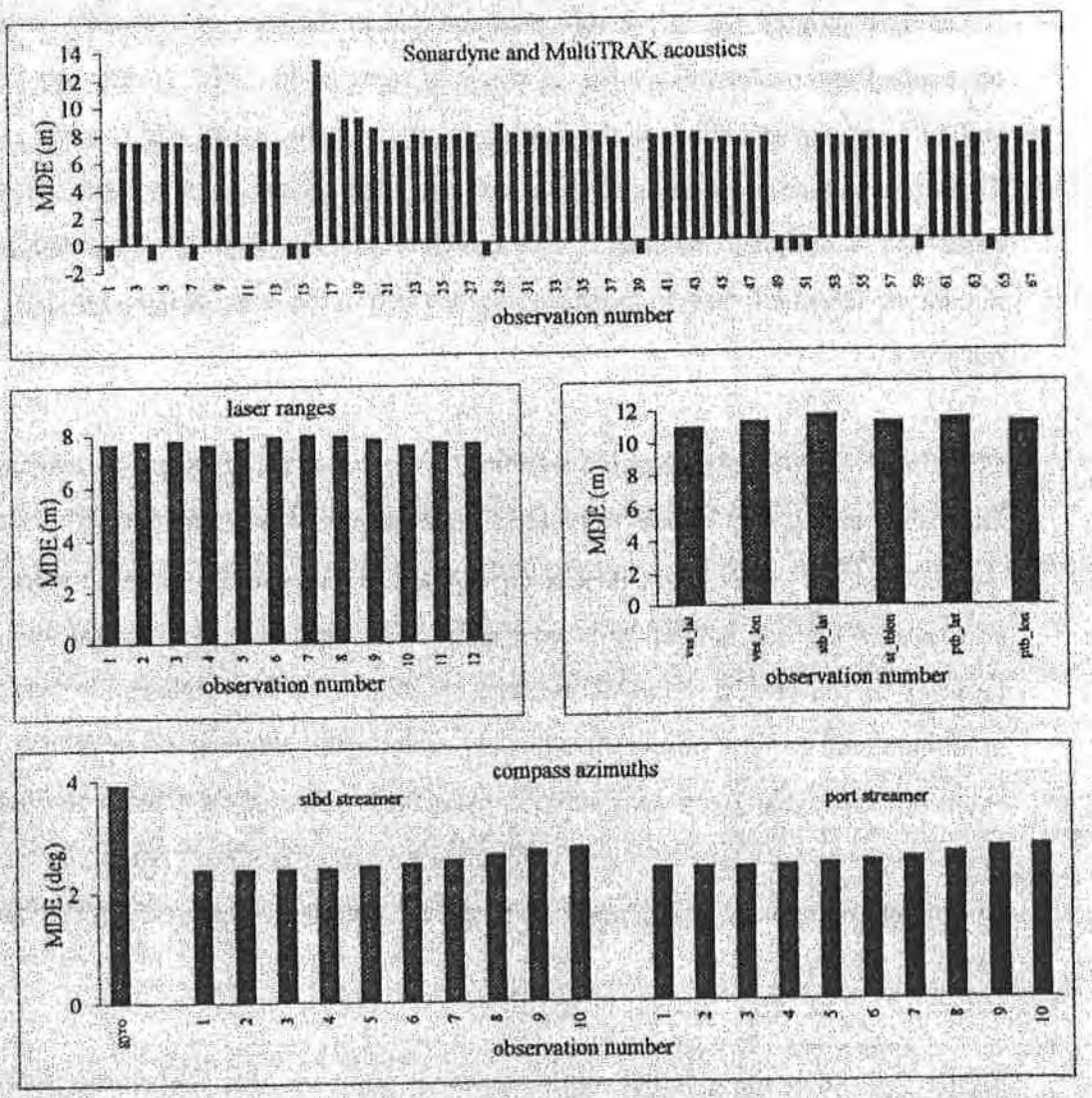

Figure 9.2: Internal reliability measures for all observations in the network, Irish Sea 1993

Although it is important to know the magnitude of any gross error that may remain undetected in each observation it is far more important to be able to investigate the effect of an undetected gross error on the state vector elements and finally on the positions of interest, namely source nodes and hydrophone groups. This aspect is discussed in the following section.

9.3.2 External Reliability

It has been pointed out in previous sections that in the case of a seismic network the concept of external reliability lies in knowing what is the effect (maximum horizontal shift) of undetected outliers in the positioning data on the source and receiver positions. This effect is then propagated to the HMP, viz. the average of the positions of a source node and a streamer receiver. These values can be directly compared with the maximum tolerated bias in position derived from the size of the bin for QA/QC purposes.

Chapter Five shows that external reliability is not as straightforward a computation as internal reliability. Each observational MDE is associated with an effect $\Delta\hat{x}_i$ in the state vector elements. This effect then is propagated at every node in the network (source and receiver) as a resultant horizontal shift. The maximum shift at any node in the network is the critical value of external reliability for this observation whereas the maximum shift for any observation for any node in the network is the critical value at each time (shotpoint). In the following paragraphs some of the results derived for the main stages of each one of these computations are discussed. Note that analysis is confined to computations at a nodal level, i.e. no attempt is made to examine what is the effect on the HMP.

Figure 9.3 shows the external reliability values computed for the source points and a sample of receivers fixed along the cables under three different circumstances. In other words these values refer to the hypothetical horizontal shifts of these nodes caused by an undetected outlier of the size of a MDE for three different observations.

Although it is important to evaluate the magnitude of these values it is far more important to examine their trends, i.e. which part of the network is significantly effected and which it is not. More specifically the following conclusions can be drawn

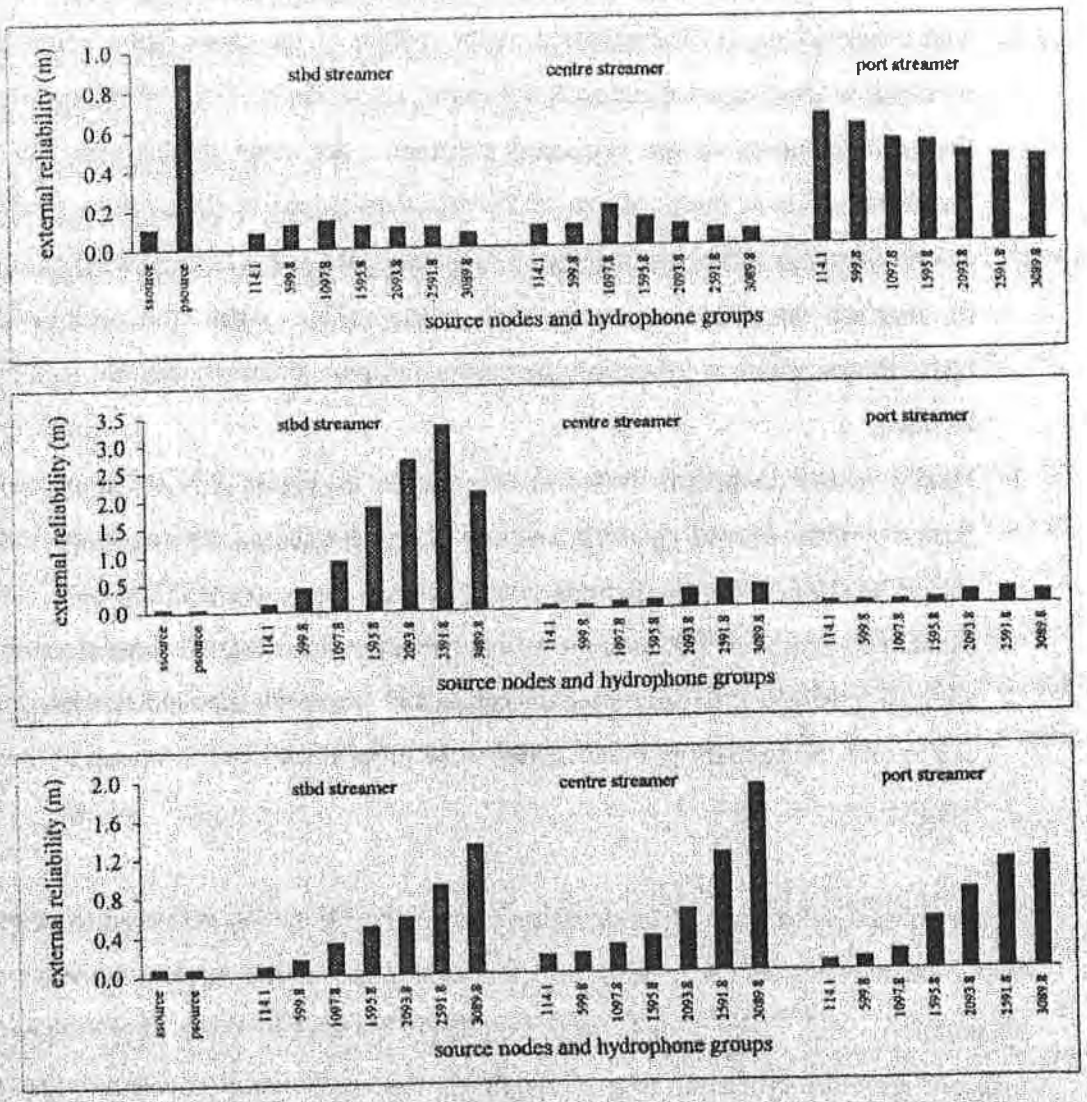

Figure 9.3: External reliability values computed for the source nodes and a sample of receiver groups caused by an outlier of the size of MDE for three observations: an outlier of 7.5 meters in the acoustic observed range between the devices fixed on the port source and the front end of the port streamer - range 22 (top), an outlier of 2.0 degrees in the tenth compass of the starboard streamer (middle), and an outlier of 11.0 meters in the latitude component of the centre tailbuoy observation (bottom), Gabon 1992

1. The plot shown at the top of Figure 9.3 depicts the hypothetical shifts caused by a gross error of the order of 7.5 meters in the acoustic range observed between the

pinger which is fixed on the port source and the acoustic device fixed at the front end of the port cable - range 22 in Figure 9.1. As is reasonable to expect the port source and the front end area of the port cable are mainly distorted. The positions of the receivers of the centre and port streamers are influenced very little.

2. The results given in the histogram in the middle of the same figure were derived assuming a gross error of almost 2.0 degrees, i.e. of the size of a MDE, occurring at the tenth compass of the starboard streamer. An error of this size will cause maximum effect at the positions of the receivers placed at the starboard cable. It can be clearly seen that the presence of tailbouy data at the starboard streamer helps to decrease the effect at the far end of the cable. Again the position of the hydrophones which are fixed on the centre and port streamers are not significantly affected.
3. Finally, in the histogram shown at the bottom of Figure 9.3, the impact on the positions of the seismic network, and how this is distributed, caused by an outlier of almost 11.0 meters in the latitude component of the centre tailbuoy observation is examined. From this histogram it is immediately evident that all three streamers are affected mostly at the rear end of the cables and especially the receivers fixed on the centre one. Note that this effect seems to be proportional to the square of the cable length.

The maximum value for each observation in the network is then extracted to produce a histogram showing the maximum effect at any node in the spread for each single observation. Such a histogram helps in making decisions as to which observations in the network are more crucial at a particular time. Figures 9.4 and 9.5 contain the results derived for both sets of data based on the MDEs shown on Figures 9.1 and 9.2 respectively. The first point to note is that only the external reliability values for the compass azimuths of the first data set are given. Analysis of the compass observations of the second set of data results in very small values that obviously seem to be unrealistic. It is unclear to date exactly what is causing the problem. Therefore an extra check on the software and data is ideally required to overcome this problem. Of course it has been mentioned in previous sections that both raw data and the results derived

from the analysis of the second data set are not as good as those derived for the first campaign - see Sections 7.4.2, 7.5.1, 8.2.1.2, 8.3.2.

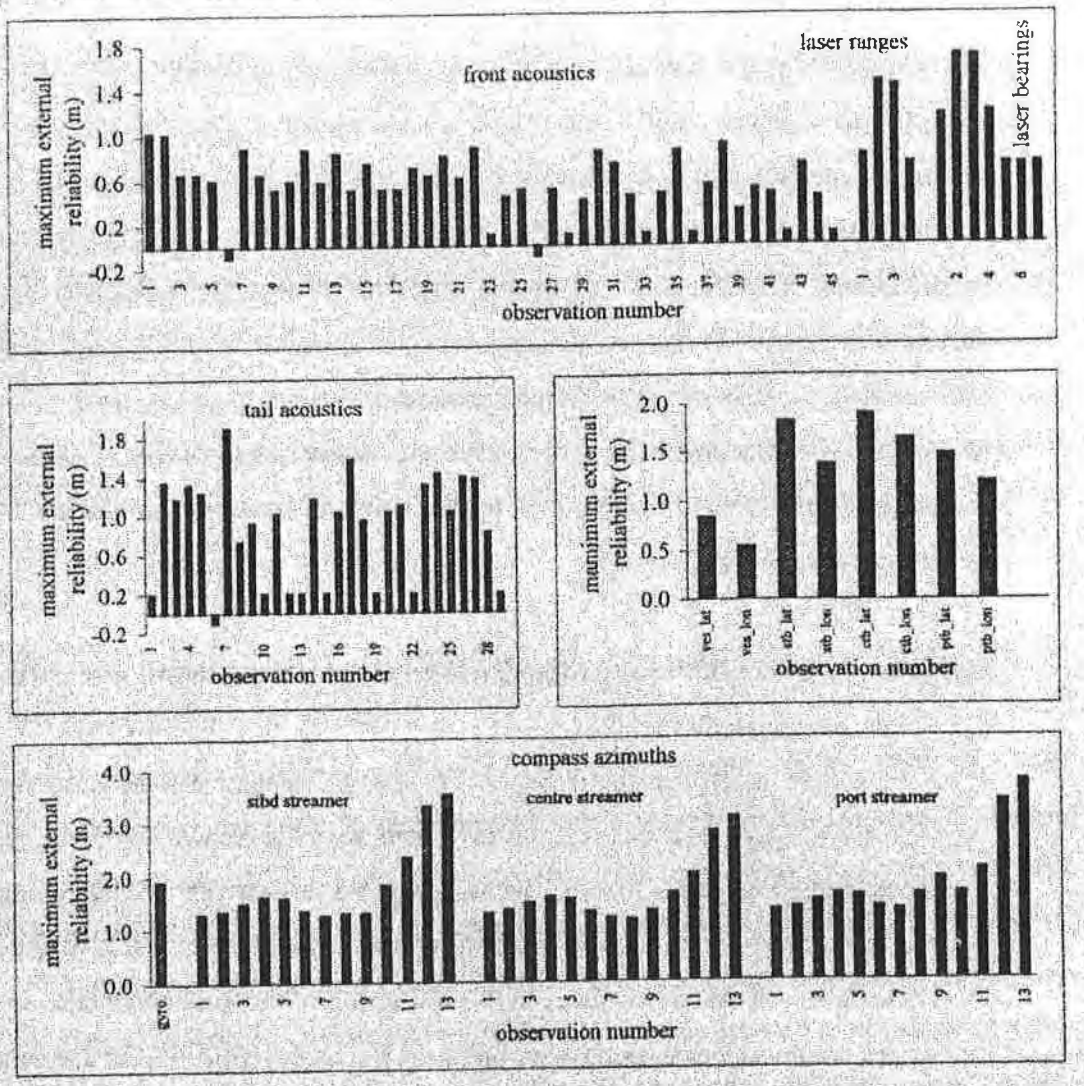

Figure 9.4: Maximum external reliability (maximum horizontal shift) computed at any node in the network, Gabon 1992

Before the specific conclusions relating to the external reliability results are fully detailed a point that emanates from this part of the analysis should be discussed. In Section 5.3.3 it is mentioned that most of the elements of the design matrix are obtained numerically because of the large number of unknown parameters contributing to the system and the complicated nature of some of the observation equations. Analysis proved that the small amount of the state vector elements needed to compute these

differentials can affect the values of the covariance matrix of the predicted residuals of the observations and therefore the reliability results. This remark becomes more important for observations with highly non-linear observation equation.

More specifically, it is the relative size of the elements of the design matrix that seems to generate the problem. In fact, this problem is mainly due to the relatively big difference in size between the blocks of elements related to polynomial coefficients of a high order and those related to polynomial coefficients of a low order. Although the matrix given by Equations 3.20 and 3.36 is almost singular, its inverse is formed successfully. However the impact of this problem becomes clearly visible when forming the inverse of the covariance matrix of the predicted residuals of the observations - which then is used to compute the internal reliability of the system. Some sort of scaling of the columns of the design matrix could be a first idea to overcome this numerical problem. Obviously this point needs further research.

The most important of the conclusions related to the results shown in Figures 9.4 and 8.5 can be summarized as follows

1. A maximum displacement of about 1.0 and 2.5 meters can be observed at any acoustic measurement in both the front end acoustic network and the full length acoustic network of the first and second data sets respectively. Similarly the tail end acoustics observed in the first campaign present a maximum effect of the order of 1.8 meters. All near zero values in this last group of measurements refer to acoustic ranges observed between devices fixed on the same cable, i.e. in the along track direction. Also analysis of the external reliability results of the laser observations lead to similar conclusions. Finally note that all negative values appearing on these histograms refer to measurements that have been rejected through the estimation process.
2. The external reliability values derived for the vessel and tailbuoy positions indicate an excellent consistency in magnitude and trends for both first and second data sets. A more detailed examination of these results shows that the external reliability values of the vessel NRP are smaller compared with those obtained for the tailbuoys although the same *a priori* standard deviation values were used. Perhaps the most

marked reason for this is due to ample redundancy at the front end of the network. Finally the last point to note from these figures, is that all latitude values are larger than the longitude ones. This phenomenon has already been discussed in Section 7.4.3.

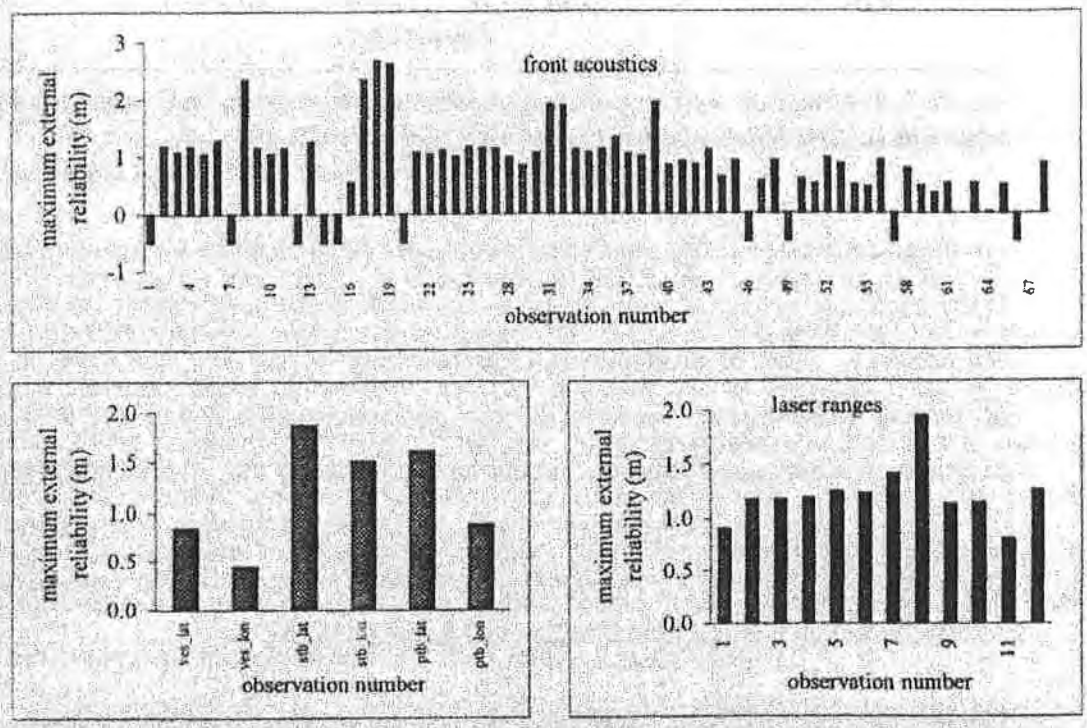

Figure 9.5: Maximum external reliability (maximum horizontal shift) computed at any node in the network, Irish Sea 1993

As expected, MDEs in the compass observations will cause maximum effect in the network positions since this part of the network is less redundant. An error of about 2.0 degrees in the gyro or in a compass unit fixed at the front end or midway along the cable will cause a displacement of maximum 2.0 meters. If the same error occurs in a compass unit fixed at the rear end of the cable this will have a maximum effect of 4.0 meters horizontal shift. The last point to note from these results is that the pattern of these values may reveal an unknown model effect. The assumption of a polynomial model to describe the shape of the streamer is the most marked reason to cause this problem. Proper tunning of the polynomial coefficients stochastic model might eliminate this effect.

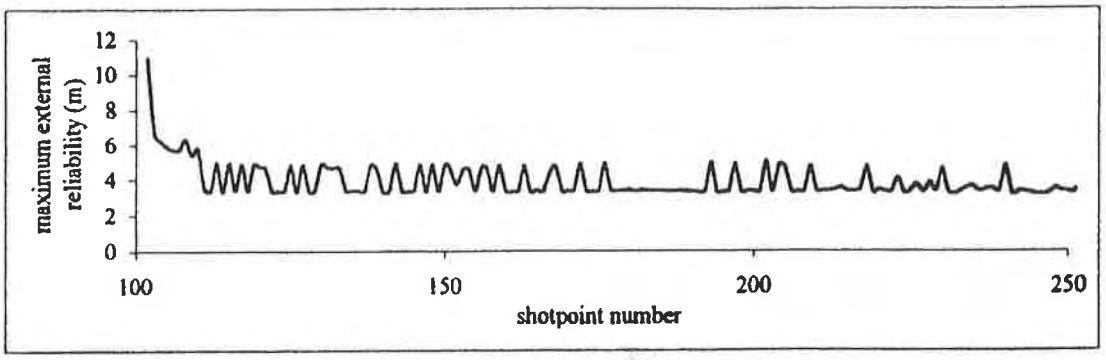

Figure 9.6: Maximum external reliability (maximum horizontal shift) computed for any node and for any observation in the network, Gabon 1992

As stated earlier, the foregoing computations shall finally lead to a single number. This is the maximum horizontal shift caused by any MDE in the observations for any node in the network. Plots of maximum external reliability in real time can assist in quickly identifying problems and trends in the raw positioning data, and therefore in making decisions whether specific sensors should be eliminated or not. These can also help in identifying problem areas that might require particular attention in post processing. A comprehensive procedure that should be adopted when specifying and using HMP external reliability may be found in Zinn and Rapatz, (1995).

Figure 9.6 gives maximum nodal (source or receiver) external reliability computed for the first set of data. The points of greatest importance can be summarized as follows

1. The first point to note is that most of the external reliability values shown in Figure 9.6 are due to outlying observations either in the compass measurements or in the tailbuoy geodetic derived positions. The single peaks of almost 6.0 meters are mainly due to low redundancy in the network caused by removing observations at the stage of data snooping.
2. External reliability at the beginning of the line is as high as 11.0 meters. Nevertheless, once the filter's operation is normalized, after a few shotpoints, external reliability is decreased by half and remains steady at this level.
3. Zinn and Rapatz, (1995), suggest that maximum HMP external reliability should not be allowed to exceed 50% more than the 2dRMS value specified for maximum HMP precision. On the analogy of this specification maximum nodal external reliability is compared with maximum nodal precision specified in a level of 2dRMS.

From Table 8.2 it can be concluded that the maximum error reaches 4.5 meters in the middle of the cables. Obviously the maximum external reliability value, shown in Figure 9.6, is far less than 7.0 meters, i.e. 50% more the maximum 2dRMS value.

9.3.3 The Effect of the Design Parameters on the Reliability Estimates

Analysis of both sets of data using a polynomial fitting model of order four and six results in smaller and larger external reliability values respectively compared with those derived for the 'standard' solution, i.e. for a polynomial model of order five. The differences in magnitude between each one of these solutions and the 'standard' one are only of the order of 0.5 meters, i.e. slightly larger than the resultant differences for precision - see Tables 8.2 and 8.4. However it should be pointed out that external reliability seems to change faster than precision, confirming that reliability is more sensitive to any abrupt changes in the positioning data and in any changes in the external forces acting on the system.

Similarly any changes in the stochastic models have an effect on the reliability results. Analysis proved that by increasing the standard deviations of the observations their MDEs increase resulting in larger variations in the state vector elements $\Delta\hat{x}_i$, and consequently in larger external reliability values. More specifically, changes in the stochastic model of the compass observations have a larger impact on the system reliability than changes in the uncertainty of any other observation type.

The stochastic model of the dynamic model is another factor that contributes to the estimation of reliability measures. It is mainly the stochastic model of the polynomial coefficients that influences the reliability of the system with all receivers deployed in the middle of the network suffering the biggest effect.

Although functional and stochastic models are important in computing the reliability of the network, it is the network geometry and observation redundancy that determine to a large extent the reliability of the system. Figures 9.7 to 9.10 give the reliability results

(internal and external) computed for the first series of trials described in Section 8.2.2. Examination of these results helps the following conclusions to be drawn

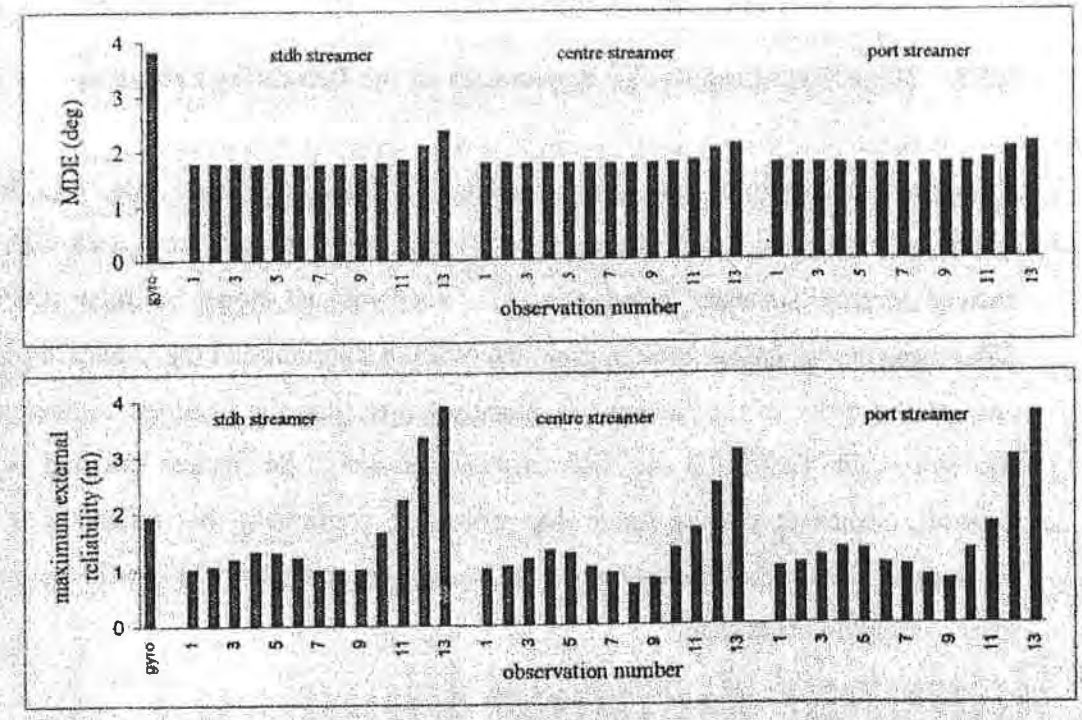

Figure 9.7: Internal reliability computed for the vessel gyro and all compass units deployed in the network, and external reliability (maximum horizontal shift) at any node caused by these MDEs. In this trial the starboard tailbuoy is eliminated, Gabon 1992

1. If only the starboard tailbuoy is eliminated (Figure 9.7) the reliability measures hardly alter. Only the compasses fixed at the rear end of the cables, especially those of the starboard streamer present slightly larger MDEs and reach 2.5 degrees. This causes a maximum shift of about 4.0 meters for some compass observations.
2. In the second trial, where the starboard tailbuoy and all tail acoustics from/to the starboard streamer are eliminated, the situation changes dramatically. The maximum horizontal shift in the network caused by a MDE of the order of 3.0 degrees in the tail end compass azimuths varies up to 8.0 meters. From the same histogram it is also clear that MDEs of more than 2.0 degrees in the centre and port streamers have an effect of less than 4.0 meters.
3. Finally, if the starboard tailbuoy, all tail end acoustics from/to the starboard streamer and the starboard streamer compass units 12 and 13 are eliminated then internal reliability exceeds 3.5 degrees in certain cases. Clearly in this uncontrolled manner it

is not surprising that external reliability at the rear end of the starboard cable shoots up and reaches 28.0 meters.

4. The MDEs and maximum external reliability related to the vessel and tailbuoy geodetic derived positions are less significant than those derived for the compass observations. Figure 9.10 suggests that in the last test the external reliability values caused by an MDE in the tailbuoy position are almost doubled, if compared with the results given in Figure 9.4. Moreover, similar to the conclusions drawn in Section 9.3.2, all latitude observations present larger external reliability values than the longitude ones.
5. In all three trials the reliability results that are related to acoustic and laser observations are not significantly affected.

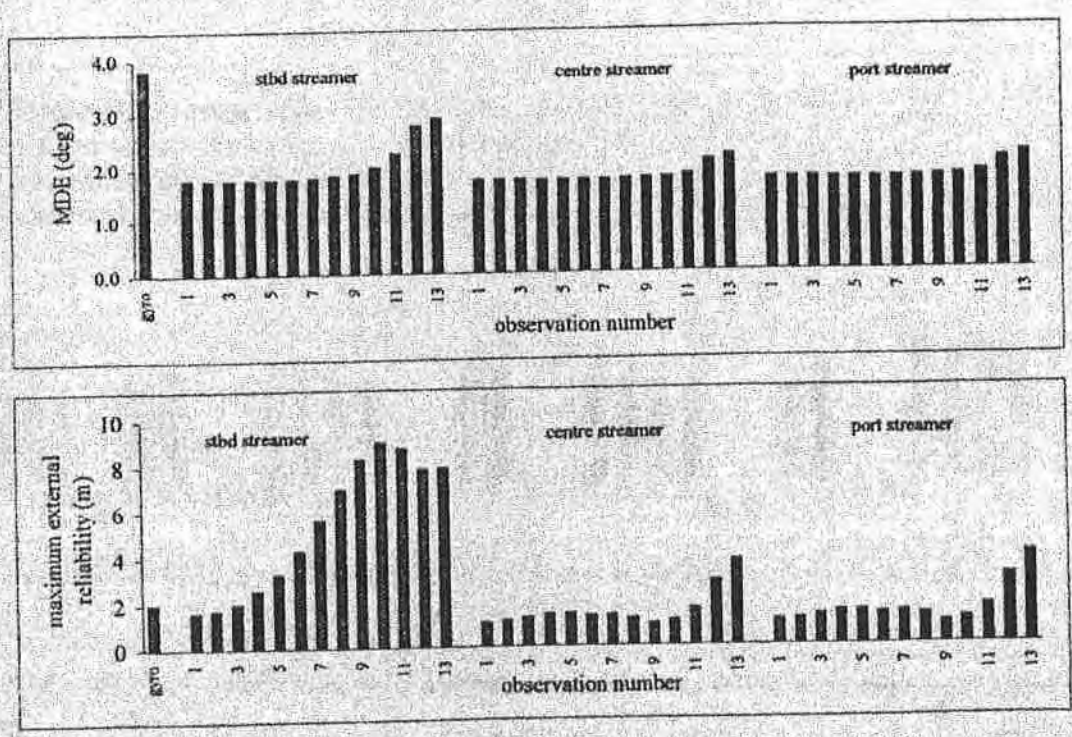

Figure 9.8: Internal reliability computed for the vessel gyro and all compass units deployed in the network, and external reliability (maximum horizontal shift) at any node caused by these MDEs. In this trial the starboard tailbuoy and all tail acoustics from/to the starboard streamer are eliminated, Gabon 1992

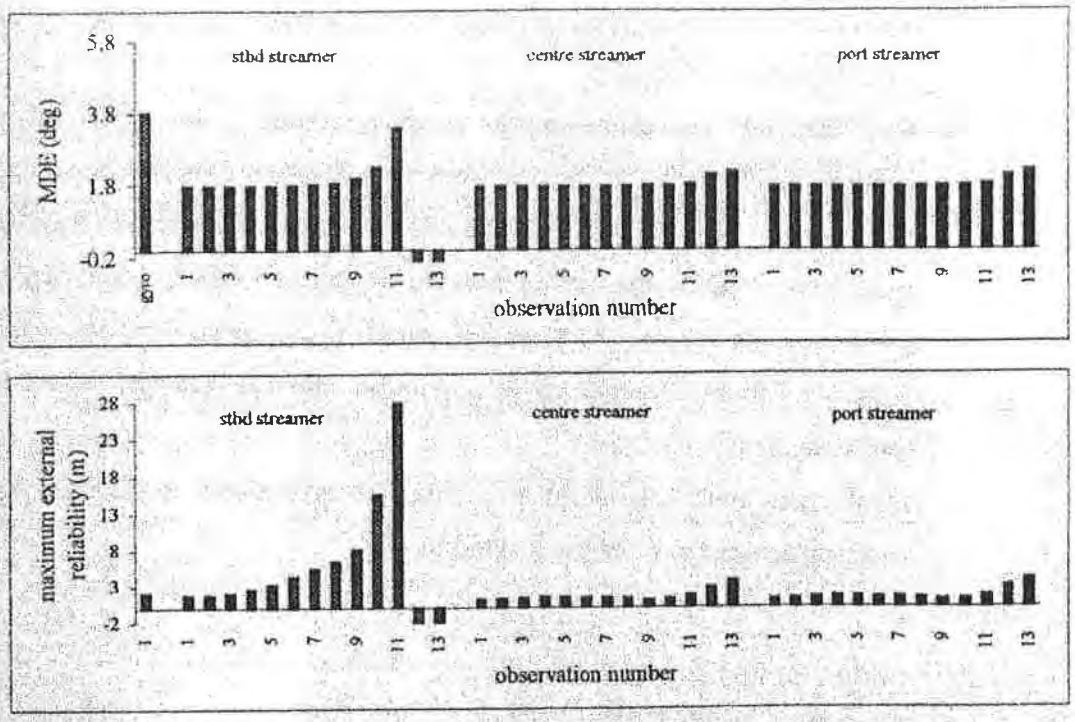

Figure 9.9: Internal reliability computed for the vessel gyro and all compass units deployed in the network, and external reliability (maximum horizontal shift) at any node caused by these MDEs. In this trial the starboard tailbuoy, all tail acoustics from/to the starboard steamer and the compass units 12, 13 of the same streamer are eliminated, Gabon 1992

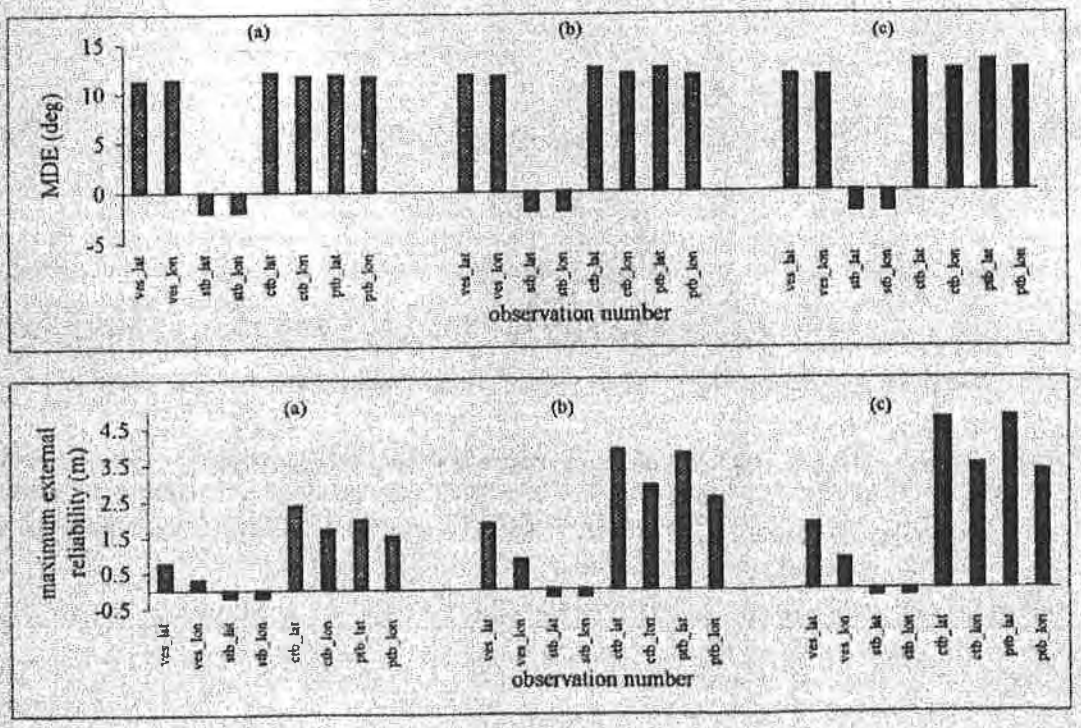

Figure 9.10: Internal reliability computed for the vessel and tailbuoy geodetic derived

positions, and external reliability (maximum horizontal shift) at any node caused by these MDEs. These results computed for three different geometry configurations, elimination of the starboard tailbuoy location (a), elimination of the starboard tailbuoy location and tail acoustics from/to the starboard streamer (b), and elimination of the starboard tailbuoy location, tail acoustics from/to the starboard tailbuoy and the starboard streamer tail compasses 12 and 13 (c), Gabon 1992

9.4 CONCLUSIONS

In this chapter the analysis of the reliability results derived from the implementation of the integrated algorithm developed in Chapter Five proved very useful for a first characterization of the quality measures for a seismic network. These are specified in terms of MDE (internal reliability) and maximum horizontal shift (external reliability). More specifically, the most important of the conclusions can be summarized as follows

1. Measures of internal reliability are primarily a function of the observational standard deviations. Internal reliability seems not to be affected significantly by any changes in the network geometry, in contrast with external reliability which is significantly affected.
2. Internal reliability is rather a straightforward computation, defined by the covariance matrix of the predicted residuals of the observations and the statistical testing parameters, while external reliability needs to be computed in several sequential steps. Analysis proved that the uncertainty matrix of the predicted residuals of the observations is sensitive to the numerical procedure used to form the design matrix.
3. Analysis of the external reliability results proved that this quality measure is highly dependent on the network geometry and observation redundancy - much more than on the functional and stochastic models.

CHAPTER TEN

CONCLUSIONS AND SUGGESTIONS FOR FUTURE WORK

This thesis has concentrated on the development of the mathematical algorithms and software for the integration of offshore surveying observables in order to determine the source, hydrophone and associated hardware positions, as well as their quality measures, in quasi-real or real-time during multi-source, multi-streamer operations. Based on the investigations carried out during this research at the design and development stage and the results obtained from the processing of the models with real positioning data the conclusions may be divided into two sections.

10.1 Design and Development of the Mathematical Algorithms

The main specific characteristics and advantages that derived from the design and development phases of this study can be summarised as follows

1. Although a rigorous and integrated approach to the problem is a clear demand by the seismic industry today, this requirement has to be reconciled with low processing time during real-time operations. The proposed model has been designed so that the size of the state vector elements (and therefore the size of all resultant matrices) to be as small as possible. It is the geometry configuration (number of vessels, floats and streamers) that determines the size of the state vector, and not (as it is the case for most other systems) the number of sensors deployed throughout the network. This issue is really emerging today since increasingly complex systems are used by the exploration industry. For instance, the proposed algorithm for a system of one vessel, three sources and six streamers needs to solve for 71 states (if a fifth polynomial order is adopted) at every time

event whatever the number of the positioning sensors. In contrast, a conventional seismic geodetic network needs to solve for more than 300 unknowns (assuming only 10 acoustic sensors and 12 compasses on each streamer, and two sensors on each gun), a number increased by an order more than four.

2. The positions of the source nodes and hydrophone groups is a direct by-product of the Kalman filter solution. This practically means that there is no need for further computations and no additional mathematical assumptions are required (most other approaches require interpolations between known positions to estimate the source and hydrophone positions).
3. By design, the whole system is split into several subsystems so that the resultant algorithm can be flexible enough to handle any geometrical configuration (i.e. any number of vessels, sources and streamers), and to describe coherently their relative positions using one set of continuous equations for each subsystem. This has been applied in such a way that new observation types can be easily incorporated into the unified system - i.e. there would be no need to expand the state vector.
4. Simplicity is a principal requirement for the computational efficiency, functionality and overall success of an operational algorithm. Single polynomial functions describe the shape of the entire streamer with only one set of coefficients and are continuous and continuously differentiable, as well as preserving ample redundancy along the cable. Moreover, given that acoustic ranges are incorporated into the integrated functional model (they are not stations in the system) there is no need for breaking the polynomial at the acoustic nodes to integrate this observation type. A n-order polynomial function has been adopted as the mathematical representation of the streamer shape. The more important of the results obtained by the preliminary tests using only compass observations can be concluded as follows
   - Polynomials of order four or less do not describe faithfully the observations. In such cases the residuals 'observed compass values - polynomial model values' may exceed 0.5 degrees.
   - Polynomials of order greater than six generate curves characterised by steep changes of gradient (particularly at the rear end of the cables) and therefore high risk of erroneous extrapolations.

- Polynomials of order five or six fit the data extremely well (no residuals more than 0.5 degrees are observed).

By design, the polynomial order is an input parameter at the system, and therefore the user can decide on the polynomial degree depending on the raw data (number of compasses, quality of the data, etc.).

Prior to the development of the mathematical models, particular attention was paid so that the final algorithm fulfills a number of design characteristics. Testing the algorithm using software validated their performance with real data. These specific characteristics are

1. *Optimal* - The estimator used is optimal in the sense that applies a stated criterion (least squares criterion) of optimality to minimize error. Moreover, the algorithm is optimal in the sense that the functional model used to describe the position of any point in the spread is determined in a rigorous mathematical way.
2. *Adaptive* - The structure of the algorithm allows for a rigorous statistical testing in order to detect and identify biases in the measurements and consequently eliminate (adapt) their effect on the filter estimates.
3. *Recursive* - No storage of observation data or results are required in order for the algorithm to perform. The algorithm's results depend only on the last event input data and the most recent previous output.
4. *Graceful* - This characteristic refers to the fact that as the quality of the data degrades, the quality of the filter results decrease only gradually.
5. *Flexible* - The algorithm is by design flexible to cope with any geometry configuration, any combination of positioning sensors and set of observations.
6. *Simple* - The basic processes of the algorithm can be described concisely in several flowcharts and diagrams (see Chapter Six).
7. *Well Structured* - The main mathematical processes split into functions that are as independent as possible. The mathematical computations are performed in a way so that changes in some modules do not affect the operation of others.

10.2 Performance of the Integrated Model with Real Marine Positioning Data

To verify the correctness of the mathematical model and the feasibility of the associated algorithms two sets of real positioning data were used to test the proposed algorithm. The configuration of the first data set consists of one vessel, two sources and three streamers (Gabon, 1992), while the geometry of the second one consists of one vessel, two sources and two streamers (Irish Sea, 1993). From all stages of the analysis is a general conclusion that the results obtained from the first set of data seem to be much more consistent in magnitude and trends compared with those obtained from the second survey. This conclusion can be, however, justified given that the raw data derived from the second campaign include more noisy, outlying and missing observations than the first one - see Appendix E. The main conclusions from these analyses are

1. Examination of the time series diagrams of the filter states and source and hydrophone positions leads to the following specific points
   - Analysis of the position and velocity of the centre of the sources and head of the streamers lead to similar conclusions for both sets of data. The first point to note is that all nodes present the same trends and variations in magnitude with time (and therefore it can be concluded, as expected, react in the same way to external forces). The maximum variations are 6.0 metre in-line and 15.0 metre cross-line throughout the surveying lines. The shot to shot differences do not exceed 1.0 metre. The time series of the velocity of the same nodes reveal an approximately white noise pattern with no substantial peaks occurring - suggesting that there is no need to model acceleration terms. Also, the hydrophone positions suggest similar patterns for all streamers at each survey. Higher differences are, however, observed at the shot to shot positions (of the order of 1.0-2.0 metre) for receivers deployed at the rear end of the cables.
   - The streamers' baseline orientation show similar patterns with time for all streamers involved in each survey. Moreover, the streamers' baseline orientation and the vessel crab angle show the same trends with time as the

gyro suggesting that streamers are affected, to some extent, by the variations in the gyro. This phenomenon is more distinct for the first set of data.

2. Assessment of the statistics of the predicted residuals of the observations shows that the mean values for most of the acoustic and laser ranges are less than 2.0 metre, but in any case less than 3 standard deviations of their *a priori* estimates. Analysis also proved that observations that present predicted residuals with high standard deviation, present also high rate of rejection, are the most noisy ones. Hence, it can be concluded that the filter is correctly identifying the outlying observations. Moreover, the mean values of all observation types seem to follow an approximately white noise pattern - representing an exceptionally strong argument that the observational and dynamic models are correct and correctly implemented. It should be stressed, however, that the (possibly) biased mean values and the relatively high standard deviation obtained for the compass observations for the second data set require further research.
3. A series of independent checks (comparison between identical quantities computed using completely different data, namely observed and filter derived values) have been carried out to assess the overall performance of the model. These tests indicate mean differences of 5.0 metre in-line and 10.0-15.0 metre cross-line for a tailbuoy position, differences less than 2.0 metre for acoustically or laser observed ranges throughout the network, and differences of the order of 1.0 degree for compasses deployed at the middle of the network (where redundancy is minimum). These tests add further confirmation that the model and its implementation are correct - at the very least they do not provide evidence to the contrary.
4. The tests carried out to study the effect of the streamer model on the final hydrophone coordinates have led to the following conclusions
   - The results obtained using polynomial fitting models of different order have led to similar conclusions with those derived from the analysis of the preliminary curve fitting tests. More specifically, analysis showed that polynomials of order four, five and six lead to similar results, namely differences less than 0.5 metre in-line for both sets of data, and 1.0 metre and 5.0 metre cross-line (worst case) for the first and second sets of data respectively. The precision of these estimates (error ellipses) changes only very little (less than 0.5 metre) for

different polynomial orders. These results suggest that polynomials can be adopted as a realistic mathematical representation of the seismic streamer shape.

- The implementation of a harmonic function model, as an alternative streamer model, proved in principle to be successful. Though the results obtained from the analysis of the first data set are absolutely consistent with those obtained using a polynomial fitting model, the results derived from the analysis of the second set of data reveal inconsistencies in magnitude of the receiver coordinates at the far end of the cables suggesting that much more research is still needed in this area and particularly on the dynamic model of the harmonic model parameters.

5. Changes in the geometry configuration of the surveying network showed that the algorithm is flexible as well as graceful. These were implemented by eliminating selected sensors, reprocessing the data and studying the results (positions and precision) in combination with the solution derived using all data. This feature of the algorithm can be used for planning as well as design purposes.
6. The effect of the stochastic models on the estimation results, namely position and precision, can be summarised as follows
   - Changes in the stochastic model of the observations are reflected in the source and hydrophone coordinates but mainly on their uncertainties. Analysis showed that if the *a priori* standard deviations of the acoustic and laser ranges are scaled down by half (from 2.0 metre to 1.0 metre), the uncertainty of the nodes in the area that the change is applied decreases by 1.0-1.5 metre. Changes in the standard deviations of the compass measurement seem to affect mainly the precision of the receivers in the cross-track direction. This phenomenon is more distinct at the middle of the cables, where the redundancy is very poor, and therefore particular attention should be paid in the determination of *a priori* uncertainties of measurements in this region.
   - Changes in the stochastic model of the dynamic model of the motion of the vessel, the guns and the streamer reference points reveal only slight changes mainly in the position and accuracy of the corresponding bodies. The stochastic model of the polynomial coefficients seem, however, to effect (in

some cases significantly) the positions of (especially) the far-end receivers. Nevertheless, it should be stressed that, this comment applies only for the results derived from the analysis of the second data set and therefore testing with more data is necessary to validate or demolish this hypothesis.

7. Assessment of the reliability analysis results has shown that
   - Internal reliability is a rather straightforward computation while external reliability needs to be computed in several sequential steps (observation, node and network level).
   - Internal reliability is a primary function of the *a priori* observational errors and seems not to be affected significantly (in contrast with external reliability) when the geometry configuration changes (Section 9.3.3).
   - External reliability proved to be sensitive to any changes of the geometry configuration and observation redundancy, i.e. areas of poor redundancy present maximum external reliability.
   - External reliability seems to change faster than precision confirming that reliability is more sensitive to any abrupt changes in the positioning data and any changes in the external forces acting on the system. Analysis also proved that maximum external reliability floors out at about 4.0-8.0 metre depending on the functional and stochastic model parameters used. This value is higher, as expected, than maximum nodal precision at 2drms level.

Generally, the whole research project has shown, for the first time, that an integrated and mathematically rigorous approach to the positioning of complicated seismic networks in real-time is practically feasible. Particularly, for the type of configurations examined, single polynomials of order five or six can be adopted as a realistic representation of the seismic streamer shape. Source nodes and hydrophone groups can be located with a positional precision of about 2.0-3.0 metre 2drms and better than 4.0-5.0 metre 2drms respectively. Maximum external reliability at any node in the network floors out between 4.0-8.0 metre. Also, analysis showed that the computational cycle time is typically less than the shot interval.

10.3 Suggestions for Future Work

Testing the integrated algorithm with more real and/or simulated data is essential in order to validate its performance in general. The ideal data sets may include configurations of different geometries as well as blocks of 'bad' data in order to test its performance in terms of robustness. More specifically, emphasis should be paid to the following points

1. *Mathematical processes* - In order to overcome any numerical problems that may relate to matrix algebra operations it is suggested that the structure of the design matrix (relative sizes of its elements) should be studied in detail and possibly applied some sort of scaling technique in groups of its elements in order to eliminate arithmetic ambiguities. Another point that is related to the mathematical procedures of such a system is the type of filter that might be used in order to provide an effective but cost effective solution to the problem. The idea of using a sequential Kalman filter (though its implementation assumes only uncorrelated observations) seems to be very attractive as an alternative since major mathematical computations (matrix operations) can be reduced to simple linear algebra computations. Finally, it is essential that software should be written in order to implement the entire DIA testing procedure for bias detection, identification and adaptation as proposed in Appendix B.
2. *Stochastic models* - Analysis showed that correct specifications of the stochastic models of the observation and dynamic models is essential for both proper 'tuning' of the filter and its capability to produce accurate and reliable quality measures. A first idea that may help in assigning 'better' values to the covariance matrix of the observations might be a dynamic observation variance estimation technique (for use in real-time), and also use of minimum (floor) standard deviation values. The basis of such an approach will be continuous monitoring of the raw observations and their innovation values and studying of their performance using linear regression analysis schemes. Similarly, an alternative to this technique might be used to improve the stochastic model of the dynamic model. For example, an independent Kalman filter algorithm with input data being only compass azimuths may help in making

decisions regarding the stochastic model of the polynomial (or other) function coefficients used to simulate the streamer shape. This concept is described in more detail in section 3.2.3.

3. *Streamer modelling* - Much more research is still needed to study the harmonic function as an alternative to model the streamer's shape. This might include studying of similar functions to the one adopted in Section 8.2.1.2, and more research on the stochastic model of harmonic function coefficients. A careful study of the time series of these state vector elements and their uncertainties (obtained based on alternative stochastic models) can be proved extremely useful in assigning 'better' values for their stochastic model and tuning the filter properly. It may also be interesting to see what effect using, for example, cubic splines (as opposed to single polynomials) would have upon the resultant hydrophone positions and their quality measures.
4. *Expansion of the algorithm/software* - All the analysis that has been discussed throughout the course of this thesis has been confined to one vessel configurations. Today, there is a lot scope to extend the current analysis techniques to multi-vessel operations. A first idea of the concept related to the design philosophy and structure that underlie the proposed algorithm is given in Appendix D. Extension of the state vector to include magnetic declination and cable stretch parameters is considered to be essential in order the real world be described in a more rigorous way. It is also considered essential to extend the algorithm's facilities to compute HMP positions and their associated quality measures.
5. *Pre-filtering* - In order that the filter operate efficiently, raw data should first be cleaned for outliers. It is suggested that, due to the relatively long cycle time of such complicated filters as the one developed here, it would be extremely useful in practice to carry out separate analyses for the front, middle and tail acoustic networks, as well as for every streamer compass group using simple least squares or Kalman filter algorithms to detect outliers. Obviously it would be the raw (edited) data that would be fed into the integrated filter - the separate filters only being for data screening. This feature can be ideally used in quasi real-time or postprocessing mode.

REFERENCES AND BIBLIOGRAPHY

Ackroyd N., and Lorimer R., (1990). *Global Navigation: A GPS User's Guide,* Lloyd's of London Press Ltd., London, pp 196.

Amrine T.L., Loree S.A., and Ridyard D., (1989). *Investigations of Interactions between Cable Leveling and Heading Measurement,* Proceedings of SEG-89, Dallas, USA, October 29 - November 2, pages 640-642.

ANON, (1986). *Geolog General Information,* Sercel, France, Issue: April 1986, 2400XEA000.

Anstey N.A., (1982). *Simple Seismics,* IHRDC, Boston, ISBN 0-934634-43-2.

Baarda W., (1968). *A Testing Procedure for Use in Geodetic Networks,* Netherlands Geodetic Commission, Publ. on Geodesy, New Series, Vol. 2(5) Delft.

Barr F.J., Wright R.M., Abriel W.L., Sanders J.I., Obkirchner S., and Womack B.A., (1990). *A Dual-Sensor Bottom-Cable 3-D Survey in the Gulf of Mexico,* Proceedings of SEG-90, San Francisco, USA, September 23-27, pages 855-858.

Barr F.J., (1993). *Seismic Data Acquisition: Recent Advances and the Road Ahead,* Proceedings of SEG-93, Washington D. C., USA, September 26-30, pages 1201-1204.

Berg O.R., and Woolverton D.G., (1985). *Seismic Stratigraphy II: An Integrated Approach to Hydrocarbon Exploration,* American Association of Petroleum Geologists, AAPG Memoir 39.

Brown R.G., and Hwang P.Y.C., (1992). *Introduction to Random Signal and Applied Kalman Filtering,* John Wiley, pp 499.

Canter P., (1989). *Evolution of Positioning in Marine 3-D Seismic,* Proceedings of SEG-89, Dallas, USA, October 29 - November 2, pages 606-609.

Celik R.N., and Cross P.A., (1994). *Implication for Quality Assesment and Quality Control from Integrated Offshore Positioning Systems*, Proceedings of Hydro-94, Aberdeen, UK.

Celik R.N., (1996). *Integration of DGPS and Conventional Systems in Offshore Surveying*, PhD Thesis, Department of Surveying, University of Newcastle upon Tyne, pp 284.

Chen W., (1992). *Integration of GPS and INS for Precice Surveying Applications*, PhD Thesis, Department of Surveying, University of Newcastle, pp 219.

Chevron Training Course, (1992). *Positioning 3-D Seismic Surveys*, Chevron Exploration and Production Services Company, School Scheme, Texas, September 14-18.

Coffen J.A., (1984). *Seismic Exploration Fundamentals*, ISBN 0-87814-295-9.

Cohen C.E., Pervan B., and Parkinson B.W., (1992). *Estimation of Absolute Ionospheric Delay Exclusively through Single-Frequency GPS Measurements*, Proceedings of ION GPS-92, Albuquerque, New Mexico.

Conner J., and Ponton B., (1994). *The Determination of Streamer Shape in Dynamic Cases*, The Hydrographic Journal, Vol. 73, July 1994, pages 3-9.

Corbett S.J., (1994). *GPS Single Epoch Ambiguity Resolution for Airborne Positioning and Orientation*, PhD Thesis, Department of Surveying, University of Newcastle upon Tyne, pp 229.

Cotton W.R., Schleicher K.L., Ridyard D., and Spinelli J.J., (1985). *Accuracy in Marine Streamer Positioning*, Proceedings of SEG-85, Washington D. C., USA.

Court I.N., (1990). *Integrated Acousticand Compass Streamer Positioning*, Proceedings of SEG-90, San Francisco, USA, September 23-27, pages 882-884.

Court I.N., (1991). *Applications of Acoustics to Source-Array and Streamer Tow-Point Positioning*, GEOPHYSICS, Vol. 56, April 1991, pages 558-564.

Court I.N., (1993a). *Applications of Acoustics to Streamer/Source Positioning*, Proceedings of SEG-93, Washington D. C., USA, September 26-30, pages 610-612.

Court I.N., (1993b). *Streamer Compass Validation and Verification*, GEOPHYSICS, Vol. 58, April 1993, pages 589-592.

Cramer H., (1946). *Mathematical Methods of Statistics*, Princeton University Press, Princeton.

Cross P.A., (1983). *Advanced Least Squares Applied to Position-Fixing*, Noth East London Polytechnic, Department of Land Surveying, ISBN 0-907382-06-1, pp 205.

Cross P.A., and Pritchett C.H., (1986). *A Kalman Filter for Real-time Positioning during Geophysical Surveys at Sea*, FIG XVIII International Congress, Toronto, Canada.

Cross P.A., (1987). *Kalman Filtering and its Application to Offshore Position-Fixing*, The Hydrographic Journal, Vol. 44, April 1987, pages 19-25.

Cross P.A., (1989). *Position: Just what does it mean?*, Proceedings of Nav-89, The Royal Institute of Navigation, London, UK.

Cross P.A., (1990). *Deriviation of Kalman Filter Equations*, Royal Institution of Chartered Surveyors/Hydrographic Society, Seminar on Kalman Filtering, University of Nottingham, UK, January 1990.

Cross P.A., Hawksbee D.J., and Nicolai R., (1994a). *Quality Measures for Differential GPS Positioning*, The Hydrographic Journal, Vol. 72, April 1994, pages 17-22.

Cross P.A., Hawksbee D.J., and Roberts W.D.S., (1994b). *Quality Measures for Offshore Differential GPS*, Department of Surveying, University of Newcastle upon Tyne, Technical Report prepared for UKOOA, c/o Enterprise Oil plc.

Davidson D.S., and Bandell A., (1990). *A Novel 3-D Marine Acquisition Technique*, Proceedings of SEG-90, San Francisco, USA, September 23-27, pages 863-866.

Digicourse Inc., (1994). *DigiCOURSE Underwater Positioning Systems*, Prospectus 8192-DC.

Dragoset B., (1990). *Proposed Ship Algorithm*, Western Atlas International Inc., Intercompany Report, January 1990.

Duncan P.M., Nelson B.H., and Wright R.M., (1989). *Acquisition of High Quality 3-D Data beneath Production Platforms*, Proceedings of SEG-89, Dallas, USA, October 29 - November 2, pages 621-623.

Durrani J., French W., and Comeaux L.B., (1987). *New Directions for Marine 3-D Surveys*, Proceedings of SEG-87, New Orleans, USA,, October 11-15, pages 177-180.

Egan M.S., and Kupoor S.J., (1990). *Shooting Direction: A 3-D Marine Survey Design Issue*, Proceedings of SEG-90, San Francisco, USA, September 23-27, pages 851-854.

Egeland G.S., (1982). *Array Shape Estimation*, Proceedings of OCEANS-82, Washington D. C., USA, pages 121-122.

Forssell B., (1991). *Radionavigation Systems*, Prentice Hall, ISBN 0-13-751058-6, pp 392.

Gao Y., Krakiwsky E.J., and Liu Z.W., (1992). *A New Algorithm for Filtering a Correlated Measurement Sequence*, Manuscripta Geodetica, Vol. 17(2).

Gelb A., (1974). *Applied Optimal Estimation*, MIT Press, pp 369.

Gerber K., (1988). *Seismic Streamer Positioning with Magnetic Compasses and Syledis*, Proceedings of HYDRO-88, London, UK, , pages 107-118.

Gikas V., and Herr W., (1994). *Positioning 3-D Seismic Surveys*, Houston, Texas, QC Tools Inc., I/O Functions - Design Specifications - Draft, Internal Report.

Gikas V., Cross P.A., and Assiama-Akuamoa A., (1995a). *A Rigorous and Integrated Approach to Hydrophone and Source Positioning during Multi-Streamer Offshore Seismic Exploration*, The Hydrographic Journal, Vol. 77, July 1995, pages 11-24.

Gikas V., Cross P.A., and Asiama-Akuamoa A., (1995b). *Development and Testing of Mathematical Algorithms for Source and Streamer Positioning during Marine Seismic Exploration*, Proceedings of the 4th International Congress of the Brazilian Geophysical Society and 1st Latin American Geophysical Conference, Rio de Janeiro, Brazil, August 20-24, pages 885-888.

Gikas V., and Cross P.A., (1996). *Reliability Assessment of Positioning for Seismic Acquisition and Processing at Sea*, Proceedings of EAGE-96, Amsterdam, Netherlands, June 3-7.

Gikas V., (1996). *A Data Snooping and Reliability Procedure for Use in Integration of Navigation Sensors in Offshore Oil Prospecting*, Proceedings of UKGA-96, Issue 7, University of Newcastle upon Tyne, UK, April 10-12.

Gilbert D., (1980). *Performance Characteristics of a Three-Dimensional Array Shape Estimation*, Analysis and Technology Inc., North Stonigton, Connecticut, 06359.

Hampson G., and Jakubowicz (1990). *Effects of Source and Receiver Motion on Seismic Data*, Proceedings of SEG-90, San Fransico, USA, September 23-27, pages 859-862.

Hofmann-Wellenhof B., Lichtenegger H., and Collins J., (1994). *GPS Theory and Practice*, Springer-Verlag, ISBN 3-211-82591-6, pp 355.

Homman J.C., and van-Ogtrop L.C., (1993). *Impact of Marine Positioning Errors on Processed Seismic Data*, Proceedings of EAGE-93, Workshop on Quality Assurance in Seismic Exploration, Stavanger, Norway, June 6.

Houston M.H., (1987). *Improving the Accuracy of Marine 3-D Seismic Surveys*, Ocean Industry, January 1987, pages 17-22.

Houtenbos A.P.E.M., (1982). *Prediction, Filtering and Smoothing of Offshore Navigation Data*, The Hydrographic Journal, Vol. 25, July 1982, pages 5-16.

Houtenbos A.P.E.M., (1989). *Integrated Processing of 3D Marine Seismic Positioning Data*, The Hydrographic Journal, Vol. 52, April 1989, pages 13-25.

Humbert K., Zinn N., and Rapatz P.J.V., (1993). *Real-Time Survey Networks in Marine Seismics*, Sea Technology, September 1993, pages 10-12.

Hume J., Monk D. J. and Ridyard D., (1994). *A Total Quality Management Approach to Assessment of the Distribution of 3D Seismic Data*, Proceedings of N.P.F. Biannual Geophysical Conference, Kristiansand, Norway, March 7.

Ingham A.E., (1975). *Sea Surveying*, John Wiley & Sons, London, UK.

Input/Output Inc., (1994). *I/O System Two Bottom Cable Acquisition System*, Prospectus PIB 49, U.S. Patent No. 4 750 156 (HPE) and 4 875 166 (Spectral Shaping Filter).

Jakubowicz H., (1981). *Locating Seismic Cables in Marine Surveys Using Cable Compasses*, Houston, Texas, Western Atlas International Inc., TD 81.07-14.01 WTR.

Jensen M.H.B., (1988). *Quality Assurance in Positioning Seismic Surveys*, The Hydrographic Journal, Vol. 48, April 1988, pages 25-36.

Jensen M.H.B., and Nicolai R., (1990). *Some Practical Examples of the Use of Standardised Statistical Testing of Positioning for Seismic and Engineering Surveys*, Proceedings of FIG XVIX Congress, Helsinki, Filand, June 10-19, pages 182-199.

Jensen M.H.B., (1992). *Quality Control for Differential GPS in Offshore Oil and Gas Exploration*, GPS World, September 1992.

Kailath T., (1968). *An innovations Approach to Least Squares Estimation Part I: Linear Filtering in Additive White Noise*, IEEE Trans. on AutomaticControl, Vol. 13(6), pages 646-655.

Kalman R.E., (1960). *A New Approach to Linear Filtering and Prediction Problems*, ASME Journal of Basic Engineering, Vol. 82, pages 34-35.

Kearey P., and Brooks M., (1994). *An Introduction to Geophysical Exploration*, Blackwell Scientific Publications, ISBN 0-632-02921-8, pp 254.

Kelland N.C., (1994). *Development in Integrated Underwater Acoustic Positioning*, The Hydrographic Journal, Vol. 71, January 1994, pages 19-27.

Kerr S.D., (1982). *Exploration Strategy*, Concepts and Techniques in Oil and Gas Exploration, Chapter Two, SEG, ISBN 0-931830-22-2, pages 13-42.

Kok J.J., (1984). *On Data Snooping and Multiple Outlier Testing*, NOAA Technical Report, NOS NGS 30, NOAA, Rockville, Md.

Krail P.M., and Brysk H., (1989). *The Shape of a Marine Streamer in a Cross Current*, GEOPHYSICS, Vol. 54, March 1989, pages 302-308.

Krail P.M., (1993). *Sub-Salt Acquisition with a Marine Vertical Cable*, Proceedings of SEG-93, Washington D. C., USA, September 26-30, pages 1376.

Lansley R.M., (1995). *The Question of Azimuths*, 4th International Congress of the Brazilian Geophysical Society and 1st Latin American Geophysical Conference, Rio de Janeiro, Brazil, August 20-24, pages 889-891.

Levin F.K., (1983). *The Effects of Streamer Feathering on Stacking*, GEOPHYSICS, Vol. 48, September 1983, pages 1165-1171.

Levin F.K., (1984). *The Effect of Binning on Data from a Feathered Streamer*, GEOPHYSICS, Vol. 49, August 1984, pages 1386-1389.

Levin F.K., (1996). *Specifying Source and Receiver Positioning Precision*, Proceedings of EAGE-96, Amsterdam, Netherlands, June 3-7.

Martens J.L.A.J.M., and Riemersma J.G., (1986). *Quality Assurance and Contract Surveys*, Proceedings of Colloquim IV, Canadian Petroleum Association, Lake Louise, Alberta, Canada, April 21-25.

McQuillin R., Bacon M., and Barclay W., (1984). *An Introduction to Seismic Interpretation*, Graham & Trotman, ISBN 0-86010-455-9, pp 287.

Merminod B., (1989). *The Use of Kalman Filters in GPS Navigation*, Kensington, NSW Australia, The University of New South Wales, Unisurv S35, pp 203.

Mertikas S., Wells D., and Leenhouts P., (1985). *Treatment of Navigational Accuracies: Proposal for the Future*, NAVIGATION: Journal of the Institute of Navigation, Vol. 32, Spring 1985, pages 68-84.

Mikhail E.M., (1976). *Observations and Least Squares*, IEP - A Dun Donnelley Publisher, ISBN 0-7002-2481-5, pp 497.

Mood A.M., and Graybill F.A., (1963). *Introduction to the Theory of Statistics*, McGraw-Hill, New York, pp 340.

Morgan J.G., Spradley L.H., Worthington G.A., and McClelland I.J., (1983). *SEG Standard Exchange Formats for Positional Data*, GEOPHYSICS, Vol. 48, pages 488-503.

Morgan J.G., (1983). *The Challenge of Precisely Positioning a 3D Seismic Survey*, NAVIGATION: Journal of the Institute of Navigation, Vol. 30, pages 261-272.

Morgan J.G., (1986). *Navigation and Positioning Report*, Ocean Industry, May 1986, pages 19-24.

Morgan J.G., (1991). *DGPS and Seismic Acquisition Workshop*, Chevron Exploration and Production Services Company, Company Report on the Workshop Held at Shell-Mex House, 22 May 1991.

Morgan J.G., (1992). *Positioning Challenges in Marine 3-D Seismic Surveys*, Ocean Industry, February 1992, pages 53-56.

Napier M., (1990). *Kalman Filter Algorithms*, Royal Institution of Chartered Surveyors/Hydrographic Society, Seminar on Kalman Filtering, University of Nottingham, UK, January 1990.

Nash J., and Ridyard D., (1987). *Real Time Marine 3-D Quality Control for Multiline Data Collection*, Proceedings of SEG-87, New Orleans, USA, October 11-15, pages 249-251.

Naylor R., (1990). *Positioning Requirements for Complex Multi-Vessel Seismic Acquisition*, The Hydrographic Journal, Vol. 58, October 1990, pages 25-32.

Nicolai R., (1988). *Statistics in Positioning Quality Control*, Proceedings of Hydro-88, The Hydrographic Society, London, UK, , pages 97-106.

Nicolai R., (1992). *UKOOA P2/91 Exchange Format for Raw Marine Positioning Data*, The Hydrographic Journal, Vol. 66, October 1992, pages 25-31.

Norton J.P., Hall M.A., and Court I.N., (1990). *Point Location Determination at Close to the Surface*, U. S. Patent No 4 912 682, 27 March 1990.

Owsley N.L., (1981). *Shape Estimation for a Flexible Underwater Cable*, Naval Underwater Systems Center, New London, Connecticut, 06320.

Paffenholz J., Monk D., and Fryar D., (1993). *Random and Systematic Errors: How Do They Affect Seismic Data Quality?*, Proceedings of SEG-93, Washington D. C., USA, September 26-30, pages 527-530.

PGS Exploration, (1996). Advertisement from First Break, EAGE, Vol.14(5), pages 209.

QC Tools Inc., (1994). *CENSUS User's Guide,* Version 4.02.

Quality Engineering and Survey Technology Ltd, (1995). *Quality Measures for Offshore DGPS,* Training Course for the Exploration Industry held at the University of Newcastle upon Tyne, January 24-26.

Rayson M., (1996). *Personal correspondence,* Quality Engineering and Survey Technology, Ltd.

Ridyard D., (1989). *Memo to Angus Jamieson JTS,* Houston, Texas, QC Tools Inc.

Ridyard D., (1993). *An Analysis of the Sensitivity of North Sea 3D Data to Measurable Quality Standards,* Proceedings of EAGE-93, Stavanger, Norway, Workshop W3, June 6.

Rigsby T.B., Cafarelli W.J., and O'neill D.J., (1987). *Bottom Cable Exploration in the Gulf of Mexico: A New Approach,* Proceedings of SEG-87, New Orleans, USA, October 11-15, pages 181-183.

Roberts W.D.S., (1993). *GPS Time Correlation and Its Implication for Precise Navigation,* PhD Thesis, Department of Surveying, University of Newcastle upon Tyne, pp 249.

Salzmann M., (1993). *Least Squares Filtering and Testing for Geodetic Navigation Applications,* Delft University of Technology, New Series, No.37, ISBN 90-6132-245-6, pp 209.

Salzmann M., (1995). *Real-Time Adaptation for Model Errors in Dynamic Systems,* Bulletin Goedesique, pages 81-91.

Schlumberger Geco-Prakla, (1996). Advertisement from the First Break, EAGE, Vol.14(5), cover page.

Sheriff R.E., (1981). *Structural Interpretation of Seismic Data,* A Continuing Education Course presented for the Dallas Geological Society, Education Course Notes Series #23, ISBN 0-89181-172-9.

Sheriff R.E., (1994). *Encyclopedic Dictionary of Exploration Geophysics,* Society of Exploration Geophysicists, ISBN 1-56080-018-6, pp 376.

Stigant J.P., (1989). *Tailbuoy Tracking for Twin Streamer 3D Surveys: A Case History*, Proceedings of OTC-89, Houston, USA, May 1-4, pages 289-297.

Stigant J.P., (1990). *Trust but Verify - A New Approach to Quality Control of Navigation and Binning during 3-D Marine Seismic Surveys*, Houston, Texas, Chevron Exploration and Production Services, Proprietary Technology - Contact CEPS Publications, Paper 49, 1990 ICGC.

Syntron Inc., (1995). *SYNTRAK 480-24TM Ocean Bottom Cable System.*

Talbot N.C., (1992). *Efficient Surveying under GPS Encryption*, Trimble Navigation, Sunnyvale, CA.

Tetley L., and Calcutt D., (1991). *Electronic Aids to Navigation: Position Fixing*, Edward Arnold, London, pp 386.

Teunissen P.J.G., and Knickmeyer E.H., (1988). *Nonlinearity and Least Squares*, CISM Journal ACSGC, Vol. 42, Winter 1988, pages 321-330.

Teunissen P.J.G., and Salzmann M.A., (1988). *Performance Analysis of Kalman Filters*, Delft University of Technology, pp 18.

Teunissen P.J.G., (1990a). *An Integrity and Quality Control Procedure for Use in Multi Sensor Integration*, Proceedings of ION GPS-90, Colorado Springs, USA, September 19-21, pages 513-522.

Teunissen P.J.G., (1990b). *Quality Control in Integrated Navigation Systems*, Proceedings of IEEE-90, Las Vegas, USA, March 20-23, pages 158-165.

Tiong-Ha S., (1990). *Multistreamer and Multisource Location: Acoustic and Laser Positioning Methods*, Proceedings of SEG-90, San Francisco, USA, September 23-27, pages 878-881.

Tompson E.H., (1969). *Introduction to the Algebra of Matrices with Some Applications*, Adam Hilger, pp 229.

UKOOA_SPC, (1986). *UKOOA P2/86 Raw Marine Positioning Data Exchange Type Format Version 1.1*, United Kingdom Offshore Operators Association Surveying and Positioning Committee.

UKOOA_SPC, (1994). *UKOOA P2/94 Raw Marine Positioning Data Exchange Type Format Version 1.1,* United Kingdom Offshore Operators Association Surveying and Positioning Committee.

UKOOA, (1994). *Guidelines for the Use of Differential GPS in Offshore Surveying,* UKOOA Publications, Issue 1, September 1994.

University of New Brunswick, (1987). *Digital Filtering,* Department of Surveying Engineering, SE 4131, Special Studies in Adjustments, September 1987.

University of New Brunswick, (1988). *Applications of Positioning,* Department of Surveying Engineering, SE 4131, Special Studies in Adjustments, September 1988.

van-Zeelst J., (1991). *Further Considerations in Positioning of 3D Seismic Surveys,* The Hydrographic Journal, Vol. 59, January 1991, pages 12-24.

Western Atlas International Inc., (1993). *TotalNet System,* Real-Time Total Network Positioning, Prospectus W94-234, Printed in USA JPC 3M.

Western Atlas International Inc., (1994a). *Sargas Differential GPS System,* Prospectus W94-234, Printed in USA JPC 3M.

Western Atlas International Inc., (1994b). *TotalNet System Operator's Manual,* Version 1.11G.

Western Atlas International Inc., (1996). Advertisement from The Leading Edge, SEG, Vol. 15(6), June 1996, pages 741-744.

Xin-Xiang J., (1995). *A Recursive Procedure for Computation and Quality Control of GPS Differential Corrections,* LGR-Series, Delft University of Technology, No. 8, ISBN 93-0928-2122, pp 84.

Zacks S., and Solomon H., (1975). *Lower Confidence Limits for the Impact Probability within a Circle in the normal Case,* Naval Research Logistics Quarterly, Vol. 22, pages 19-30.

Zeijlmaker L., (1990). *Streamer and Source Positioning during NA 3D Seismic Surveys in 1989,* Proceedings of the workshop of the Hydrographic Society (Netherlands Branch), 16th February 1990.

Zinn N., (1991). *Horizontal Midpoint (HMP) Accuracy in Marine Seismic*, Proceedings of SEG-91, Houston, USA.

Zinn N., and Rapatz P.J.V., (1993). *Positioning Networks in 3-D Marine Seismic*, Proceedings of OTC-93, Houston, USA, May 3-6.

Zinn N., and Humbert K., (1994). *The Cost of Reliability in Marine Seismic Networks*, Proceedings of EAGE-94, Viena, Austria, June 6-10.

Zinn N., and Rapatz P.J.V., (1995). *Reliability Analysis in Marine Seismic Networks*, The Hydrographic Journal, Vol. 76, April 1995, pages 11-18.

Zinn N., (1996). *Personal correspondence*, Western Atlas International Inc.

APPENDIX A

KALMAN FILTER NOTATIONAL CONVENTIONS

	Cross	Gelb	Merminod	Teunissen
Model Parameters				
Time index	i	k	i	k
Number of observations	m	l	m	m
Number of states	n	n	n	n
Vector of observations	l	z	l	y
Estimate of the state vector	x	x	$\dot{x} + \delta x$	x
Design matrix	A	H	A	A
Observed-computed vector	b	b	$\dot{v}$	y
Vector of residuals	v	-v	-v	-e
Covariance of observations	C_l	R	Q_{ll}	R
Transition matrix	M	Φ	Φ	Φ
Dynamic model noise	y	w	w	d
Covariance of dynamic model noise	C_y	D	Q_{ww}	Q
From time t_{i-1} to time t_i				
Predicted state	$\hat{x}_i(-)$	$\hat{x}_i(-)$	$\tilde{x}$	$\hat{x}_{i\|i-1}$
Predicted covariance	$C_{\hat{x}_i}(-)$	$P_i(-)$	$Q_{\tilde{x}\tilde{x}}$	$P_{i\|i-1}$
Filtered state	$\hat{x}_i(+)$	$\hat{x}_i(+)$	$\hat{x}$	$\hat{x}_{i\|i}$
Filtered covariance	$C_{\hat{x}_i}(+)$	$P_i(+)$	$Q_{\hat{x}\hat{x}}$	$P_{i\|i}$
Gain matrix	G_i	K_i	K	K_i
Covariance of the predicted residuals	$C_v(-)$	D_v	Q_{vv}	Q_v

	Cross	Gelb	Merminod	Teunissen
From time t_i to time t_{i-1}				
Smoothed state	$\hat{x}_{i-1}(s)$	$\hat{x}(t\|T)$	$\hat{\hat{x}}$	$\hat{x}_{i-1\|i}$
Smoothed covariance	$C_{\hat{x}_{i-1}}(s)$	$P(t\|T)$	$Q_{\hat{\hat{x}}\hat{\hat{x}}}$	$P_{i-1\|i}$
Smoothing matrix	S_i		J	J

APPENDIX B

STATISTICAL TESTING OF THE KALMAN FILTER

The following discussion regarding the statistical testing phases associated to the DIA procedures follows Salzmann (1993), Salzmann (1995), and Xiang (1995), and the reader is referred to these texts for further details.

As it is mentioned in Section 4.3 two kinds of test statistics can be considered. Local model tests that are carried out based on the information of a particular epoch, and the global tests using information of a number of epochs. Here, only the local model tests are discussed for the detection and identification steps.

B.1 Detection

The objective of the detection phase of the DIA procedure is to test the overall validity of the mathematical model under the null hypothesis H_o and it is carried out by the so-called Local Overall Model (LOM) test statistic. The two alternative hypotheses to detect model error at epoch t_i are (Xiang, 1995; Roberts and Cross, 1993)

$$\begin{aligned} H_0&: \quad \hat{v}_i \sim N\left(0,\ C\hat{v}_i(-)\right) \\ H_A&: \quad \hat{v}_i \sim N\left(K_i\nabla_i,\ C\hat{v}_i(-)\right) \end{aligned} \qquad \text{B.1}$$

where

K	is a m_i-by-b matrix specifying the type of error that is being sought (assumed known)
∇	is a b-by-1 vector specifying the whereabouts of the error (unknown)
m_i	is the degrees of freedom (the number of observations) at epoch t_i

The size of b depends on the type of model error within the alternative hypothesis, i.e. whether or not the assumed bias is of the same size at every observation and which

observations are biased, and it ranges from 1 to m_i. If b is taken equal to one, which is the one-dimensional case, the vector ∇ becomes scalar and the matrix K becomes a vector denoted by e.

The uniformly-most-powerful-invariant (UMPI) test statistic for detecting model errors in the null hypothesis is given by

$$T_i = v_i(-)^T C v_i(-)^{-1} v_i(-) \qquad \text{B.2}$$

$$T_{LOM_i} = T/m_i \qquad \text{B.3}$$

and consequently the UMPI test for testing H_0 against H_A reads reject H_0 in favour of H_A if

$$T_{LOM_i} \geq F_\alpha(m_i, \infty, 0) \qquad \text{B.4}$$

where $F_\alpha(m_i, \infty, 0)$ is the α percentile central F-distribution value with m_i and ∞ degrees of freedom.

B.2 Identification

After a misspecification has been detected various alternative hypotheses should be assumed in order to identify the bias(es). This specification is probably the most difficult task in the process of quality control and depends on the experience and level of knowledge of the measurement and dynamic models. In the case in which only errors in the measurement model occur the predicted residuals are used to determine the observation with the most likely model error. This uses the data snooping Local Slippage (LS) test statistic (Xiang, 1995; Roberts and Cross, 1993)

$$t_{LS_i} = \frac{e^T C \hat{v}_i(-)^{-1} \hat{v}_i(-)}{\sqrt{e^T C \hat{v}_i(-)^{-1} e}} \qquad \text{B.5}$$

The Local Slippage test is carried out for every observation. The most likely bias is said to have occurred at the observation for which $\left|t_{LS_i}\right|$ becomes maximum and hence this observation is rejected. Thereafter the LOM test statistic is computed to detect for any other outliers remaining in the data. These tests are repeated recursively until no further blunders are detected.

B.3 Adaptation

Finally, after identification of the most likely hypothesis, adaptation of the filter is required in order to eliminate the effect of biases in the data on the filter estimates. In order to compute the effect on the filter estimates it is necessary to know the size of the biases in the observations ∇. When only a single error is identified in the observations, from Equation 4.14 it can be concluded that (Xiang, 1995; Salzmann, 1995)

$$\hat{\nabla}_i = \left(e_i^T C_{v_i}^{-1} e_i\right)^{-1} e_i^T C_{v_i}^{-1} e_i \qquad \text{B.6}$$

The adapted filtered state at epoch i can be written as

$$\hat{x}_i^{\alpha} = \hat{x}_i^0 - \Delta x_i \qquad \text{B.7}$$

where

$\hat{x}_i^{\alpha}$ is the state vector solution associated to H_0
x_i^0 is the state vector solution associated to H_A

upon substituting Equation 4.21 into B.7 the filtered state becomes

$$\hat{x}_i^{\alpha} = \hat{x}_i^0 - K_i e_i \nabla_i \qquad \text{B.8}$$

APPENDIX C

DESIGN MATRIX COMPUTATIONS

As stated in Section 5.3.3, due to the complex nature of most of the observation equations involved in the system, the design matrix is obtained numerically. The procedure for an obsesrvation l_i with raw (non-linear) observation equation

$$F_i(x) = l_i + v_i \qquad \text{C.1}$$

is as follows. The A_{ik} element of the design matrix A for the i-observation for the k-element of the state vector x, is defined by

$$A_{ik} = \frac{\partial F_i(x)}{\partial x_k} \qquad \text{C.2}$$

The value of A_{ik} at epoch j obtained in a numerical way is given by the equation

$$A_{ik} = \frac{F_i^{\circ}(x + \delta x_k)\big|_j - F_i^{\circ}(x)\big|_j}{\delta x_k} \qquad \text{C.3}$$

where

$F_i^{\circ}(x)\big\|_j$	is the computed value of $F_i(x)$ at time j
$F_i^{\circ}(x + \delta x_k)\big\|_j$	is the computed value of $F_i(x + \delta x_k)$ at time j
δx_k	represents a small change in the k-element of the state vector x

The most common observation types involved in a modern marine seismic survey are listed in Section 5.3.2. For these types of data a number of observation equations can be formed depending on the subsystem (vessel, float, streamer) types on which the measurement devices are fixed. A pattern of the design matrix for all possible combinations is given in the following table. Its full elements are denoted by a cross sign - all other elements are equal to zero.

OBSERVATIONS	UNKNOWNS	VESSEL						FLOAT - i						FLOAT - j						STREAMER - i							STREAMER - j					
		φ	λ	$\dot{\varphi}$	$\dot{\lambda}$	c		X	Y	$\dot{X}$	$\dot{Y}$			X	Y	$\dot{X}$	$\dot{Y}$			X	Y	$\dot{X}$	$\dot{Y}$	α	c_t		X	Y	$\dot{X}$	$\dot{Y}$	α	c_t
VESSEL OBS.	vessel latitude	+																														
	vessel longitude		+																													
	vessel gyro		+		+	+	+																									
REDUCED RANGES	vessel → float	+		+	+	+	+	+	+																							
	vessel → streamer	+		+	+	+	+													+	+			+	+		+	+				+
	float i → float j							+	+					+	+																	
	float → streamer							+	+											+	+			+	+		+	+				+
	streamer i → streamer i																			+	+			+	+		+	+				+
	streamer i → streamer j																			+	+			+	+		+	+				+
REDUCED DIRECTIONS	vessel → float	+		+	+	+																										
	vessel → streamer	+		+	+	+														+	+			+	+		+	+				+
	float i → float j							+	+					+	+																	
	float → streamer							+	+											+	+			+	+		+	+				+
	streamer i → streamer i																			+	+			+	+		+	+				+
	streamer i → streamer j																			+	+			+	+		+	+				+
COMPASS OBS.	compass azimuth																															
TAILBUOY OBS.	tailbuoy latitude	+																			+											
	tailbuoy longitude		+																	+							+					

APPENDIX D

GENERAL INPUT STRUCTURE AND FUNCTION DESIGN SPECIFICATIONS FOR USE BY THE NCL_NET POSITIONING ALGORITHM DURING MULTI-VESSEL SEISMIC OPERATIONS

D.1 INTRODUCTION

This section is an introductory design specification proposal developed to provide the general layout of the types of structures and function declarations required to initiate the mathematical processes of the NCL_NET positioning algorithm. As mentioned in Chapter Six the input information which is required to implement the proposed algorithm is split into three areas; control, state vector and observations.

- The control area is meant to extract, standardize in structure and transfer to the math part of the computations, all header information described in the UKOOA raw positioning data formats P2/86 and P2/91 (or from other exchange formats).
- The state area consists of the types of structures required to assign values (initial or from a previous epoch solution) for the network unknowns as defined in NCL_NET algorithm (see Section 5.3.1).
- The observation area contains the types of structures used to extract, standardize in structure and transfer to the math part of the computations all measurement data records described in the UKOOA raw positioning data formats P2/86 and P2/91 or from other exchange formats.

This appendix is divided into two parts. In the first part the basic structure declarations for the three areas discussed above are given while, in the latter, the basic function definitions used to activate the filter processes are presented. In fact, the algorithm described in Chapter Five is extended in this discussion to multi-vessel configurations

and therefore, this development specification is assumed to be suitable for multi-vessel operations as well.

It should be stressed, however, that the following is only a draft specification that aims at providing the basic idea of the standardization of the raw positioning data and the state vector for use by the generalized NCL_NET algorithm. It is likely, therefore, that these definitions may be change at the implementation stage of this work but, it is believed, always adhering to the philosophy presented here.

D.2 STRUCTURE DEFINITIONS

D.2.1 Control Information

As set of structures are defined to organize the information which is held under this area. These are summarized as follows.

A. General and Surveying Definition Information - Following the UKOOA standards (Nicolai, 1992) a set of structures is formed per seismic line to provide all requisite information needed to define the survey parameters and other relevant information. More specifically a structure of type MODEL is defined.

MODEL structure

```
typedef struct
    {
        PARTICIPANTS INFO participants info;   /* structure of type PARTICIPANTS INFO */
        AREA INFO area info;                   /* structure of type AREA INFO */
        GEODETIC INFO geodetic info;           /* structure of type GEODETIC INFO */
        PROJECTION INFO projection info;       /* structure of type PROJECTION INFO */
        RELEVANT INFO relevant info ;          /* structure of type RELEVANT INFO */
    } MODEL;
```

- The structure of type PARTICIPANTS INFO consists all the information related to the client, the geophysical contractor, processing contractor, etc.
- The structure of type AREA INFO contains all relevant information regarding the survey area.
- The structure of type GEODETIC INFO includes datum information and all parameters needed for datum transformations.
- The structure PROJECTION INFO contains the name of projection used, origin of grid, origin of latitude, scale factor, etc.
- The structure RELEVANT INFO contains information such as number of systems (vessels), maximum number of observations, etc.

At the implementation stage the MODEL structure may extend to include other additional information parameters.

B. Positioning Information - This part attempts to determine all the requisite parameters needed to define the geometry configuration of the seismic survey systems. It is very likely that the final operational software requires this information prior to handling the event data as many other positioning processing software (Nicolai, 1992). For multi-vessel operations the geometry configuration is conceptually split into three types of layers; system, body, device and the body layer into vessel, float and streamer. For each one of those entities one structure is defined. More specifically

B1. For each system (vessel with floats and streamers) involved in the survey one structure of type SYSTEM is defined

SYSTEM structure

```
typedef struct
    {
        int  ves_type;          /*  pilot vessel= 0, slave vessel= 1  */
        DEV_DEF  mydev_def;     /*  structure of type DEV_DEF  */
        int  float_ num;        /*  number of floats  */
        int  str_num;           /*  number of streamers  */
        int  tb_num;            /*  number of tailbuoys  */
        int  gun_num;           /*  number of guns  */
        int  hyph_num;          /*  number of hydrophones  */
    } SYSTEM;
```

Example:
For a configuration of two systems an array of structures of type SYSTEM is defined

```
SYSTEM  mysys[1];
```

For instance, if the first system is assumed to involve two floats, three streamers and ten acoustic devices this is declared by the following structure elements

```
mysys[0].float_num= 2;    mysys[0].str_num= 3;      mysys[0].mydev_def.acoustic_num= 10;
```

B2. For each vessel, float and streamer one structure of type VESSEL, FLOAT, STREAMER is defined respectively.

VESSEL structure

```
typedef struct
    {
        int sys_num;            /*  first system= 1, second system=2, ...  */
        DEV_DEF  mydev_def;     /*  structure of type DEV_DEF */
        double  x;              /*  nominal x-coordinate of this system vessel with respect to the
                                pilot vessel fixed coordinate system  */
        double  y;              /*  nominal y-coordinate of this system vessel with respect to the
                                pilot vessel fixed coordinate system  */
```

```
        double z;                /*  nominal z-coordinate of this system vessel with respect to the
                                 pilot vessel fixed coordinate system */
    } VESSEL;

/*-------------------------------------------------------------------------*/
```

FLOAT structure

```
typedef struct
    {
        int sys_num;             /*  first system= 1, second system=2, ... */
        DEV_DEF  mydev_def;      /*  structure of type DEV_DEF */
        int  gun_num;            /*  number of guns (energy sources) */
        double  x;               /* nominal x-coordinate of the float centre with respect to its system
                                 vessel fixed coordinate system */
        double  y;               /* nominal y-coordinate of the float centre with respect to its system
                                 vessel fixed coordinate system */
        double  z;               /* nominal z-coordinate of the float centre with respect to its vessel
                                 fixed coordinate system */
    } FLOAT;

/*-------------------------------------------------------------------------*/
```

STREAMER structure

```
typedef struct
    {
        int sys_num;             /*  first system= 1, second system=2, ... */
        DEV_DEF  mydev_def;      /*  structure of type DEV_DEF */
        int  tb;                 /*  active tailbuoy= 0,  tailbuoy disable= -1 */
        int  hyph_num;           /*  number of hydrophones */
        int  str_coef_num;       /*  number of streamer model parameters (polynomial order) */
        double  x;               /* nominal x-coordinate of the streamer reference point with respect
                                 to its system vessel fixed coordinate system */
        double  y;               /* nominal y-coordinate of the streamer reference point with respect
                                 to its system vessel fixed coordinate system */
        double  z;               /* nominal z-coordinate of the streamer reference point with respect
                                 to its vessel fixed coordinate system */
    } STREAMER;
```

B3. To perform NCL_NET algorithm three types of devices should be considered; measurement devices, guns (energy sources) and, hydrophones (seismic receivers). For each type of these devices an array of structures of type DEVICE, GUN, HYDROPHONE is formed respectively, depending on the number of devices in each category. These are

DEVICE structure

```
typedef struct
    {
        int  system_num;         /*  system number */
        int  body_type;          /*  body type:  vessel= 1, float= 2, streamer= 3 */
        int  body_num;           /*  body number */
        int  dev_type;           /*  device type:  acoustic= 1, laser= 2, compass= 3, gps= 4, syledis=
                                 5, gyrocompass= 6 */
```

```
        double  x;          /*  nominal x-coordinate with respect to this device body coordinate
                            system  */
        double  y;          /*  nominal y-coordinate with respect to this device body coordinate
                            system  */
        double  z;          /* nominal z-coordinate with respect to this device vessel coordinate
                            system  */
    } DEVICE;
```

Example:
For a configuration consisting of 30 measurement devices an array of structures DEVICE is defined

```
DEVICE  mydev[29];
```

The structure elements for the third device will be

```
mydev[2].system_num
mydev[2].body_type
mydev[2].body_num
mydev[2].dev_type
mydev[2].x
mydev[2].y
mydev[2].z
```

```
/*-------------------------------------------------------------------------*/
```

GUN structure

```
typedef struct
    {
        int  system_num;    /*  system number  */
        int  body_num;      /*  body number  */
        double  x;          /*  nominal x-coordinate with respect to its float fixed coordinate
                            system */
        double  y;          /*  nominal y-coordinate with respect to its float fixed coordinate
                            system  */
        double  z;          /*  nominal z-coordinate with respect to the vessel fixed coordinate
                            system  */
    } GUN;
```

```
/*-------------------------------------------------------------------------*/
```

HYDROPHONE structure

```
typedef struct
    {
        int  system_num;    /*  system number  */
        int  body_num;      /*  body number  */
        double  offset;     /*  nominal offset from the streamer reference point  */
        double  z;          /*  nominal z-coordinate with respect to the vessel fixed coordinate
                            system  */
    } HYDROPHONE;
```

C. Network Information - An array of structures is formed in order to define the observation connecting nodes involved within the network. This information is used to assign all necessary attributes for every observation which are necessary at the

mathematical computations stage. In the case of compass or absolute position observations the structure to_dev of type DEVICE is not used. The size of this array is equal to the total number of observations.

NETWORK structure

```
typedef struct
    {
        int obs_type;           /* observation type */
        DEVICE from_dev;        /* structure to define the attributes of the device 'from' */
        DEVICE to_dev;          /* structure to define the attributes of the device 'to' */
    } NETWORK;
```

Four observation types are defined in NCL_NET. These include; slope ranges, directions (between two nodes), azimuths (single node) and absolute positions. It is possible that these types might split into sub-types such as acoustic and laser ranges etc. It should be mentioned that, for all other data such as; pseudo-ranges, carrier phase, range differences, angles, time, velocities, it is assumed that after they are reduced, they fall in one of the above mentioned observation types.

Example:
If the fifth observation is an acoustically observed range between the first device on the first streamer of the first system and the second device of the third streamer of also the first system, this can be expressed using a structure mynet of type NETWORK as

```
mynet[4].obs_type= 1;

mynet[4].from_dev.system_num= 0;
mynet[4].from_dev.body_type= 3;
mynet[4].from_dev.body_num= 0;
mynet[4].from_dev.dev_type= 1;
mynet[4].from_dev.x= ?
mynet[4].from_dev.y= ?
mynet[4].from_dev.z= ?

mynet[4].to_dev.system_num= 0;
mynet[4].to_dev.body_type= 3;
mynet[4].to_dev.body_num= 2;
mynet[4].to_dev.dev_type= 1;
mynet[4].to_dev.x= ?
mynet[4].to_dev.y= ?
mynet[4].to_dev.z= ?
```

Previously a structure of type DEV_DEF was used. This is defined as follows

DEV_DEF structure

```
typedef struct
    {
        int acoustic_num;       /* number of acoustic devices */
        int laser_num;          /* number of laser devices */
        int compass_num;        /* number of compass devices */
        int gps_num;            /* number of gps devices */
        int syledis_num;        /* number of syledis devices */
        int gyrocompass_num;    /* number of gyrocompass devices (on the vessel) */
    } DEV_DEF
```

D.2.2 State Vector Information

The state vector definition, detailed in Section 5.3.1, for one vessel deployment is extended here for multi-vessel configurations. The position of the NRP of the pilot or master vessel is considered in geodetic coordinates while, the positions of the NRP's of all other (slave) vessels are computed with respect to the local topographic system which has its origin at the NRP of the pilot vessel. Therefore, for the pilot vessel and for each one slave vessel, float and streamer is formed one structure of the type VES_PLT_UKWN, VES_UKWN, FLOAT_UKWN and STR_UKWN respectively.

Hence, the state vector is defined as a dynamic array the size of which is dependent on the number of systems and bodies defined in the MODEL and SYSTEM structures.

VES_PLT_UKWN structure

```
typedef struct
    {
        double lat;             /* pilot vessel ellipsoidal latitude of the NRP */
        double lon;             /* pilot vessel ellipsoidal longitude of the NRP */
        double lat_v;           /* pilot vessel ellipsoidal latitude velocity of the NRP */
        double lon_v;           /* pilot vessel ellipsoidal longitude velocity of the NRP */
        double crab;            /* pilot vessel crab angle */
    } VES_PLT_UKWN;
```

```
/*-------------------------------------------------------------------------*/
```

VES_UKWN structure

```
typedef struct
    {
        int ves_num;            /* vessel number */
        double east;            /* vessel easting with respect to the pilot vessel NRP */
```

```
        double  north;          /*  vessel northing with respect to the pilot vessel NRP  */
        double  east_v;         /*  vessel easting velocity with respect to the pilot vessel NRP  */
        double  north_v;        /*  vessel easting velocity with respect to the pilot vessel NRP  */
        double  crab;           /*  vessel crab angle  */
    } VES_UKWN;
```

FLOAT_UKWN structure

```
typedef struct
    {
        double  east;           /*  easting of the centre of float  */
        double  north;          /*  northing of the centre of float  */
        double  east_v;         /*  easting velocity of the centre of float  */
        double  north_v;        /*  northing velocity of the centre of float  */
    } FLOAT_UKWN;

/*-------------------------------------------------------------------------*/
```

STR_UKWN structure

```
typedef struct
    {
        double  east;           /*  easting of the reference point of streamer  */
        double  north;          /*  northing of the reference point of streamer  */
        double  east_v;         /*  easting velocity of the reference point of streamer  */
        double  north_v;        /*  northing velocity of the reference point of streamer  */
        double  dir_angle;      /*  streamer base-line direction angle  */
        double  coef[sc];       /*  streamer model coefficients  */
    } STR_UKWN;
```

D.2.3 Observations

For every time event and for every observation one structure has to be formed. The elements of this structure are defined as follows

OBS structure

```
typedef struct
    {
        TIME time;              /*  structure of type TIME  */
        NETWORK  net;           /*  structure of type NETWORK  */
        double  val;            /*  observation value  */
        double  weight;         /*  observation weight  */
    } OBS;
```

Example:
If the tenth observation is an acoustic range made from the vessel hull the 'from' node can be described using a structure myobs of type OBS as

```
myobs[9].mynet.from_dev.dev_type= 1;
```

TIME structure

```
typedef struct
    {
        int hour;          /* hours (GMT) */
        int min;           /* minutes (GMT) */
        int sec;           /* seconds (GMT) */
    } TIME;
```

The year and day of year information is held in the MODEL structure to minimize memory requirements.

D.3 GENERAL INPUT FUNCTION DECLARATIONS TO INITIATE NCL_NET MATHEMATICAL COMPUTATIONS

In this section the function declarations required to pass the input information to the mathematical computations are given. At this stage, five general functions are defined to carry out this task. The input arguments to these functions are the structures defined in the control, state vector and observation steps discussed earlier. In the following paragraphs their declaration statements are given

Function Name : set_control

Purpose : To pass in the control information into the math computation part.

Input :
: MODEL *mymod - pointer to a structure of type MODEL
: SYSTEM *mysys - pointer to an array of structures of type SYSTEM
: VESSEL *myves - pointer to an array of structures of type VESSEL
: FLOAT *myfloat - pointer to an array of structures of type FLOAT
: STREAMER *mystr - pointer to an array of structures of type STREAMER
: DEVICE *mydev - pointer to an array of structures of type DEVICE
: GUN *mygun - pointer to an array of structures of type GUN
: HYDROPHONE *myhp - pointer to an array of structures of type HYDROPHONE
: DEV_DEF *mydev_def - pointer to an array of structures of type DEV_DEF

Output : Error code
-1= Number of observations exceeds max_obs_num
-2= Number of devices exceeds max_num_dev
-3= Number of vessels exceeds max_ves_num
-4= Number of floats exceeds max_float_num
-5= Number of streamers exceeds max_str_num
-6= Number of guns exceeds max_gun_num
-7= Number of hydrophones exceeds max_hp_num

Declaration : long set_control (MODEL *mymod, SYSTEM *mysys, VESSEL *myves, FLOAT *myfloat, STREAMER *mystr, DEVICE *mydev, GUN *mygun, HYDROPHONE *myhp, DEV_DEF *mydev_def);

/*----------*/

Function Name : set_network

Purpose : This function describes the observation geometry (observation connecting nodes).

Input :
: long obs_num - total number of observations
: NETWORK *mynet - pointer to an array of structures of type NETWORK

Output : Error code
0= successful
-1= Cannot allocate memory to save table

Declaration : long set_net (long obs_num, NETWORK *mynet);

Function Name : set_state

Purpose : To compute the state vector size and return to the caller the state vector size and a dynamic array containing the state vector elements.

Input
: VES_PLT_UKWN *myvpu - a pointer to a structure VES_PLT_UKWN
: VES_UKWN *myvu - a pointer to an array of structures VES_UKWN
: FLOAT_UKWN *myfu - a pointer to an array of structures FLOAT_UKW
: STR_UKWN *mysu - a pointer to an array of structures STR_UKWN
: SYSTEM *mysys - a pointer to an array of structures SYSTEM

Output
: long *st_vec_size - a pointer to long variable that contains the state vector size in number of elements
: double *state_vec - a pointer to an array that contains the state vector elements

: Error code 0= successful
-1= Cannot allocate memory to save table

Declaration : long set_state (VES_PLT_UKWN *myvpu, VES_UKWN *myvu, FLOAT_UKWN *myfu, STR_UKWN *mysu, SYSTEM *mysys, long *st_vec_size, double *state_vec);

/*----------*/

Function Name : calc_net

Purpose : To provide the mathematical part the information required for every observation.

Input
: long shot_no - shotpoint number counter
: double *state_vec - a pointer to the state vector array
: OBS *myobs - a pointer to an array of structures OBS
: SYSTEM *mysys - a pointer to an array of structures SYSTEM

Output
: double *state_vec - a pointer to the state vector array

: Error code 0= successful
-1= Cannot allocate memory to save table

Declaration : long set_state (long shot_no, double *state_vec, OBS *myobs, SYSTEM *mysys);

/*----------*/

Function Name : done_process ( )

Purpose : To inform the math computation part that all the events have been processed, so that the math computation can perform clean up such as free memory and close files etc.

Input : None

Output
: double *state_vec - a pointer to the state vector array
: double *state_cov_mat - a pointer to the state vector matrix

: Error code 0= successful

Declaration : long done_process ( );

APPENDIX E

DESCRIPTION OF THE RAW MARINE POSITIONING DATA

E.1 GABON 3D SEISMIC SURVEY

E.1.1 General Description

A. Job Information

Client	: Elf Gabon
Geophysical contractor	: GECO-Prakla Inc., Energy Innovations Inc.
Vessel name	: GECO Searcher
Start of line	: 24 November 1992

B. Area and Grid Definition

Area name	: 3D Palomide/Mandaros
Datum	: m' poraloko
Semimajor ellipsoidal axis	: 6378249.2 metre
Inverse flattering	: 293.4660
Magnetic declination	: -5.98 degrees
Gyro correction	: -0.40 degrees
Line number	: 0315
Line direction	: 58.0 degrees
Grid cells	: 25.0 metre cross-line, 6.25 metre in-line
Shotpoint interval	: 18.75 metre

C. Survey Configuration Information

Number of vessels	: One
Number of seismic sources	: Two
Source separation	: 50.0 metre
Number of streamers	: Three
Streamer length	: 3153 metre
Streamer separation	: 100 metre
Receiver group interval	: 12.45 metre

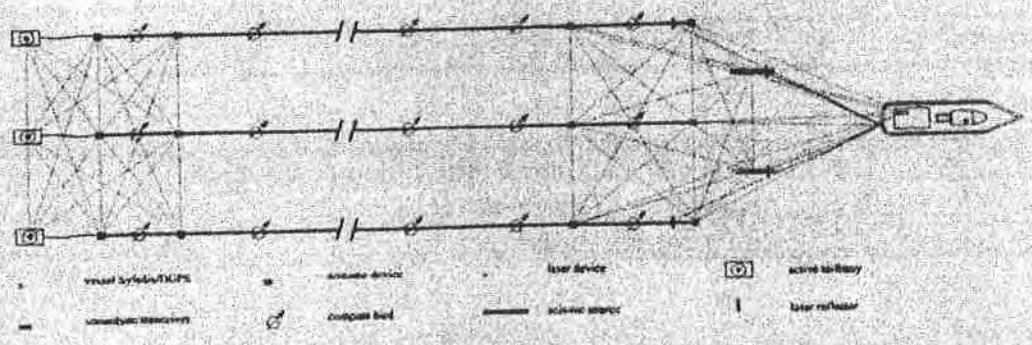

Figure E.1 Geometry configuration sketch, Gabon (1992)

E.1.2 Navigation Sensors' Information

Primary navigation was accomplished with both Syledis and DGPS. In addition, active components on the vessel included an acoustic pinger, an echo sounder, and a laser device which was fixed at the stern of the vessel. The Syledis positioning was provided by five stations situated along the coast of Gabon.

All three tailbuoys were equipped with Syledis radiopositioning receivers as well as acoustic pods. Front and tail-end positioning utilised an acoustic network consisting of SONARDYNE acoustic units. To assist the computation of streamer orientation, 13 depth controller/compass (DigiCOURSE 396 & 5011) units were deployed at each streamer. In summary, the survey configuration consisted of the following of navigation sensors

- Vessel Syledis, DGPS, gyro, acoustic pinger, echo sounder and a laser device
- 8 SONARDYNE acoustic transceivers at the front-end network
- 7 SONARDYNE acoustic transceivers at the tail-end network
- 4 laser reflectors
- 13 compass birds at every streamer
- Tailbuoy Syledis and acoustic pods

E.1.2.1 Navigation Sensor Offsets

The offset values shown in the following tables correspond to the vessel, source, (and other float), and streamer coordinate systems which defined in Figures E.2 and 5.2.

Table E1. Vessel and tailbuoy positioning sensors, Gabon 1992

Navigation sensor	Reference point	*x* / offset	*y*	*z* / height
vessel Syledis	NRP	-0.8	0.0	23.7
vessel DGPS	NRP	0.0	-0.8	20.0
stbd tailbuoy Syledis	stbd str. ref. point	3077.9	--	1.3
centre t/b Syledis	centre str. ref. point	3076.1	--	1.3
port t/b Syledis	port str. ref. point	3076.9	--	1.3

Table E2. Front-end SONARDYNE TRINAV acoustic network sensors, Gabon 1992

Acoustic device	Reference point	*x* / offset	*y*	*z* / height
acoustic pinger B1T1	NRP	0.0	-1.0	-6.5
acoustic transceiver G1T1	stbd source centre	0.0	-12.5	-7.8
acoustic transceiver G2T1	port source centre	0.0	-12.5	-7.8

Acoustic device (contd.)	Reference point	*x* / offset	*y*	*z* / height
acoustic transceiver S1T1	stbd str. ref. point	-114.1	--	-6.0
acoustic transceiver S1T2	stbd str. ref. point	71.2	--	-6.0
acoustic transceiver S2T1	centre str. ref. point	-114.0	--	-6.0
acoustic transceiver S2T2	centre str. ref. point	71.2	--	-6.0
acoustic transceiver S3T1	port str. ref. point	-112.0	--	-6.0
acoustic transceiver S3T2	port str. ref. point	71.2	--	-6.0

Table E3. Tail-end SONARDYNE TRINAV acoustic network sensors, Gabon 1992

Acoustic device	Reference point	*x* / offset	*y*	*z* / height
acoustic transceiver S1T4	stbd str. ref. point	2959.6	--	-6.0
acoustic transceiver F1T1	stbd str. ref. point	3073.7	--	-4.8
acoustic transceiver S2T3	centre str. ref. point	2859.6	--	-6.0
acoustic transceiver S2T4	centre str. ref. point	2959.6	--	-6.0
acoustic transceiver F2T1	centre str. ref. point	3071.9	--	-4.8
acoustic transceiver S3T4	port str. ref. point	2959.6	--	-6.0
acoustic transceiver F3T1	port str. ref. point	3072.7	--	-4.8

Table E4. Front-end laser network sensors, Gabon 1992

Laser device	Reference point	*x* / offset	*y*	*z* / height
laser sensor B1R1	NRP	0.8	-50.5	8.0
laser reflector G1H1	stbd source centre	0.0	-9.6	0.6
laser reflector G2H2	port source centre	0.0	-9.6	0.6
laser reflector S1H1	stbd str. ref. point	-113.1	--	0.8
laser reflector S3H1	port str. ref. point	-111.0	--	0.8

Table E5. Compass Birds - starboard streamer, Gabon 1992

Compass device	Reference point	*x* / offset	*y*	*z* / height
7531 / 1	stbd str. ref. point	-62.3	--	-6.0
6018 / 2	stbd str. ref. point	21.5	--	-6.0
7330 / 3	stbd str. ref. point	220.7	--	-6.0
3512 / 4	stbd str. ref. point	519.7	--	-6.0
7225 / 5	stbd str. ref. point	818.2	--	-6.0
7549 / 6	stbd str. ref. point	1117.2	--	-6.0
6562 / 7	stbd str. ref. point	1415.8	--	-6.0
7563 / 8	stbd str. ref. point	1714.8	--	-6.0
7617 / 9	stbd str. ref. point	2013.3	--	-6.0
7055 / 10	stbd str. ref. point	2312.3	--	-6.0
7529 / 11	stbd str. ref. point	2610.8	--	-6.0
7016 / 12	stbd str. ref. point	2909.9	--	-6.0
5983 / 13	stbd str. ref. point	2989.5	--	-6.0

TableE6. Compass Birds - centre streamer, Gabon 1992

Compass device	Reference point	*x* / offset	*y*	*z* / height
5553 / 1	centre str. ref. point	-62.2	--	-6.0
7039 / 2	centre str. ref. point	21.5	--	-6.0
7558 / 3	centre str. ref. point	220.7	--	-6.0
3233 / 4	centre str. ref. point	519.7	--	-6.0
6132 / 5	centre str. ref. point	818.2	--	-6.0
4002 / 6	centre str. ref. point	1117.2	--	-6.0
7312 / 7	centre str. ref. point	1415.8	--	-6.0
4425 / 8	centre str. ref. point	1714.8	--	-6.0
3308 / 9	centre str. ref. point	2013.3	--	-6.0
3291 / 10	centre str. ref. point	2312.3	--	-6.0
7543 / 11	centre str. ref. point	2610.8	--	-6.0
3691 / 12	centre str. ref. point	2909.9	--	-6.0
4417 / 13	centre str. ref. point	2989.5	--	-6.0

Table E7. Compass Birds - port streamer, Gabon 1992

Compass device	Reference point	*x* / offset	*y*	*z* / height
7027 / 1	port str. ref. point	-62.3	--	-6.0
5556 / 2	port str. ref. point	21.5	--	-6.0
7607 / 3	port str. ref. point	220.7	--	-6.0
7072 / 4	port str. ref. point	519.7	--	-6.0
3005 / 5	port str. ref. point	818.2	--	-6.0
6863 / 6	port str. ref. point	1117.2	--	-6.0
3367 / 7	port str. ref. point	1415.8	--	-6.0
6230 / 8	port str. ref. point	1714.8	--	-6.0
4317 / 9	port str. ref. point	2013.3	--	-6.0
6212 / 10	port str. ref. point	2312.3	--	-6.0
4025 / 11	port str. ref. point	2610.8	--	-6.0
8094 / 12	port str. ref. point	2909.9	--	-6.0
7539 / 13	port str. ref. point	2989.5	--	-6.0

E.1.2.2 Acoustic and Laser Observables Definition

At the front-end of the streamers a total number of 45 acoustic ranges were measured while 29 acoustic ranges were observed at the tail network. In addition to this, 4 laser ranges and 7 directions from the vessel to energy sources and streamers we observed. The observation connecting nodes are given in the following tables.

Table E8. Front-end acoustic and laser ranges network, Gabon 1992

From node	To node	Range	From node	To node	Range
B1T1	G1T1	1	S1T1	S3T1	26
B1T1	G2T2	2	S1T1	S3T2	27
B1T1	S1T1	3	S1T2	S1T1	28
B1T1	S1T2	4	S1T2	S2T1	29
B1T1	S2T1	5	S1T2	S2T2	30
B1T1	S2T2	6	S1T2	S3T2	31
B1T1	S3T1	7	S2T1	S1T1	32
B1T1	S3T2	8	S2T1	S2T2	33
G1T1	G2T2	9	S2T1	S3T1	34
G1T1	S1T1	10	S2T2	S1T2	35
G1T1	S1T2	11	S2T2	S2T1	36
G1T1	S2T1	12	S2T2	S3T1	37
G1T1	S2T2	13	S2T2	S3T2	38
G1T1	S3T1	14	S3T1	S1T1	39
G1T1	S3T2	15	S3T1	S1T2	40
G2T1	G1T1	16	S3T1	S2T1	41
G2T1	S1T1	17	S3T1	S3T2	42
G2T1	S1T2	18	S3T2	S1T1	43
G2T1	S2T1	19	S3T2	S2T1	44
G2T1	S2T2	20	S3T2	S3T1	45
G2T1	S3T1	21	B1R1	S1H1	46
G2T1	S3T2	22	B1R1	G1H1	47
S1T1	S1T2	23	B1R1	G2H1	48
S1T1	S2T1	24	B1R1	S3H1	49
S1T1	S2T2	25			

Table E9. Front-end bearings network, Gabon 1992

From node	To node	Bearing	From node	To node	Bearing
B1R1	S1H1	1	S1T1	S1T2	5
B1R1	G1H1	2	S2T1	S2T2	6
B1R1	G2H1	3	S3T1	S3T2	7
B1R1	S3H1	4			

Table E10. Tail-end acoustic ranges network, Gabon 1992

From node	To node	Range	From node	To node	Range
S1T4	F1T1	1	S2T4	S3T4	16
SIT4	S2T3	2	F2T1	F3T1	17
S1T4	S2T4	3	F2T1	S1T4	18
S1T4	S3T4	4	F2T1	S2T4	19
F1T1	F2T1	5	F2T1	S3T4	20
F1T1	F3T1	6	S3T4	F1T1	21
F1T1	SIT4	7	S3T4	F3T1	22
F1T1	S2T4	8	S3T4	SIT4	23
S2T3	F1T1	9	S3T4	S2T3	24
S2T3	F2T1	10	S3T4	S2T4	25
S2T3	F3T1	11	F3T1	F1T1	26
S2T3	S2T4	12	F3T1	S1T4	27
S2T4	F2T1	13	F3T1	S2T4	28
S2T4	S1T4	14	F3T1	S3T4	29
S2T4	S2T3	15			

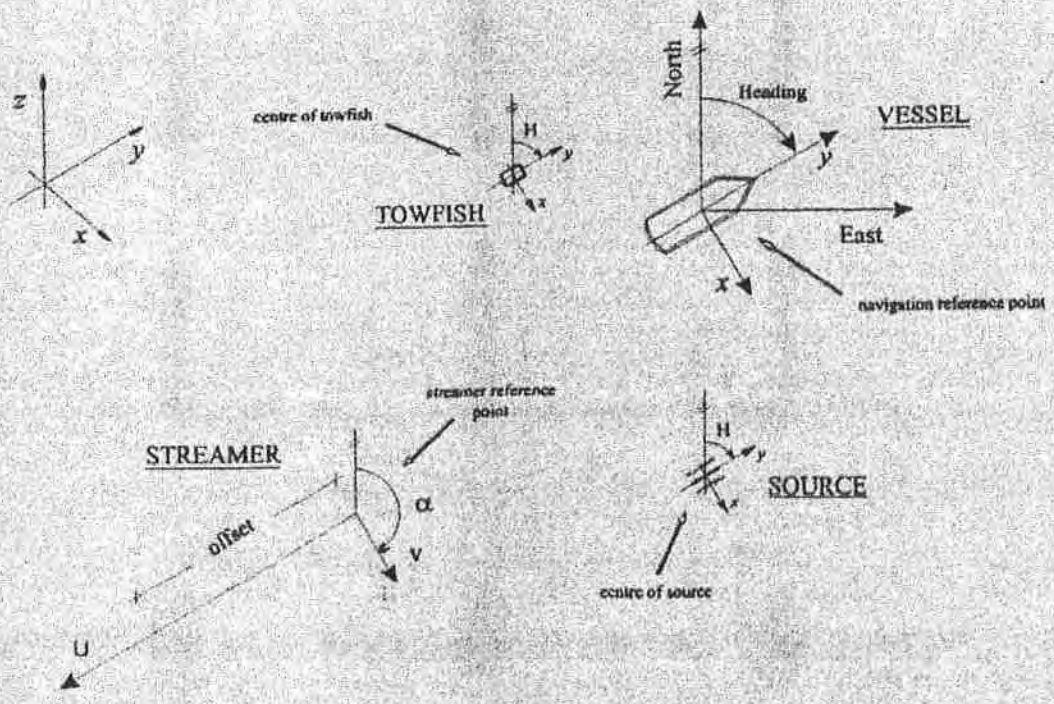

Figure E.2 Seismic network "body-fixed" coordinate systems

E.1.2.3 Survey Configuration Diagrams

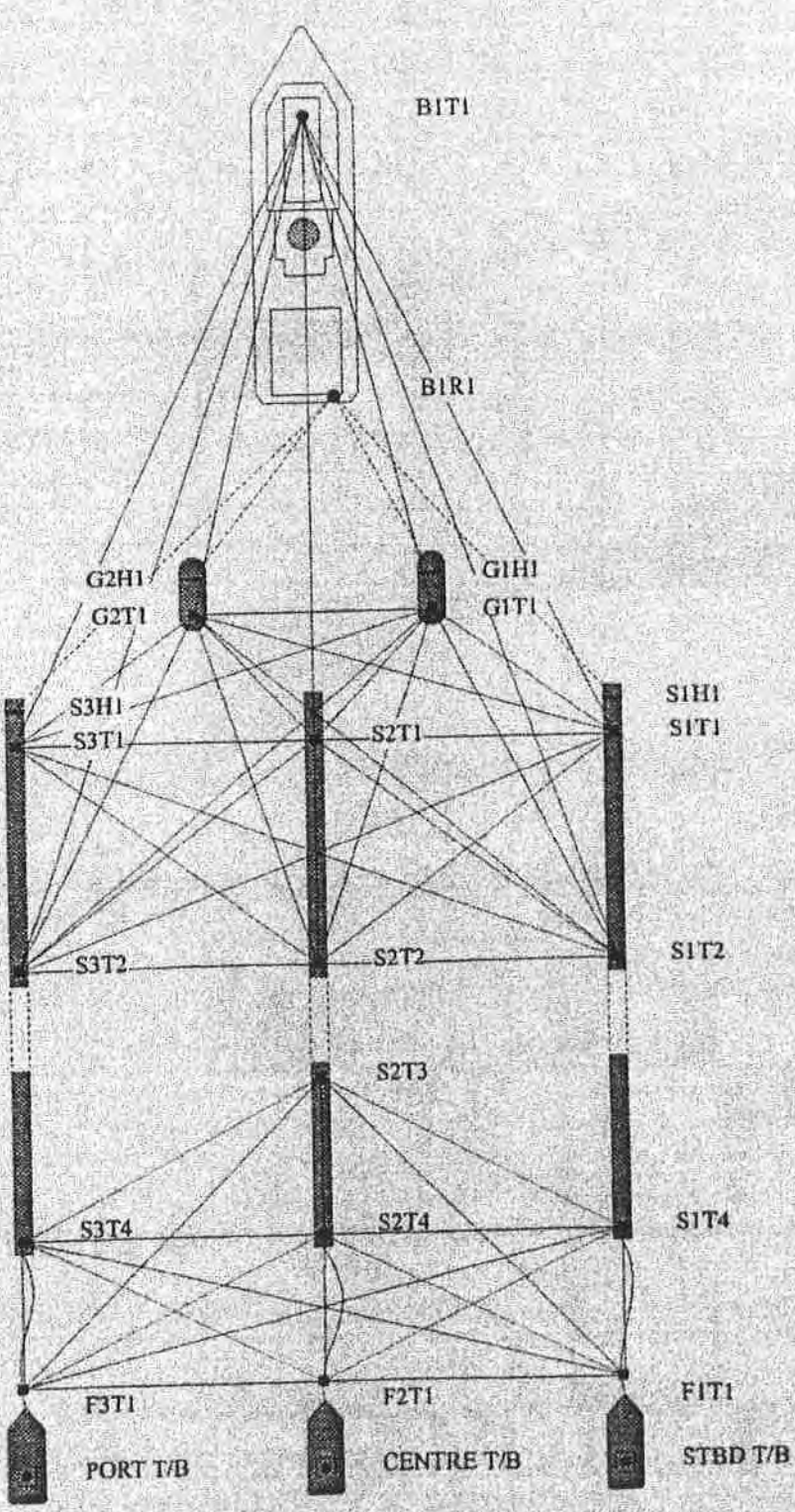

Figure E.3 Front-end and tail-end SONARDYNE acoustic network, and front-end laser network, Gabon 1992

E.1.3 Time Series Diagrams of Raw Positioning Data

E.1.3.1 Vessel and Tailbuoy Positioning and Gyro

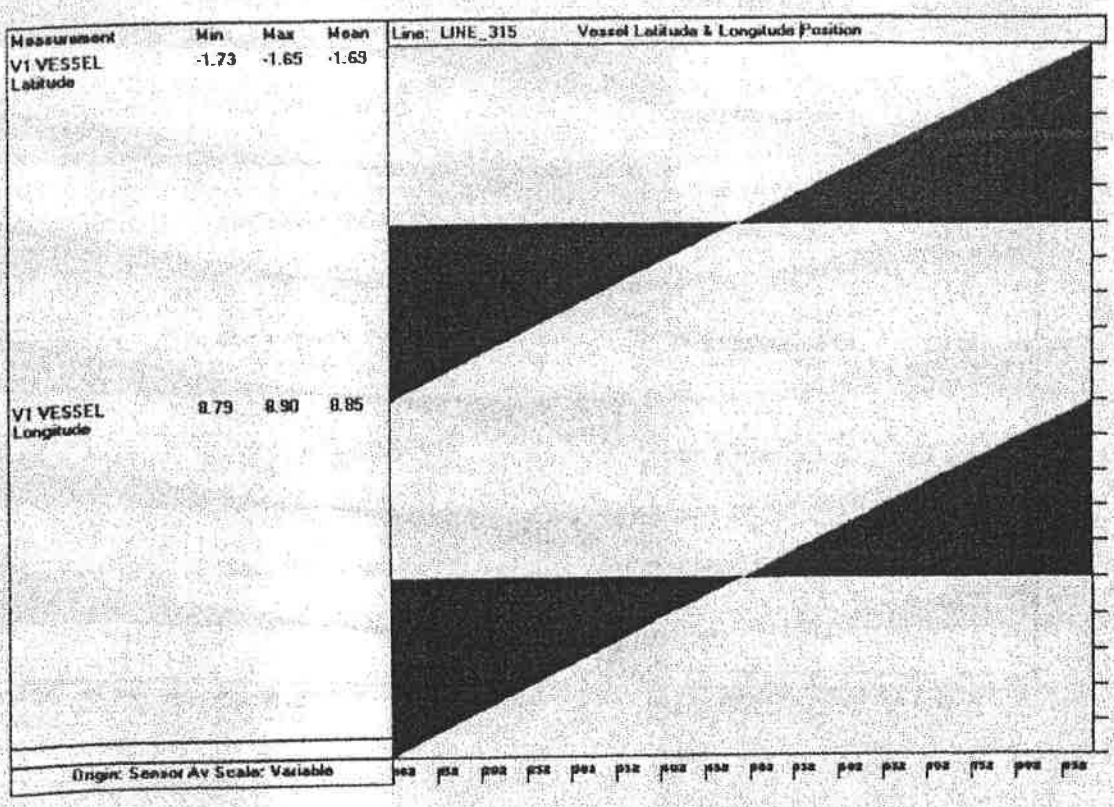

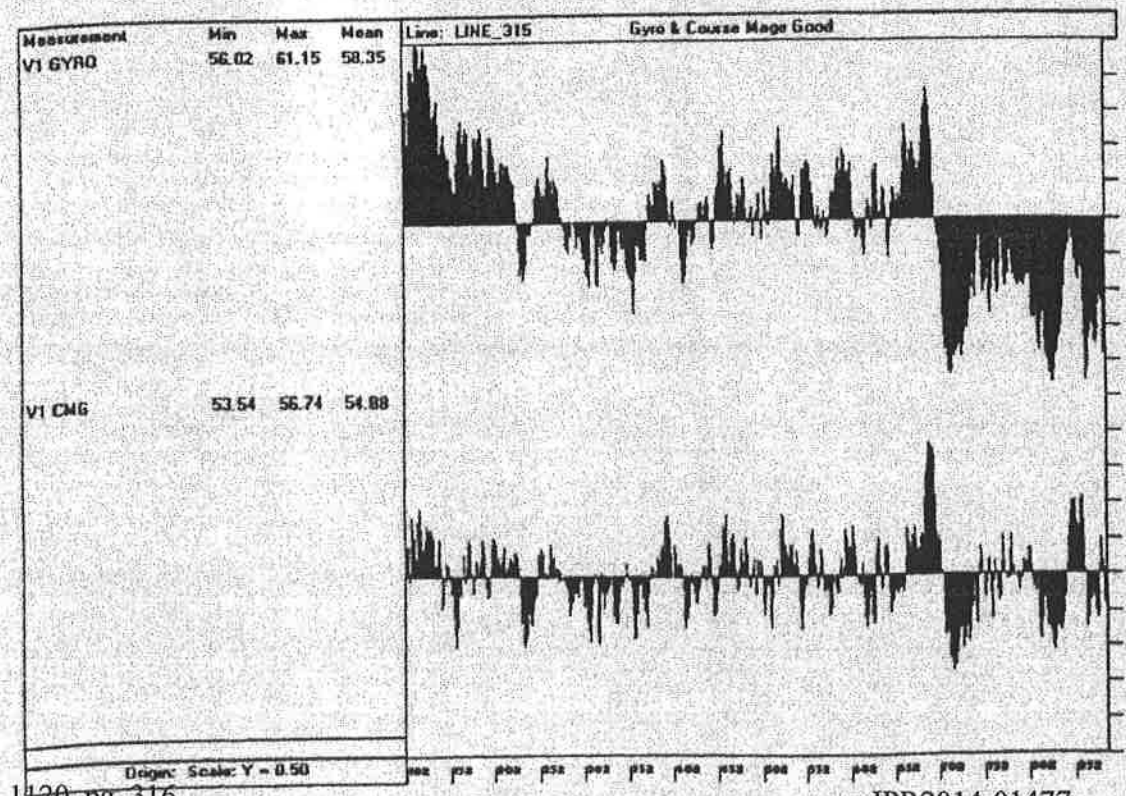

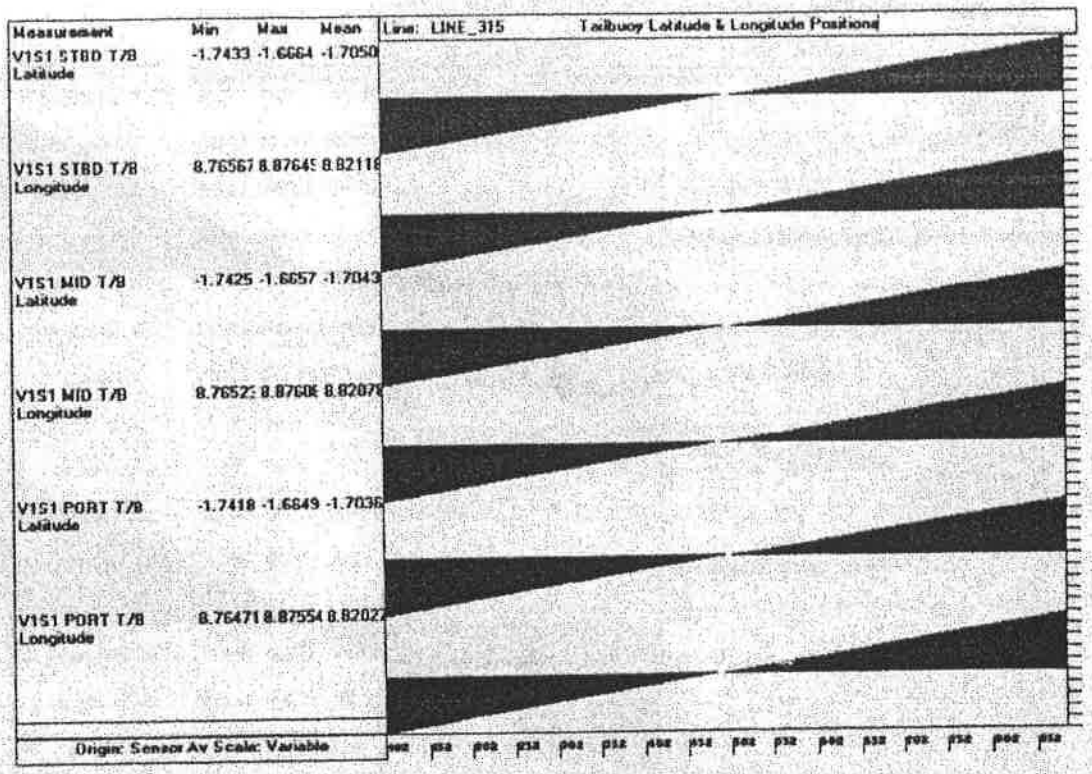
Measurement
Min
Max
Mean
Line: LINE_315
Tailbuoy Latitude & Longitude Positions
V1S1 STBD T/B Latitude
-1.7433
-1.6664
-1.7050
V1S1 STBD T/B Longitude
8.76567
8.87649
8.82118
V1S1 MID T/B Latitude
-1.7425
-1.6657
-1.7043
V1S1 MID T/B Longitude
8.76525
8.87608
8.82078
V1S1 PORT T/B Latitude
-1.7418
-1.6649
-1.7036
V1S1 PORT T/B Longitude
8.76471
8.87554
8.82027
Origin: Sensor Av Scale: Variable

E.1.3.2 Front-end and Tail-end Acoustic and Laser Networks

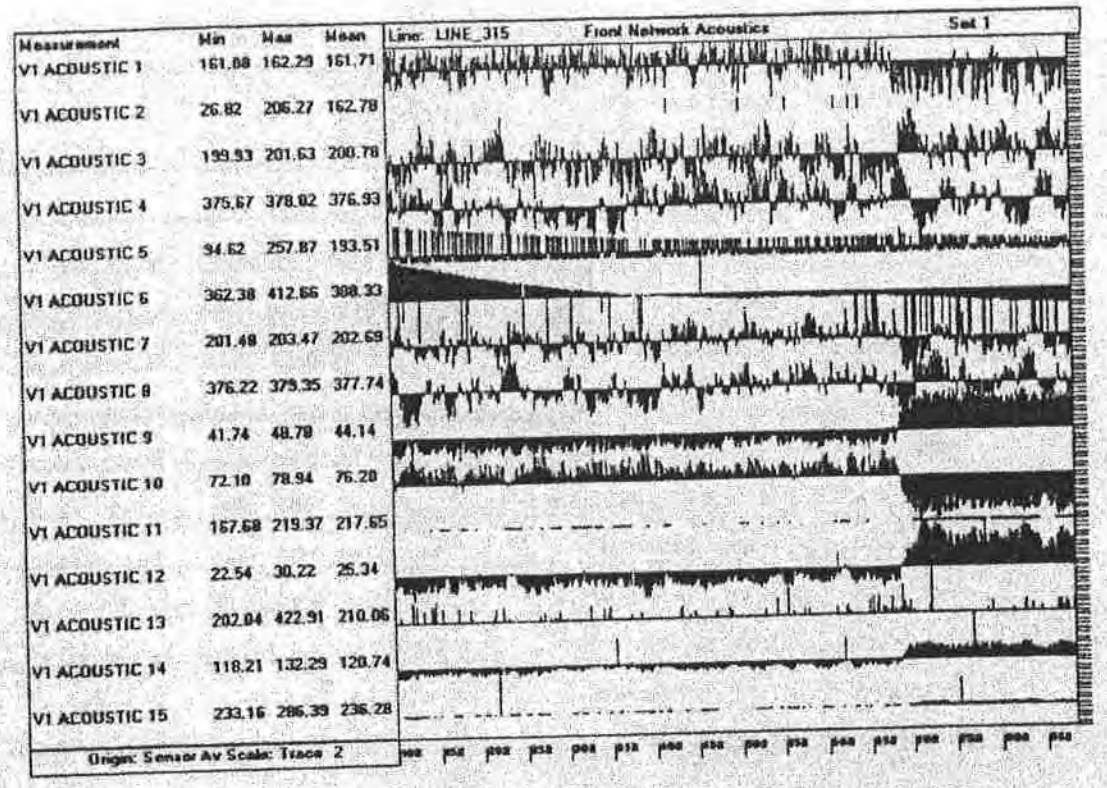

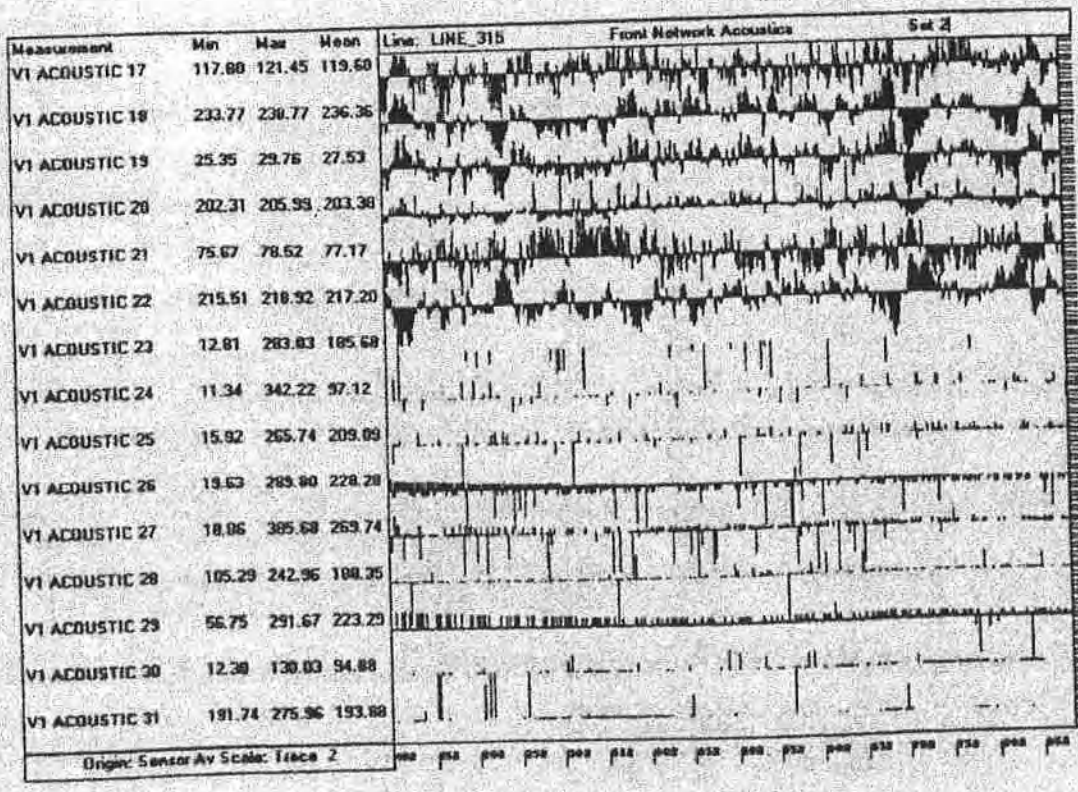

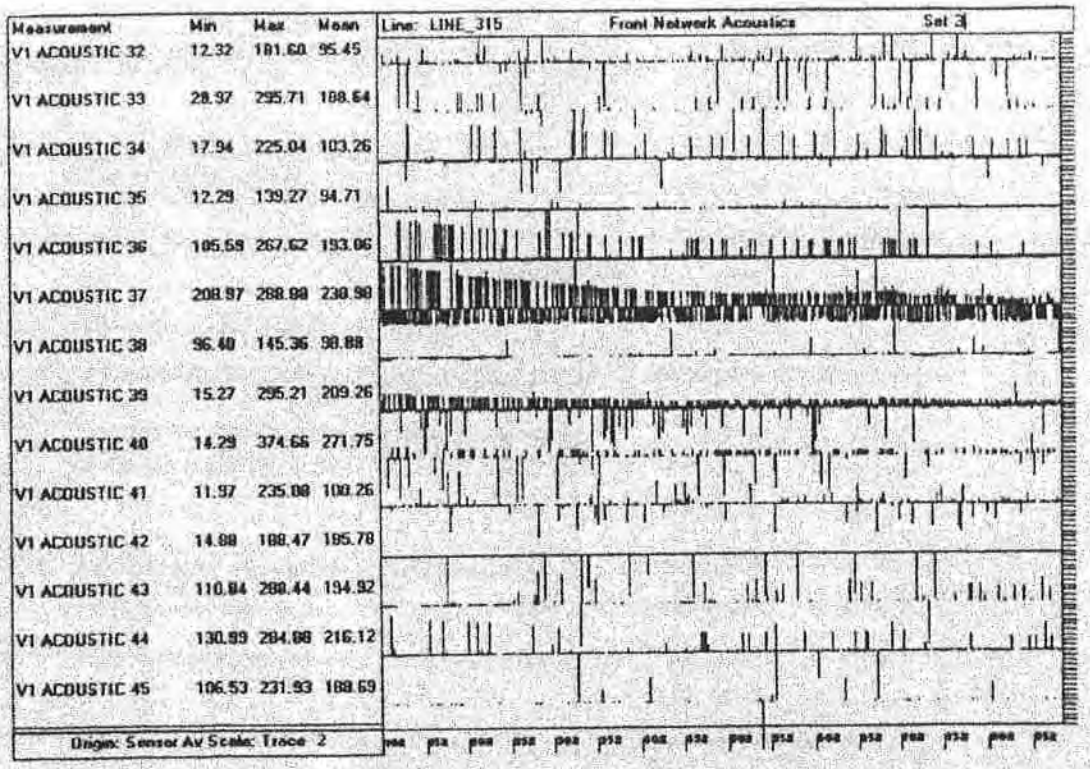

Measurement	Min	Max	Mean
V1 ACOUSTIC 32	12.32	181.60	95.45
V1 ACOUSTIC 33	28.97	295.71	188.64
V1 ACOUSTIC 34	17.94	225.04	103.26
V1 ACOUSTIC 35	12.29	139.27	94.71
V1 ACOUSTIC 36	185.58	267.62	193.06
V1 ACOUSTIC 37	208.97	288.88	230.88
V1 ACOUSTIC 38	96.40	145.36	98.88
V1 ACOUSTIC 39	15.27	295.21	209.26
V1 ACOUSTIC 40	14.29	374.66	271.75
V1 ACOUSTIC 41	11.97	235.08	108.26
V1 ACOUSTIC 42	14.88	188.47	195.78
V1 ACOUSTIC 43	110.84	288.44	194.92
V1 ACOUSTIC 44	130.99	284.88	216.12
V1 ACOUSTIC 45	106.53	231.93	188.69

Origin: Sensor Av Scale: Trace 2

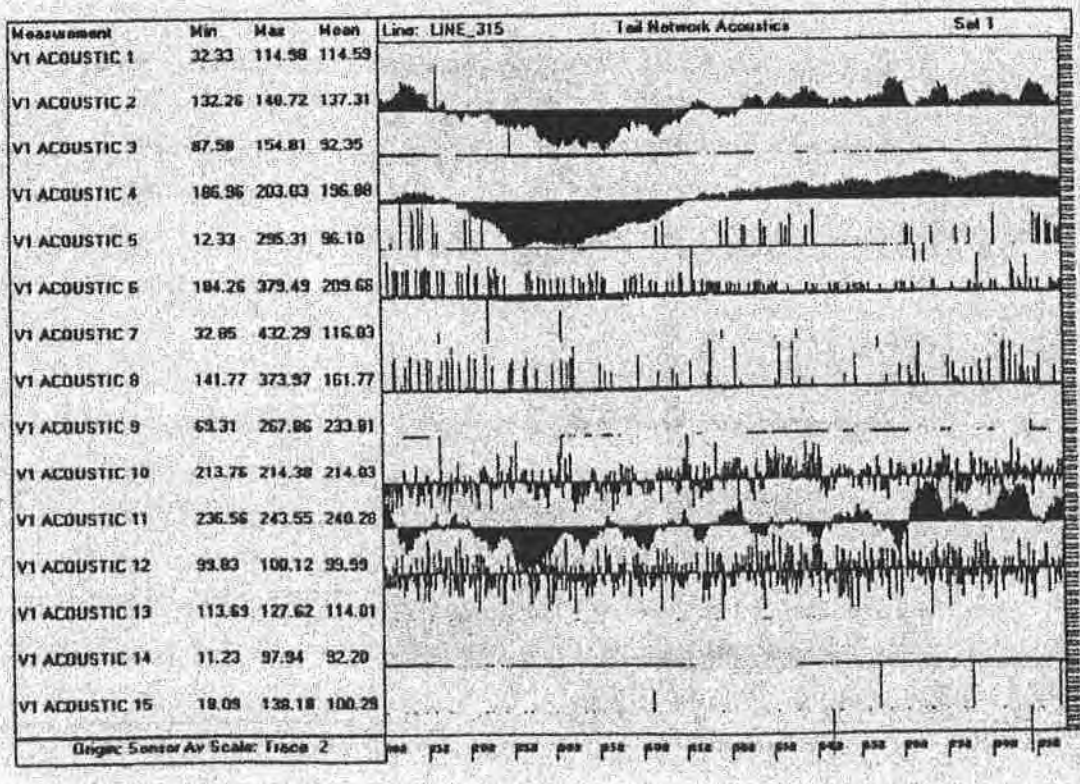

Measurement	Min	Max	Mean
V1 ACOUSTIC 1	32.33	114.58	114.59
V1 ACOUSTIC 2	132.26	148.72	137.31
V1 ACOUSTIC 3	87.58	154.81	92.35
V1 ACOUSTIC 4	186.96	203.03	196.98
V1 ACOUSTIC 5	12.33	295.31	96.10
V1 ACOUSTIC 6	184.26	379.49	209.68
V1 ACOUSTIC 7	32.85	432.29	116.03
V1 ACOUSTIC 8	141.77	373.97	161.77
V1 ACOUSTIC 9	63.31	267.86	233.91
V1 ACOUSTIC 10	213.75	214.38	214.03
V1 ACOUSTIC 11	236.56	243.55	240.28
V1 ACOUSTIC 12	93.83	108.12	99.99
V1 ACOUSTIC 13	113.69	127.62	114.01
V1 ACOUSTIC 14	11.23	97.94	92.20
V1 ACOUSTIC 15	18.09	138.18	100.28

Origin: Sensor Av Scale: Trace 2

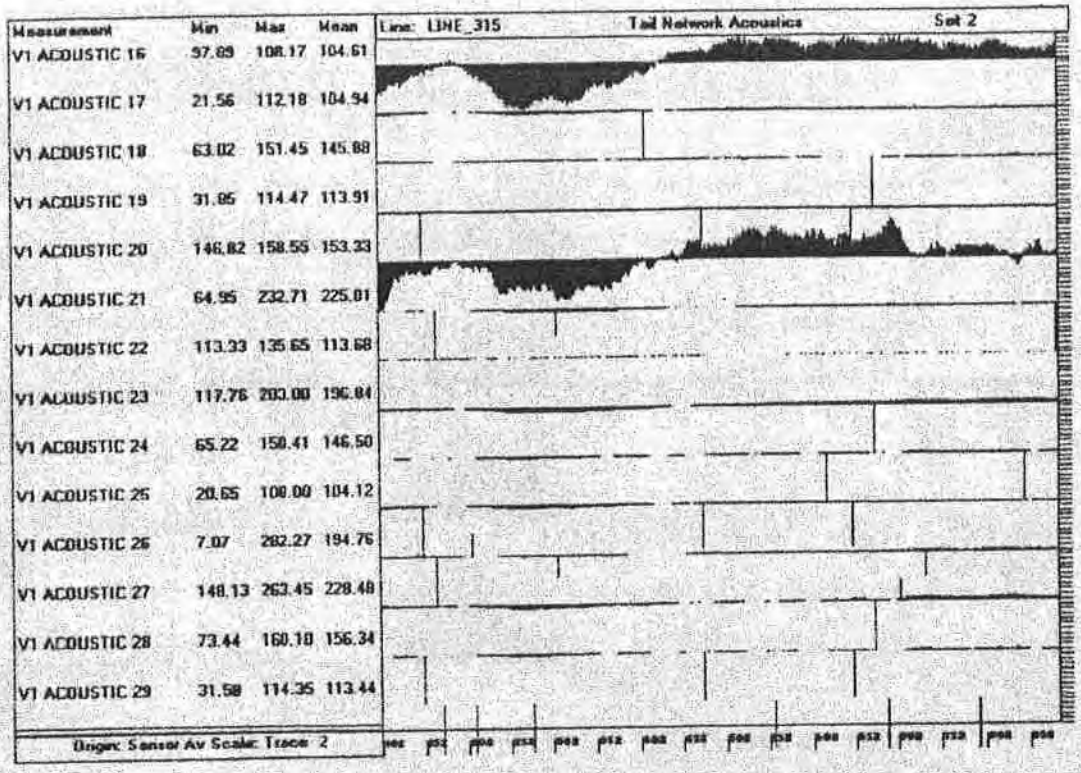
Measurement Min Max Mean
V1 ACOUSTIC 16 97.69 108.17 104.61
V1 ACOUSTIC 17 21.56 112.18 104.94
V1 ACOUSTIC 18 63.02 151.45 145.88
V1 ACOUSTIC 19 31.85 114.47 113.91
V1 ACOUSTIC 20 146.82 158.55 153.33
V1 ACOUSTIC 21 64.95 232.71 225.01
V1 ACOUSTIC 22 113.33 135.65 113.68
V1 ACOUSTIC 23 117.76 200.00 196.84
V1 ACOUSTIC 24 65.22 150.41 146.50
V1 ACOUSTIC 25 20.65 108.00 104.12
V1 ACOUSTIC 26 7.07 282.27 194.76
V1 ACOUSTIC 27 148.13 263.45 228.48
V1 ACOUSTIC 28 73.44 160.10 156.34
V1 ACOUSTIC 29 31.58 114.35 113.44
Origin: Sensor Av Scale: Trace 2
Line: LINE_315
Tail Network Acoustics
Set 2

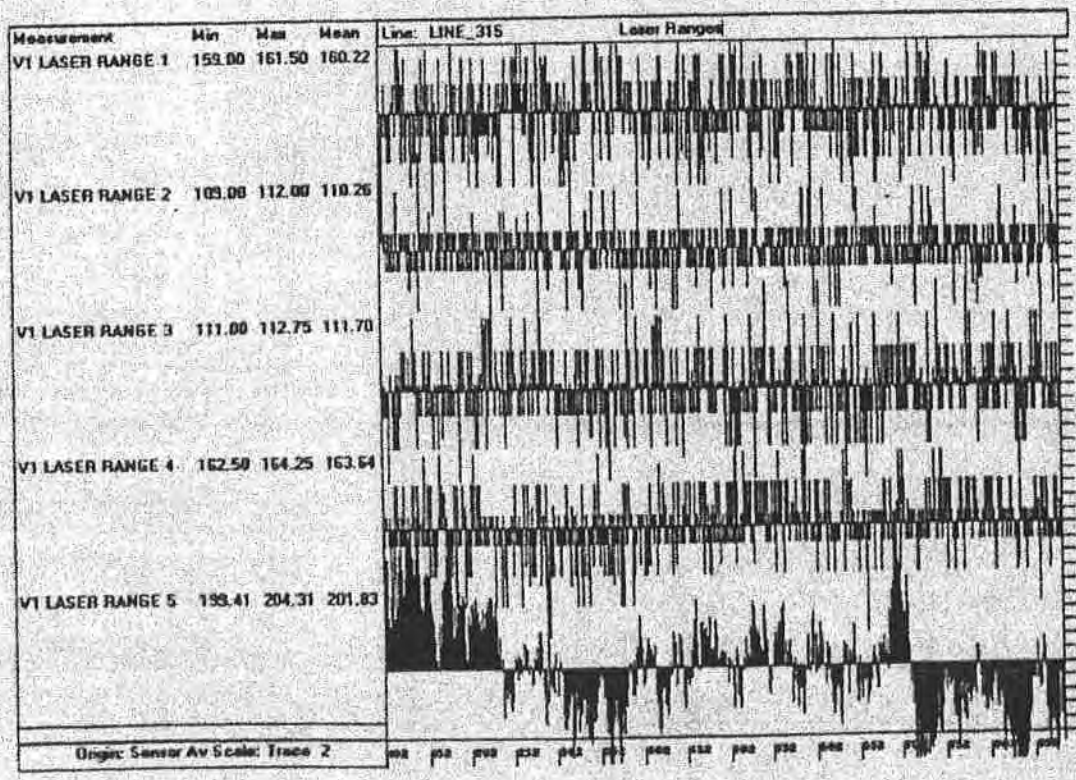
Measurement Min Max Mean
V1 LASER RANGE 1 159.00 161.50 160.22
V1 LASER RANGE 2 109.00 112.00 110.26
V1 LASER RANGE 3 111.00 112.75 111.70
V1 LASER RANGE 4 162.50 164.25 163.64
V1 LASER RANGE 5 199.41 204.31 201.83
Origin: Sensor Av Scale: Trace 2
Line: LINE_315
Laser Ranges

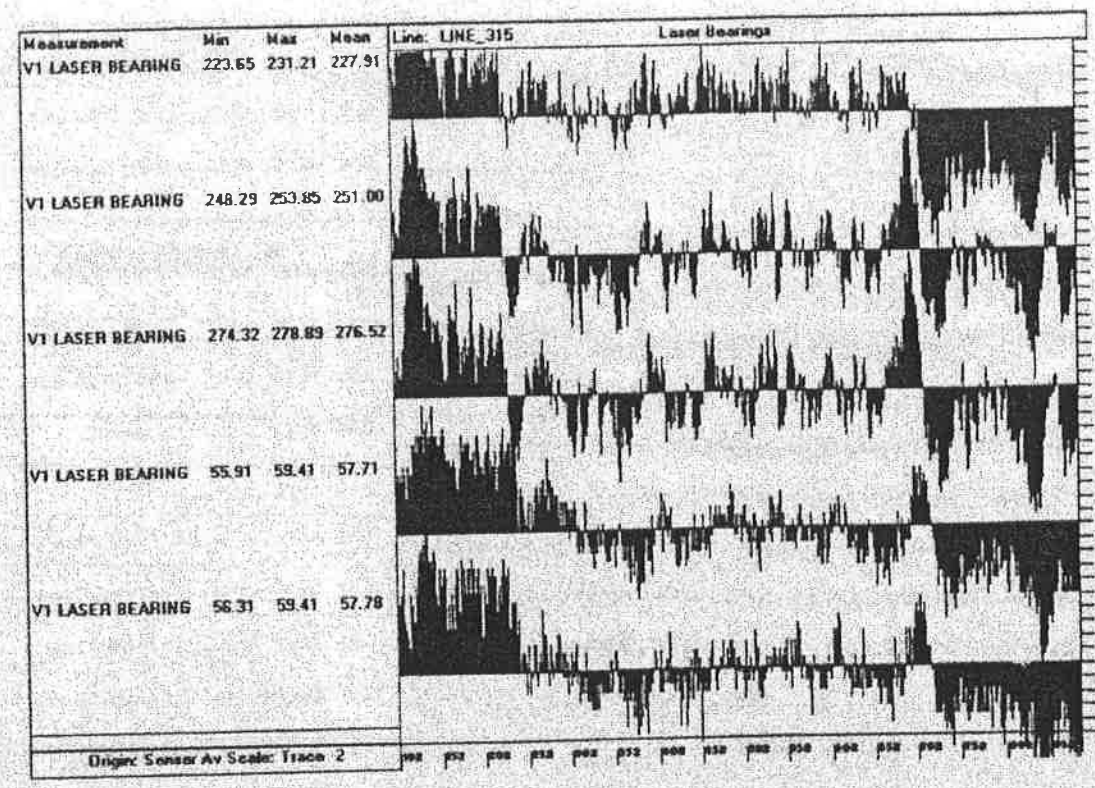
Measurement Min Max Mean
V1 LASER BEARING 223.65 231.21 227.91
V1 LASER BEARING 248.29 253.85 251.00
V1 LASER BEARING 274.32 278.89 276.52
V1 LASER BEARING 55.91 59.41 57.71
V1 LASER BEARING 56.31 59.41 57.78
Origin: Sensor Av Scale: Trace 2
Line: LINE_315
Laser Bearings

E1.3.3 Compass Azimuths

Measurement	Min	Max	Mean
V1S1 COMPASS 1	61.30	65.10	63.52
V1S1 COMPASS 2	61.90	65.40	63.70
V1S1 COMPASS 3	62.70	65.50	64.01
V1S1 COMPASS 4	62.60	65.50	63.84
V1S1 COMPASS 5	62.50	65.00	63.51
V1S1 COMPASS 6	62.90	65.30	63.95
V1S1 COMPASS 7	62.90	65.50	64.06
V1S1 COMPASS 8	62.50	65.50	63.64
V1S1 COMPASS 9	63.00	66.10	64.12
V1S1 COMPASS 10	62.90	66.40	64.21
V1S1 COMPASS 11	62.90	66.80	64.38
V1S1 COMPASS 12	62.90	67.20	64.43
V1S1 COMPASS 13	63.30	67.20	64.73

Origin: Global Av Scale: Trace 2

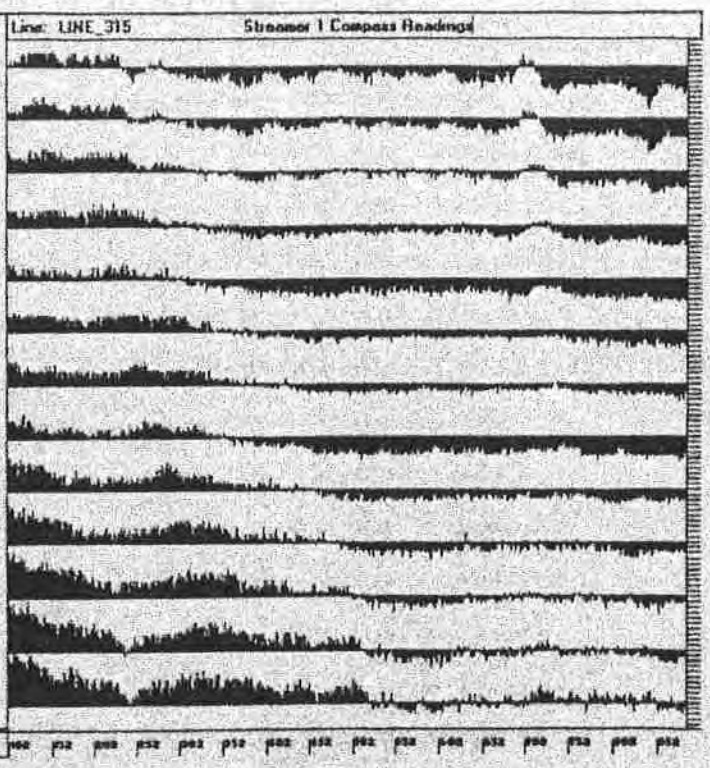

Measurement	Min	Max	Mean
V1S2 COMPASS 1	62.40	65.00	64.03
V1S2 COMPASS 2	62.30	65.40	63.77
V1S2 COMPASS 3	62.00	65.50	63.96
V1S2 COMPASS 4	62.30	65.00	63.47
V1S2 COMPASS 5	62.80	65.50	63.90
V1S2 COMPASS 6	62.80	65.40	63.93
V1S2 COMPASS 7	63.00	65.70	64.03
V1S2 COMPASS 8	63.20	66.00	64.13
V1S2 COMPASS 9	61.20	66.20	64.24
V1S2 COMPASS 10	60.60	66.40	64.15
V1S2 COMPASS 11	63.20	66.80	64.52
V1S2 COMPASS 12	62.20	66.80	63.89
V1S2 COMPASS 13	62.80	67.40	64.28

Origin: Global Av Scale: Trace 2

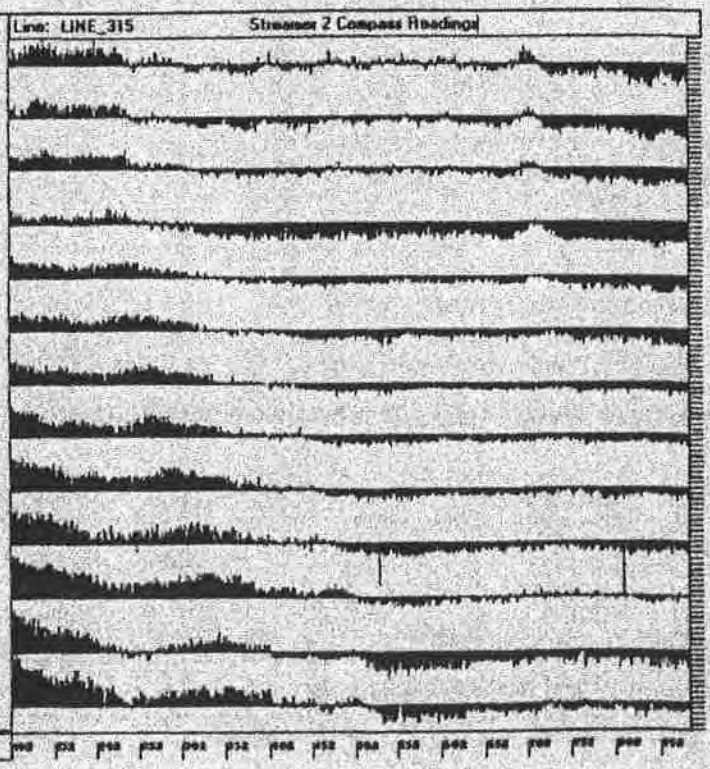

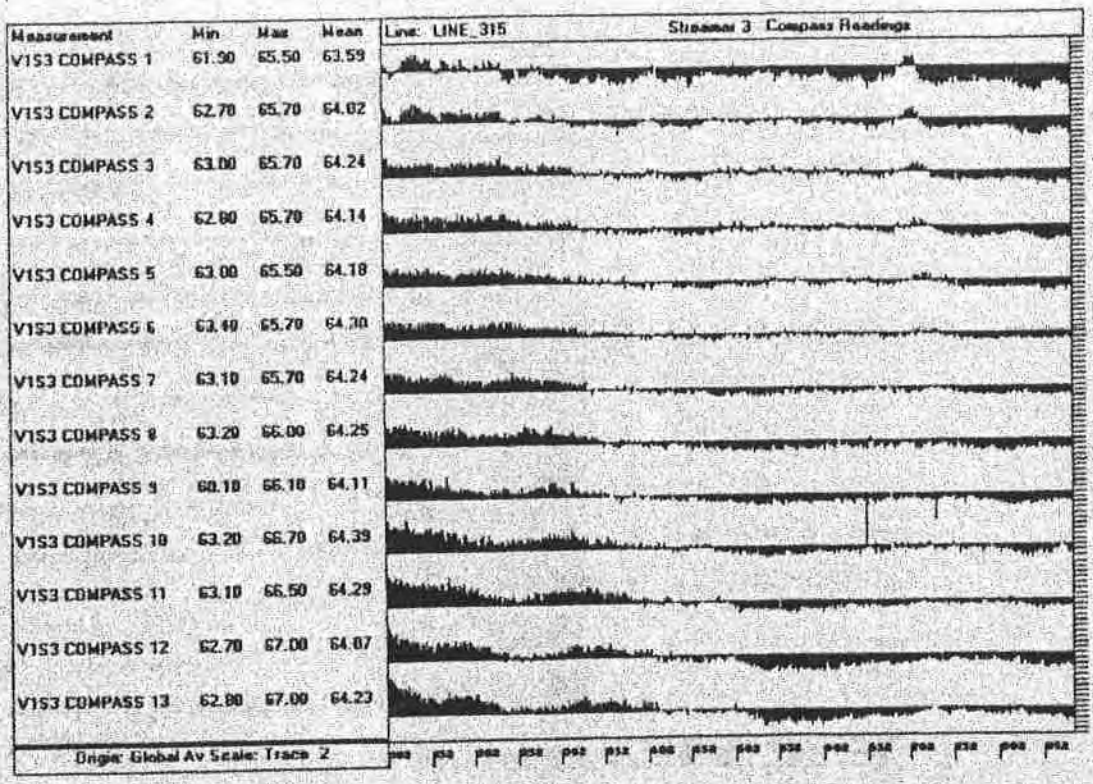

Measurement	Min	Max	Mean
V1S3 COMPASS 1	61.90	65.50	63.59
V1S3 COMPASS 2	62.70	65.70	64.02
V1S3 COMPASS 3	63.00	65.70	64.24
V1S3 COMPASS 4	62.80	65.70	64.14
V1S3 COMPASS 5	63.00	65.50	64.18
V1S3 COMPASS 6	63.40	65.70	64.30
V1S3 COMPASS 7	63.10	65.70	64.24
V1S3 COMPASS 8	63.20	66.00	64.25
V1S3 COMPASS 9	60.10	66.10	64.11
V1S3 COMPASS 10	63.20	66.70	64.39
V1S3 COMPASS 11	63.10	66.50	64.29
V1S3 COMPASS 12	62.70	67.00	64.07
V1S3 COMPASS 13	62.80	67.00	64.23

Origin: Global Av Scale: Trace 2

Line: LINE_315 Streamer 3 Compass Readings

E.2 IRISH SEA 3D SEISMIC SURVEY

E.2.1 General Description

A. Job Information

Geophysical contractor	: Horizon Exploration Limited
Vessel name	: PACIFIC HORIZON
Start of line	: 9 September 1993

B. Area and Grid Definition

Area name	: North Wales
Datum	: ED
Semimajor ellipsoidal axis	: 6378388.0 metre
Inverse flattering	: 297.0000
Magnetic declination	: -6.20 degrees
Gyro correction	: -0.00 degrees
Line number	: UK93-419
Line direction	: 270.0 degrees
Grid cells	: 25.0 metre cross-line, 12.5 metre in-line
Shotpoint interval	: 12.5 metre

C. Survey Configuration Information

Number of vessels	: One
Number of seismic sources	: Two (two inner and two outer sources)
Source separation	: 50.0 metre
Number of streamers	: Two
Streamer length	: 1950 metre
Streamer separation	: 100 metre
Receiver group interval	: 12.5 metre

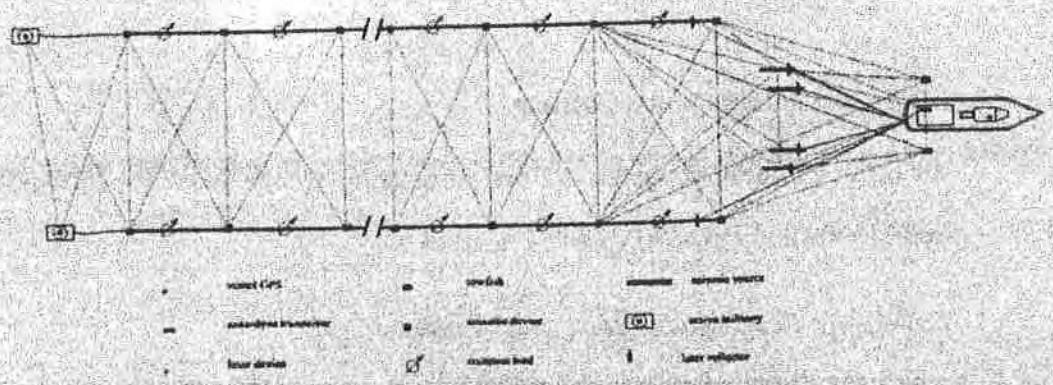

Figure E.4 Geometry configuration sketch, Irish Sea (1993)

E.2.2 Navigation Sensors

Primary positioning was accomplished with Syledis while secondary positioning was by means of DGPS. In addition, tailbuoys equipped with RGPS were employed in conjunction with front and tail acoustic networks to locate both source and receivers. Both tailbuoys were equipped with acoustic pods.

Front-end positioning utilised an acoustic network consisting of SONARDYNE acoustic units. Active components included two hull pingers and two source pingers. A separate acoustic network consisting of SYNTRON echo pods was installed to provide streamer and tail-end positioning. transponders were located under both RGPS tailbuoys and at fixed positions up both starboard and port streamers. A relatively new feature added for this survey was the use of a SYNTRON MultiTRAK system. These bird/compass/acoustic units were positioned down each cable to provide the normal compass/depth control. In addition, these acoustic pingers/receivers provided a full-length acoustic network for total cable positioning. It should be, however, mentioned that ranging data was collected at approximately every other shotpoint. In summary, the survey configuration consisted of the following sensors

- Vessel Syledis, DGPS, gyro, two acoustic pinger and a laser device
- 10 SONARDYNE acoustic devices at the front-end network
- 24 MultiTRAK acoustic units deployed along the length of the cables
- 6 laser reflectors
- 10 compass bird units fixed on each streamer
- Tailbuoy Syledis and acoustic pods

E.2.2.1Navigation Sensor Offsets

All offset coordinates given bellow correspond to the local (body-fixed) coordinate frames shown in Figures E.2 and 5.2.

Table E11. Vessel and tailbuoy positioning sensors

Navigation Sensor	Reference point	*x* / offset	*y*	*z* / height
vessel Syledis	NRP	0.8	0.3	24.8
vessel DGPS	NRP	0.6	-1.1	24.3
stbd t/b Syledis	stbd str. ref. point	2063.2	--	-7.0
port t/b Syledis	port str. ref. point	2111.6	--	-7.0

Table E12. Front-end SONARDYNE acoustic network sensors

Acoustic device	Reference point	*x* / offset	*y*	*z* / height
fore hull pinger 1	NRP	-0.4	35.5	-6.4
aft hull pinger 2	NRP	0.9	-0.4	-6.4
stbd towfish 3	port towfish centre	0.0	0.0	-7.0
port towfish 4	stbd towfish centre	0.0	0.0	-7.0
stbd streamer diverter 5	port str. ref. point	-89.0	--	-7.0
outer stbd source 6	o port source centre	0.0	-3.5	-5.0
inner stbd source 7	i port source centre	0.0	-3.5	-5.0
inner port source 8	i stbd source centre	0.0	-3.5	-5.0
outer port source 9	o stbd source centre	0.0	-3.5	-5.0
port streamer diverter 10	stbd str. ref. point	-89.0	--	-7.0

Table E13. MultiTRAK acoustic network sensors

Acoustic device	Reference point	*x* / offset	*y*	*z* / height
transmit & receive 61/12B	stbd str. ref. point	-87.6	--	-7.0
receive only 62/11B	stbd str. ref. point	-14.4	--	-7.0
receive only 63/10B	stbd str. ref. point	62.7	--	-7.0
receive only 64/9B	stbd str. ref. point	137.7	--	-7.0
transmit & receive 65/8B	stbd str. ref. point	436.9	--	-7.0
transmit only 66/7B	stbd str. ref. point	736.1	--	-7.0
transmit & receive 67/6B	stbd str. ref. point	1035.3	--	-7.0
transmit & receive 68/5B	stbd str. ref. point	1334.5	--	-7.0
receive only 69/4B	stbd str. ref. point	1633.7	--	-7.0
receive only 70/3B	stbd str. ref. point	1857.9	--	-7.0
transmit & receive 71/2B	stbd str. ref. point	1932.9	--	-7.0
transmit & receive 72/1B	stbd str. ref. point	2063.2	--	-7.0
transmit & receive 21/12A	port str. ref. point	-87.6	--	-7.0
transmit & receive 22/11A	port str. ref. point	-14.4	--	-7.0
receive only 23/10A	port str. ref. point	62.7	--	-7.0
transmit only 24/9A	port str. ref. point	137.7	--	-7.0
receive only 25/8A	port str. ref. point	436.9	--	-7.0
receive only 26/7A	port str. ref. point	736.1	--	-7.0
receive only 27/6A	port str. ref. point	1035.3	--	-7.0
transmit & receive 28/5A	port str. ref. point	1334.5	--	-7.0
transmit & receive 29/4A	port str. ref. point	1633.7	--	-7.0
receive only 30/3A	port str. ref. point	1857.9	--	-7.0
receive only 31/2A	port str. ref. point	1932.9	--	-7.0
transmit & receive 32/1A	port str. ref. point	2111.6	--	-7.0

Table E14. Front-end laser network sensors

Laser device	Reference point	*x* / offset	*y*	*z* / height
laser sensor LS	NRP	0.0	0.0	24.3
laser reflector LR1	stbd str. ref. point	-89.0	--	0.8
laser reflector LR2	port str. ref. point	-89.0	--	0.8
laser reflector LR3	o stbd source centre	0.0	-3.5	0.8
laser reflector LR4	i stbd source centre	0.0	-3.5	0.8
laser reflector LR5	i port source centre	0.0	-3.5	0.8
laser reflector LR6	o port source centre	0.0	-3.5	0.8

Table E15. Compass Birds - starboard streamer

Compass device	Reference point	*x* / offset	*y*	*z*/ height
1	stbd str. ref. point	-14.3	--	-7.0
2	stbd str. ref. point	62.3	--	-7.0
3	stbd str. ref. point	137.3	--	-7.0
4	stbd str. ref. point	436.5	--	-7.0
5	stbd str. ref. point	735.7	--	-7.0
6	stbd str. ref. point	1034.9	--	-7.0
7	stbd str. ref. point	1334.1	--	-7.0
8	stbd str. ref. point	1633.3	--	-7.0
9	stbd str. ref. point	1857.5	--	-7.0
10	stbd str. ref. point	1932.5	--	-7.0

Table E16. Compass Birds - port streamer

Compass device	Reference point	*x* / offset	*y*	*z* / height
1	port str. ref. point	-14.3	--	-7.0
2	port str. ref. point	62.3	--	-7.0
3	port str. ref. point	137.3	--	-7.0
4	port str. ref. point	436.5	--	-7.0
5	port str. ref. point	735.7	--	-7.0
6	port str. ref. point	1034.9	--	-7.0
7	port str. ref. point	1334.1	--	-7.0
8	port str. ref. point	1633.3	--	-7.0
9	port str. ref. point	1857.5	--	-7.0
10	port str. ref. point	1932.5	--	-7.0

E.2.2.2 Acoustic and Laser Observables Definition

The front-end SONARDYNE acoustic network consisted of a total number of 43 ranges while the full-length MultiTRAK acoustic network consisted of 24 ranges. The raw laser data have been converted into DX and DY values.

Table E17. SONARDYNE and MultiTRAK acoustic networks

From node	To node	Range	From node	To node	Range
1	2	1	7	6	35
1	10	2	7	5	36
1	9	3	6	1	37
1	8	4	6	2	38
1	6	5	6	3	39
1	5	6	6	10	40
2	1	7	6	9	41
2	3	8	6	8	42
2	10	9	6	5	43
2	9	10	29/4A	70/3B	44
2	8	11	29/4A	69/4B	45
2	6	12	29/4A	68/5B	46
2	5	13	28/5A	69/4B	47
4	1	14	28/5A	68/5B	48
4	10	15	28/5A	67/6B	49
3	1	16	22/11A	64/9B	50
3	2	17	22/11A	61/12B	51
3	10	18	71/2B	31/2A	52
3	9	19	71/2B	30/3A	53
3	5	20	71/2B	32/1A	54
9	1	21	68/5B	29/4A	55
9	2	22	68/5B	28/5A	56
9	10	23	68/5B	27/6A	57
9	5	24	67/6B	27/6A	58
8	1	25	66/7B	27/6A	59
8	2	26	65/8B	25/8A	60
8	10	27	61/12B	22/11A	61
8	9	28	61/12B	62/11B	62
8	6	29	61/12B	21/12A	63
8	5	30	32/1A	31/2A	64
7	1	31	32/1A	71/2B	65
7	2	32	32/1A	72/1B	66
7	10	33	72/1B	71/2B	67
7	9	34	72/1B	32/1A	68

E.2.2.3 Survey Configuration Diagrams

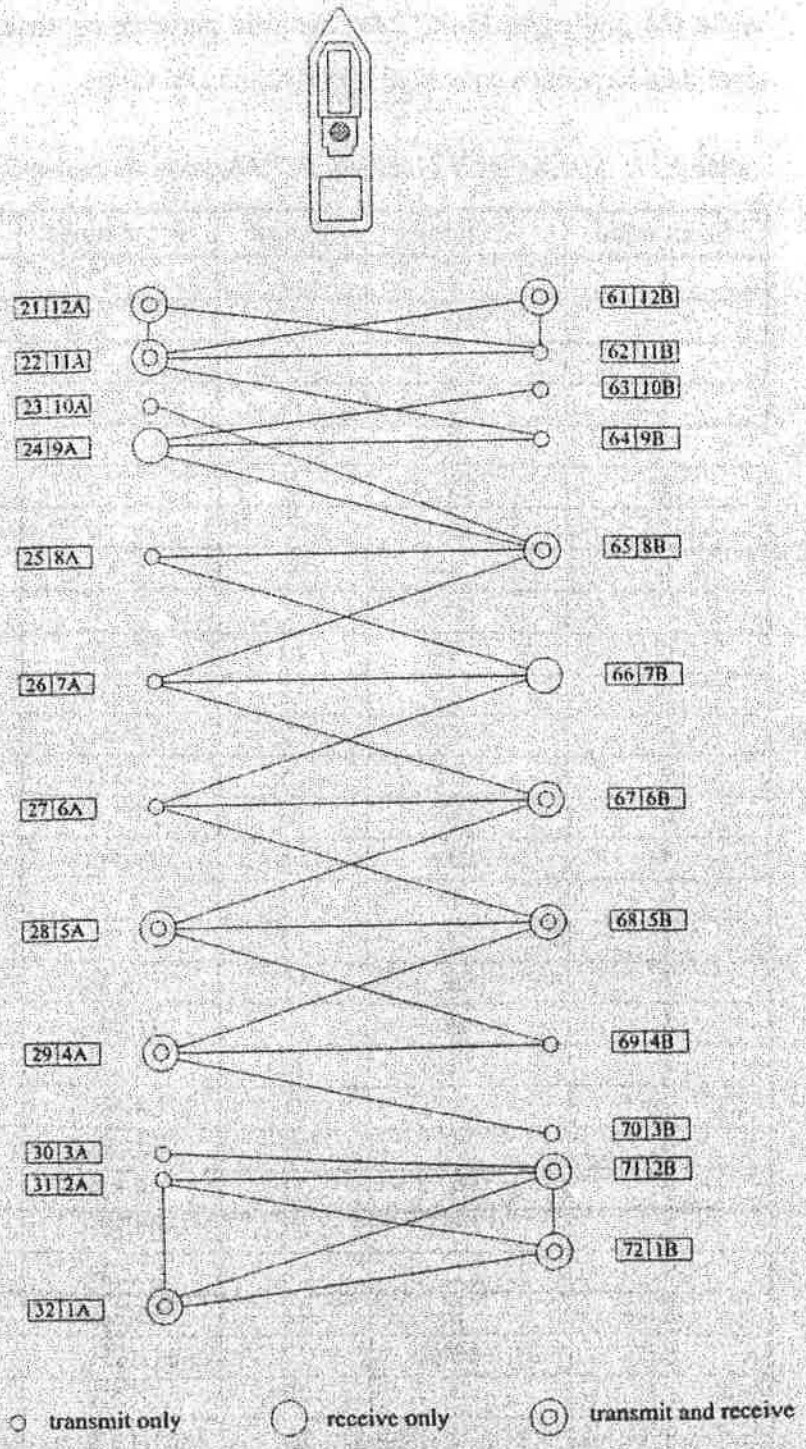

Figure E.5 MultiTRAK acoustic network, Irish Sea 1993

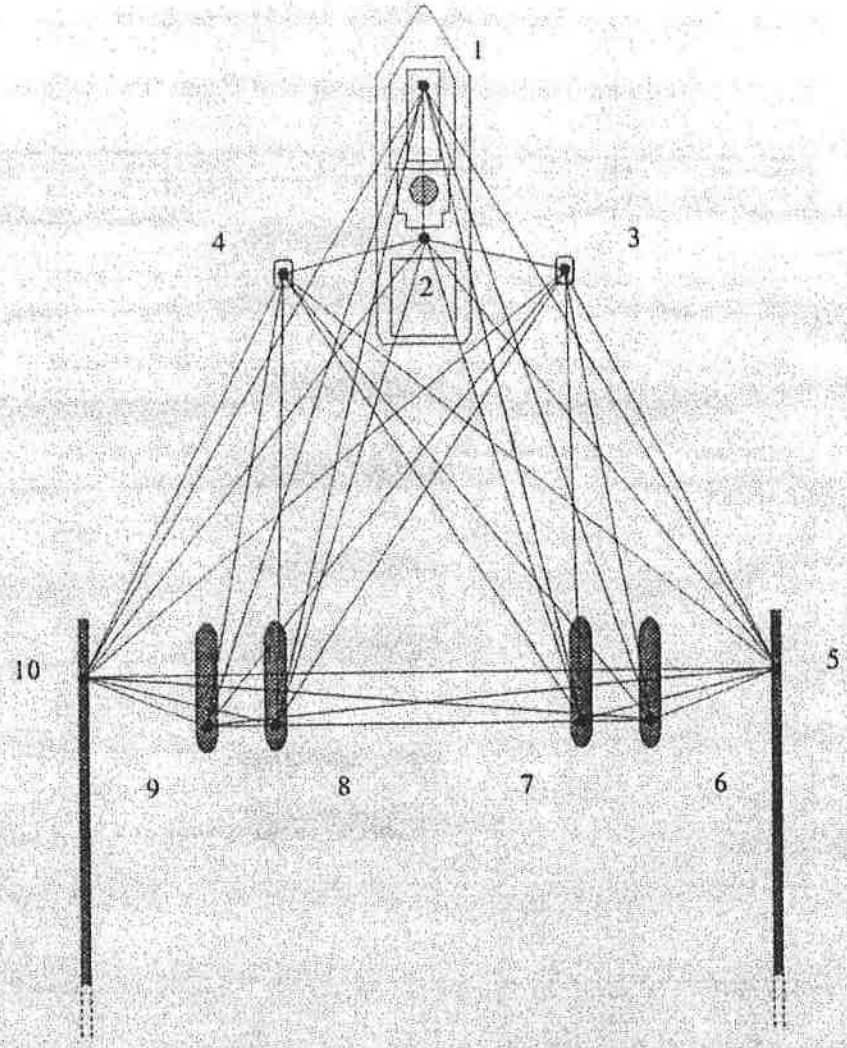

P286 node	DESCRIPTION
1	fore hull pinger
2	aft hull pinger
3	starboard towfish
4	port towfish
5	starboard streamer diverter
6	starboard outer float
7	starboard inner float
8	port inner float
9	port outer float
10	port streamer diverter

Figure E.6 Front-end SONARDYNE acoustic network, Irish Sea 1993

E.2.3 Time Series Diagrams of Raw Positioning Data

E.1.3.1 Vessel and Tailbuoy Positioning and Gyro

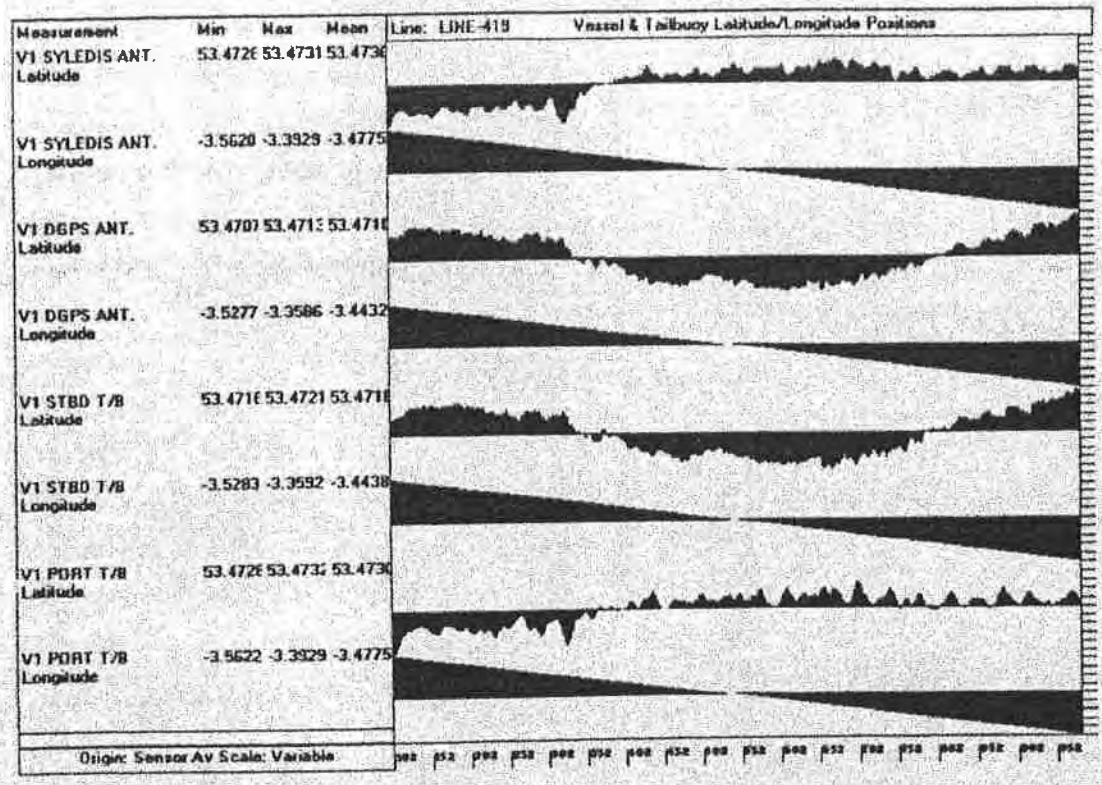

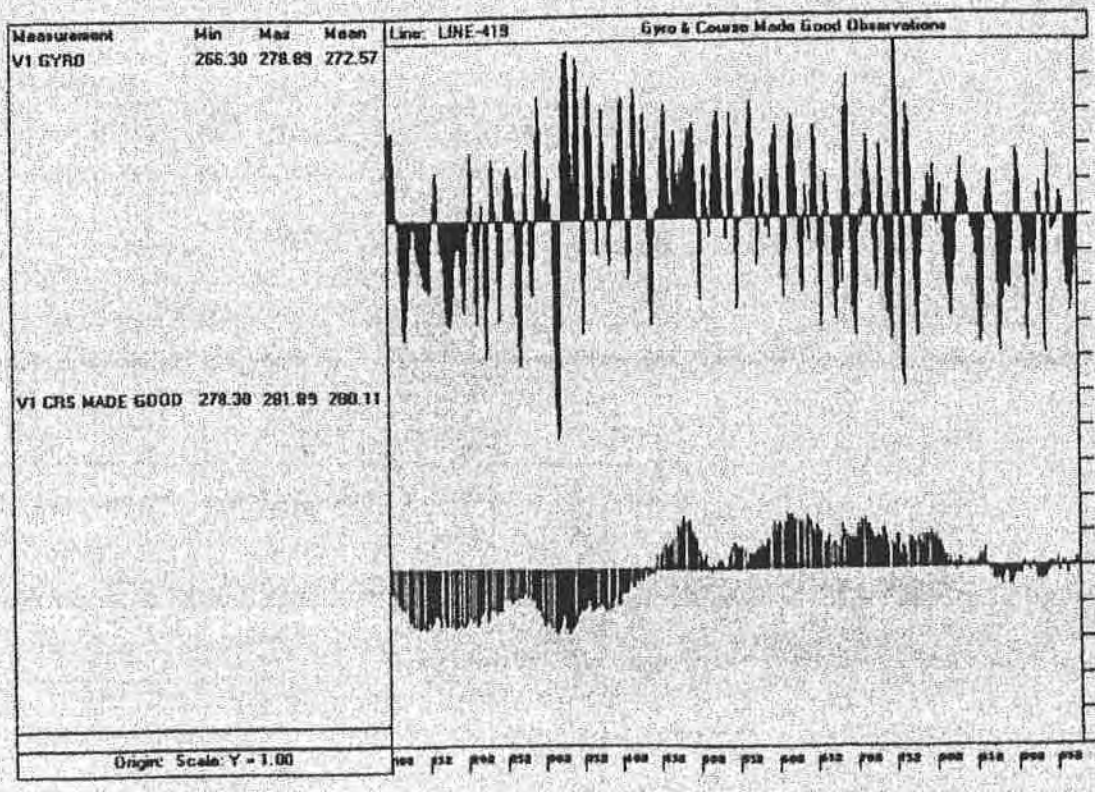

E.1.3.2 Acoustic and Laser Networks

Measurement	Min	Max	Mean
V1 ACOUSTIC 1	34.47	34.71	34.57
V1 ACOUSTIC 2	107.40	135.43	131.63
V1 ACOUSTIC 3	52.83	138.23	130.80
V1 ACOUSTIC 4	85.71	147.01	130.35
V1 ACOUSTIC 5	19.77	139.30	130.89
V1 ACOUSTIC 6	130.67	141.20	135.38
V1 ACOUSTIC 7	34.61	101.26	34.82
V1 ACOUSTIC 8	17.68	19.35	18.34
V1 ACOUSTIC 9	99.15	112.16	101.09
V1 ACOUSTIC 10	43.63	108.58	98.50
V1 ACOUSTIC 11	94.91	110.98	96.58
V1 ACOUSTIC 12	97.54	106.99	99.46
V1 ACOUSTIC 13	31.51	174.44	104.86
V1 ACOUSTIC 14	40.65	84.21	49.72
V1 ACOUSTIC 15	10.29	104.70	83.39

Origin: Sensor Av Scale: Trace 2

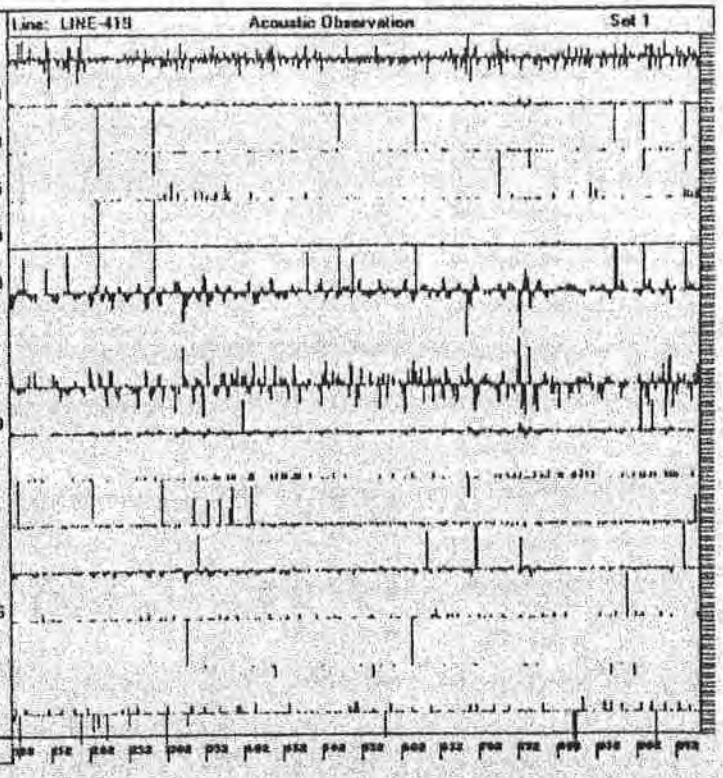

Measurement	Min	Max	Mean
V1 ACOUSTIC 16	5.15	50.31	49.52
V1 ACOUSTIC 17	17.66	98.51	18.52
V1 ACOUSTIC 18	19.69	113.25	103.74
V1 ACOUSTIC 19	1.49	107.14	97.74
V1 ACOUSTIC 20	19.81	100.84	86.78
V1 ACOUSTIC 21	128.52	133.43	131.11
V1 ACOUSTIC 22	96.26	99.43	97.89
V1 ACOUSTIC 23	17.21	20.75	18.98
V1 ACOUSTIC 24	83.02	96.21	91.52
V1 ACOUSTIC 25	25.70	131.84	130.85
V1 ACOUSTIC 26	88.21	97.57	96.47
V1 ACOUSTIC 27	15.51	28.14	26.00
V1 ACOUSTIC 28	1.57	424.72	10.19
V1 ACOUSTIC 29	55.19	76.85	63.97
V1 ACOUSTIC 30	74.79	92.25	91.65

Origin: Sensor Av Scale: Trace 2

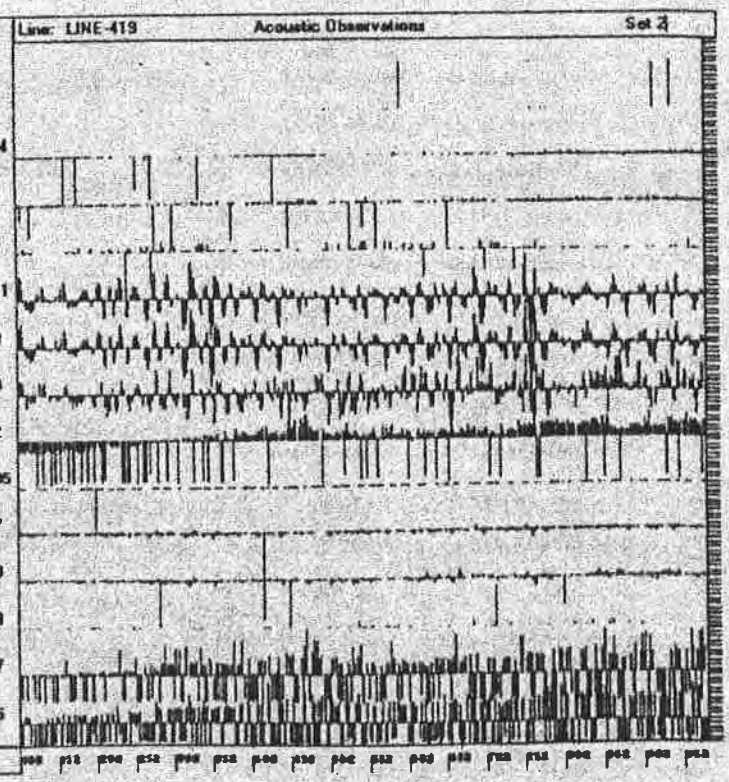

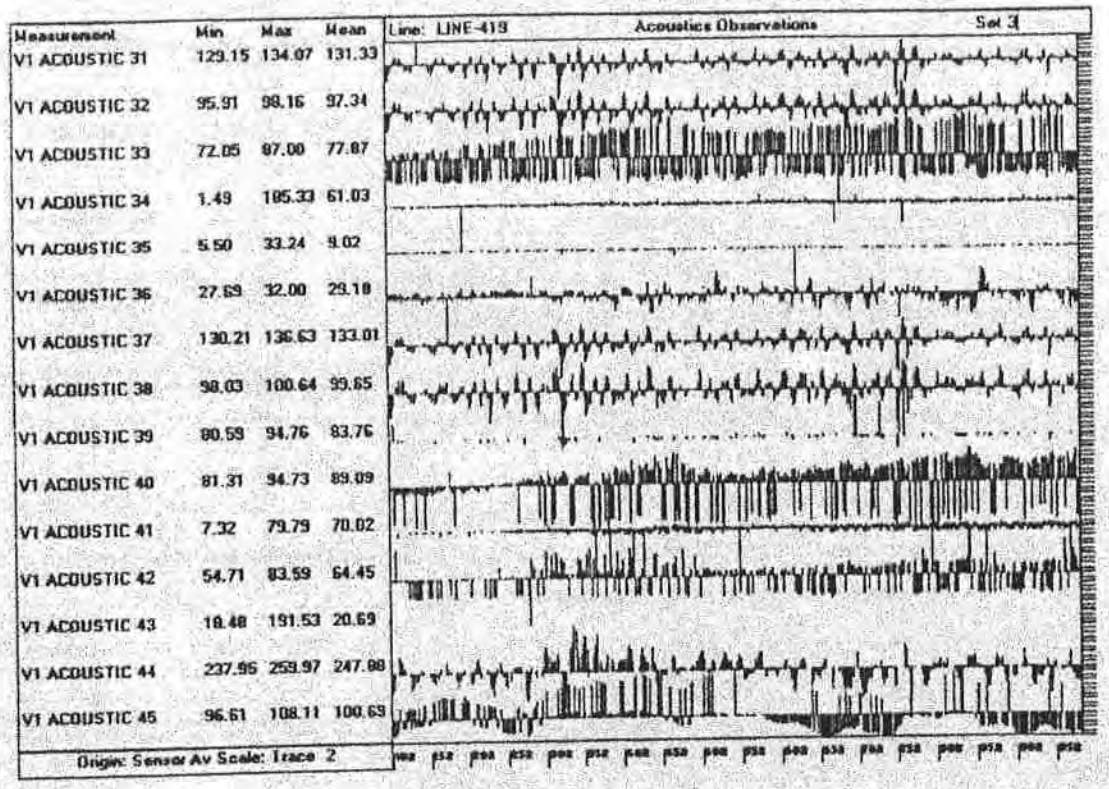

Measurement	Min	Max	Mean
V1 ACOUSTIC 31	129.15	134.07	131.33
V1 ACOUSTIC 32	95.91	98.16	97.34
V1 ACOUSTIC 33	72.05	97.00	77.87
V1 ACOUSTIC 34	1.49	185.33	61.03
V1 ACOUSTIC 35	5.50	33.24	9.02
V1 ACOUSTIC 36	27.69	32.00	29.18
V1 ACOUSTIC 37	130.21	136.63	133.01
V1 ACOUSTIC 38	98.03	100.64	99.65
V1 ACOUSTIC 39	80.59	94.76	83.76
V1 ACOUSTIC 40	81.31	94.73	89.09
V1 ACOUSTIC 41	7.32	79.79	70.02
V1 ACOUSTIC 42	54.71	83.59	64.45
V1 ACOUSTIC 43	19.48	191.53	20.69
V1 ACOUSTIC 44	237.96	259.97	247.98
V1 ACOUSTIC 45	96.61	108.11	100.69

Origin: Sensor Av Scale: Trace 2

Line: LINE-419 Acoustics Observations Set 3

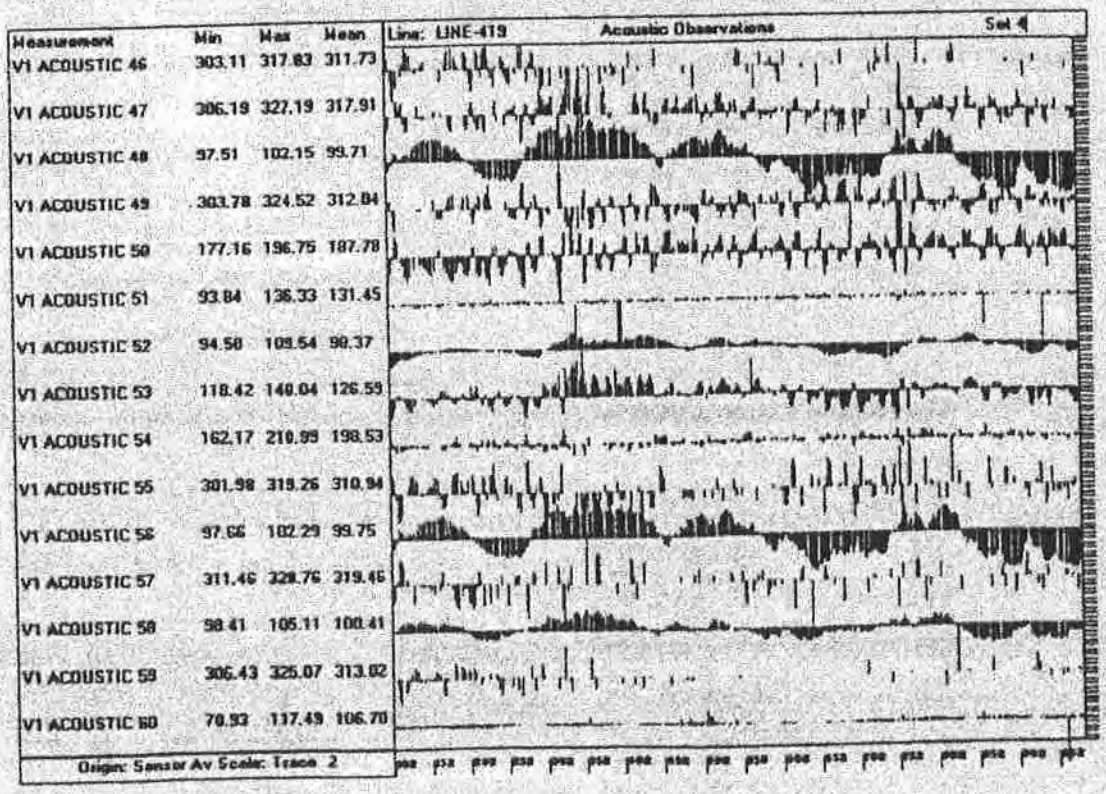

Measurement	Min	Max	Mean
V1 ACOUSTIC 46	303.11	317.83	311.73
V1 ACOUSTIC 47	306.19	327.19	317.91
V1 ACOUSTIC 48	97.51	102.15	99.71
V1 ACOUSTIC 49	303.78	324.52	312.84
V1 ACOUSTIC 50	177.16	196.75	187.78
V1 ACOUSTIC 51	93.84	136.33	131.45
V1 ACOUSTIC 52	94.58	109.54	98.37
V1 ACOUSTIC 53	118.42	140.04	126.59
V1 ACOUSTIC 54	162.17	210.99	198.53
V1 ACOUSTIC 55	301.98	315.26	310.94
V1 ACOUSTIC 56	97.66	102.29	99.75
V1 ACOUSTIC 57	311.46	328.76	319.46
V1 ACOUSTIC 58	98.41	105.11	100.41
V1 ACOUSTIC 59	306.43	325.07	313.02
V1 ACOUSTIC 60	70.93	117.49	106.70

Origin: Sensor Av Scale: Trace 2

Line: LINE-419 Acoustic Observations Set 4

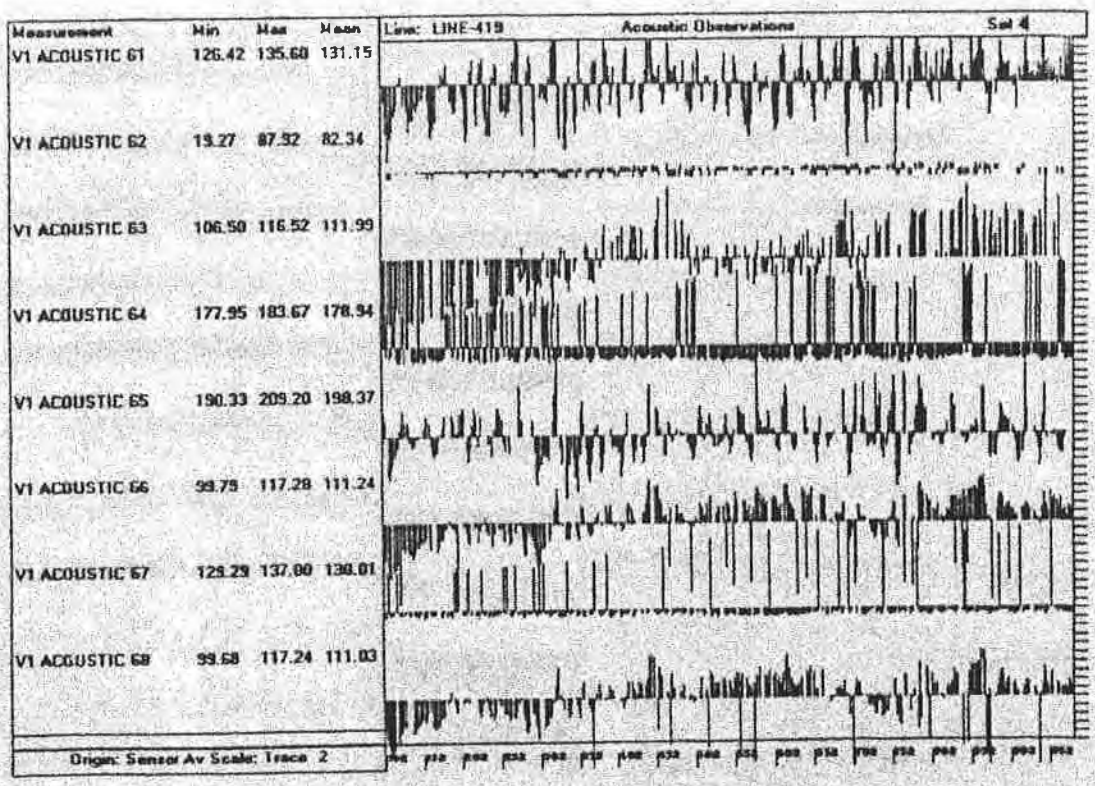

Measurement	Min	Max	Mean
V1 ACOUSTIC 61	126.42	135.60	131.15
V1 ACOUSTIC 62	19.27	87.32	82.34
V1 ACOUSTIC 63	106.50	116.52	111.99
V1 ACOUSTIC 64	177.95	183.67	178.94
V1 ACOUSTIC 65	190.33	209.20	198.37
V1 ACOUSTIC 66	99.75	117.28	111.24
V1 ACOUSTIC 67	129.29	137.00	130.01
V1 ACOUSTIC 68	99.68	117.24	111.03

Origin: Sensor Av Scale: Trace 2

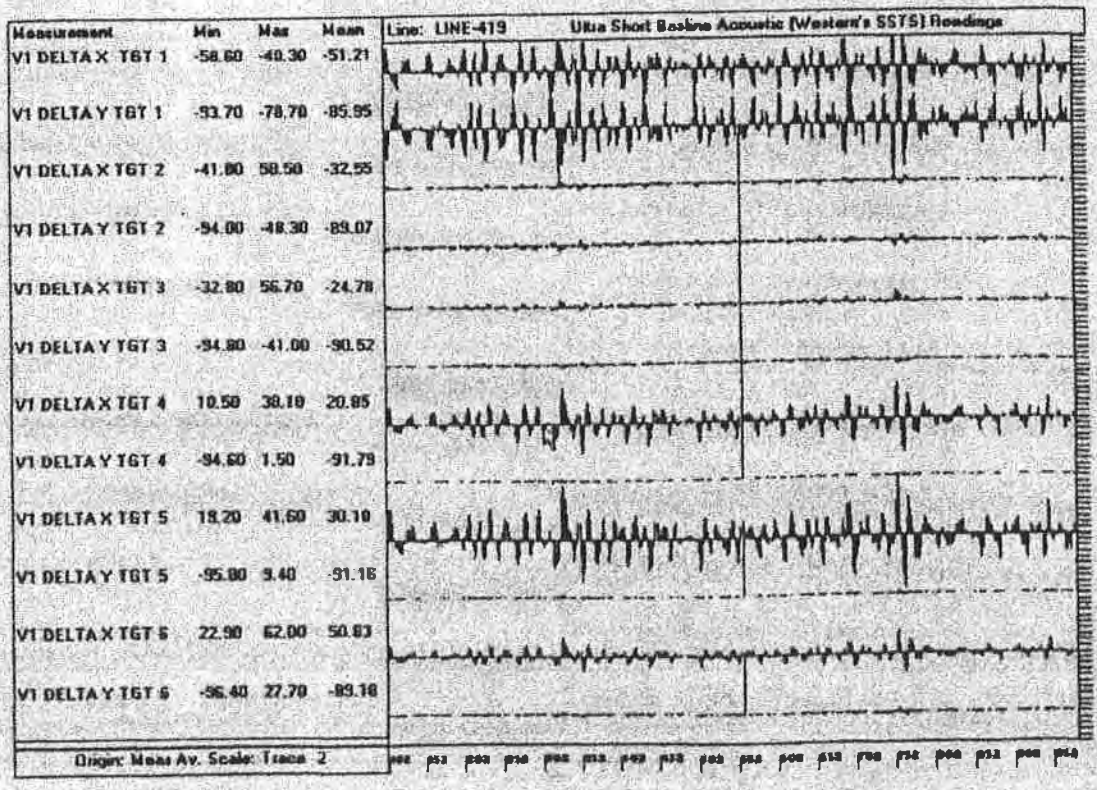

Measurement	Min	Max	Mean
V1 DELTA X TGT 1	-58.60	-49.30	-51.21
V1 DELTA Y TGT 1	-93.70	-78.70	-85.95
V1 DELTA X TGT 2	-41.80	58.50	-32.55
V1 DELTA Y TGT 2	-94.00	-48.30	-89.07
V1 DELTA X TGT 3	-32.80	56.70	-24.78
V1 DELTA Y TGT 3	-94.80	-41.00	-90.52
V1 DELTA X TGT 4	10.50	38.10	20.85
V1 DELTA Y TGT 4	-94.60	1.50	-91.79
V1 DELTA X TGT 5	18.20	41.60	30.10
V1 DELTA Y TGT 5	-95.80	9.40	-91.16
V1 DELTA X TGT 6	22.90	62.00	50.83
V1 DELTA Y TGT 6	-96.40	27.70	-89.16

Origin: Meas Av. Scale: Trace 2

E1.3.3 Compass Azimuths

Measurement	Min	Max	Mean
V1S1 COMPASS 1	278.30	281.80	280.11
V1S1 COMPASS 2	278.70	281.90	280.34
V1S1 COMPASS 3	279.10	282.00	280.60
V1S1 COMPASS 4	278.70	281.60	280.27
V1S1 COMPASS 5	279.00	281.80	280.50
V1S1 COMPASS 6	279.00	281.60	280.34
V1S1 COMPASS 7	278.80	281.70	280.05
V1S1 COMPASS 9	278.50	282.10	280.19
V1S1 COMPASS 9	277.80	282.00	279.72
V1S1 COMPASS 10	277.30	283.00	280.22

Origin: Global Av Scale: Trace 2

Line: LINE-419 Streamer 1 Compass Readings

Measurement	Min	Max	Mean
V1S2 COMPASS 1	278.30	282.10	280.28
V1S2 COMPASS 2	279.20	282.70	281.05
V1S2 COMPASS 3	278.90	282.00	280.61
V1S2 COMPASS 4	279.00	281.60	280.44
V1S2 COMPASS 5	278.70	281.50	280.22
V1S2 COMPASS 6	279.60	282.10	280.91
V1S2 COMPASS 7	279.40	282.00	280.75
V1S2 COMPASS 8	278.50	281.60	280.17
V1S2 COMPASS 9	277.80	282.00	280.01
V1S2 COMPASS 10	276.50	282.50	280.26

Origin: Global Av Scale: Trace 2

Line: LINE-419 Streamer 2 Compass Readings